Title	Synthesis and characterization of new metal-organic frameworks by the use of 2-Pyridyl oximes or alcohols in combination with poly-carboxylic ligands
Author(s)	Mylonas-Margaritis, Ioannis
Publication Date	2022-01-27
Publisher	NUI Galway
Item record	http://hdl.handle.net/10379/17014

"Synthesis and Characterization of New Metal-Organic Frameworks by the Use of 2-Pyridyl Oximes or Alcohols in Combination with Poly-carboxylic Ligands"

Ioannis Mylonas-Margaritis

Thesis for the degree of Ph.D.

OÉ Gaillimh
NUI Galway

Supervisor: Dr. Constantina Papatriantafyllopoulou

Head of School: Prof. Olivier Thomas

August 2021

School of Chemistry

College of Science and Engineering

National University of Ireland, Galway

Δεν αναπτύσσετε θάρρος με το να είστε ευχαριστημένοι στις καθημερινές σας προσωπικές σχέσεις. Το αναπτύσσετε με την συμβίωση δύσκολες στιγμές και αψηφώντας τις αντιξοότητες.

You don't develop courage by being happy in your relationships everyday. You develop it by surviving difficult times and challenging adversity.

EPICURUS *(Philosopher of the 4th century BC)*

To those who positively contributed to developing critical thinking, strong ethics and being able to recognize the right and wrong in life.

I declare the work in this thesis to be original work carried out by myself and the collaborators acknowledged herein. This work has not been submitted to any other academic institution.

Ioannis Mylonas-Margaritis

Acknowledgements

First of all, I would like to thank my supervisor Dr. Constantina Papatriantafyllopoulou for offering me a Ph.D. position in Ireland giving me the chance to become an international scientist. I had the opportunity to fulfill my dream and research interests, studying coordination polymers and Metal-Organic Frameworks. Also, I am grateful for her guidance and her support during my studies.

During the course of my Ph.D. studies, I had the opportunity to work with a great scientist Prof. Pat McArdle. I am glad that he came into my life. Without being my supervisor he supported our research. During the short time that I worked with him, I had the chance to learn more about crystallography and the Irish culture. He is a great teacher and his enthusiasm for research fascinates me. He truly has become one of my mentors.

I would also like to acknowledge my internal examiner Dr. Andrea Erxleben for giving me access to the X-ray facilities of the School. Without it, I would not have the opportunity to obtain my results, since all of my samples were analyzed through X-ray diffraction.

Thank you, Prof. Anastasios Tasiopoulos for our collaboration. Without providing access to your X-ray diffractometer in Cyprus, during the period that ours was out of order, my Ph.D. could not be completed on time. You are a great academic and person. From our discussions, I have gained a lot. I really appreciate the time and effort of your students Dr. Katerina Skordi and Dr. Andreas Kourtelaris.

Thank you, Dr. Constantinos Efthymiou for helping me to be accommodated in Ireland and for our nice discussions. Getting a different perspective was always nice.

A big thank you to all technical officers in the School of Chemistry, Kelly Karen, Judy Buckley, Dermont McGrath, Gerry Reilly, Bernie Conroy, Róisin Doohan, Seamus Collier, Marian Vingoles, Ger Fahy, and Seamus Kellehan.

Thank you, Ciaran O'Malley and Nora Crushell for being my best friends and colleagues and a part of this long journey.

I have to acknowledge the impact of my academic "father" in my academic career, Prof. Spyros P. Perlepes. He was the one, who introduced me to the field of Inorganic Chemistry, once he asked me to join his group, during the 3rd year of my undergraduate studies, when I started working in his research lab. I worked in his group for four years (a period equal to my Ph.D. studies). Working close to him was a great opportunity for me, as I gained a broad knowledge of many different objectives, not only science. His passion for science is always an inspiration. He provided me with many opportunities as he appreciated that I was working hard, and he has contributed a lot in this long journey. No matter what, I will always consider him my "dad" for all the good and bad moments. Working with him was the key factor in being able to complete my Ph.D. studies.

During my BSc. and MSc. Studies, I had the pleasure to be a student of Prof. Vassilios Nastopoulos and interact with him. He is a great mentor and teacher. His strong personality and morals are his key features, that I will always admire and follow in my life. His research integrity is an inspiration. I am glad that he was always open for any type of discussion, without being afraid to state his opinion and always being able to see any perspective. I do not know if I am allowed to consider him a friend, but he will always be my beloved teacher.

A big thank you to all of my friends as they are a big part of my life and for their support at any step of it. It was challenging for all of us to keep in touch while being abroad for that long, since I could not go back home. Even COVID-19 proved to us that we can always be there for each other no matter the challenges.

No reason to state their names, as those who are reading this small paragraph, know that they are acknowledged in each step of my daily life.

Last but not least, I would like to thank my family. Stavroula and Stelios for understanding and for supporting my decision to move abroad and pursue my dream in Ireland. Your love and support are the key points that make me capable to deal with any type of difficulty in life. Your morals will always be the key point that I follow to every aspect of my life. Being my school teachers and always tough on me contributed in a positive way to my life so far. Thank you for being so mindful. Dad's health will always worry me, but mum's personality will always offer balance. Of course, I have to acknowledge my brother Dimitris (Mitsos), who always supported me in his own unique way, I love you, bro. Dimitris Apostolakis is a member of this family too. No matter what is going on in my life, he has the unique ability to make me smile within a couple of seconds. Julie Alexandropoulou, is like a second mother to me, as she has always treated me like one of her children (Giannis and Dimitris). Since I met her in Patras during my undergraduate studies, she is always there for me. My "brother", first student and friend Aristotelis Kontos, whose non-emotional way of thinking was the reason to ask him for a second opinion for everything.

Table of Contents

Abbreviation List

CO_2	Carbon Dioxide
CO	Carbon Monoxide
N_2O	Nitrous Oxide
CCl_2F_2	Dichlorodifluoromethane
CHF_3	Fluoroform
SF_6	Sulfur hexafluoride
NF_3	Nitrogen trifluoride
CrO_4^{2-}	Chromate
As(III)	Arsenate
SMMs	Single-Molecule Magnets
MV-MOFs	Multivariant MOFs
0D	Zero Dimensional
1D	One Dimensional
2D	Two Dimensional
3D	Three Dimensional
H_2pyaox	Pyridine-2-amidoxime
H_2bdc	1,4-benzenedicarboxylic acid
H_3btc	1,3,5-benzenetricarboxylic acid
X-ray	X-radiation
SCM	Single Chain Magnetization

MOFs	Metal-organic frameworks
pxrd	Powder X-ray diffraction
DMF	Dimethyl formamide
MeCN	Acetonitrile
Et_2O	Diethyl ether
Et_3N or NEt_3	Triethylamine
CH_3ONa	Sodium Methoxide
H_2O	Water
mL	Milliliter
°C	Degrees Celsius
h	Hour
Å	Angstrom
mpkoH	2-methyl pyridyl ketoxime
H_4pma	1,2,4,5-benzenetetracarboxylic acid or pyromellitic acid
UV-Vis	Ultraviolet Visible
EDX	Energy Dispersive X-ray Analysis
DC	Direct Current
SBU	Secondary Building Unit
Ru-MOFs	Ruthenium Metal-Organic Frameworks
Ln-MOFs	Lanthanide Metal-Organic Frameworks

R.T.	Room Temperature
min	Minute(s)
T	Tesla
K	Kelvin
cm	Centimeter
H	Heisenberg Hamiltonian
S	Spin
g	g-factor
EPR	Electron Paramagnetic Resonance
IR	Infrared
H_2pdm	2,6-pyridinedimethanol

First Author Publications

- I. Mylonas-Margaritis, M. Winterlich, C. Efthymiou, P. McArdle, Th. Lazarides, C. Papatriantafyllopoulou, "New insights into oximic ligands: synthesis and characterization of 1D chains by the use of pyridine 2-amidoxime and polycarboxylates", *Polyhedron* **2018** 151, 360-368.

- I. Mylonas-Margaritis, A. Gérard, K. Skordi, J. Mayans, A.Tasiopoulos, Patrick McArdle, C. Papatriantafyllopoulou, "From 1D Coordination Polymers to Metal Organic Frameworks by the Use of 2-Pyridyl Oximes", *Materials MDPI* **2020**, 13(18) (2020) 4084.

- I. Mylonas-Margaritis, J. Mayans, P. McArdle, C. Papatriantafyllopoulou, "ZnII and CuII-Based Coordination Polymers and Metal Organic Frameworks by the Use of 2-Pyridyl Oximes and 1,3,5-Benenetricarboxylic acid", *Molecules MDPI* **2021** 26(2), 491.

- I. Mylonas-Margaritis, J. Mayans, W. Tong, P. Farràs, A. Escuer, P. McArdle, Constantina Papatriantafyllopoulou, "Synthesis and Characterization of New Coordination Compounds by the Use of 2-Pyridinemethanol and Di- or Tricarboxylic Acids", *CrystEngCommun* **2021**, DOI: *HTTPS://DOI.ORG/10.1039/D1CE00659B* .

- I. Mylonas-Margaritis, C. G. Efthymiou, J. Mayans, A.. Escuer, P. McArdle, C. Papatriantafyllopoulou, "Metal-organic frameworks by the simultaneous use of 2,6-pyridinedimethanol & terephthalate" (manuscript in preparation)

Conference Presentations

- I. Mylonas-Margaritis, J. Mayans, A. Tasiopoulos, P. McArdle, C. Papatriantafyllopoulou, "Moving from traditional coordination chemistry to MOFs for the investigation of new families of MOFs with unique properties", 15th International conference on materials chemistry (MC15), July 12-15 2021, Online Poster Presentation

- I. Mylonas-Margaritis, J. Mayans, A. Tasiopoulos, P. McArdle, C. Papatriantafyllopoulou, "Moving from traditional coordination chemistry to MOFs for the investigation of new families of MOFs with unique properties", 2nd International School on Porous Materials: MOF2021, Lake Como School of Advanced Studies, June 21-25 2021, Online Poster Presentation

- I. Mylonas-Margaritis, C. G. Efthymiou, K. Skordi, J. Mayans, A. Tasiopoulos, P. McArdlr, C. Papatriantafyllopoulou, "Novel Metal-Organic Frameworks by the simultaneous use of carboxylates and pyridyl oximes/pyridine alcohols", Inorganic Ireland Symposium 2021, Galway, Ireland, May 14 2021, Online Poster Presentation

- I. Mylonas-Margaritis, C. G. Efthymiou, P. McArdle, C. Papatriantafyllopoulou, "A new class of coordination polymers and MOFs by the combination of chelate and bridging organic ligands", 3rd European Conference on Metal organic Frameworks and Porous Polymers (EUROMOF2019), Paris, October 27-30, 2019, Poster Presentation

- I. Mylonas-Margaritis, C. G. Efthymiou, P. McArdle, C. Papatriantafyllopoulou, "Metal complexes, 1D coordination polymers and MOFs by the use of oximes in the presence of polytopic carboxylic

acids", 14th International Conference on Materials Chemistry (MC14), University of Birmingham, July 8-11, 2019, Poster Presentation.

- I. Mylonas-Margaritis, C. G. Efthymiou, P. McArdle, A. Escuer, C. Papatriantafyllopoulou, "Metal complexes, 1D coordination polymers and MOFs by the use of oximes in the presence of polytopic", 1st International School on Advanced Porous Materials, Como, Villa del Grumello, June 17-21 2019, Poster Presentation.

- I. Mylonas-Margaritis, C. G. Efthymiou, Th. Lazarides, P. McArdle, A. Escuer, C. Papatriantafyllopoulou, "Using pyridine amidoximes in the presence of polytopic carboxylic acids for the synthesis of novel coordination polymers", 6th International Conference on Multifunctional, Hybrid and Nanomaterials, Sitges, Spain, March 11-15 2019, Oral Presentation.

- I. Mylonas-Margaritis, C. G. Efthymiou, Th. Lazarides, P. McArdle, A. Escuer, C. Papatriantafyllopoulou, "Coordination Polymers from the Use of Pyridine Amidoximes and Polytopic Carboxylic Acids", Inorganic Ireland Symposium 2018, Belfast, Ireland, December 17, 2018, Poster Presentation.

- I. Mylonas-Margaritis, C. G. Efthymiou, Th. Lazarides, P. McArdle, A. Escuer, C. Papatriantafyllopoulou, "By the simultaneous use of pyridine amidoximes and polycarboxylates is formed a new class of coordination polymers and MOFs", 50 Years of Coordination Chemistry (A Meeting of the Coordination and Organometallic Chemistry Discussion Group), University College Dublin, Ireland, December 3-4, 2018, Poster Presentation.

- I. Mylonas-Margaritis, C. G. Efthymiou, Th. Lazarides, P. McArdle, C. Papatriantafylopoulou, "1D- Coordination Polymers and metal complexes from the combination of 2-pyridyl oximes with polycarboxylic acids", 8th North America-Greece-Cyprus Workshop on Paramagnetic Materials, Sparta, Greece, June 18-22, 2018, Invited Oral Presentation.

Abstract

The aim of this project is the synthesis and characterization of novel mixed-ligand coordination polymers and metal-organic frameworks (MOFs) and their further study as magnetic sensors for the adsorption of non-environmental friendly species. For the synthesis of the mixed-ligand MOFs, pyridyl oximes or pyridyl alcohols have been used for the stabilization/formation of inorganic secondary building units (sbus), whereas di-, tri- and tetra- topic carboxylates (1,4- benzene-dicarboxylic acid/terephthalate, 1,3,5- benzene-tricarboxylic acid or trimesic acid, 1,2,4,5-benzenetetracarboxylic acid or pyromellitic acid) have been employed as pillars. The compounds were synthesized under solvothermal conditions. The choice of linkers is crucial for the properties of the synthesized materials. Pyridyl oximes and alcohols are broadly used in the field of Single-Molecule Magnets (SMMs) and have proved to stabilize small and high nuclearity metal complexes with interesting magnetic properties; however, they have not been systematically explored in the field of MOFs. Polycarboxylates were one of the first family of linkers used in the field of MOFs for the formation of stable 2D and 3D networks. Combining these two categories of organic linkers, we targeted the isolation of small or high nuclearity novel secondary inorganic units and MOFs with interesting topologies and magnetic properties. The main drawback of investigating mixed-ligand systems is that there are more than one product (bi-products) that can be isolated during this process before the final coordination polymer or MOF is precipitated. As such, mixed ligand systems are not generally high yielding or thermodynamically stable and for this reason, an in-depth understanding and investigation is required to understand the conditions upon which they precipitate/crystallize and to be able to isolate the intermediate products in absence of the final coordination polymer or MOF. This can be achieved by modifying the synthetic conditions. All synthesized

compounds were characterized through single-crystal and powder X-ray crystallography, infrared spectroscopy, thermogravimetric analysis, with magnetic studies obtained for relevant products. The capacity of representative MOFs to encapsulate and detect environmentally hazardous species was also investigated.
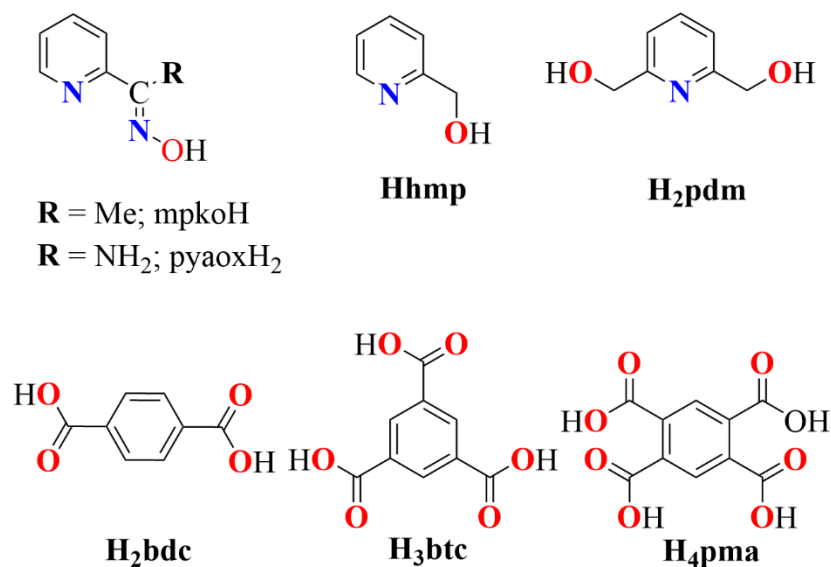
Scheme 1. Representation of the ligands, which were used for the formation of MOFs: (top, left) pyridyl-oximes, (top, middle) 2-pyridine-methanol (Hhmp), (top, right) 2,6,-pyridine-dimethanol (H$_2$pdm), (bottom, left) benzene-1,4-dicarboxylic acid or terephthalic acid (H$_2$bdc); (bottom, middle) benzene-1,3,5-tricarboxylic acid or trimesic acid (H$_3$btc) , (bottom, right) 1,2,4,5-benzenetetracarboxylic acid or pyromellitic acid (H$_4$pma).

The investigation of the combination of pyrdine-2-amidoxime (pyaoxH$_2$) with 1,4- benzene-dicarboxylic acid (H$_2$btc) and 1,3,5-benezene-tricarboxylic acid (H$_3$btc) led to isolation of one-dimensional coordination polymers

$[Zn(bdc)(pyaoxH_2)(DMF)]_n$, $\{[Ni(bdc)(pyaoxH_2)_2]\cdot 2DMF\}_n$, $[Mn(bdc)(pyaoxH_2)_2]\cdot 2DMF\}_n$, $[Ni(Hbtc)(pyaoxH_2)_2]_n$ and a mononuclear complex $[Ni(Hbtc)(pyaoxH_2)_2]_n]\cdot 2H_2O$. This system was expanded further with the employment of benzene-1,3,5-tricarboxylic acid and pyridine-2-amidoxime ($pyaoxH_2$) or 2-methyl- pyridyl ketoxime (mpkoH) in Zn^{II} and Cu^{II} chemistry. Five novel coordination polymers and MOFs have been isolated and characterized, namely $[Zn(H_2btc)_2(pyaoxH_2)_2]\cdot 2H_2O$, $[Zn(Hbtc)(pyaoxH_2)_2]_n$, $[Cu(Hbtc)(pyaoxH_2)]_n$, $[Cu(Hbtc)(mpKoH)]_n$ and $[Cu_2(Hbtc)_2(mpkoH)_2(H_2O)_2]\cdot 4H_2O$. The Dc magnetic susceptibility of $[Cu(Hbtc)(pyaoxH_2)]_n$ was carried out and revealed the presence of weak exchange interactions between the metal centers; where the experimental data were fitted with a theoretical model and fittings parameter being $J = -0.16(1)$ cm^{-1} and $g = 2.085(1)$. The isotropic g value was also confirmed by electronic paramagnetic resonance (EPR) spectroscopy. Also, reactivity studies were performed in presence of metal cations.

Expanding further the exploration of this unique combination, by the use of a tetra-topic carboxylate, nine new compounds have been isolated and characterized. Among them, $[Zn_2(pma)(pyaoxH_2)_2(H_2O)_2]_n$ and $[Cu_4(OH)_2(pma)(mpko)_2]_n$ are the first MOFs of this combination with the latter displaying a novel 3,4,5,8-c net topology. Coordination polymers were isolated through this combination leading to $[Zn_2(pma)(pyaoxH_2)_2]_n$, $[Cu_2(pma)(pyaoxH_2)_2(DMF)_2]_n$, and $[Cu_2(pma)(mpkoH)_2(DMF)_2]_n$. Discrete metal complexes were also isolated through this synthetic investigation leading to $[Zn(H_2pma)(pyaoxH_2)(H_2O)_2]$, two isostructural dinuclear complexes $[M_2(pma)(pyaoxH_2)_2(H_2O)_6]$ where M^{II} = Co, Mn and $[Zn_2(pma)(mpkoH)_2(H_2O)_4]\cdot 2H_2O$. The $[Cu_4(OH)_2(pma)(mpko)_2]_n$ is stable under different chemical conditions and for this reason, it was further studied for

the encapsulation of Fe^{3+} ions. The encapsulation of iron was investigated through a variety of techniques, namely, UV-vis, EDX, and magnetism studies. The MOF itself and the loaded MOF were studied magnetically and it was revealed that this could be a nice example for the further investigation of MOFs as magnetic sensors, as it selectively adsorbs Fe^{3+}.

As the combination of pyridyl-oximes and carboxylates was studied in-depth, we continued to investigate the behavior of an analogue family of small rigid ligands, pyridine alcohols. The oximic group (-N-OH) of pyridyl-oximes was replaced by the hydroxyl group (-OH) of pyridine alcohols. This combination was introduced for the first time in the field of coordination polymers and MOFs. The simultaneous use of 2-pyridinemethanol (hmpH) with benzene-1,4-dicarboxylic acid (H_2bdc) or 1,3,5-benzenetricarboxylic acid (H_3btc) led to the isolation of five new coordination compounds $[M_2(Hbtc)_2(Hhmp)_4]\cdot DMF$ ($M=Co^{II}$; Ni^{II}), $[Ni(bdc)(Hhmp)_2]_n\cdot 4H_2O$, $[Zn_2(bdc)(hmp)_2]_n\cdot DMF$ and $[Fe_3(bdc)_3(Hhmp)_2]_n$. $[Zn_2(bdc)(hmp)_2]_n\cdot DMF$ and $[Fe_3(bdc)_3(Hhmp)_2]_n$ are the first examples of metal-organic frameworks bearing hmp^- while the Zn-MOF exhibits an unprecedented 4,4,4-c net with point symbol $\{3^2.10^3.11\}\{3^2.10^4\}_2$. Regarding the Fe-MOF, this is based on a trinuclear linear Fe^{II} secondary building unit and possesses a 3,4,6T2 topology with point symbol $\{4^2.8^3.10\}_3\{4^3\}_2\{4^6.8^6.10^3\}$. This compound was magnetically studied and revealed the existence of antiferromagnetic coupling between the Fe^{II} cations with a superexchange value of $J = -8.46$ cm^{-1}.

In order to investigate the impact of an additional hydroxyl group on the identity of the isolated species, the pyridinemethanol was replaced by 2,6-pyridinedimethanol. The combination of 2,6-pyridinedimethanol (H_2pdm) with 1,4-benzene dicarboxylic acid (H_2bdc), led to three new MOFs $[M_3(bdc)_3(Hpdm)_2]_n\cdot DMF$ (where M^{II} = Zn, Mn), $[Mn_3(bdc)_3(H_2pdm)_2]_n$, and

$[Mn_3(bdc)_3(DMF)_4]_n$ and a mononuclear metal complex $[Ni(H_2pdm)_2](bdc)$, which forms a strong 3D-hydrogen bonding network.

Overall, the initial combination of 2-pyridyl oximes or alcohols with polycarboxylates provided access to twelve novel MOFs adopting new topologies, eight coordination polymers, and nine metal complexes. Also, it was proved that the $[Cu_4(OH)_2(pma)(mpko)_2]_n$ is suitable for the sensing of Fe^{3+} with sensing capacity 129.89 mg Fe/g MOF.

xxx

Chapter 1: Introduction

1. Materials/Compounds for Environmental Applications

Technological development has indisputably provided essential benefits in humanity in regards to transportation, communication, energy, food industry, and others. Unfortunately, such technological advancements often have a negative impact on the environment; for instance, toxic gases such as CO_2, CO, N_2O, CCl_2F_2, CHF_3, SF_6, NF_3, etc, which are released from cars, factories, and other sources are responsible for the greenhouse effect. Also, chemical species like heavy metals (e.g. Cd(II), Hg(II), Pb(II), Cr(III), Co(II), Fe(III)), dyes, toxic ions (e.g. CrO_4^{2-}, As(III), etc), pharmaceuticals and personal care products are responsible aquatic pollution. (**Figure 1**) Consequently, living organisms, including humans, are severely affected.[1]

One of the main concerns of the European Union (EU) and governments worldwide is environmental pollution; the EU has planned to be climate-neutral with net-zero greenhouse emissions by 2050 in order to preserve the planet for future generations. As a consequence, interest has turned to renewable energy and the elimination of released gas emissions from households, farming, factories, and private and public transportation. One efficient approach in this direction is the development of appropriate filters/membranes, which will be able to entrap CO_2, CO, or other gases and convert them to useful sources or non-toxic/pollutant alternatives such as methane, methanol, and formic acid.[2] Such membranes are based on the employment of porous materials with the capacity to encapsulate a variety of different guest molecules into their pores.

Figure 1. Top: the air pollution due to toxic gases (CO_2, CO, CH_4, N_2O, CCl_2F_2, CHF_3, SG_6, NF_3) is responsible for the green-house effect. Bottom: the water pollution contributes to the poisoning of living organisms and destruction of the eco-system.

Classical porous materials like silicates, metal oxides, activated carbon, and zeolites have been studied and have shown good performance in a range of applications. Silicates find applications as microchips, quartz crystals, glass manufacturing, and ceramics. Activated carbons have been broadly applied on membranes for the removal of chlorine and other organic compounds from water. Zeolites can be employed for catalysis, adsorption of gases, ion exchange membranes, and waste treatment. However, the control or modification of the pore size of the above-mentioned materials can be challenging; hence, the development of alternative materials/compounds with tuneable porosity is essential for the efficient encapsulation and detection of different types of guest molecules.[3] To this end, hybrid multifunctional materials have attracted intense research interest over the recent years. Such species combine two or more physical properties (e.g. photoluminescence, magnetism, catalytic activity, porosity, etc.), whose synergy often enhances their performance in applications,

including sensing, catalysis, drug delivery, spintronics, photonics, adsorption of a wide variety of guest molecules, gas storage, separation, electronics, etc. One representative category of hybrid multifunctional material is the metal-organic frameworks (MOFs), which will be described in more detail in the next pages.
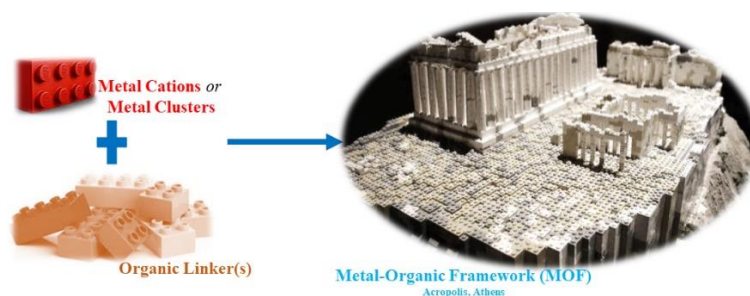
Figure 2. Representation of the formation of MOFs.

2. Metal-Organic Frameworks (MOFs)

Metal-Organic Frameworks (MOFs) are hybrid porous crystalline materials, which consist of inorganic and organic secondary building units (SBUs).[4] The organic ligand is the pillar/linker, connecting the inorganic SBUs, which can be either a metal cation or a metal cluster (**Figure 2**). These type of compounds were discovered approximately four decades ago and have now been officially recognized by IUPAC. Over the last few decades many research groups have been working in the field, including Richard Robson, Gérard Férey, Omar Yaghi, Susumu Kitagawa, Michael Zaworotko, Mathew Rosseinsky, Mohamed Eddaoudi, and others. (**Figure 3**).
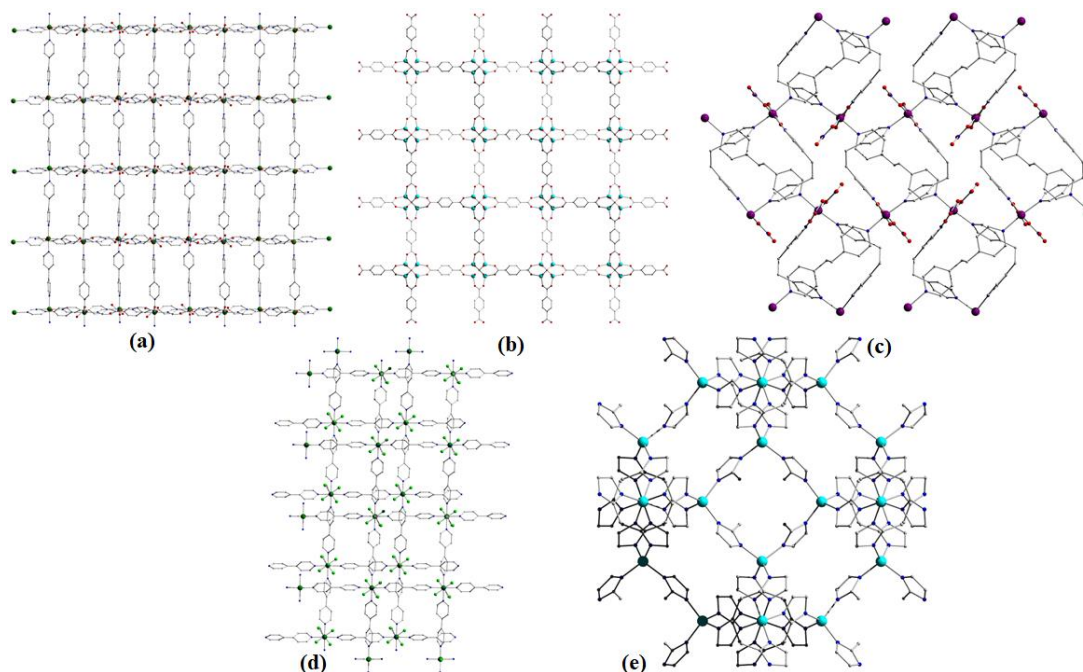
Figure 3. Examples of well-known MOFs and coordination polymers reported in the literature. (a) $[Cu_2(4,4'\text{-bpy})_5(H_2O)_4]_n$ [5], (b)MOF-5 [6], (c) $[Co(NO_3)_2(1,2\text{-bis}(4\text{-pyridy})ethane_{1.5}]_n$ [7], (d) $\{[Cu(PF_6)(4,4'\text{-bpy})_2(MeCN)]\cdot PF_6\cdot 2MeCN\}_n$ [8], (e) ZIF-8 [9].

Due to their porosity, MOFs are excellent candidates for the encapsulation of a variety of adsorbates such as gases (CO_2, CO, SO_2, Xe, H_2, N_2, etc.) and environmental pollutants. The framework can be modified by the addition of functional groups that favor suitable intermolecular interactions stabilizing guest molecules of different shape or size into their pores. Furthermore, they often affect the structural conformation of the MOF resulting in the pore expansion or contraction depending on the presence of a guest molecule in the MOF pores. This phenomenon is known as the breathing effect and is a unique property of MOFs. The first examples of MOFs show that the

nature of the linker influences the breathing effect, and initially, it had been suggested that they should bear alkyl chains that provide flexibility into the system. Later on, it was proved that the linkers do not have to be fully flexible but semi-rigid, in order for the materials to have increased breathing and stability. It is worth mentioning that there are materials whose properties (e.g. porosity, magnetism) change due to external stimuli such as light or temperature and have attracted the interest of the scientific community. A representative example of MOFs, based on this special category is the spin-crossover MOFs, which are temperature based and such an example are the Hoffman type MOFs.[10]

Another unique property of MOFs is interpenetration, which improves their structural flexibility and stability. Interpenetration or catenation is expressed as polymeric analogs of catenanes or rotaxanes, and the formation of entanglement. This phenomenon is significantly observed and reported in MOFs. Interpenetration results in the decrease of the pore volume while also affecting the surface area. Although interpenetration is merely based on a self-assembly process, one possible way to control it is by adjusting the bridging ligands. By using bulky ligands and adding functional groups on the pillars, it is possible to change the degree of interpenetration. Also, by modifying the reaction conditions (such as solvent, temperature, the concentration of reagents) it is possible to influence the interpenetration effect.[11]

There is an increasing need for synthesizing and characterizing new MOFs with enhanced stability and porosity for employing them in different technological and environmental applications. In the last few decades a wide variety of coordination polymers and metal-organic frameworks has been characterized and studied for potential applications or are promising candidates for future applications such as drug delivery, gas purification or separation, catalysis (e.g. conversion of CO or CO_2 to useful molecules), electrochemistry, separations

(e.g. chromatography), sensing, water splitting, and others. In regards to the separation of species either in the liquid or gaseous phase, this is essential for purity and their further use in absence of other reagents.

For example, Plana's group published in 2020 the synthesis and characterization of a water-stable Cu@MOF, abbreviated as mCB-MOF-1, (**Figure 4**) with carborane-ditopic acid used as a ligand. This molecule was previously used in biofuels for the separation of butanol from ethanol and acetone contaminants. For the same application, zeolites had been tested and used in the past, but as they are hydrophilic, their performance was poor.[12] Another example is the separation of ethane and ethylene. Li's group developed a calcium based MOF by the use of 1,2,4,5-tetrakis(4-carboxyphenyl)-benzene). This MOF has a preference to adsorb ethane over ethylene from mixtures that contain both species. This separation is essential as ethylene is widely used for a variety of industrial applications, including the production of polyethylene.[13]
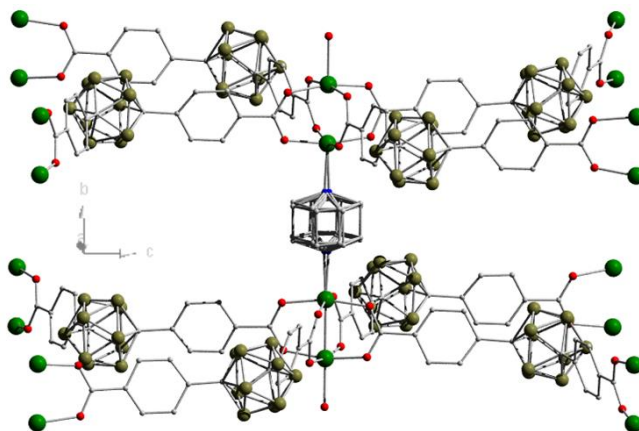
Figure 4. Representation of the crystal structure of the mCB-MOF-1.[12]

The use of MOFs is also paramount for sensing applications, and in particular, for the detection of species, which are harmful either for the ecosystem

or the living species. For example, Biswas's group developed a Cd(II) fluorescent MOF, by the use of quinoline-2,6-dicarboxylic acid, for the encapsulation and detection of dichromate in water. This molecule was able to selectively adsorb dichromate even from mixtures with chromates, sulfonates, acetates, bromides, nitrates, and other anions.[14] Recently, Liu's group used a calcium-based MOF for the encapsulation of sulfur hexafluoride at low concentrations; sulfur hexafluoride is also responsible for the greenhouse effect. They were able to detect and selectively encapsulate and separate sulfur hexafluoride from a mixture containing nitrogen.[15] Another example, of detection of biological importance, is the recognition and sensing of glutathione, which is responsible for the damage of DNA and RNA. Yao's group developed an electrochemical sensor based on an Au@Cu-MOF. The Cu-MOF was loaded with Au nanoparticles. They demonstrated that the loaded MOF with Au nanoparticles had higher sensitivity to the detection of glutathione (GSH). This sensor device can be used for the detection of glutathione in vegetable and serum samples.[16]

Catalysis and conversion of molecules to other useful sources is also a big part of the worldwide economy and solutions have to be found in order to reduce the energy cost and the industrial cost of production. Regarding the reduction of CO_2, Zhang's group developed bimetallic Ni(II)/Ti(IV) bimetallic MOFs for the photocatalytic reduction of CO_2 to CO, CH_4, and H_2. The necessity of growing new materials for the reduction of carbon dioxide is the use of milder conditions than is currently available. They proved that the mixed MOF had better photocatalytic activity than the homometallic titanium analogue. As an example, the 50%NiTi-MOF shows an increased yield of CO and of course increased CH_4 yield compared with the Ti-MOF. The 75%NiTi was much more efficient and the conversion yield was further increased. This is due to the fact

that further increase of Ni, affects the charge transfer process.[17] Hijikata's group used known MOFs such as MIL-125-NH$_2$, UiO-66-NH$_2$, HKUST-1, MIL-101, Zn-MOF-74 and MIL-121, and loaded them with Pt nanoparticles for the conversion of acetic acid to ethanol while avoiding the production of ethyl acetate as a reaction by-product. They also proved that the MIL-125-NH$_2$ has better performance in this catalytic reaction than the other MOF that had been tested.[18]

3. Synthetic Approaches Towards New MOFs

The wide range of technological, biomedical, and environmental applications of MOFs have increased the need for the development of synthetic approaches for the isolation of new such species with desirable stability and controlled porosity. Over the last three decades, a wide variety of techniques have been developed and are briefly described below:[19]

1. solvothermal synthesis: this is the most commonly employed synthetic approach for the development of coordination polymers and MOFs. It does not require specific equipment apart from an oven and a closed flask (tube, vial, autoclave). Reagents are added either at once or in multiple steps. The system is heated until the boiling point of the solvent or solvent mixture and the product is isolated after a specific time either as a powder, semi-crystalline form or as crystals. It is the most common technique that is employed for the production of MOFs on a gram scale.[20]

2. microwave-assisted synthesis: in this case, the reaction takes place in a microwave oven and the system is heated at a higher rate than the classical solvothermal approach. It is useful for the production of MOF nanoparticles and the material is more homogeneous in shape and morphology.[21]

3. electrochemistry: this approach offers the advantage of the production of MOFs in a continuous manner. Milder conditions are used and the reaction time is decreased compared with solvothermal synthesis. The production of material ranges from minutes to a few hours. It is suitable for the development of materials in film or coating form. There are four different types of electrochemical synthesis of MOFs: a) anodic dissolution, b) cathodic electrosynthesis, c) galvanic displacement, and d) electrophoretic deposition. In cases of direct electrosynthesis like (a) and (b), the MOFs are synthesized using an electrochemical reaction which occurs on the surface of the electrode. But in methods, where the synthesis is indirect, the MOFs are pre-synthesized following certain procedures and the electrochemical reaction is one of the intermediate steps.[22]

4. mechanochemical and sonochemical synthesis: this is a greener and solvent-free approach for the production of MOFs. There are three different categories of mechanochemical synthesis, a) neat grinding, where the use of solvent is avoided, b) liquid-assisted grinding, where a catalytic amount of solvent is used for the faster production of the material, as it increases the mobility of the reagent, and c) ion-liquid assisted grinding, where a catalytic amount of solvent and salt additives are used.[23]

5. post-synthetic modification (PSM): this entails the targeted modification of a MOF after it has been synthesized. The aim of this technique is to alter the porosity and/or other physical properties of the material, as well as the insertion of functional groups in desirable positions in the framework, enhancing its encapsulation or sensing capacity.[24]

4. Synthetic parameters that affect the MOF synthesis

A variety of synthetic parameters in MOF synthesis (such as the nature of the organic linker, solvents, temperature, the presence or absence of organic polymers and surfactants, and the metal source) can influence the identity and crystallinity of the product.

1. Organic linkers: Until now, an extensively broad library of organic ligands (such as carboxylates, pyridines, azoles, imidazolates, etc) have been used for the synthesis of new metal-organic frameworks (**Figure 5**). One of the first categories of linkers, which was broadly used for the synthesis of MOFs, are the carboxylic acids (terephthalate, biphenyl-dicarboxylate, naphthalene-dicarboxylic acid, trimesic acid, and others). The size of the linkers was increased, to increase the size of the pores of the synthesized compounds. The aforementioned were introduced and extensively studied by G. Férey, O.Yaghi, S. Kitagawa, and others and have given structurally interesting compounds, including the MIL family MOFs, MOF-5, IR-MOFs, and others.

Oxalate   **BDC**   **BDC-NH₂**   **BDC-(OH)₂**   **1,3-BTC**   **BPDC**   **H₂L**   **PDC**

H₂oba   **H₃BTC**   **H₃PBTC**   **H₃BTB**

H₃BTTB   **H₄L**
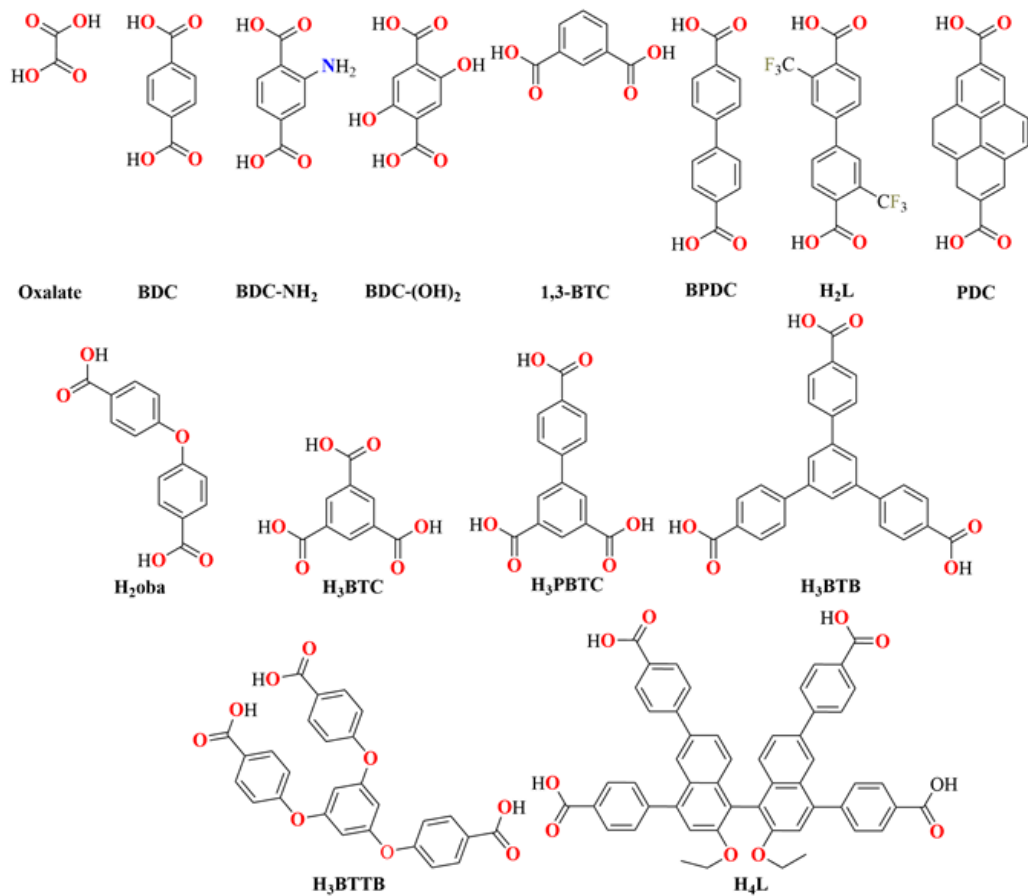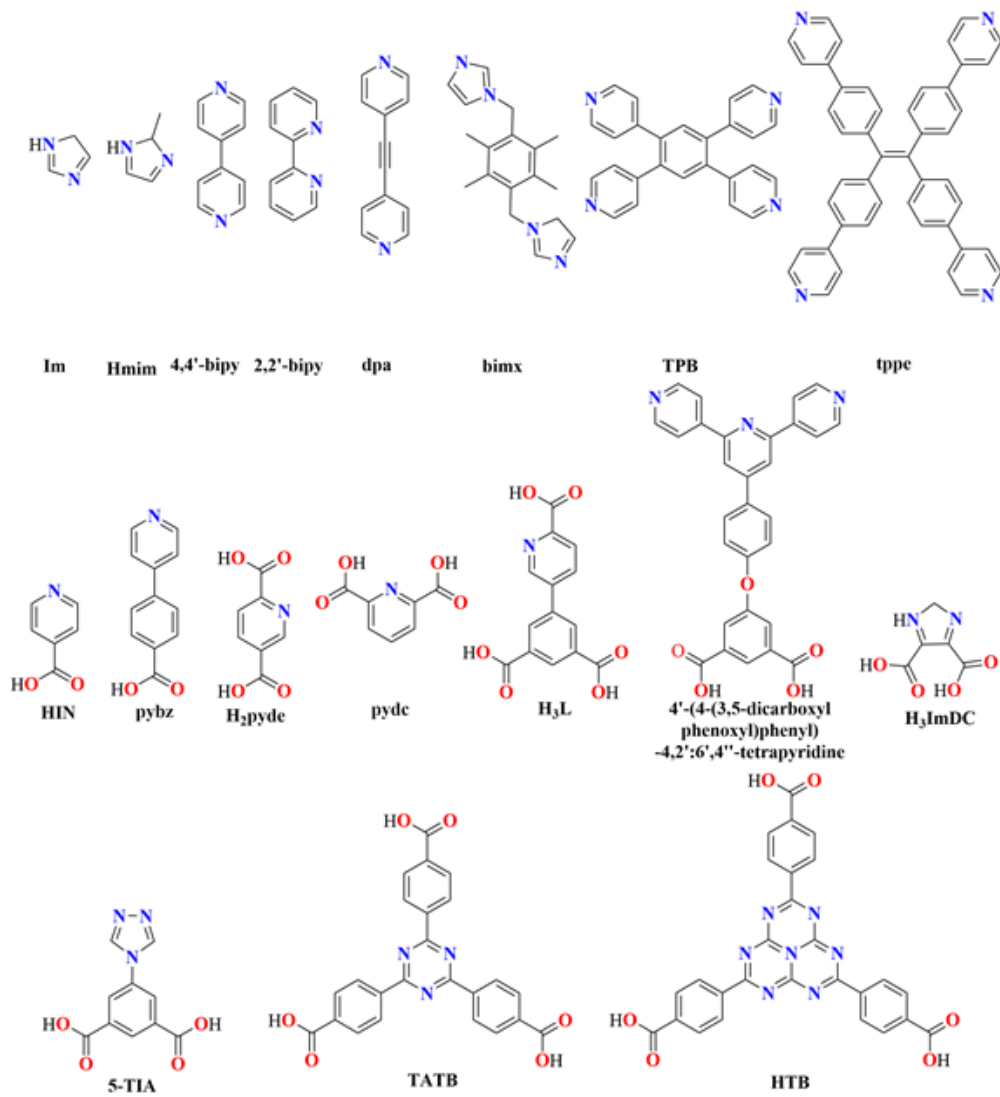
Figure 5. Organic ligands used in the literature for the synthesis of MOFs.

2. Solvents: It is well known that the nature of the solvent is crucial for the solubility of the reagents, affects the crystallization and in some cases the identity of the product. A broad range of solvents have been used for the synthesis and crystallization of new MOFs (**Figure 6**). They can act as templates influencing the crystal growth and the final-morphology. The nature of the solvent is crucial as it affects the nature of interactions (e.g. Van der Waals, π-π stacking..) and the hydrogen bonding, through which compounds are stabilized and, sometimes, the change of the solvent leads to different reaction products.[25]

3. Metal cations: The influence of the metal is evident by changing the oxidation state from +2 to +3. This change will affect parameters such as the coordination number, specific surface area, the shape and the size of the cavities, the structural geometry, the accessibility to the metal sites, the hydrophilicity, and the stability leading to species with different structural features and properties.

4. Temperature: The choice of the temperature is based on the boiling point of the used solvent or mixture of solvents. There are cases, where in high temperatures the solvents are decomposed forming other species and those are stabilizing MOFs are coordinated. An example is *N,N*-dimethylformamide, in an autoclave system DMF can be hydrolyzed to formic acid and this can either coordinate or its presence to be crucial for the stabilization of a compound by either coordinating or acting as a modulator.
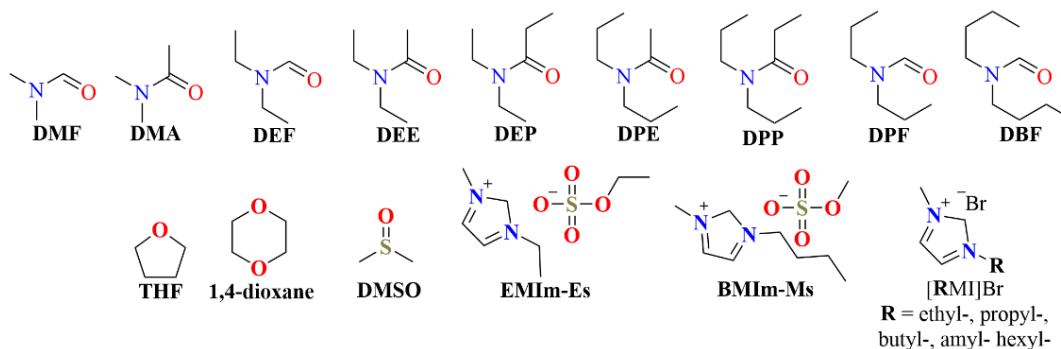
Figure 6. Solvents for the synthesis of MOFs.

5. Organic polymers and surfactants: For the template synthesis of MOFs, compounds such as organic polymers or surfactants have been used. They give the opportunity to pre-synthesize coordination polymers with regulated sizes, shapes and they influence also crystal growth. (**Figures 7-8**) For example, Zhang's group used as surfactant the poly-ethylene glycol (PEG), which is an inexpensive, worldwide commercially available, and environmentally friendly surfactant. In the presence of the surfactant, they were able to isolate eight metal-organic frameworks, but in its absence or by its replacement with an organic solvent such as ethylene glycol or methanol or *N,N*-dimethylformamide, no crystals were precipitated. This surfactant was chosen based on its melting point, charge and its ability to coordinate metals.[26]
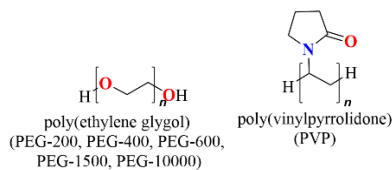
Figure 7. Organic polymers for the template synthesis of MOFs.
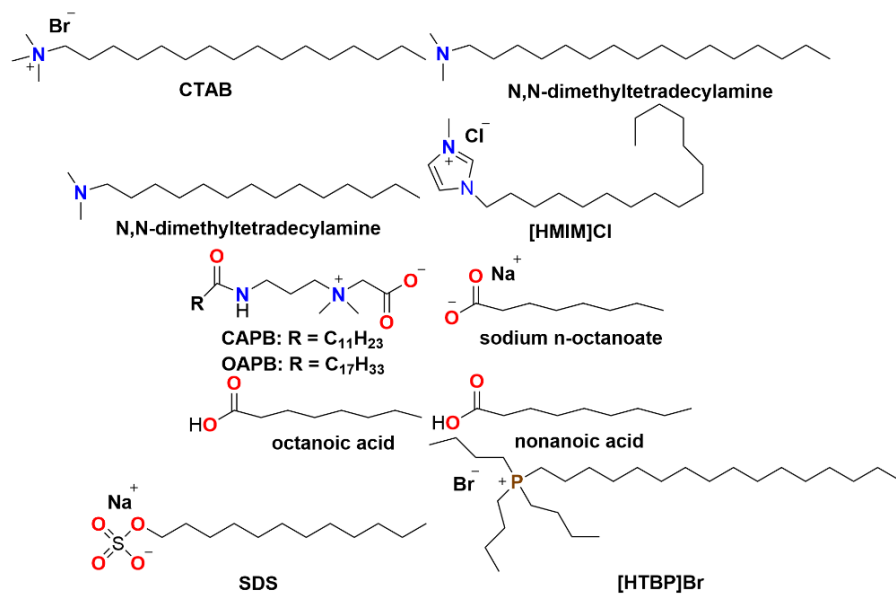
Figure 8. Surfactants for the template synthesis of MOFs.

5. Mixed-Ligand Approach for the Synthesis of New MOFs

In the last decade, the mixed-ligand approach for the development of MOFs has attracted considerable attention from the scientific community, for the development of new MOFs with enhanced properties. Representative examples of this synthetic approach will be described below. In a separate sub-chapter, it will be described a family of small rigid ligands (pyridyl-oximes and pyridyl alcohols) from the field of single-molecule magnets (SMMs), which were used as co-ligands for the formation of novel metal-organic frameworks in this research thesis.

a) Synthesis of novel Mixed-Ligand MOFs

Multivariant MOFs (MV-MOFs) are classified as a category of compounds in which multiple organic groups or metal cations (variate units) are used for the isolation of frameworks with the same topology; they lead to heterogeneity and affect the properties (eg, porosity) of the product. This synthetic approach is also known as the multicomponent isoreticular approach and it was introduced by Yaghi and co-workers. The ratio of the variate units and the synthetic conditions used can vary based on the targeted properties of the reaction product. O. Yaghi introduced the multi-variant/multivariate MOFs (MV-MOFs), and one of the first compounds that he studied was the MVs of MOF-5. MOF-5 is synthesized by the use of terephthalic acid; in order to synthesize its MVs analogues, they used derivatives of terephthalic acid, to favor the isolation of products with the same topology by adding functional groups on 1 and 4 positions (**Figure 9**). The compounds were characterized through powder X-ray diffraction, NMR spectroscopy, sorption studies and a few of them through single crystal X-ray diffraction. They found out that the MV MOF with free alkene groups in the pores, had the maximum uptake 84% of hydrogen, but the one with extra aromatic rings has 400% better selectivity for CO_2 compared to MOF-5.[27] Later on, other scientists worked with mixed ligand systems, such as different sizes of multi-pyridine ligands, combinations of pyridines and carboxylates, etc. The combination of different ligands has led to MOFs with unique topologies and also compounds with interesting properties. As each organic compound has a specific property, the combination of different kinds could lead to inorganic compounds, which will combine these features leading to a new class of hybrid materials.[28]
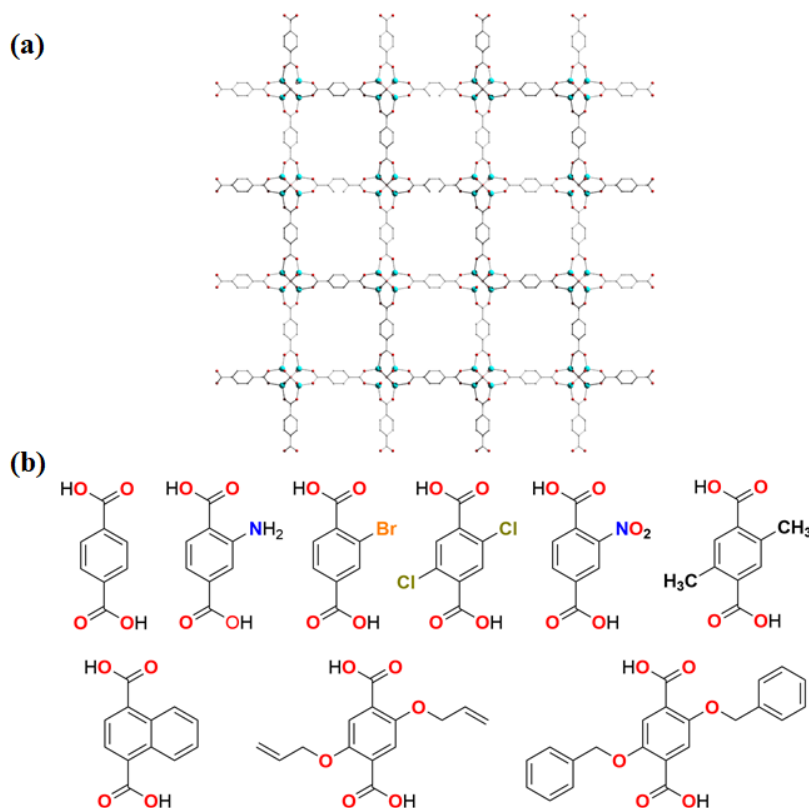
Figure 9. The ligands, which were used for the formation of the MVs of MOF-5.[27]

Carboxylates, pyridine-based linkers, and azolates were the first class of linkers, which were studied for the formation of MOFs. Until now, they are extensively used, as they form stable compounds. Moreover, in order to increase the ligation capability of the ligands and also introduce other properties to the product, different scientific groups have employed a variety of other linkers, including phosphonates, sulfydryls, alcohols, catechols, Schiff-base ligands, and others.[29] For example, the group of K. Biradha developed an elongated Schiff based pyridine linker and by combining it with di-topic carboxylates (4,4'-oxybisbenzoic acid (OBA) and benzene-1,3-diacrylic acid (BDA)), they

developed a class of novel MOFs based on Co^{II} and Cd^{II} metal cations for the deployment of proton conductors, sensing of water vapors, and dye sorption.[30] Also, A. Kumar and his team have published a Zn^{II} based mixed ligand MOF, by the use of a di-carboxylate (4,4'-(1,3-phenylenebis(methyleneoxu))dibenzoic acid; pbd) and a common di-topic N-donor linker (4,4'-bipyridine; 4,4'-bpy) for the development of fluorescent sensors for the selective detection and encapsulation of picric acid.[31] A schematic representation of the organic linkers discussed above is shown in **Figure 11**.
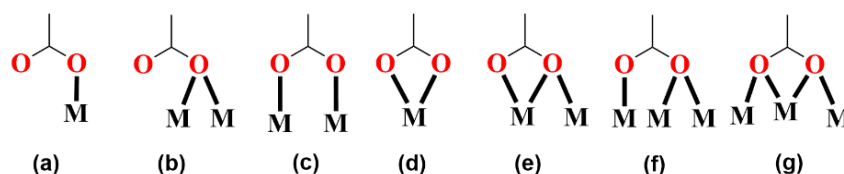
Figure 10. The literature reported coordination modes of the carboxylate group (a) η^1, (b) η^2:μ_2, (c) η^1:η^1:μ_2, (d) η^1:η^1, (e) η^1:η^2:μ_2, (f) η^1:η^2:μ_2, (g) η^2:η^2:μ_3.[32]
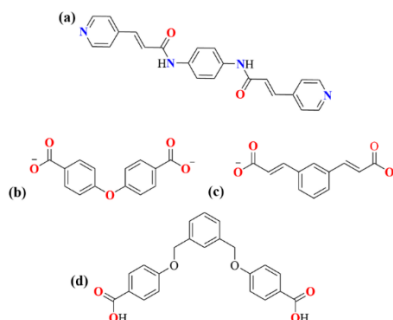
Figure 11. (a) bis-pyridyl-tris-amide ligand; (b) the deprotonated form of 4,4'-oxybisbenzoic acid (OBA); (c) the deprotonated form of benzene-1,3-diacrylic acid (BDA); (d) 4,4'-(1,3-phenylenebis(methyleneoxy))dibenzoic acid (pbd).

Azolates have provided access to a family of stable MOFs (ZIFs) and they have been extensively studied for a plethora of applications; hence, many

scientists have used a variety of combinations[33] in order to develop new frameworks for sensing applications. For example, Qu's group reported the synthesis and characterization of two copper-based MOFs, namely $[Cu_5(Hbtc)_4(trz)_2(H_2O)_4](H_2O)_2$ and $[Cu_2(btc)(trz)](H_2O)_3$) by the use of 1,2,4-triazole and 1,3,5-benzenetricarboxylic acid. The anti-esophageal cancer activity of the MOFs was assessed and proved that Cu(II) cation plays a crucial role in the anticancer activity of human esophageal cancer cells EC109, EC8712, and KYSE150.[34]

Other mixtures of azolate-based ligands have also been used for the development of a new class of MV-MOFs. For example, Cui's group combined the 1,4-bis(imidazole-1-1-ylmethyl)benzene (L_1) or the 4,4'-bis(imidazolyl)diphenyl ether in presence of captobenzoic acid (L_2) for the formation of two Co-MOFs ((a) $[Co(L_1)(bimb)·H_2O·OH]_n$ and (b) $[Co(L_2)(bidpe)]_n$) and their further study for the photocatalytic dye degradation of the methylene blue (MB). The band gap (E^g) is 2.69 eV and 2.60 evV respectively and the equipotential point (pH_{pzc}) is 4.47 and 4.40.[35] Another example by the design of multi-podal linker and its combination with di-topic carboxylates is from E. V. Alexandrov's group, where they developed a tripodal N,O-donor tris-[4-(2'methylimidazol-yl)phenyl)phosphine oxide linker and they combined it with naphthalene-2,6-dicarboxylic acid or 4,4'-stibenedicarboxylic acid for the formation of two novel Cd(II) MOFs {[$Cd_3(2,6-ndc)_3(tmpo)_2$]·$8H_2O·4DMF$; [$Cd_2(bpedc)(tmpo)_2$]·$2NO_3·4H_2O·2DMF$, where 2,6-H_2ndc = naphthalene-2,6-dicarboxylic acid, H_2bpedc = 4,4'-stibenedicarboxylic acid, tmpo = tris[4-(2'-methylimidazol-yl)phenyl]phosphine oxide}, and their further photoluminescence studies.[36]

Recently, Papaefstathiou's group targeted for the first time the synthesis of MOFs which act as single-molecule magnets (SMMs), by the use of a small

rigid ligand in the presence of poly-carboxylates. In particular, they introduced di-2-pyridyl ketone in the field of MOFs by the simultaneous use of a binary mixture of benzene-1,3,5-triphosphonic acid, trimesic acid, 5-hydroxy-isophthalic acid or pyromellitic acid for the formation of novel Cu(II) mixed-ligand MOFs. In the first case, a Cu_4-based MOF ($\{[Cu_4\{(py)_2C(OH)O\}_2(btec)_{1.5}(H_2O)_3]\cdot 4H_2O\}_n$) was isolated; dc magnetic susceptibility studies revealed that the exchange interactions between the metal centers are antiferromagnetic. The other ligand combinations provided access to ferromagnetic Cu_2 dimers with the formula $\{[Cu_2\{(py)_2C(OH)O\}(btc)(H_2O)]_n$; $[Cu_2\{(py)_2C(OH)-O\}(bdc)_{1.5}(H_2O)]_n$; $[Cu_2\{(py)_2C(OH)O\}(5\text{-HO-}bdc)_{1.5}(H_2O)]_n \}$.[37]

b) Small rigid ligands from the field of Single-Molecule Magnets

b1) Pyridyl-oximes

Coordination chemistry has been the most powerful tool for the construction of molecular magnetic systems. Single-Molecule Magnets (SMMs) are discrete molecules that function as nanoscale magnetic particles below a blocking temperature. They derive their properties from the combination of a large ground-state spin (*S*) and a magnetoanisotropy of the Ising-type (negative zero-field splitting parameter, D). Also, they display quantum tunneling of magnetization (QTM) and quantum phase interference, properties of the microscale. The term was first employed in 1996, but the first reported single-molecule magnet was in 1991, a Mn_{12} metal cluster $[Mn_{12}O_{12}(OAc)_{16}(H_2O)_4]$ (**Figure 12**). Molecular-based magnets can find applications in information storage devices, MRI agents, magnetic refrigeration, among others. 1D

coordination polymers of paramagnetic metal ions can display single-chain magnetism (SCM) behavior, i.e. they can exhibit slow relaxation of magnetization stemming from strong intrachain exchange interactions between high spin structural building units along the chain [38] SCMs are excellent candidates for applications in high-density information storage, molecular spintronics, and quantum computation, etc.[39] One dimensional polymers are also studied as molecular ferromagnets, synthetic metallic conductors, non-linear optical or ferroelectric materials.[40]
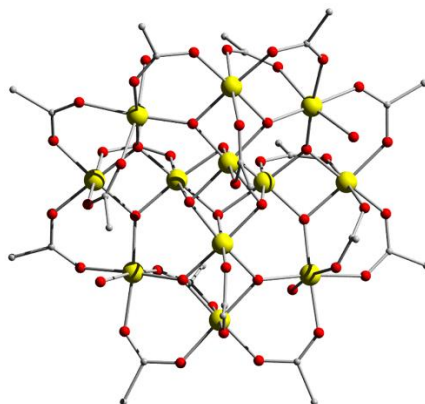
Figure 12. Representation of the Mn_{12} metal cluster $[Mn_{12}O_{12}(OAc)_{16}(H_2O)_4]$. Color: Mn, yellow; O, red; C, grey.

One family of ligands that has attracted considerable interest in the field of SMMs is the 2- pyridyl-oximes. S. Perlepes and G. Christou introduced them in the field of Single-Molecule Magnets and they demonstrated that these types of compounds are promising candidates for the formation of metal complexes and coordination polymers, which display interesting magnetic behavior. (**Figure 13**)

R = H; paoH
R = Me; mpkoH
R = Ph; ppkoH
R = 2-pyridyl; (py)pkoH
R = CN; pckoH
R = NH$_2$; pyaoxH$_2$
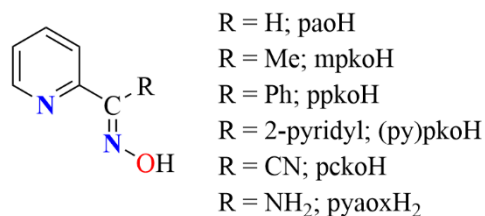
Figure 13. General representation of the 2-pyridyl oximes.

2-pyridyl oximes often combine more than one functional groups, which can link more than two or three metal cations (**Figures 14-15**) at the same time leading to the formation of small or high nuclearity metal complexes (**Figure 16**). A close inspection of the Cambridge Structural Database (CSD) reveals that the vast majority of compounds reported with these ligands are discrete metal clusters. [41] An example of high nuclearity metal complexes, which present magnetic properties are the Ni$_{12}$ and Ni$_{16}$ by the use of pyaoxH$_2$. [Ni$_{12}$(pyaox)$_6$(pyaoxH)$_6$(MeOH)$_2$Cl$_2$]Cl$_4$·5MeOH and [Ni$_{16}$(pyaox)$_8$(pyaoxH)$_8$(MeOH)$_4$](SO$_4$)$_4$·10H$_2$O·26MeOH are recent examples of Ni(II) and pyridine-2-amidoxime displaying high nuclearities and present ferromagnetic exchange between the Ni(II) ions resulting in a spin ground state $S = 6$ and $S = 8$ respectively. (**Figure 16**) Also, it was the first time, where it was observed the fourth type (d) ligand's coordination mode (**Figure 14**).[47]
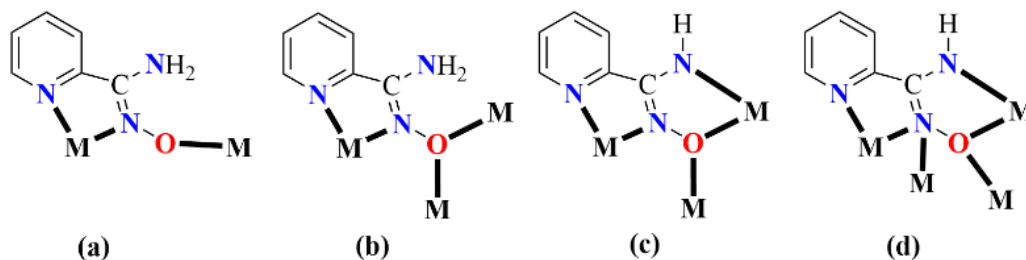
Figure 14. The literature reported coordination modes of pyaoxH$_2$. (a) η^1:η^1:η^1:μ, (b) η^1:η^1:η^2:μ_3, (c) η^1: η^1: η^1: η^2:μ_3, (d) η^1: η^2: η^1: η^2:μ_4.[42]
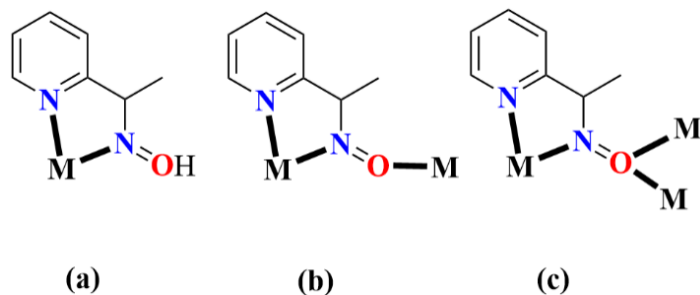
Figure 15. The literature reported coordination modes of Hmpko. (a) η^1:η^1, (b) η^1:η^1:η^1:μ_2 **[43]**, and (c) η^1: η^1: η^2:μ_3.[44]
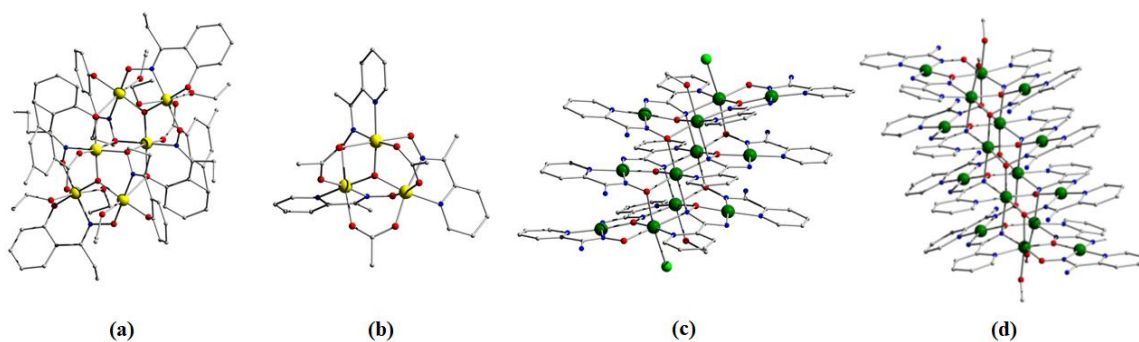
Figure 16. (a) $[Mn^{III}_6O_2(Et\text{-}sao)_6(O_2CPh(Me)_2)_2(EtOH)_6]$[45], (b) $[Mn^{III}_3O(O_2CR)_6(py)_3](ClO_4)$ (R = Me, Et, Ph)[46], (c) $[Ni_{12}(pyaox)_6(Hpyaox)_6(MeOH)_2Cl_2]Cl_4\cdot 5MeOH$ & (d) $[Ni_{16}(pyaox)_8(Hpyaox)_8(MeOH)_4](SO_4)_4\cdot 10H_2O\cdot 26MeOH$ [47].

b2) Pyridyl-alcohols

2-hydroxymethylpyridine (Hhmp) has provided access to approximately five hundred compounds, the majority of which are discrete metal complexes. Hhmp has also been extensively used in the field of Single-Molecule Magnets (SMMs) providing complexes with small or high nuclearities, (**Figure 18**) which have

presented interesting magnetic properties.[48] For instance, [Mn$_4$(hmp)$_4$(OH)$_2$Mn(dcn)$_6$]·2MeCN·2THF is a coordination polymer, where its asymmetric unit is linked through dicyanamide molecules and the metal core is formed and stabilized via the hydroxymethylpyridine. The tetranuclear metal cluster adopts a rhombic core. The oxidation state of the manganese cations Mn(1), Mn(2), and Mn(3) can be assigned as divalent, trivalent and divalent respectively. The compound is a 3D ferrimagnet (T_c = 4.1 K) and consists of SMM Mn4 building units (S =9) and paramagnetic bridges Mn^{II} (S =5/2). Among the reported compounds, there are many complexes, which have terminal acetate or benzoates linkers and analogues of them.[49]

Until now, there are two examples in the literature for the simultaneous use of 2-pyridinemethanol with di-topic linkers, leading to one-dimensional polymers. The first example was by S. Onaha, where they used a fluorinated-terephthalate linker for the formation of the polymer chain and the formula of the one-dimensional polymer was Mn(C$_5$NH$_4$-2-CH$_2$OH)$_2$(C$_6$F$_5$CO$_2$)$_2$. The second example was reported by S. Gao being a two-dimensional complex with the formula Cu$_4$(pmo)$_4$(C$_4$H$_4$O$_4$)$_2$·H$_2$O; it has been synthesized by the employment of succinate in the reaction system. This compound was magnetically studied and it was found that there are ferromagnetic couples between the copper(II) cations.[50] The crystallographically established coordination modes of Hhmp are presented in **Figure 17**.
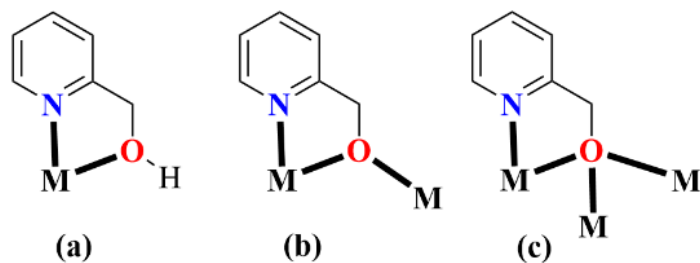
Figure 17. The literature reported coordination modes of Hhmp in its neutral or anionic form (hmp-). (a) $\eta^1:\eta^1$ [51], (b) $\eta^1:\eta^2:\mu_2$ [52], (c) $\eta^1:\eta^3:\mu_3$ [53].
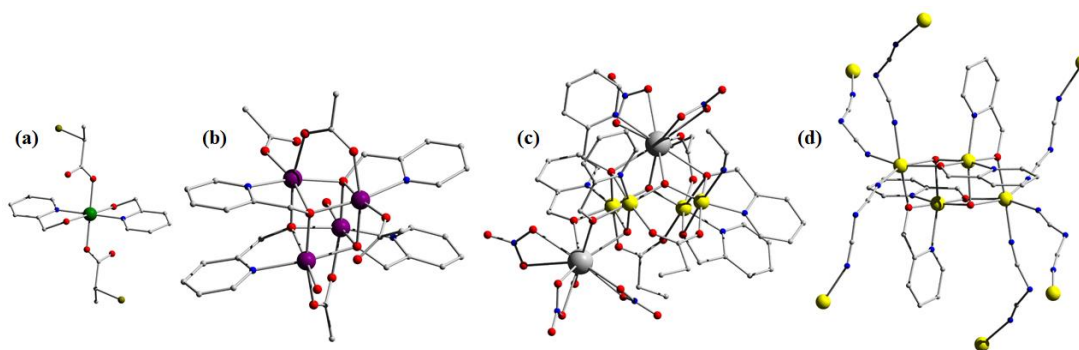
Figure 18. Coordination compounds by the use of Hhmp. (a) $[Cu(CH_3CHBrCO_2)_2(2\text{-}pyme)_2]$ [54]; (b) $[Co^{II}_4(hmp)_4(\mu\text{-}OAc)_2(\mu_2\text{-}OAc)_2(H_2O)_2]$ [55]; (c) $[Mn_4Ln_2O_2(OH)(hmp)_5(EtCO_2)_3(MeCN)(NO_3)_5(H_2O)]$ $(Ln^{III} = La, Nd)$ [56]; (d) $[Mn_4(hmp)_4(OH)_2Mn(dcn)_6]\cdot2MeCN\cdot2THF$ [57].

Recently, Tasiopoulos' group has employed amino-alcohols for the template synthesis of carboxylate MOFs by the use of trimesic acid (H₃btc) and Zn(II) for the formation of six MOFs with novel topologies. This family of compounds was called MOAAF (metal organic amino-alcohol framework) and the members of this family are the: a) (MOAAF-1) $(teoaH)_2[Zn(btc)_{1.33}]$ where teaoH = amino-alcohol triethanolamine, b) (MOAAF-2) $(NH_2Me_2)_2(hmpipH)[Zn_3(btc)_3]$ where hmpipH = 2-(hydroxymethyl)piperidine, c) (MOAAF-3)

(NH$_2$Me$_2$)(tbdmaH)$_2$[Zn$_3$(btc)$_3$] where tbdmaH= Ntert-butyl-dimethylamine, d) (MOAAF-4) (NH$_2$Me$_2$)(bhepH$_2$)[Zn$_3$(btc)$_3$] where bhepH$_2$ = 1,4-bis(2-hydroxyethyl)-piperazine, e) (MOAAF-5) (NH$_2$Me$_2$)[Zn$_4$(btc)$_3$(mdeoa)$_2$] where mdeoaH$_2$ = *N*-methyldiethanolamine, and f) (MOAAF-6) (NH$_2$Me$_2$)[Zn$_4$(btc)$_3$(hem)$_2$] where hemH = 4-(2-hydroxyethyl)morpholine.[58] Employing the single-crystal-to-single (SCSC) transformation of [Eu$_2$(ClP)$_2$(DMF)$_2$(H$_2$O)$_2$], UCY-8 MOF. They were able to replace the coordinated solvents (e.g. pyridine, 2-hydroxymethyl-phenol) with terminally ligated organic ligands, including Hhmp.[59] Aiming at the isolation of mixed-ligand MOFs by the simultaneous use of two different pyridine-alcohol based derivatives in presence of pyridine-3,5-dicarboxylic acid, they managed the synthesis and characterization of two two-dimensional MOFs ([Zn(PDC)(3Hhmp)]$_n$·nDMF·0.5nH$_2$O, [Co(PDC)(3Hhmp)$_2$]$_n$·0.25nDMF), one zero-dimensional binuclear complex ([Zn(PDC)(Hhmp)$_2$]$_2$·2DMF) and a one-dimensional polymer chain ([Cu(PDC)(3Hhmp)$_2$]$_n$·0.5nDMF·1.5nH$_2$O) by the simultaneous use of H$_2$pdc and 3-hydroxymethylpyridine (3hmpH) or 2-hydroxymethylpyridine (Hhmp). Through this study, it is revealed that a small change at the position of the co-ligand's hydroxyl group, influences and leads to the stabilization of molecules with completely different dimensionality as revealed in the case of Zn(II).

So far, almost one hundred nighty eight compounds have been submitted at the CCDC database by the use of 2,6-pyridinedimethanol (H$_2$pdm). Many scientific groups have reported small and high nuclearity metal complexes (**Figure 20**) by the simultaneous use of H$_2$pdm and carboxylates. The use of benzoate and H$_2$pdm with 3d metal cations led to the formation of [M^{II}(H$_2$pdm)$_2$][M^{II}(Ph(COO)$_4$] (where M^{II} = Co, Mn, Zn; Ph(COOH) = benzoate acid). All the compounds were studied as heterogeneous catalysts for the

conversion of epoxides to cyclic carbonates in a solvent-free environment.[60] Another rare example is the stabilization of two co-crystallized metal clusters, a trimer and tetramer, $\{[Cu_3(O_2CMe)_2(pdm)_2(MeOH)_2][Cu_4(O_2CMe)_2(Hpdm)_4]\}$ $(ClO_4)_2 \cdot 4MeOH$, which is the outcome of the reaction between the $[Cu_2(O_2CMe)_4(H_2O)_2]$ with pdmH$_2$ in presence of LiClO$_4$ in MeOH. The two metal complexes are stabilized through a strong hydrogen bond (D$\cdots$A = 2.632 Å, D-H-A = 156.6°). The magnetic susceptibility at room-temperature is 1.67 cm^3 K mol^{-1}, which is lower than the expected value for seven uncoupled spins (2.625 cm^3 K mol^{-1} with g = 2.0). More literature reported compounds synthesized by the use of carboxylates and H$_2$pdm are summarized in **Table 1**.[70]
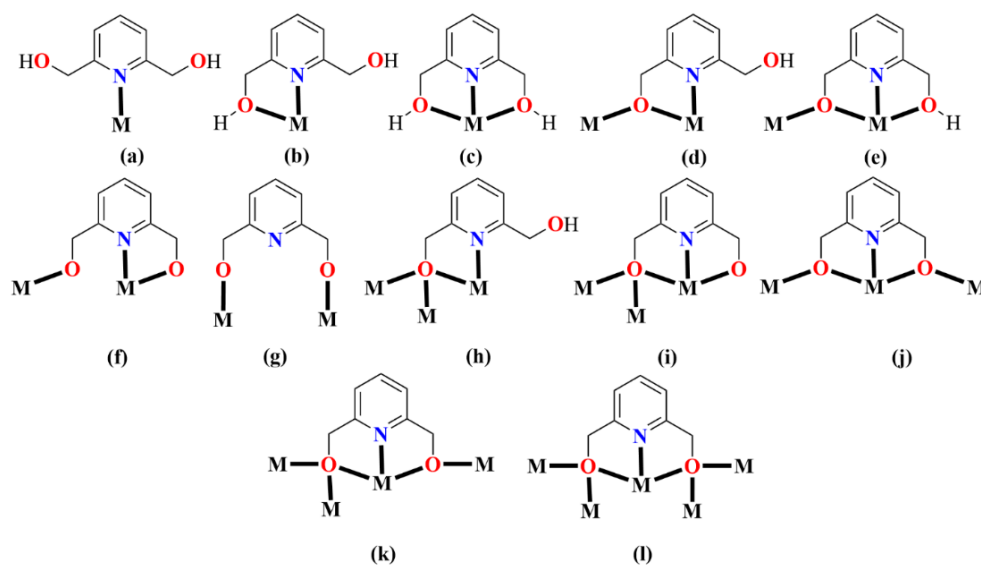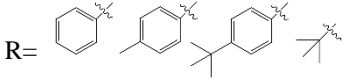
Figure 19. The literature reported coordination modes of H$_2$pdm. (a) η^1 [63], (b) η^1:η^1 [64], (c) η^1:η^1: η^1 [65], (d) η^2:η^1: μ [66], (e) η^2:η^1: η^1: μ, (f) η^1:η^1: η^1 [67], (g) η^1: η^1 [68], (h) η^3:η^1: μ_3 [69], (i) η^3:η^1: η^1:μ_3 [70], (j) η^2:η^1: η^2:μ_3 [71], (k) η^3:η^1: η^2:μ_4 [72], (l) η^3:η^1: η^3:μ_5 [73].

Table 1. Examples of metal complexes, which have been synthesized by the use of H_2pdm and carboxylates.

Metal Cation	Carboxylate	Compound	Ref.
Mn(II)	acetate	$[Mn_4(O_2CMe)_2(Hpdm)_6](ClO_4)_2$	61
Mn(II)	propanate	$[Mn_9(O_2CEt)_{12}(pdm)(Hpdm)_2(L)2]$	62
Zn(II)	R= Ph or Bu	$[Zn_6(OH)_2(O_2CR)_8(H_2pdm)]$	63
Zn(II)	acetate	$[Zn_4(Hpdm)_2] \cdot (OCMe)_4$	64
		$[Zn(H_2pdm)(OCMe)_2]$	
Ni(II)	acetate	$[Ni_4(Hpdm)_4(OCMe)_4]$	65
Ni(II)	R= (structures)	$[Ni_4(Hpdm)_4(OCR)_4]$	
Ni(II)	dnbz = 3,5-dinitrobenzoato	$[Ni(H_2pdm)_2](dnbz)_2$	66
Co(II)	dnbz = 3,5-dinitrobenzoato	$[Co(H_2pdm)_2](dnbz)_2$	67
Ni(II)	acetate	$[Ni(diethylenetriamine)(H_2pdm)_2]$ $(PF_6)(OOCMe)(H_2O)$ or $(ClO_4)_2$	68, 69
Cu(II)	acetate	$[Cu_4(O_2CMe)_2(Hpdm)_4][Cu_3(O_2CMe)_2(pdm)_2(MeOH)]$	70
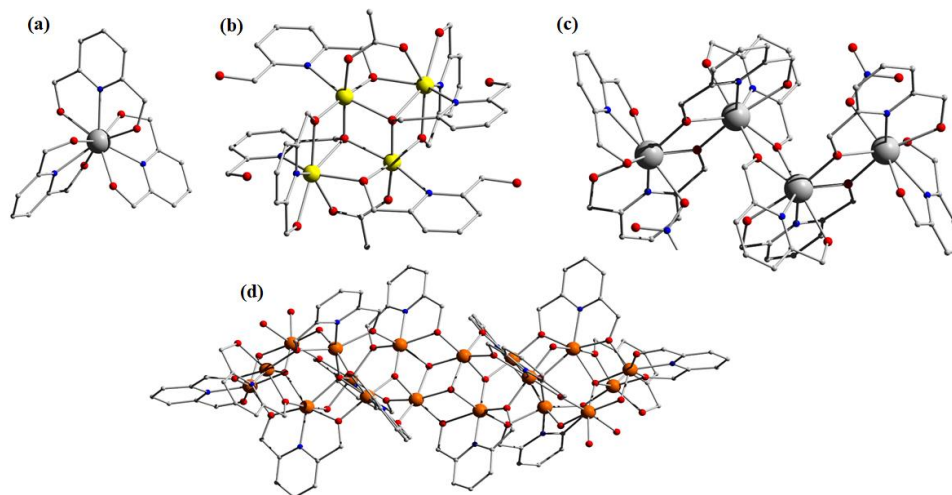
Figure 20. Schematic representation of the crystal structure of representative metal clusters by the use of H$_2$pdm. (a) [Er(H$_2$pydm)$_3$](NO$_3$)$_3$ [75]; (b) [Mn$_4$(O$_2$CMe)$_2$(Hpdm)$_6$][ClO$_4$]$_2$ [76]; (c) [Ln$^{III}_4$(NO$_3$)$_2$(pdmH)$_6$(pdmH$_2$)$_2$](NO$_3$)$_4$ (Ln^{III} = Eu^{III}, Gd^{III}, Tb^{III}, Dy^{III}, Ho^{III}, Er^{III}, Yb^{III}) [77]; (d) [Fe$_{18}$O$_6$(OH)$_8$(pdm)$_{10}$(pdmH)$_4$(H$_2$O)$_4$](ClO$_4$)$_{10}$ [78].

6. MOFs as sensors

Metal-Organic Frameworks are suitable to be used as sensors, as some of them exhibit either photoluminescence or magnetic properties with a few combining both. The encapsulation of guest molecules into their pores has the potential to affect the physical properties of the MOF, which is desirable for the development of sensors. Over the last decade, extensive research has taken place for the use of coordination polymers as photoluminescence sensors for different environmental pollutants. Through those studies, it is proven that the metal-organic frameworks can encapsulate and detect heavy metal cations, anions, personal care, and pharmaceutical products.[79]

An example of luminescent MOF for sensing is from Zahao's group, where they synthesized a tetranuclear Zn(II) MOF (denoted as NUS-1) by the use of 4,4'-(2,2-diphenylethene-1-1,diyl)benzoic acid. This compound was used for the encapsulation and further study as a fluorescent sensor for a variety of volatile organic molecules such as benzene, toluene, o-xylene, p-xylene, and mesitylene. Through fluorescence, they proved the encapsulation of the species into the pores of the MOF and as the guest molecules enhance the fluorescence, they developed a turn-on fluorescent sensor for organic volatiles. Crystals of the MOF NUS-1 were soaked in various VOCs by following photoluminescence tests, and in the majority of the cases, the color difference was obvious with a naked eye upon illumination of the samples with ultra-violet light. The PL comparison of the samples was with a loaded NUS-1 with pristine ($\lambda_{fl} = 486$ nm), and they had highlighted that the sample loaded with benzene ($\lambda_{fl} = 504$ nm) gave the largest red shift (18nm) and in case of the mesitylene ($\lambda_{fl} = 458$ nm) the largest blue shift (28nm). They highlighted that these shifts possibly occur due to the conformation change of the dangling phenyl rings of the NSUI-1's linker upon exposure to analytes.

Another example of a fluorescent sensor is based on a Zn@MOF with a dinuclear sbu synthesized using terephthalic acid and a 2,5-di(4-piridyl)thiazolo[5,4-d]thiazole. This Zn@MOF presents photoluminescent properties due to its ligand and was used for the detection of mercury. The MOF itself has a major adsorption band at 240nm which gradually decreases with the addition of mercury and at the end of the addition, a new absorption peak appeared at 210nm. The thiazole ligand has functional groups, which are suitable for the coordinative encapsulation of mercury. Once the mercury was adsorbed, the MOF changes color and the rapid encapsulation (less than 3 min) is obvious with the naked eye. The removal capacity of Hg(II) was 1428 mg/g, which is the highest observed

until now. Also, the same MOF is suitable for the removal of Pb(II) with a capacity of 434 mg/g. They had also obtained competitive studies in presence of other metal cations ions (Cp, Cu, Cd) in oxidation state and the MOF was showing a preference to the mercury.[80]

Fluorescence is not always suitable for the detection of any kind of chemical compound, as not all of them are photoluminescence active. For this reason, other supplementary techniques like EDX, SEM, XPS, ICP, single-crystal-transformation, and magnetism have been used to bear witness to the selective encapsulation of the desired species.[81] Magnetism is also a powerful tool that can be used for the identification of the guest molecule and to identify the kind of interactions between the host and the guest molecule. Each compound has a magnetic fingerprint, being either paramagnetic or ferromagnetic. The encapsulation of a guest molecule alters the fingerprint; a representative such example was reported by Suzuki's group, where they developed a non-magnetic MOF, the UiO-66(Zr) which was loaded with the ferri-magnetic $MgFe_2O_4$ nanoparticles and they used it as a magnetic sensor for swing adsorption of CO_2. The release of CO_2 after adsorption was 100% under 42 mT magnetic field.[82]

Through the above-mentioned approach by Suzuki for the development of magnetic MOFs as sensors, the material is losing part of its porosity, even if it is effective. To retain the porosity of the materials and at the same time to present magnetic properties, another approach has been proposed where it is based on the pre-design synthesis of them. To this end, two different synthetic approaches have been proposed: 1) a metal complex which presents magnetic behavior will react with pillars for the formation of the framework, and 2) the mixed-ligand approach, in which small rigid ligands are able to coordinate and stabilize many metal cations will be mixed with linkers suitable to form the network acting as pillars.[83]

7. Aim of the Research Project

Pyridyl-oximes and pyridyl-alcohols have been extensively studied in the field of metal complexes as SMMs, stabilizing homo- and hetero-metallic metal complexes with small or high nuclearities[84] (**Figure 21**). Taking into account this knowledge, and aiming at the expansion of the family of MOFs that possess interesting magnetic properties, we decided to introduce this family of ligands into the field of MOFs and explore their potential to lead to new such species. To this end, 2-pyridyl oximes and alcohols were combined with carboxylate linkers (**Figure 22**) that have been extensively used in the field of MOFs, and favour the formation of novel mixed-ligand / multi-variant MOFs with novel structural features and properties.
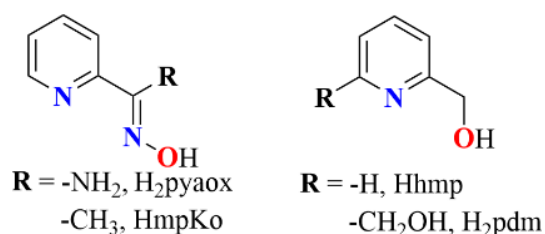
Figure 21. Representation of the oximes (left) and pyridine-alcohols (right).
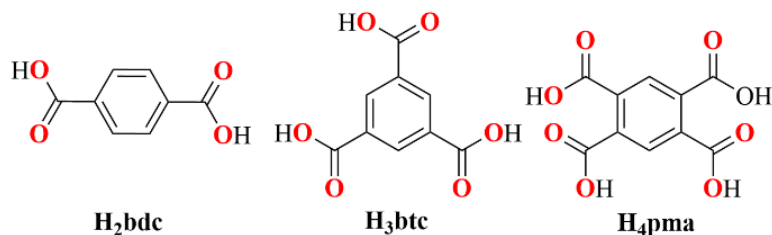
Figure 22. Representation of the carboxylates, which were used for the formation of MOFs. (left) benzene-1,4-dicarboxylic acid or terephthalic acid

(H$_2$bdc); (middle) benzene-1,3,5-tricarboxylic acid or trimesic acid (H$_3$btc) , (right) 1,2,4,5-benzenetetracarboxylic acid or pyromellitic acid (H$_4$pma).

From the synthetic point of view for the development of a secondary building unit, there are two different synthetic approaches: a) the pre-design of the inorganic secondary building unit as a metal complex and its further reaction with a polytopic linker for the formation of the network and b) the straight-forward reaction of the organic ligands with the metal salts. For this project, both synthetic approaches were thoroughly investigated with the first one been proven the most fruitful.
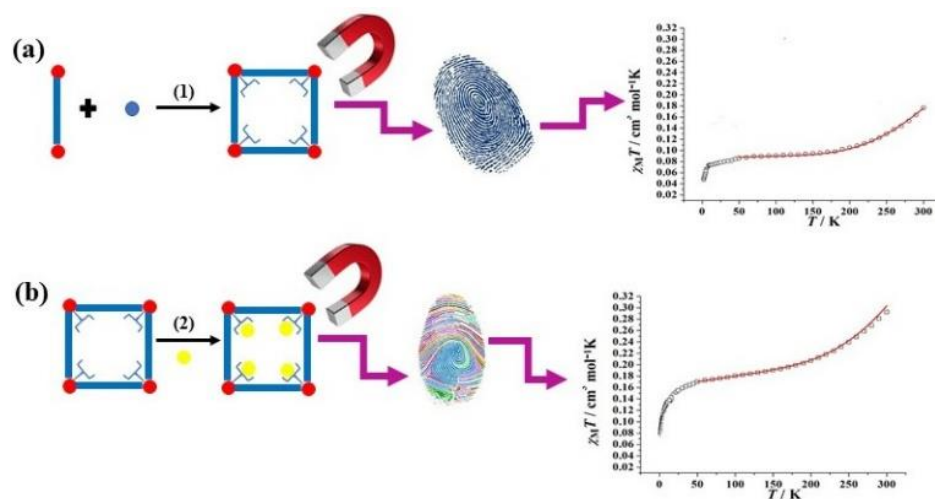
Figure 23. Representation of experimental strategy for magnetic sensing. (a) the formation of the MOF and its magnetic studies and (b) the encapsulation of compound/chemical species and the magnetic studies of the MOF with the encapsulated compound.

For the determination of the crystal structures of the MOFs and the characterization of their physical properties, a variety of techniques was used,

including single-crystal X-ray crystallography, powder X-ray crystallography, infrared spectroscopy, thermogravimetric analysis, and magnetism. Single-crystal X-ray crystallography was used for the determination of the crystal structures of the synthesized compounds. Powder X-ray crystallography was used for the comparison of the powder-diffraction spectra of the bulk compounds with the known crystal structure, and also for the assessment of the stability of the MOF after exposure to different chemical environments. Infrared spectroscopy and thermogravimetric analysis were used for the characterization of the synthesized compounds. Magnetism studies were carried out for the compounds that bear more than one metal ion in their SBU.. The capacity of the stable MOFs to encapsulate environmentally hazardous species will be investigated through liquid state UV-spectrometry, infrared spectroscopy, powder X-ray diffraction, and thermogravimetric analysis. Magnetism studies have also been performed to investigate the impact of the presence of the guest molecule on the magnetic properties of the pristine MOF.

References

1. a) Hoornweg, D.; Bhada-Tata, P.; Kennedy, C. *Nature* **2013**, 502, 615-617. b) Ukaogo, P. O. ; Ewuziw, U. ; Onwuka, C. V.; "Environmental pollution: causes, effects, and the remedies", *Microorganisms for Sustainable Environmnet and Health, Elsevier* **2020**, 419-429.

2. Environment policy: general principles and basic framework https://www.europarl.europa.eu/factsheets/en/sheet/71/environment-policy-general-principles-and-basic-framework .

3. a) Rangnekar, N.; Mittal, N.; Elyassi, B.; Caro, J.; Tsapatsis, M. *Chem. Soc. Rev.* **2015** 44 7128-7154. b) Blay, V.; Bobadilla, L. F.; Cabrera Garcia, A.

"Zeolites and Metal-Organic Frameworks" *Amsterdam University Press* **2018** p. 13-24, 209-234, 307-342.

4. a) Batten, S. R.; Champness, N. R.; Chen, X.-M.; Garcia-Martinez, J.; Kitagawa, S.; Öhrström, L.; O' Keefee, M.; Suh, M. P.; Reedjik, J. *Pure Appl. Chem.* **2013** 85, 1715-1724. b) Hoskins, F. B.; Robson, R. *J. Am. Chem. Soc.* **1989** 111, 15, 5962-5964. c) Abrahams, F. B.; Hoskins, B. F.; Robson, R. *J. Am. Chem. Soc.* **1991** 113, 9, 360-3607. d) Batten, R. S.; Hoskins, F. B.; Robson, R. *J. Am. Chem. Soc.* **1995** 117, 19, 5385-5386. e) Hoskins, F. B.; Robson, R.; Slizys, A. D. *J. Am. Chem. Soc.* **1997** 119, 12, 2952-2953. f) Kitagawa, S.; Kitaura, R.; Noro, Sh.-inchiro *Angew. Chem. Int. Ed.* **2004** 43, 2334-2375. g) Chui, Y. S.; Lo, M.-F. S.; Charmant, P. H. J.; Orpen, A. G.; Williams, D. I. *Science* **1999** 283, 5405, 1148-1150.

5. Noro, Sh.; Kitaura, R.; Kondo, M.; Kitagawa, S.; Ishii, T.; Matsuzaka, H.; Yamashita, M. *J. Am. Chem. Soc.* **2002** 124, 11, 2568-2583.

6. Li, H.; Eddaoudi, M.; O'Keeffe, M.; Yaghi, O. M. *Nature* **1999** 402, 276-279.

7. Hennigar, T. L.; MacQuarrie, D. C.; Losier, P.; Rogers, R. D.; Zaworotko, M. *Angew. Chem. Int. Ed.* **1997** 36, 9, 972-973.

8. Noro, S.; Kitaura, R.; Kondo, M.; Kitagawa, S.; Ishii, T.; Matsuzaka, H.; Yamashita, M. *J. Am. Chem. Soc.* **2002,** 124, 11, 2568-2583.

9. Shekhah, O.; Swaidan, R.; Belmabkhout, Y.; Plessis, M. du; Jacobs, T.; Barbour, L. J.; Pinnau, I.; Eddaoudi, M. *Chem. Commun.* **2014** 50, 2089-2092.

10. a) Alhamani, M.; Doan, H.; Cheng, C. -H. *Materials MDPI* **2014**, 7, 3198-3250. b) Murdock, C. R.; Hughes, B. C.; Lu, Z.; Jekins, D. M. *Coordination Chemistry Reviews* **2014** 258-259, 119-136. c) Magott, M.; Gawel, B.; Sarewicz, M.; Reczyński, M.; Ogorzaly, K.; Makowski, W.; Pinkowicz, D. *Chem. Sci.* **2021** 12, 9176-9188.

11. Zarekarizi, F.; Joharian, M.; Morsali, A. *J. Mater. Chem. A* **2018** 6, 19288-19329.

12. Gan, L.; Chidambaram, A.; Fonquernie, P. G.; Light, M. E.; Choquesillo-Lazarte, D.; Huang, H.; Solano, E.; Fraile, J.; Viňas, C.; Teixidor, F.; Navarro, J. A. R.; Stylianou, K. C.; Planas, J. G. *J.A.C.S.* **2020** 142(18), 8299-8311.

13. Lin, Y.; Wang, H.; Luo, D.; Lin, F.; Li, J. *New J. Chem.* **2020** 44, 11933-11936.

14. Gogoi, C.; Biswas, S. *Crystal Growth & Design* **2021** 21(5), 2680-2689.

15. Wang, T.; Chang, M.; Yan, T.; Ying, Y.; Yang, Q.; Liu, D. *Ind. Eng. Chem. Res.* **2021** 60, 5976-5983.

16. Xie, J.; Cheng, D.; Li, P.; Xu, Z.; Zhu, X.; Zhang, Y.; Li, H.; Liu, X.; Liu, M.; Yao, S. *ACS Applied Nano Materials* **2021** 4(5), 4853-4862.

17. Chen, S.; Xu, X.; Gao, H.; Wang, J.; Li, A.; Zhang, X. *J. Phys. Chem. C* **2021** 125, 17, 9200-9209.

18. Yoshimaru, S.; Sadakiyo, M.; Maeda, N.; Yamauchi, M.; Kato, K.; Pirilllo, J.; Hijikata, Y. *ACS Appl. Mater. Interfaces* **2021** 13, 17, 19992-20001.

19. a) Rowsell, J. L. C.; Yaghi, O. M. *Mircoporous and Mesoporous Materials* **2004** 73, 3-14. b) Rubio-Martinez, M.; Avci-Camur, C.; Thornton, A. W.; Imaz, I.; Maspoch, D.; Hill, M. R. *Chem. Soc. Rev.* **2017** 46, 3453-3480.

20. a) McKinstry, C.; Cathcart, R. J.; Cussen, E. J.; Fletcher, A. J.; Patwardhan, S. V.; Sefcik, J. *Chemical Engineering Journal* **2016** 285, 718-725. b) Zhang, B.; Luo, Y.; Kanyuck, K.; Saenz, N.; Reed, K.; Zavalij, P.; Mowery, J.; Bauchan, G. *RSC Adv.* **2018** 8, 33059-33064.; c) Rubio-Martinez, M.; Avci-Camur, C.; Thornton, A. W.; Imaz, I.; Maspoch, D.; Hill, M. R. *Chem. Soc. Rev.* **2017** 46, 3453-3480.

21. a) Abedin Jhan, N.; Hwa Jhung, S. *Coord. Chem. Rev.* **2015** 285, 11-23. b) Rubio-Martinez, M.; Avci-Camur, C.; Thornton, A. W.; Imaz, I.; Maspoch, D.; Hill, M. R. *Chem. Soc. Rev.* **2017** 46, 3453-3480.

22. a) Al-Jutubi, H.; Gascon, J.; Sudhölter, E. J. R.; Rassaei, L. *ChemElectroChem* **2015** 2 (4), 462-474. b) Rubio-Martinez, M.; Avci-Camur, C.; Thornton, A. W.; Imaz, I.; Maspoch, D.; Hill, M. R. *Chem. Soc. Rev.* **2017** 46, 3453-3480. c) Ghoorchian, A.; Afkhami, A.; Madrakian, T.; Ahmadi, M. *Metal-Organic Frameworks for Biomedical Applications*, *Woodhead Publishing*, **2020**,177-195.

23. a) Chen, D.; Zhao, J.; Zhang, P.; Dai, S. *Polyhedron* **2019** 162, 59-64. b) James, S. L.; Adams, C. J.; Bolm, C.; Braga, D.; Collier, P.; Friščić, T.; Grepioni, F.; Harris, K. D. M.; Hyett, G.; Jones, W.; Krebs, A.; Mack, J.; Maini, L.; Guy Orpen, A.; Parkin, I. P.; Sharouse, W. C. ; Steed, J. W.; Waddell, D. C. *Chem. Soc. Rev.* **2012** 41, 413-447.

24. a) Garibay, S. J.; Wang, Z.; Tanable, K. K.; Cohen, S. M. *Inorg. Chem.* **2009** 48, 7341-7349. b) Wang, Z.; Cohen, S. M. *Chem. Soc. Rev.* **2009** 38, 1315-1329.

25. a) Tanaka, D.; Kitagawa, S. *Chem. Mater.* **2008** 20, 922–931. b) Majano, G.; Martin, O. ; Hammes, M. ; Smeets, S. ; Baerlocher, C. ; Pérez-Ramírez, J. *Adv. Funct. Mater.* **2014** 24, 3855–3865. c) Qin, T.; Gong, J.; Ma, J.; Wang, X.; Wang, Y.; Xu, Y.; Shen, X.; Zhu, D. *Chem. Commun.* **2014** 50, 15886–15889. d) Ding, R.; Huang, C.; Lu, J.; Wang, J.; Song, C.; Wu, J.; Hou, H.; Fan, Y. *Inorg. Chem.* **2015** 54, 1405–1413. e) Santra, A.; Bharadwaj, P.K. *Cryst. Growth Des.* **2014** 14, 1476–1485. f) Huang, X.-C.; Zhang, J.-P.; Lin, Y.-Y.; Chen, X.-M. *Chem. Commun.* **2005** ,2232– 2234. g) Shi, Q.; Xu, W.-J.; Huang, R.-K.; Zhang, W.-X.; Li, Y.; Wang, P.; Shi, F.-N.; Li, L.; Li, J.;

Dong, J. *J. Am. Chem. Soc.* **2016** 138, 16232–16235. h) Javanmardi, H.; Abbasi, A.; Bagheri, H. *Analytica Chimica Acta* **2021** 1125, 231-246.

26. a) Gao, J.; Ye, K.; He, M.; Xiong, W.-W.; Cao, W.; Lee, Z. Y.; Wang, Y.; Wu, T.; Huo, F.; Liu, X.; Zhang, Q. *J. Solid State Chem.* **2013** 206, 27–31. b) Zhao, J.; Wang, Y.; Dong, W.; Wu, Y.; Li, D.; Liu, B.; Zhang, Q. *Chem. Commun.* **2015** 51, 9479–9482. c) Wu, Y.-P.; Zhou, W.; Zhao, J.; Dong, W.-W.; Lan, Y.-Q.; Li, D.-S.; Sun, C.; Bu, X. *Angew. Chem. Int. Ed.* **2017** 56, 13001–13005. d) Qiu, L.-G.; Xu, T.; Li, Z.-Q.; Wang, W.; Wu, Y.; Jiang, X.; Tian, X.-Y.; Zhang, L.-D. *Angew. Chem. Int. Ed.* **2008** 47, 9487–9491.

27. a) Dutta A.; Pan, Y.; Liw, J. -Q.; Kumar, A. *Coordination Chemistry Review*s **2021** 445, 214074. b) Deng, H.; Doonan, C. J.; Furukawa, H.; Ferreira, R. B.; Towne, J.; Knobler, C. B.; Wang, B.; Yagi, O. M. *Science* **2010** 327, 846-850. c) Furukawa, H.; Cordova, K. E.; O'Keefee, M.; Yaghi O. M. *Science* **2013** 341, 123044-1 – 1230444-12. d) Ji, Z.; Li, T.; Yaghi, O. M. *Science* **2020** 369, 674-680. e) Hetal, A.; Yamani, Z. H.; Cordoova, K. E.; Yaghi, O. M. *National Science Review* **2017** 4,3, 296-298.

28. a) Kleist, W.; Jutz, F.; Maciejewski, M.; Baiker, A. *Eur. J. Inorg. Chem.* **2009** 24, 3552-3561. b) Burrows, A. D. *CrystEngComm.* **2011** 13, 3623-3642.

29. a) Freund, R.; Canossa, S.; Cohen, S. M.; Yan, W.; Deng, H.; Guillerm, V.; Eddaoudi, M.; Madden, D. G.; Fairen-Jimenez, D.; Lyu, H.; Macreadie, L. K.; Ji, Z.; Zhang, Y.; Wang, B.; Haase, F.; Wöll, C.; Zaremba, O.; Andreo, J.; Wuttke, S.; Diercks, C. S. *Angew. Chem. Int. Ed.* **2021** DOI: *HTTPS://DOI.ORG/10.1002/ANIE.202101644*; b) Fan, L.; Liu, X.; Zhang, L.; Kong, X.; Xiao, Z.; Fan, W.; Wang, R.; Sun, D. *Journal of Molecular Structure* **2019** 1197, 87-95. c) Khullara, S.; Thakurb, S.; Mandalb, S. K. *Inorg. Chim. Acta* **2020** 502, 119281.

30. Konavarapu, S. K.; Goswami, A.; Ganesh Kumar, A.; Banerjeeb, S.; Biradha, K. *Inorg. Chem. Front.* **2019** 6,184-191.

31. Wang, J.; Pan, Y.; Lu, L.; Xiong, Y. F.; Fang, L.; Luo, W.; Wu, X.; Kumar, A. *Journal of Molecular Structure* **2019** 1196, 194-200.

32. Gao, J.; Ye, K.; He, M.; Xiong, W.-W.; Cao, W.; Lee, Z.Y.; Wang, Y.; Wu, T.; Huo, F.; Liu, X.; Zhang, Q. *J. Solid State Chem.* **2013** 206, 27–31.

33. a) Vizuet, J. P.; Howlett, Th. S.; Lewis, A. L.; Chroust, Z. D.; McCandless, G. T.; Balkus, K. J. *Inorg. Chem.* **2019** 58, 8, 5031–5041. b) Zhaoa, F.-H.; He, Y. -C.; Shen, C.-Y.; Wang, D. -L.; Lia, Z.-L.; Lia, S.-Y.; Guoa, W.-Y.; Youa, J.-M. *Inorg. Chim. Acta* **2019** 492, 60-65.

34. Zhu, K.; Chen, L.; Jin, X.; Qu, C. *Structural Chemistry* **2019** 30, 1485-1484.

35. Zuo, W.; Fan, Y.; Yang, L.; Cui, L. *Journal of Inorganic and Organometallic Polymers and Materials* **2020** 30, 2105-2113.

36. Ma, R.; Guo, X.; Sun, Y.; Wang, F.; Sun, S.; Zhou, T.; Liu, S.; Guo, H.; Alexandrov, E. V. *Inorg. Chim. Acta* **2019** 496, 119032.

37. a) Fridelli, A. M.; Kessler, V. G.; Escuer, A.; Papaefstathiou, G. S. *CrystEngComm* **2017**, 19, 4355-4367. b) Fidelli, A. M.; Armakola, E.; Demadis, K. D.; Kessler, V. G.; Escuer, A.; Papaefstathiou, G. S. *Eur. J. Inorg. Chem.* **2018** 1, 91-98.

38. a) Coulon, C. ; Miyasaka, H. ; Clérac, R. ; *Struct. Bonding* **2006** 122, 163-206. b) Jeon, I. -R ; Clérac, R. *Dalton Trans.* **2012** 41, 9569-9586. c) Miyasaka, H.; Julve, M.; Yamashita, M.; Clérac, R. *Inorg. Chem.* **2009** 48, 3420-3437. d) Bernot, K.; Luzon, J.; Sessoli, R.; Vindigni, A.; Thion, J.; Richeter, S.; Leclercq, D.; Larionova, J.; Van der Lee, A. *J. Am. Chem. Soc.* **2008** 130, 1619-1627. e) Wang, T.-T.; Ren, M.; Bao, S.-S.; Liu, B.; Pi, L.;

Cai, Z.-S.; Zheng, Z. -H.; Xu, Z.-L.; Zheng, L.-M. *Inorg. Chem.* **2014** 53, 3117-3125. f) Gatteschi, D.; Sessoli, R. *Angew. Chem., Int. Ed.* **2003** 42, 268-297.; g) Papatriantafyllopoulou, C.; Zartilas, S.; Manos, M. J.; Pichon, C.; Clérac, R.; Tasiopoulos, A. J. *Chem. Commun.* **2014** 50, 14873-14876.

39. a) Bogani, L.; Wernsdorfer, W. *Molecular spintronics using single-molecule magnets. Nat. Mater.* **2008**, 7, 179-186. b) Leuenberger, M. N.; Loss, D. *Nature* **2001** 410, 789.

40. a) Chen, L.; Ji, Q.; Wang, X.; Pan, Q.; Cao, X.; Xu, G.; *Cryst. Eng. Comm.* **2017** 19, 5907-5914. b) Hui, J.; Kishida, H.; Ishiba, K.; Takemasu, K.; Morikawa, M.; Kimizuka, N. *Chem Eur. J.* **2016** 40**,** 14213-14218. c) Wang, H. -N.; Meng, X.; Dong, L.-Z.; Chen, Y.; Li, S.-L.; Lan, Y. -Q. *J. Mater. Chem. A* **2019**, 7, 24059-24091. d) Givaja, G.; Amo-Ochoa, P.; Gomez-Garcia, C.; Zamora, F.; *Chem. Soc. Rev.* **2012** 41, 115-147. e) Yue, Q.; Gao, E.-Q. *Coord. Chem. Rev.* **2019**, 382, 1-31.

41. a) Tomsa, A.-R.; Li, Y.; Blanchard, S.; Herson, P.; Boubekeur, K.; P. Gouzerh, K.; Proust, A. *J. Cluster. Sci.* **2014** 25 825-838. b) Alexandropoulos, D. I.; Mowson, A. M.; Pilkington, M. ; Bekiari, V.; Christou, G.; Stamatatos, Th. C. *Dalton Trans.* **2014** 43, 1965-1969. c) Stamatatos, Th. C.; Foguet-Albiol, D.; Stoumpos, C. C.; Raptopoulou, C. P.; Terzis, A.; Wernsdorfer, W.; Perlepes, S. P.; Christou, G. *Polyhedron* **2007** 26, 2165-2168. d) Stamatatos, Th. C.; Foguet-Albiol, D.; Lee, S.-C.; Stoumpos, C. C.; Raptopoulou, C. P.; Terzis, A.; Wernsdorder, W.; Hill, S. O.; Perlepes, S. P.; Christou, G. *J. Am. Chem. Soc.* **2007** 129, 9484-9499. e) Wang, H.-S.; Zhang, Z.C.; Song, X.-J.; Zhang, J.-W.; Zhou, H.-B.; Wang, J.; Song, Y.; You, X.-Z. *Dalton Trans.* **2011** 20, 2703-2706. f) Stoumpos, C. C.; Stamatatos, Th. C.; Psyharis, V.; Raptopoulou, C. P.;

Christou, G.; Perlepes, S. P. *Polyhedron* **2008** 27, 3703-3709. g) Mowson, A. M.; Nguygen, T. N.; Abboud, K. A.; Christou, G. *Inorg. Chem.* **2013** 52, 12320-12322. h) Stamatatos, Th. C.; Gogiet-Albiol, D.; Stoumpos, C. C.; Raptopoulou, C. P.; Terzis, A.; Wernsdorfer, W.; Perlepes, S. P.; Christou, G. *J. Am. Chem. Soc.* **2005** 127, 15380-15381. i) Stamatatos, Th. C.; Fogiet-Albiol, D.; Stoumpos, C.; Raptopoulou, C. P.; Terzis, A.; Wernsdorfer, W.; Perlepes, S. P.; Christou, G. *Polyhedron* **2007** 26, 2165-2168. j) Gkioni, C.; Boudalis, A. K.; Sanakis, Y.; Psycharis, V.; Raptopoulou, C. P. *Polyhedron* **2009** 28, 3221.

42. Efthymiou, C. G.; Cuhna-Silva, L.; Perlepes, S. P.; Brechin, E. K.; Inglis, R.; Evangelisti, M.; Papatriantafyllopoulou, C. *Dalton Trans.* **2016** 45, 17409-17419.

43. Polyzou, C. D. ; Nikolaou, H.; Papatriantafyllopoulou, C. ; Psycharis, V. ; Terzis, A. ; Raptopoulou, C. P. ; Escuer, A. ; Perlepes, S. P. *Dalton Trans.* **2012** 41, 13755-13764.

44. Efthymiou, C. G. ; Raptopoulou, C. P. ; Terzis, A. ; Perlepes, S. P. ; Escuer, A. ; Papatriantafyllopoulou, C. *Polyhedron* **2010** 29, 627-633.

45. Milios, C. J. ; Vinslava, A.; Wernsdorfer, W.; Moggach, S. ; Parsons, S. ; Perlepes, S. P. ; Christou, G. ; Brechin, E. *J. Am. Chem. Soc.* **2007** 129, 2754-2755.

46. Stamatatos, Th. C.; Foguet-Albiol, D.; Lee, S.-C.; Stoumpos, C.; Raptopoulou, C. P.; Terzis, A.; Wernsdorfer, W.; Hill, S. O.; Perlepes, S. P.; Christou, G. *J. Am. Chem. Soc.* **2007** 129, 30, 9484-9499.

47. Efthymiou, C. G. ; Cuhna-Silva, L. ; Perlepes, S. P. ; Brechin, E. K. ; Inglis, R. ; Evangelisti, M. ; Papatriantafyllopoulou, C. *Dalton Trans.* **2016** 45, 17409-17419.

48. a) Fraser, H. W. L.; Nichol, G. S.; Uhrin, D.; Nielsen, U. Gr.; Evangelisti, M.; Schnack, J.; Brechin, E. K. *Dalton Trans.* **2018** 47, 11834-11842. b) Fraser, H. W. L.; Nichol, G. S.; Baldansuren, A.; Mcinnes, E. J. L.; Brechin, E. *Dalton Trans.* **2018** 47, 15530-15537. c) Bagai, R.; Wernsdorfer, W.; Abboud, K. A.; Christou, G. *Polyhedron* **2018** 142, 49-57. d) Melnic, S.; Shoca, S.; Benniston, A. C.; Waddell, P. G. *CrystEngComm.* **2017** 19, 3674-3681. e) Sun, L.; Chen, H.; Chen, Ch. *RSC Advances* **2016** 6, 12408-12413. f) Jooper, T. N.; Inglis, R.; Lorusso, G.; Ujma, J.; Perdita; Barran, E.; Uhrin, D.; Schnack, J.; Piligkos, S.; Evangelisti, M.; Brechin, E. K. *Inorg. Chem.* **2016** 55, 10535-10546. g) Dermitzaki, D.; Lorusso, G.; Raptopoulou, C. P.; Psycharis, V.; Escuer, A.; Evangelisti, M.; Perlepes, S. P.; Stamatatos, Th. *Inorg. Chem.* **2013** 52, 10235-10237. h) Feuersenger, J.; Prodius, D.; Mereacre, V.; Clérac, R.; Anson, C. E.; Powell, A. K. *Polyhedron* **2013** 66, 257-263. i) Hooper, Th. N.; Scnack, J.; Piligkos, St.; Evangelisti, M.; Brechin, E. K. *Angew. Chem. Int. Ed.* **2012** 51, 4633-4636. j) Wang, H.-Sh.; Zhang, Z.-Ch.; Song, X.-J.; Zhang, J.-W.; Zhou, H.-B.; Wang, J.; Song, Y.; You, X.-Z. *Dalton Trans.* **2011** 40, 2703-2706. k) Saha, A.; Abboud, K. A.; Christou, G. *Inorg. Chem.* **2011** 50, 12774-12784. l) Stamatatos, Th. C.; Poole, K. M.; Abboud, Kh. A.; Wernsdorfer, W.; O'Brien, T. A.; Christou, G. *Inorg. Chem.* **2008** 47, 5006-5021. m) Hiraga, H.; Miyasaka, H.; Nakata, K.; Kajiwara, T.; Takaishi, Sh.; Oshima, Y.; Nojiri, H.; Yamashita, M. *Inorg. Chem.* **2007** 46, 9661-9671. n) Stamatatos, Th. C.; Boudalis, A. K.; Pringouri, K. V.; Raptopoulou, C. P.; Terzis, A.; Wolowska, J.; Mcinness, E. J. L.; Perlepes, S. P. *Eur. J. Inorg.* **2007** 5098-5104. o) Miyasaka, H.; Nakata, K.; Lecren, L.; Coulon, Cl.; Nakazawa, Y.; Fujisaki, T.; Sugiura, K.; Yamashita, M.; Clérac, R. *J. Am. Chem. Soc.* **2006** 128, 3770-3783. p) Stamatatos, Th. C.; Abboud, K. A.; Wernsdoerfer,

W.; Christou, G. *Angew. Chem. Int. Ed.* **2006** 45, 4134-4137. q) Lecren, L.; Roubeau, O.; Coulon, Cl.; Li, Y.-G. ; Goff, X. F. L.; Wernsdorfer, W. *J. Am. Chem. Soc.* **2005** 127, 17353-17363. r) Miyasaka, H.; Nakata, K.; Sugiura, K.; Yamashita, M.; Clérac, R. *Angew. Chem. Int. Ed.* **2004** 43, 707-711. s) Saňudo, E. C.; Wernsdoerfer, W.; Abboud, K. A.; Christou, G. *Inorg. Chem.* **2004** 43, 4137-4144..

49. a) Evangelisti, F.; Güttinger, R.; Moré, R.; Luber, S.; Patzke, G. R. *J. Am. Chem. Soc.* **2013** 135, 18734-18737. b) Sun, L.; Chen, H.; Ma, C.; Chen, C. *RSC Advances* **2016** 6, 12408-12413. c) Wang, P.; Shannigrahi, S.; Yakovlev, N. L.; Andy Hor, T. S. *Chem. Asian J.* **2013** 8, 2943-2946. d) Pham, L.; Abboud, K. A.; Wernsdoerfer, W.; Christou, G. *Polyhedron* **2013** 66, 205-211. e) Bizilj, K.; Hardin, S. G.; Hoskins, B.F.; Oliver, P. J.; Tiekink, E. R. T.; Winter, G. *Aust. J. Chem.* **1986** 39, 1035-1042. f) Wang, H.-S.; Zhang, Z.-C.; Song, X.-J.; Zhang, J.-W.; Zhou, H.-B.; Wang, J.; Song, Y.; You, X.-Z. *Dalton Trans.* **2011** 40, 2703-2706. g) Hooper, T. N.; Schnack, J.; Piligkos, S.; Evangelisti, M.; Brechin, E. K. *Angew. Chem. Int. Ed.* **2012** 51, 4633-4636. h) Wang, P.; Shannigrahi, S.; Yakovlev, N. L.; Andy Hor, T. S. *Inorg. Chem.* **2012** 51, 12059-12061. i) Hooper, T. N.; Inglis, R.; Lorusso, G.; Ujma, J.; E. Barran, P.; Uhrin, D.; Schnack, J.; Piligkos, S.; Evangelisti, M.; Brechin, E. K. *Inorg. Chem.* **2016** 55, 10535-10546. j) Stamatatos, Th. C.; Boudalis, A. K.; Pringouri, K. V.; Raptopoulou, C. P.; Terzis, A.; Wolowska, J.; McInnes, E. J. L.; Perlepes, S. P. *Eur. J. Inorg. Chem.* **2007** 5098-5104. k) Brechin, E. K.; Knapp, M. J.; Huffman, J. C.; Hendrickson, D. H.; Christou, G. *Inorg. Chim. Acta* **2000** 297, 389-399. l) Feuersenger, J. G.; Prodius, D.; Mereacre, V.; Clérac, R. ; Anson, C. E. ; Powell, A. K. *Inorg. Chem. Commun.* **2011** 14, 1851-1854. m) Wang, P.; Shannigrahi, S.; Yakovlev, N. L.; Andy Hor, T.

S. *Dalton Trans.* **2014** 43, 182-187. n) Feng, P. L.; Beedle, C. C.; Koo, C.; Wernsdorfer, W.; Nakano, M.; Hill, S.; Hendrickson, D. N. *Inorg. Chem.* **2008** 47, 3188-3204. o) Cowley, A. H.; Cushner, M.; Fild, M.; Gibson, J. A. *Inorg. Chem.* **2011** 14, 1851-1855. p) Papatriantafyllopoulou, C.; Abboud, K. A.; Christou, G. *Polyhedron* **2013** 52, 196-206. q) Pham, L.; Abboud, K. A.; Wernsdorfer, W.; Christou, G. *Polyhedron* **2013** 66, 205-211. r) Moncol, J.; Jomova, K.; Zelenicky, L.; Lis, T.; Valko, M. *Acta Crystallogr. Sect. C Struct. Chem.* **2011** 67, m318-m320. s) Feng, P. L.; Beedle, C. C.; Wernsdorfer, W.; Koo, C.; Nakano, M.; Hill, S.; Hendrickson, D. *Inorg. Chem.* **2007** 46, 8126-8128. t) Tesouro Vallina, A.; Lecren, L.; Li, Y.-G.; Roubeau, O.; Clérac, R. *Z. Anorg. All. Chem.* **2007** 633, 2400-2407. u) Sun, L.; Chen, H.; Chen, C. *Appl. Organomet. Chem.* **2017** 31, e3846. v) Bagai, R.; Wernsdorfer, W.; Abboud, K. A.; Christou, G. *Polyhedron* **2018** 142, 49. w) Taguchi, T.; Wernsdorfer, W.; Abboud, K. A.; Christou, G. *Inorg. Chem.* **2010** 49, 10579-10589. x) Melnic, S.; Shova, S.; Benniston, A. C.; Waddell, P. G. *CrystEngComm* **2017** 19, 3674-3681. y) Boskovic, C.; Brechin, E. K.; Streib, W. E.; Folting, K.; Hendrickson, D. N.; Christou, G. *Chem. Commun.* **2001** 467-468.

50. a) Ito, M.; Onaka, S. *Inorg. Chim Acta* **2004** 357, 1039-1046. b) Gek Ang, S.; Wang Sun, B.; Gao, S. *Inorg. Chem. Commun.* **2004** 7, 795-798.

51. a) Yilmaz, V. T.; Guney, S.; Andac, O.; Harrison, W. T. A. *Polyhedron* **2002** 21, 2393-2402. b) Sun, L.; Chen, H.; Ma, C.; Chen, C. *RSC Advances* **2016** 6, 12408-12413.

52. Hiraga, H.; Miyasaka, H.; Kajiwara, K.; Takaishi, S.; Oshima, Y.; Nojiri, H.; Yamashita, M. *Inorg. Chem.* **2007** 46, 23, 9661-9671.

53. Yang, E. C.; Harden, N.; Wernsdorfer, W.; Zakharov, L. N. ; Brechin, E. K.; Rheingold, A. L.; Christou, G.; Hendrickson, D. N. *Polyhedron* **2003** 22 1857-1863.

54. Moncol, J.; Mdra, M.; Lönnecke, P.; Koman, M.; Melnik, M.; *J. Coord. Chem.* **2004** 57, 1065-1078.

55. Evangelisti, F.; Güttinger, R.; Moré, R.; Luber, S.; Patzke, G. R. *J. Am. Chem. Soc.* **2013** 135, 18734-18737.

56. Sun, L. ; Chen, H. ; Ma, C.; Chen, C.; *RSC Advances* **2016** 6, 12408-12413.

57. Miyasaka, H. ; Nakata, K. ; Sugiura, K. ; Yamashito, M.; Clérac, R. *Angew. Chem. Int. Ed.* **2004** 43, 707-711.

58. Manos, M. J. ; Moushi, E. E. ; Papaefstathiou, G. S. ; Tasiopoulos, A. J. *Cryst. Growth Des.* **2012** 12, 5471-5480.

59. a) Kyprianidou, E. J.; Lazarides, Th.; Kaziannis, S.; Kosmidis, C.; Itskos, G.; Manos, M. J.; Tasiopoulos, A. J. *J. Mater. Chem. A* **2014** 5258-5266. b) Moushi, E. E.; Kourtellaris, A.; Andreou, E.; Fidelli, A.; Papaefstathiou, G. S.; Plakatouras, J. C.; Tasiopoulos, A. J. *CrystEngComm* **2020** 22, 2083-2096.

60. Kundu, A.; Saikia, S.; Majumber, M.; Sengupta, O.; Bhattacharya, B.; G. Chandra De, B. ; Ghosh, S. *ACS Omega* **2009** 4, 5221-5232.

61. a) Brechin, E. K.; Huffman, J. C.; Christou, G.; Yoo, J.; Nakano, M.; Hendrickson, D. N. *Chem. Commun.* **1999** 783-784. b) Cardona-Serra, S.; Clemente-Juan, J. M.; Coronado, E.; Martí-Gastaldo, C.; Navarro-Moratalla, E. *Eur. J. Inorg. Chem.* **2013** 1903. c) Yoo, J.; Brechin, E. K.; Yamaguchi, A.; Nakano, M.; Huffman, J. C.; Maniero, A. L.; Brunel, L.-C.; Awaga, K.; Ishimoto, H.; Christou, G.; Hendrickson, D. N. *Inorg. Chem.* **2000** 39, 3615-3623.

62. Boskovic, C.; Wernsdorfer, W.; Folting, K.; Huffman, J. C.; Hendrickson, D. N.; Christou, G. *Inorg. Chem.* **2002** 411, 5107-5118

63. Katsoulakou, E.; Dermitaki, D.; Konidaris, K. F.; Moushi, E. E.; Raptopoulou, C. P.; Psycharis, V.; Tasiopoulos, A. J.; Bekiari, V.; Manessi-Zoupa, E.; Perlepes, S. P.; Stamatatos, Th. C. *Polyhedron* **2013** 52, 467-475.

64. Anselmo, D.; Escudero-Adán, E. C.; Benet-Buchholz, J.; Kleij, A. W. *Dalton Trans.* **2009** 7368-7373.

65. a) Hocking, R. K.; Chang, S. L. Y.; MacFarlane, D. R.; Spiccia, L. *Aust. J. Chem.* **2012** 65, 608-614. b) Boa, A. N.; Crane, J. D.; Kowalczyk, R. M.; Sultana, N. H. *Eur. J. Inorg. Chem.* **2005** 872-878. c) Korzekwa, J.; Scheurer, A.; Heinemann, F. W.; Kroener, W.; Gieb, K.; Müller, P. *J. Coord. Chem.* **2017** 70, 626-641.

66. Titiş, J.; Chrenková, V.; Rajnák, C.; Moncol, J.; Valigura, D.; Boča, R. *Dalton Trans.* **2019** 48, 11647-11650.

67. Valigura, D.; Rajanák, C.; Moncol, J.; Titis, J.; Boča, R. *Dalton Trans.* **2017** 46, 10950-10956.

68. Hamaguchi, T. *Inorg. Chim. Acta* **2015** 427, 144-149.

69. Parimala, S.; Kandaswamy, M.; Nissa, M. N.; Velmurugan, D. *J. Coord. Chem.* **2003** 56, 261-274.

70. Stamatatos, Th. C.; Vlahopoulou, G. C.; Raptopoulou, C. P.; Terzis, A.; Escuer, A.; Perlepes, S. P. *Inorg. Chem.* **2009** 48 4610-4612.

71. Rochon, F. D.; Beauchamp, A. L.; Bensimon, C. *Can. J. Chem.* **1996** 74, 2121-2130.

72. Winter, S.; Seichter, W.; Weber, E. *J. Coord. Chem.* **2004** 57 997-1014.

73. Winter, S.; Seichter, W.; Weber, E. *J. Coord. Chem.* **2004** 57, 997-1014.

74. a) Brechin, E. K.; Yoo, J.; Nakano, M.; Huffman, J. C.; Hendrickson, D. N.; Christou, G. *Chem. Commun.* **1999** 783-784. b) Chakraborty, A.; Gurunatha, K. L.; Muthulakshmi, A.; Dutta, S.; Pati, S. K.; Maji, T. K. *Dalton Trans.* **2012** 41, 5879-5888.

75. Madanhire, T.; Abrahams, A.; Hosten, E.; Betz, R. *J. Coord. Chem.* **2017** 70, 3252-3274.

76. Brechin, E. K.; Huffman, J. C.; Christou, G.; Yoo, J.; Nakano, M.; Hendrickson, D. N. *Chem. Commun.* **1999** 783-784.

77. Alexandropoulos, D. I.; Cuhna-Silva, L.; Bekiari, V.; Christou, G.; Stamatatos, Th. C. *Inorg. Chem.* **2017** 70, 3220-3229

78. Taguchi, T.; Thompson, M. S.; Abboud, K. A.; Christou, G. *Dalton Trans.* **2010** 39, 9131-9139.

79. a) Karmakar, A.; Samanta, P.; Dutta, S.; Ghosh, S. K., *Chem. Asian J.* **2019** 14(24), 4506-4519. b) Ricco, R.; Styles, M. J.; Falcaro, P. "*Metal Organic Frameworks (MOFs) for Environmental Applications*", *Elsevier* **2019** 383-426. c) Samanta, P.; Let, S.; Mandal, W.; Duttta, S.; Ghosh, S. K. *Inorg. Chem. Front.* **2020** 7, 1801-1821. d) Fang, X.; Zong, B.; Mao, S. *Nano-Micro Letters* **2018** 10(64), 1-19).

80. a)Zhang, M.; Feng, G.; Song, Z.; Zhou, Y. -P.; Chao, H. -Y.; Yuan, D.; Tan, T. T. Y.; Guo, Z.; Hu, Zh.; Zhong Tang, B.; Liu, B.; Zhao, D. *J. Am. Chem. Soc.* **2014** 136, 20, 7241-7244. b) Safaei, S.; Kazemian, H.; Junk, P. C. *Journal of Solid State Chemistry* **2021** 300, 122267.

81. a) Aulakh, D.; Pyser, J. B.; Zhang, X.; Yakovenko, A. A.; Dunbar, K. R.; Wriedt, M. *J. Am. Chem. Soc.* 2015 137, 9257-9257. b) Zhao, X.; Liu, S.; Tang, Z.; Niu, H.; Cai, Y.; Meng, W.; Wu, F.; Giesy, J. P. *Scientific Reports* **2015** 5, 11849. c) Aulakh, D.; Liu, L.; Varghese, J. R.; Xie, H.; Islamoglu, T.; Duell, K.; Kung, C.-W.; Hsiung, C.-E.; Zhang, Y.; Drout, R. J.; Farha,

O. K.; Dunbar, K. R.; Han, Y.; Wriedt, M. *J. Am. Chem. Soc.* **2019** 141, 2997-3005. d) Maya, F.; Palomino Cabello, C.; Frizzarin, R. M.; Estela, J. M.; Turnes Palomino, G.; Cerda, V. *Trends in Analytical Chemistry* **2017** 90, 142-152.

82. Sadiq, M. M.; Li, H.; Hill, A.J.; Falcaro, P.; Hill, M. R.; Suzuki, K. *Chem. Mater.* **2016** 28, 6219-6226.

83. a) Katsenis, A. D.; Brechin, E. K.; Papaefstathiou, G. S. *Encyclopedia of Inorganic and Bioinorganic Chemistry* **2014** 245-258. b) Coronado, E.; Mínguez Espallargas, G. *Chem. Soc. Rev.* **2013** 42, 1525-1539. c) Mínguez Espallargas, G.; Coronado, E. *Chem. Soc. Rev.* **2018** 47, 533-557. d) Ricco, R.; Malfatti, L.; Takahashi, M.; Hillad, A. J.; Falcaro, P. *J. Mater.Chem. A.* **2013** 1, 13033-13045. e) Kurmoo, M. *Chem. Soc. Rev.* **2009** 38, 1353-1379

84. a) Mijasaka, M.; Nakata, K.; Lecren, L.; Coulon, C.; Nakazawa, Y.; Fujisaki, T.; Sugiura, K.; Yamashita, M.; Clerac, R. *J. Am. Chem. Soc.* **2006** 128, 3770-3783.; b) Stamatatos, Th. C.; Abboud, K. A.; Wernsdorfer, W.; Christou, G. *Polyhedron* **2007** 26, 2095-2100.

Chapter 2: Publications

2.1 Brief description of the paper

In this article are represented the first examples of coordination polymers by the simultaneous of di- and tri- carboxylates (terephthalic acid or 1,4-benzene-dicarboxylic acid and trimesic acid or 1,3,5-benzenetricarboxylic acid) and pyrdine-2-amidoxime.

New insights into oximic ligands: Synthesis and characterization of 1D chains by the use of pyridine 2-amidoxime and polycarboxylates

Dedicated to Professor Spyros Perlepes, an inspiring teacher and mentor, and a great scientist, on the occasion of his 65th birthday.

Ioannis Mylonas-Margaritis ª, Meghan Winterlich ª, Constantinos G. Efthymiou ª, Theodore Lazarides ᵇ, Patrick McArdle ª, Constantina Papatriantafyllopoulou ª

Show more ∨

+ Add to Mendeley   ⤳ Share   🔖 Cite

Abstract

The initial study of the ligand blend pyridine-2-amidoxime (pyaoxH$_2$)/1,4-benzenedicarboxylic (H$_2$bdc) or 1,3,5-benzenetricarboxylic acid (H$_3$btc) provided access to four 1D coordination polymers, [Zn(bdc)(pyaoxH$_2$)(DMF)]$_n$ (**1**), {[Ni(bdc)(pyaoxH$_2$)$_2$]·2DMF}$_n$ (**2**·2DMF), {[Mn(bdc)(pyaoxH$_2$)$_2$]·2DMF}$_n$ (**3**·2DMF) and [Ni(Hbtc)(pyaoxH$_2$)$_2$]$_n$ (**5**), and the discrete (0D) compound [Ni(H$_2$btc)$_2$(pyaoxH$_2$)$_2$]·2H$_2$O (**4**·2H$_2$O), whose further polymerization yielded **5**. These compounds are the first metal coordination polymers bearing pyaoxH$_2$ and rare examples of such species with any type of a 2-pyridyl oxime. The crystal structures of the compounds have been determined by single crystal X-ray crystallography, whereas their identity, purity and stability were confirmed by pxrd studies. Thermal stability studies were performed in **1**, **2**·2DMF, **4**·2H$_2$O and **5**. The photoluminescence properties of **1** have been studied and revealed a maximum emission peak at 440 nm and a visible shoulder at 467 nm, assigned to the pyaoxH$_2$ and bdc^{2-} ligands, respectively.

Author's contribution:

I. Mylonas-Margaritis: All the synthetic work, preparation of first draft, tables, figures.

Dr. Constantinos Efthymiou: Advisor and analyzed the photoluminescence data,.

Prof. Theodore Lazarides: Collection of the photoluminescence data.

Prof. Patrick McArdle: Collection and analysis of the crystallographic data.

Dr. Constantina Papatriantafyllopoulou: Managed the project **and** reviewed the manuscript before the submission and during the revision process.

New insights into oximic ligands: Synthesis and characterization of 1D chains by the use of pyridine 2-amidoxime and polycarboxylates

Ioannis Mylonas-Margaritis [a], Meghan Winterlich a, Constantinos G. Efthymiou [a], Theodore Lazarides [b],Patrick McArdle [a], Constantina Papatriantafyllopoulou [a,*]

[a] School of Chemistry, National University of Ireland Galway, H91 TK 33 Galway, Ireland

[b] Department of Chemistry, Aristotle University of Thessaloniki, 541 24 Thessaloniki, Greece

*Corresponding author. Tel: +353 9 493462

E-mail address: *CONSTANTINA.PAPATRIANTAFYLLOPO@NUIGALWAY.IE*

Abstract

The initial study of the ligand blend pyridine-2-amidoxime (pyaoxH$_2$)/1,4-benzenedicarboxylic (H$_2$bdc) or 1,3,5-benzenetricarboxylic acid (H$_3$btc) provided access to four 1D coordination polymers, [Zn(bdc)(pyaoxH$_2$)(DMF)]$_n$ (**1**),{[Ni(bdc)(pyaoxH$_2$)$_2$]·2DMF}$_n$(**2**·2DMF), [Mn(bdc)(pyaoxH$_2$)$_2$]·2DMF}$_n$ (**3**·2DMF) and [Ni(Hbtc)(pyaoxH$_2$)$_2$]$_n$ (**5**), and the discrete (0D) compound [Ni(H$_2$btc)$_2$(pyaoxH$_2$)$_2$]·2H$_2$O (**4**·2H$_2$O), whose further polymerization yielded **5**. These compounds are the first metal coordination polymers bearing pyaoxH$_2$

and rare examples of such species with any type of a 2-pyridyl oxime. The crystal structures of the compounds have been determined by single crystal X-ray crystallography, whereas their identity, purity and stability were confirmed by pxrd studies. Thermal stability studies were performed in **1**, **2**·2DMF, **4**·2H2O and **5**. The photoluminescence properties of **1** have been studied and revealed a maximum emission peak at 440 nm and a visible shoulder at 467 nm, assigned to the pyaoxH$_2$ and bdc^{2-} ligands, respectively.

1. Introduction

The synthesis and characterization of metal coordination polymers has attracted a significant amount of increasing attention the last decades because of their applications in gas storage[1], catalysis[2], sensing[3], drug delivery[4], etc. Such species are comprised of linked repeating structural units that form 1D chains, 2D nets or 3D frameworks and often display interesting molecular topologies and architectures. They also provide valuable opportunities for the discovery of intriguing phenomena, including the interpenetration of networks[5], the breathing effect[6] and the single chain magnetism (SCM) behaviour[7]. The first two are phenomena that are encountered in metal–organic frameworks, one category of coordination polymers, which are described as crystalline porous materials built from inorganic structural units, connected through organic linkers[8]; the interpenetration refers to more than one polymeric networks catenated with each other[5], and the breathing effect, also known as gate-opening effect, is relevant to the enlargement or shrinkage of the pores' diameter upon the insertion of a guest molecule into the MOFs' framework[6]. Both phenomena dominate the shapes and/or sizes of the pores of the MOF and, as such, play a crucial role in the

isolation of species suitable for gas adsorption and drug deli-very applications. On the other hand, SCMs are 1D polymeric chains that exhibit slow relaxation of magnetisation stemming from strong intrachain exchange interactions between high spin structural building units along the chain[7]. SCMs are excellent candidates for applications in high-density information storage, molecular spintronics and quantum computation, etc.[9]. The structural features and physical properties of the coordination polymers are mainly affected by the size and coordination ability of the organic ligand and the nature of the metal ion; weaker interactions (hydrogen bonding, π–π stacking, etc.) play also a crucial role as they dictate the packing of polymeric chains, hence affecting the architecture of the overall framework. There is a wide range of ligands that can bridge metal ions, leading to the formation of a coordination polymer [10]; these can be classified as: (i) monoatomic anions, e.g. C^{l-}, Br^-, O^{2-}, S^{2-}, etc., (ii) small molecules (anionic or neutral, inorganic or organic) with significant polymerization capability, i.e., SO_4^{2-}, PO_4^{3-}, acetate, formate, CN^-, NCO^-, SCN^-, oxalate, tetracyanoethylene, azides, pyrazine, pentant arm polyols etc.[7g,11–12], and (iii) N- and O-donor polytopic ligands, which act as linkers, connecting metal ions or metal clusters. The latter type of ligands, such as polycarboxylates, polyimidazolates, polypyridyls, etc., are rigid and have the ability to lead to robust multidimensional systems.[8c,13–15]
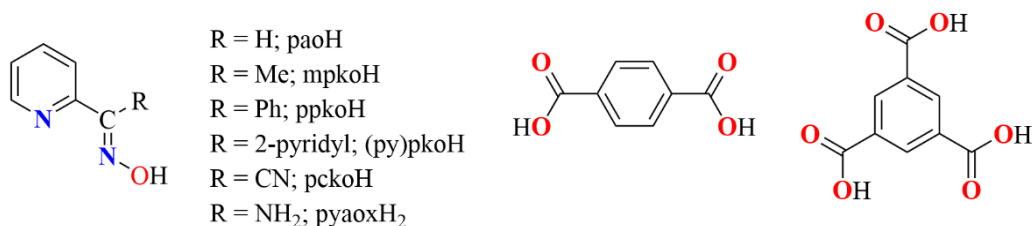
Scheme 1. The ligands discussed in this paper: 2-pyridyl oximes (left), 1,4-benzenedicarboxylic acid (H$_2$bdc, middle) and 1,3,5-benzenetricarboxylic acid (H$_3$btc, right).

The intense research efforts of several research groups around the world have resulted in an enormous library of coordination polymers. Nevertheless, the isolation of new such species remains a hot research field not only for bringing them closer to their technological applications, but also for the discovery of new phenomena, as described above. A key factor towards this direction is the development of new synthetic strategies with the investigation of new reaction systems and unexplored ligands often being a promising route. One family of ligands that have been extensively employed in coordination chemistry are the oximes; oximates have the ability to bridge a large number of metal ions favouring also ferromagnetic interactions between the paramagnetic metal centres [16]. One broad family of oximic ligands are the 2-pyridyl oximes (**Scheme 1**).[17] It is noteworthy that, although such ligands have been key ''players'' in several areas of single-molecule and single-chain magnetism[18], they have not been systematically investigated in the field of coordination polymers. Note that the enormous work of Prof. Perlepes, to whom this paper is dedicated, has significantly contributed to the development of the coordination chemistry of 2-pyridyl oximes.[17] Among these ligands, pyridine-2-amidoxime (pyaoxH$_2$) has received substantially less attention in comparison with the other members of this

family. Recently we employed pyaoxH$_2$ for the synthesis of polynuclear Ni^{II} clusters with interesting magnetic properties.[19] Expanding this work, we then studied the ligand blend pyaoxH$_2$/1,4-benzenedicarboxylic (H$_2$bdc) or 1,3,5-benzenetricarboxylic acid (H$_3$btc) as a means to isolate coordination polymers bearing pyaoxH$_2$ or its anions.[14,15] The presence of the amino functionality is expected to improve the host–guest interactions of the resulting polymers due to its coordination capability, potential for deprotonation and hydrogen bonding effects, hence the isolation of such species is strongly desirable. Herein, we describe the synthesis and characterization of the first metal coordination polymers containing pyaoxH$_2$ or its anions, namely [Zn(bdc)(pyaoxH$_2$)(DMF)]$_n$ (**1**), {[Ni(bdc)(pyaoxH$_2$)$_2$]·2DMF}$_n$ (**2**·2DMF), {[Mn(bdc)(pyaoxH$_2$)$_2$]·2DMF}$_n$ (**3**·2DMF) and {[Ni(Hbtc)(pyaoxH$_2$)$_2$]}$_n$ (**5**). The discrete (0D) compound [Ni(H$_2$btc)$_2$(pyaoxH$_2$)$_2$]·2H$_2$O (**4**·2H$_2$O) has been also isolated, which was then polymerized leading to **5**. The crystal structures and physical properties (photoluminescence properties for **1**, thermal stability studies) of these compounds are discussed below.

2. Experimental

2.1. General and physical measurements

All manipulations were performed under aerobic conditions using materials (reagent grade) and solvents as received. pyaoxH$_2$ was prepared as described elsewhere.[20] WARNING: Perchlorate salts are potentially explosive; such compounds should be used in small quantities, and treated with utmost care at all times.

Elemental analyses (C, H, N) were performed by the in-house facilities of the National University of Ireland Galway, School of Chemistry. IR spectra (4000–400 cm^{-1}) were recorded on a Perkin-Elmer Spectrum 400 FT-IR spectrometer. Powder X-ray diffraction data (pxrd) were collected using an Inex Equinox 6000 diffractometer. The photoluminescence spectrum of **1** was acquired at ambient temperature on a Perkin Elmer LS 55 fluorimeter equipped with a red sensitive Hamamatsu R928 photomultiplier tube. The spectrum was corrected using the correction function provided in the instrument's software. TGA experiments were performed on a STA625 thermal analyzer from Rheometric Scientific (Piscataway, New Jersey). The heating rate was kept constant at 10 °C/min, and all runs were carried out between 20 and 600 °C. The measurements were made in open aluminum crucibles, nitrogen was purged in ambient mode, and calibration was performed using an indium standard.

2.2. Compounds preparation

2.2.1. [Zn(bdc)(pyaoxH$_2$)(DMF)]$_n$ (1)

Zn(ClO$_4$)$_2$·6H$_2$O (0.037 g, 0.10 mmol) and pyaoxH2 (0.027 g, 0.20 mmol) were added to a vial containing H$_2$bdc (0.017 g, 0.10 mmol) in DMF (5 ml). The resultant solution was put in the oven and heated at 100 °C for 24 h, after which X-ray quality colorless crystals of **1** were formed. The crystals were collected by filtration, washed with cold MeCN (2 ml) and Et$_2$O (2 x 5 ml), and dried in air. Yield 35%. Anal. Calc. for **1**·2H$_2$O: C, 42.92; H, 4.66; N, 11.78 Found: C, 43.05; H, 4.95; N, 12.01%. IR data: v (cm^{-1}) = 1649m, 1567m, 1502m, 436w, 1369s, 1255w, 1103m, 1064w, 1034w, 1018m, 887w, 842m, 745s, 665m.

2.2.2. {[Ni(bdc)(pyaoxH₂)₂]·2DMF}ₙ (2·2DMF)

Ni(NO₃)₂·6H₂O (0.058 g, 0.20 mmol), pyaoxH₂ (0.027 g, 0.20 mmol) and Et₃N (56 μl, 0.40 mmol) were added to a vial containing H₂bdc (0.017 g, 0.10 mmol) in DMF (10 ml). The brown solution was put in the oven and heated at 100 °C for 24 h, after which X-ray quality blue needles of **2**·2DMF were formed. The crystals were collected by filtration, washed with cold MeCN (2 ml) and Et₂O (2 x 5 ml) and dried in air; yield 40%. Anal. Calc. for **2**·2DMF: C, 48.54; H, 5.01; N, 17.42 Found: C, 48.63; H, 4.96 N, 17.87%. IR data: v (cm^{-1}) = 3610w, 3356w, 3319w, 3069w, 1654m, 1572m, 1499m, 1372s, 1304w, 1263w, 1130m, 1016m, 812s, 789m, 749s, 692w, 659w.

2.2.3. {[Mn(bdc)(pyaoxH₂)₂]·2DMF}ₙ (3·2DMF)

This complex was prepared in the same manner as complex **2**·2DMF but using Mn(NO₃)₂·6H₂O (0.025 g, 0.10 mmol) instead of Ni(NO₃)₂·6H₂O. Small polyhedral crystals were formed and collected by filtration, washed with cold MeCN (2 ml) and Et₂O (2 x 5 ml) and dried in air; yield 63%. Anal. Calc. for **3**·2DMF: C, 44.73; H, 4.62; N, 16.05 Found: C, 44.50; H, 4.84; N, 16.39%. IR data: v (cm^{-1}) = 3610w, 3384w, 3315w, 3066w, 1650m, 1594m, 1492m, 1369s, 1304w, 1260w, 1130m, 1016m, 803s, 792m, 749s, 690m, 659w.

2.2.4. [Ni(H₂btc)₂(pyaoxH₂)₂]·2H₂O (4·2H₂O)

Ni(ClO₄)₂·6H₂O (0.037 g, 0.10 mmol) and pyaoxH₂ (0.027 g, 0.20 mmol) were added to a vial containing H₃btc (0.021 g, 0.10 mmol) in H₂O (10 ml). The pale pink solution was put in the oven (100 °C) and heated for 24 h, after which X-ray quality greenish crystals of **4**·2H₂O were formed. The crystals were collected by filtration, washed with cold MeCN (2 ml) and Et₂O (2x 5 ml) and dried in air;

yield 60%. Anal. Calc. for **4**·2H$_2$O: C, 45.77; H, 3.58; N, 10.67 Found: C, 44.52; H, 3.86; N, 11.09%. IR data: m (cm^{-1}) = 3414w, 3314w, 1726w, 1697m, 1670m, 1600s, 1572w, 1543s, 1499w, 1438w, 1408w, 1368s, 1327w, 1281w, 1247w, 1255w, 1176m, 1153w, 1097m, 1026m, 921w, 845w, 789m, 745s, 692m, 662m.

2.2.5. {[Ni(Hbtc)(pyaoxH$_2$)$_2$}$_n$ (5)

Method A: Ni(ClO$_4$)$_2$·6H$_2$O (0.073 g, 0.20 mmol), pyaoxH$_2$ (0.027g, 0.20 mmol) and CH$_3$ONa (0.011, 0.2 mmol) were added to a vial containing H$_3$btc (0.021 g, 0.10 mmol) in H$_2$O (15 ml). The cloudy brown-yellow solution was put in the oven (100 °C) and heated for 24 h, after which X-ray quality blue crystals of **5** were formed. The crystals were collected by filtration, washed with cold MeCN (2 ml) and Et$_2$O (2 x 5 ml) and dried in air; yield 75%. Anal. Calc. for **5**: C, 46.61; H, 3.35; N, 15.53 Found: C, 46.80; H, 3.28; N, 15.11%. IR data: v (cm^{-1}) = 3469w, 3349w, 3305w, 3182w, 2565w, 1721m, 1682m, 1606s, 1530m, 1430w, 1408w, 1363s, 1303w, 1408w, 1227m, 1166m, 1110w, 1098m, 1025s, 1014m,

937w, 896w, 875m, 812w, 788s, 757m, 747m, 714s, 688w, 664m.

Method B: **4** (0.08 g, 0.1 mmol) was added in a vial containing a solution of CH$_3$ONa 0.016 g, 0.3 mmol) in DMF (10 ml). The solution was heated at 100 °C for one day, after which crystals of **5** were formed, collected by filtration, washed with MeCN (2 x 5mL), and dried under vacuum. Yield: 20%. The product was identified as **5** by IR spectral comparison with authentic material.

2.2.6. Single-crystal X-ray crystallography

Single crystal diffraction data of **1**, **2**·2DMF, **4**·2H$_2$O, and **5** were collected using an Oxford Diffraction Xcalibur CCD diffractometer using graphite-monochromated Mo Ka radiation (k = 0.71073 Å) at room temperature. The

structures were solved using SHELXT [21], embedded in the OSCAIL software.[22] Non-hydrogen atoms were refined anisotropically and hydrogen atoms were in calculated positions. Graphics were produced with DIAMOND.[23] An initial search for reciprocal space revealed monoclinic cell for **3**·2DMF with dimensions identical with the corresponding of **2**·2DMF; however, the crystals were small and diffracted poorly, and despite our efforts to grow bigger crystals, full solution of their crystal structures was not feasible.

Crystallographic data can be found in **Table 1**. CIF files can be obtained free of charge at *WWW.CCDC.CAM.AC.UK/CONTS/RETRIEVING.HTML* or from the Cambridge Crystallographic Data Centre, Cambridge, UK with the REF codes 1832944–1832947 for **1**, **2**·2DMF, **4**·2H$_2$O, and **5**, respectively.

Table 1 Crystallographic data for complexes **1**, **2**·2DMF, **4**·2H$_2$O, and **5**.

Complex	1	2·2DMF	4·2H$_2$O	5
Empirical formula	C$_{17}$H$_{18}$N$_4$O$_6$Zn	C$_{26}$H$_{32}$N$_8$NiO$_8$	C$_{30}$H$_{24}$N$_6$NiO$_{16}$	C$_{21}$H$_{18}$N$_6$NiO$_8$
Formula weight	439.72	643.30	783.26	541.12
Crystal system	Triclinic	Monoclinic	Monoclinic	Orthorhombic
Space group	*P-1*	*P2$_1$/*c	*P2$_1$/*n	*P 2$_1$ 2$_1$ 2$_1$*
a (Å)	8.4118(6)	16.9280(5)	16.0203(6)	8.9093(2)
b (Å)	9.2489(6)	9.8151(3)	26.0789(8)	14.4089(3)

c (Å)	13.5705(6)	18.6765(5)	17.0418(7)	17.8770(4)
α (º)	96.814(5)	90	90	90
β (º)	102.630(5)	105.455(3)	114.319(4)	90
γ (º)	113.888(7)	90	90	90
V (Å^3)	916.23(11)	2990.89(16)	6488.1(5)	2294.93(9)
Z	2	4	8	4
ρ_{calc} (g cm^{-3})	1.594	1.429	1.604	1.566
Radiation, λ (Å)	0.71073	0.71073	0.71073	0.71073
μ (mm^{-1})	1.384	0.710	0.686	0.906
Temperature (K)	293(2)	297.1(6)	298.0(1)	299.0(2)
Measd/independent reflns (R_{int})	5715/ 3213 (0.0233)	5265/4445 (0.0259)	45690/11359 (0.0297)	16221/4040 (0.0334)
Parameters refined	267	410	1003	347
GoF (on F^2)	1.020	1.007	1.106	1.072
R_1^a ($I > 2\sigma(I)$)	0.0299	0.0365	0.0533	0.0257
wR_2^b ($I > 2\sigma(I)$)	0.0672	0.0891	0.1159	0.0614

$(\Delta\rho)_{max}/(\Delta\rho)_{min}$	0.343/-0.259	0.308/ -0.292	0.631/-0.575	0.377/-0.268
(e Å^{-3})				

[a] $R_1 = \Sigma(|F_o|-|F_c|)/\Sigma(|F_o|)$.

[b] $wR_2 = \{\Sigma[w(F_o{}^2-F_c{}^2)^2]/\Sigma[w(F_o{}^2)^2]\}^{1/2}$.

3. Results and discussion

3.1. Synthesis

Our group has been investigating the use of pyridine-2-amidoxime, pyaoxH$_2$, in Ni^{II} cluster chemistry as a method for the isolation of new metal clusters with interesting structural features and magnetic properties. These studies led to the isolation of two ferromagnetic multiple-decker Ni$^{II}{}_{12}$ and Ni$^{II}{}_{16}$ clusters consisting of parallel Ni$_4$ layers.[19] These promising results prompted us to further explore the coordination chemistry of this ligand with other 3d metal ions and also employ poly-carboxylic acids, such as 1,4-benzenedicarboxylic (H$_2$bdc) or 1,3,5-benzenetricarboxylic acid (H$_3$btc) as a means to isolate coordination polymers; it is noteworthy that such carboxylates have not been previously investigated in combination with any type of a 2-pyridyl oxime, whereas they have been a fruitful source of coordination polymers.[14,15] As such, it was a matter of interest to study the ligand blend pyaoxH$_2$/H$_2$bdc or H$_3$btc in 3d metal chemistry; thus, a variety of experiments were performed towards this direction, studying how the different synthetic parameters (presence/absence or kind of

base, metal ratio of the reactants, metal sources, etc.) affect the identity of the isolated product.

The reaction mixture of $Zn(ClO_4)_2 \cdot 6H_2O$/pyaoxH$_2$/H$_2$bdc (1:2:1) in DMF gave a colorless solution from which crystals of $[Zn(bdc)(pyaoxH_2)(DMF)]_n$ (**1**) were subsequently isolated. The stoichiometric equation of the reaction that lead to the formation of **1** is presented in Eq. (**1**).

$$Zn(ClO_4)_2 \cdot 6H_2O + pyaoxH_2 + H_2bdc + DMF \xrightarrow{DMF}$$
$$[Zn(bdc)(pyaoxH_2)(DMF)]_n + 2\,H^+ + 2\,ClO_4^- + 6\,H_2O\ (1)$$
$$\mathbf{1}$$
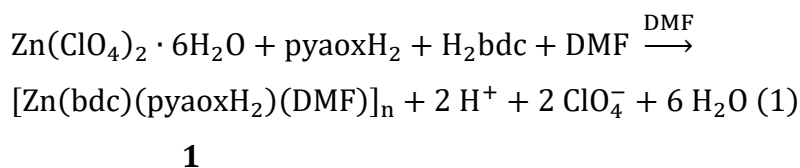
In order to favour the deprotonation of the pyaoxH$_2$ ligand in **1**, we added base into the reaction mixture; many experiments were performed using different bases and reaction conditions, and in all cases we isolated a polycrystalline material that could not be further characterized. By following a similar synthetic procedure in Ni^{II} and Mn^{II} chemistry, we were able to isolate two new 1D-coordination polymers, namely $\{[M(bdc)(pyaoxH_2)_2] \cdot 2DMF\}_n$ (M = Ni, **2**; Mn, **3**). The formation of **2** and **3** is summarized in the stoichiometric Eq. (**2**).

$$M(NO_3)_2 \cdot xH_2O + 2\,pyaoxH_2 + H_2bdc \xrightarrow{DMF}$$
$$[M(bdc)(pyaoxH_2)_3]_n + 2\,H^+ + 2\,NO_3^- + x\,H_2O\ (2)$$
$$M = Ni, \mathbf{2}; Mn, \mathbf{3}$$
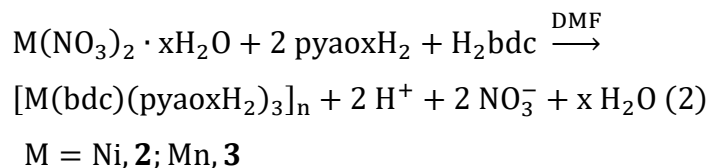
As a next step, we employed H3btc in the Ni^{II}/pyaoxH$_2$ and in the absence of base we were able to isolate the mononuclear compound $[Ni(H_2btc)_2(pyaoxH_2)_2] \cdot 2H_2O$ (**4**·2H$_2$O), whereas in the presence of excess of

CH$_3$ONa, we isolated and characterized the new 1D polymer [Ni(Hbtc)(pyaoxH$_2$)$_2$]$_n$ (**5**). It is noteworthy that **5** can be also formed by the reaction of **4**·2H$_2$O and CH$_3$ONa in a 1:3 M ratio in DMF. The stoichiometric equations of the reactions that lead to the synthesis of **4** and **5** are shown in the Eqs. (**3**) and (**4**).

$$Ni(ClO_4)_2 \cdot 6H_2O + 2\ pyaoxH_2 + 2\ H_3btc \xrightarrow{H_2O}$$
$$[Ni(H_2btc)_2(pyaoxH_2)_2]_n + 2\ H^+ + 2\ ClO_4^- + 6\ H_2O \ (3)$$
$$\textbf{4}$$

$$Ni(ClO_4)_2 \cdot 6H_2O + 2\ pyaoxH_2 + 2\ H_3btc \xrightarrow{H_2O}$$
$$[Ni(Hbtc)_2(pyaoxH_2)_2]_n + 2\ H^+ + 2\ ClO_4^- + 6\ H_2O \ (4)$$
$$\textbf{5}$$
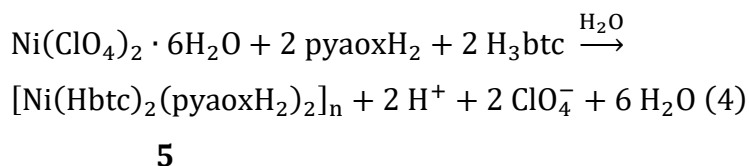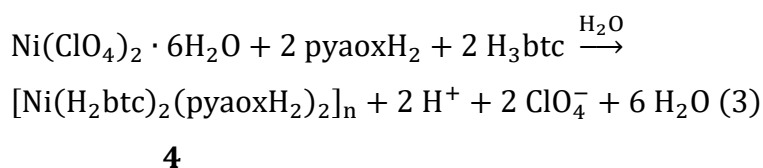
3.2. Description of structures

Representations of the molecular structures and supramolecular networks of **1**, **2**·DMF, **4**·2H2O and **5** are shown in **Figures 1–4**. Selected interatomic distances and angles are listed in **Tables 2–5**.

Compound **1** crystallizes in the triclinic space group P-*1*. Its that one of the free O atoms (O2) of the bdc^{2-} ligand is in close proximity to the metal ion (Zn1–O2 = 2.59(2) Å); although this is beyond the bonding distance range, the formation of a pseudo-bond could be considered. This is not the case for the second uncoordinated O atom (O4) in bdc^{2-} ligand, whose distance from the metal ion is

3.48(2) Å. Zn1 is 5-coordinate adopting a tetragonal pyramidal geometry (s = 0.3) with the O3, N1, O1, N2 atoms occupying the basal plane vertices and the O6 atom the apical position.[24]

The wavy-shaped chains in **1** are lying on parallel planes, which are vertical to the a axis. The distance between two Zn atoms of neighboring chains and of the same wave phase is 8.4 Å. The shortest $Zn\cdots Zn$ distance is 7.6 Å, being among two Zn atoms of neighboring chains and of an opposite wave phase. It is noteworthy that the shortest interchain metal$\cdots$metal distances (8.4 Å and 7.5 Å) are shorter than the intrachain ones (10.9 Å and 11.2 Å). The packing of the 1D chains lead to the formation of a 2D network (Fig. S1 in the Supplementary Material). Intrachain hydrogen bonds stabilize the crystal structure of **1**; these are formed between the oximic group (O5), which is the donor, and the carboxylic group of the bdc^{2-} ion (O4), which acts as the acceptor ($O5\cdots O4$ = 2.58(2) Å, $H1(O5)\cdots O4$ = 1.884(2) Å, $O5-H1(O5)\cdots O4$ = 169.89(8)°). Furthermore, interchain hydrogen bonds are formed between: (1) the amino N atom of the $pyaoxH_2$ ligand (N3) and the O atom belonging to a DMF molecule (O6) from a neighbouring chain ($N3\cdots O6$ = 3.14(2) Å, $H1(N3)\cdots O6$ = 2.461(2) Å, N3-$H1(N3)\cdots O6$ = 139.8°), and (2) the N3 atom and the carboxylate O atom (O2) from a different neighbouring chain, ($N3\cdots O2$ = 3.14(2) Å, $H2(N3)\cdots O2$ = 2.359 (2) Å, N3-$H2(N3)\cdots O2$ = 157.4°), stabilizing the supramolecular network in **1**.
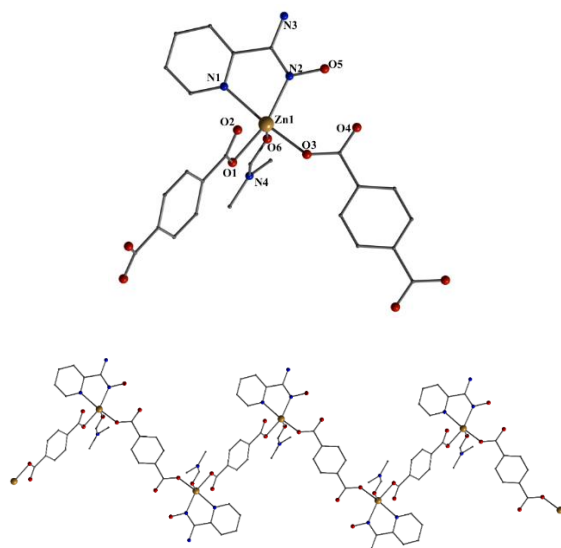
Figure 1. Representations of the repeating unit (top) and a part of the 1D chain of **1** (bottom). Colour code: Zn^{II}, orange; N, blue; O, red; C, grey. The hydrogen atoms are omitted for clarity.

Table 2 Selected interatomic distances (Å) and angles (°) for **1**.

Bonds			
Zn1-O3	2.0229	Zn1-O1	2.0280(16)
Zn1-N2	2.0528(19)	Zn1-O6	2.0989(17)
Zn1-N1	2.1944(18)		
Angles			
O3-Zn1-O1	90.06(7)	O3-Zn1-N2	99.18(7)

O1-Zn1-N2	153.24(8)	O3-Zn1-O6	94.34(7)
N2-Zn1-O6	107.48(7)	O3-Zn1-N1	171.75(8)
O1-Zn1-N1	92.96(7)	N2-Zn1-N1	75.09(7)
O6-Zn1-N1	92.11(7)		

2·2DMF crystallizes in the monoclinic space group P2_1/c. Its structure consists of [Ni(bdc)(pyaoxH$_2$)$_2$] repeating units, which result in the formation of a 1D chain, and DMF solvate molecules. The coordination sphere of the metal is completed by two neutral N,N'-bidentate chelating pyaoxH$_2$ ligands and two carboxylates. Ni1 is six coordinated with an octahedral coordination geometry. The coordination environment around the Ni^{2+} ion can be symbolized as {N$_4$O$_2$}, consisting of four N atoms coming from two different pyaoxH$_2$ ligands and two O atoms from two different carboxylates. The two O atoms, as well as the two pyridyl N atoms are displayed in a cis arrangement, while the two imine N atoms are placed in trans positions. The amino N and the oximic O atoms of each pyaoxH$_2$ ligand remain uncoordinated. The dicarboxylic ligand links two neighboring Ni^{2+} ions adopting a syn, syn- η^1:η^1: μ bridging fashion. **1** and **2·**2DMF possess similar structural features with their main difference being the replacement of the coordinated DMF molecule in **1** by a chelating pyaoxH$_2$ ligand in **2·**2DMF. This also results in the increase of the coordination number (cn) of the metal ion by one (**1**, cn = 5; **2**, cn = 6). The chains in **2·**2DMF are arranged in a parallel fashion along c axis, stabilized by two different intramolecular hydrogen bonding interactions: (1) The oximic group (O2, donor) of one of the pyaoxH$_2$ ligands is strongly hydrogen bonded to one O atom (O4,

acceptor) from the bdc^{2-} ligand (O2···O4 = 2.619(2) Å, H2(O2)···O4 = 1.802(2) Å, O2-H2(O2)···O4 = 174.87(7)°), and (2) N5 of the NH$_2$ group of one of the pyaoxH$_2$ ligands acts as the donor atom forming a hydrogen bond with the O8 atom of a lattice DMF molecule (N5···O8 = 2.926(2) Å, H1(N5)···O8 = 2.139(2) Å, N5-H1(N5)···O8 = 173.42(7)°). Similar to **1**, the packing of the 1D chains in **2·**2DMF lead to the formation of a 2D network (**Figure S2** in the Supplementary Material); in this case, all the metal atoms are located in the same plane with the shortest interchain metal···metal distance being 8.9 Å.
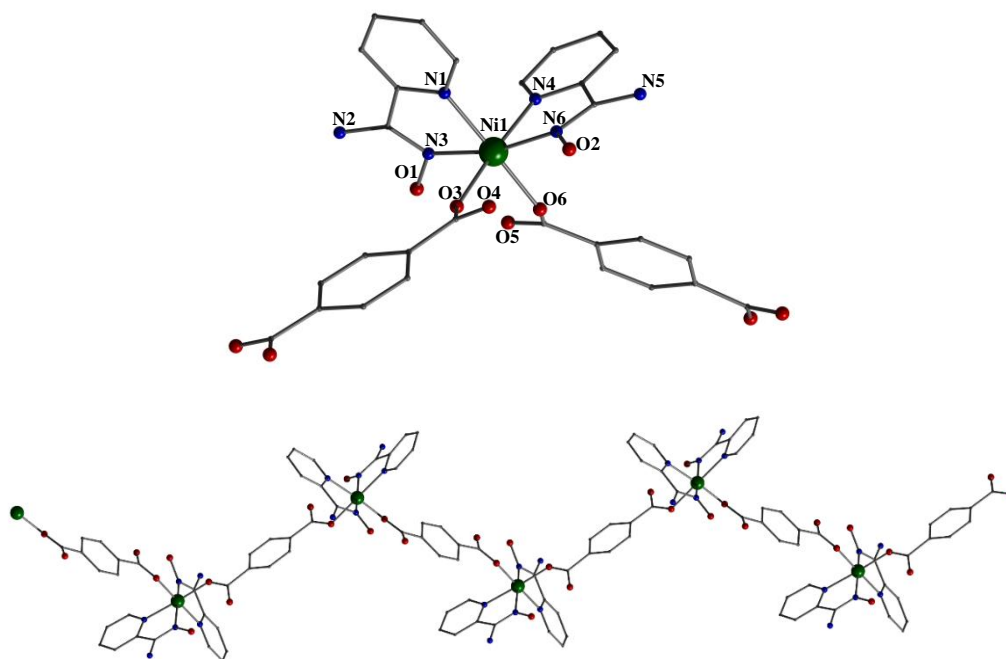
Figure 2. Representations of the repeating unit (top) and a part of the 1D chain of **2** (bottom). Colour code: Ni^{II}, green; N, blue; O, red; C, grey. The hydrogen atoms and solvent molecules are omitted for clarity.

Table 3 Selected interatomic distances (Å) and angles (°) for **2**.[a]

Bonds

Ni1-O3	2.0332(13)	Ni1-N6	2.0380(16)
Ni1-O6′	2.0432(13)	Ni1-N3	2.0492(16)
Ni1-N4	2.0962(16)	Ni1-N1	2.1084(16)

Angles

O3-Ni1-N6	101.72(6)	O3-Ni1-O6′	90.28(6)
N6-Ni1-O6′	87.55(6)	O3-Ni1-N3	87.30(6)
N6-Ni1-N3	166.91(7)	O6′-Ni1-N3	102.02(6)
O3-Ni1-N4	176.10(6)	N6-Ni1-N4	77.25(6)
O6′-Ni1-N4	85.92(6)	N3-Ni1-N4	94.36(6)
O3-Ni1-N1	89.24(6)	N6-Ni1-N1	93.37(7)
O6′-Ni1-N1	179.03(6)	N3-Ni1-N1	77.11(6)
N4-Ni1-N1	94.57(7)		

[a] Symmetry code: (′) = x, $\frac{1}{2}$-y, $\frac{1}{2}$+z

4·2H$_2$O crystallizes in the monoclinic space group P$2_1/n$ and its structure consists of two crystallographically independent mononuclear complexes with the formula [Ni(H$_2$btc)$_2$(pyaoxH$_2$)$_2$] and two lattice H$_2$O molecules. Each Ni^{II} atom is linked to two neutral N,N'-bidentate chelating pyaoxH$_2$ and two monodentate H$_2$btc$^-$ ions. The metal atom is six coordinated displaying an octahedral coordination geometry. The coordination sphere of **4** consists of four N donor atoms coming from two different chelating pyaoxH$_2$ ligands and two carboxylic O atoms belonging to two different tricarboxylic ligands. The two pyridyl N as well as the two O atoms adopt a cis arrangement, while the two imine N atoms of the oximic group are located on trans positions.

There is an amount of intramolecular and intermolecular hydrogen bonding that stabilize the crystal structure of **4**·2H$_2$O, involving the neutral carboxylic groups (O11 and O19) of the H$_2$btc$^-$ ions, the free NH$_2$ groups (N3 and N12) of the pyaoxH$_2$ ligands and the O atoms of the oximic groups (O2, O15, O1 and O16) as donors, and O atoms (O28, O8, O5, O25, O4, O24, O10 and O18) coming from different H$_2$btc$^-$ ions as acceptors. The metric parameters of the crystallographically established, independent hydrogen bonds are listed in Table S1 in the Supplementary Material.
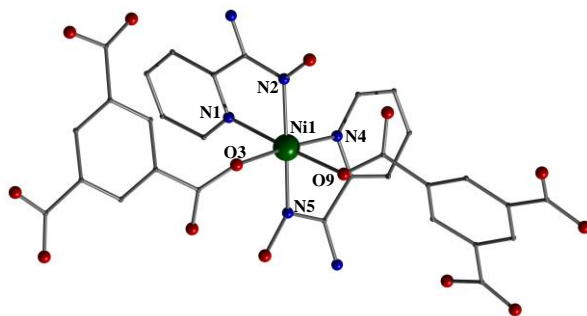
Figure 3. Representation of the molecular structure of **4**·2H2O. Colour code: Ni^{II}, green; N, blue; O, red; C, grey. The hydrogen atoms and solvate molecules are omitted for clarity.

Table 4 Selected interatomic distances (Å) and angles (°) for **4**·2H$_2$O.

Bonds			
Ni2-N11	2.051(2)	Ni2-N8	2.055(3)
Ni2-O17	2.064(2)	Ni2-N10	2.068(3)
Ni2-N7	2.069(3)	Ni2-O23	2.100(2)
Ni1-N2	2.044(3)	Ni1-N5	2.045(3)
Ni1-N4	2.068(3)	Ni1-O3	2.073(2)
Ni1-N1	2.078(3)	Ni1-O9	2.100(2)
Angles			
N11-Ni2-N8	173.69(12)	N11-Ni2-O17	98.45(9)

N8-Ni2-O17	85.44(10)	N11-Ni2-N10	77.69(10)
N8-Ni2-N10	98.52(11)	O17-Ni2-N10	175.95(10)
N11-Ni2-N7	97.39(11)	N8-Ni2-N7	77.84(10)
O17-Ni2-N7	86.17(10)	N10-Ni2-O23	87.25(10)
N7-Ni2-O23	175.30(9)	N2-Ni1-N5	173.76(12)
N2-Ni1-N4	98.41(11)	N5-Ni1-N4	77.74(10)
N2-Ni1-O3	85.97(10)	N5-Ni1-O3	97.98(10)
N4-Ni1-O3	175.53(10)	N2-Ni1-N1	77.57(10)
N5-Ni1-N1	97.78(11)	N4-Ni1-N1	95.33(11)
O3-Ni1-N1	86.44(10)	N2-Ni1-O9	98.35(9)
N5-Ni1-O9	86.42(10)	N4-Ni1-O9	87.07(10)
O3-Ni1-O9	91.44(9)	N1-Ni1-O9	175.51(10)
N1-Ni1-O9	175.51(10)		

5 crystallizes in the orthorhombic space group P$2_12_12_1$. Its structure consists of [Ni(Hbtc)(pyaoxH$_2$)$_2$] repeating units, which result in the formation of a 1D chain. The coordination sphere of the metal ion is completed by two neutral *N,N'*-bidentate chelating pyaoxH$_2$ ligands and two carboxylates. The repeating unit in

5 is similar to the discrete compound **4**·2H$_2$O with the only difference being that the carboxylate ion in **5** is doubly deprotonated, instead of singly deprotonated in **4**·2H$_2$O, linking the neighboring units. Ni is six coordinated with an octahedral coordination geometry. The coordination sphere of the metal ion in **5** can be symbolized as {N$_4$O$_2$}; the arrangement of the donor atoms is similar to that in **2**. The tricarboxylic ligand links two Ni^{2+} ions, adopting a syn, anti-η^1: η^1: μ bridging fashion. The two coordinated carboxylic groups are located in meta positions, while the third carboxylic group, which is protonated, remains uncoordinated.

There are strong intramolecular and intermolecular hydrogen bonding interactions in **5** with the former including neutral and deprotonated O atoms (O8 and O5) of two different Hbtc^{2-} ions, that act as donors and acceptors, respectively. The intermolecular hydrogen bonds are formed between oximic (O2) and free NH$_2$ (N2) groups of the pyaoxH$_2$ ligand and the O atom (O4, acceptor) of a Hbtc^{2-} ion from a neighboring chain. The metric parameters of the hydrogen bonds are listed in **Table S2** in the Supplementary Material. The supramolecular 2D network in **5** is similar to that in **2**·2DMF (**Figure S11**).
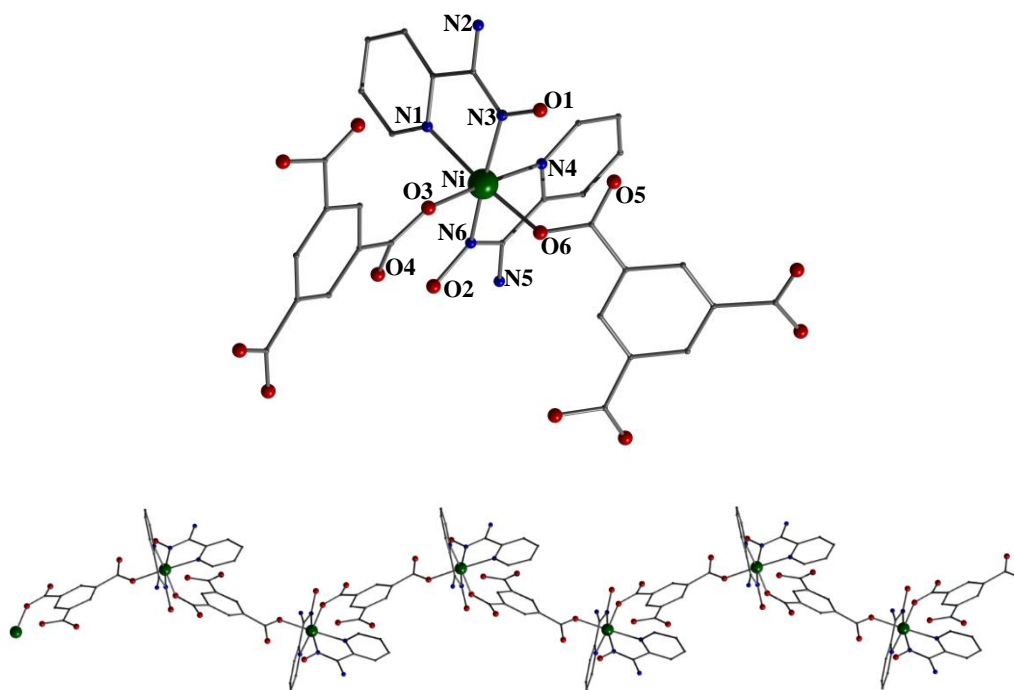
Figure 4. Representations of the repeating unit (top) and a part of the 1D chain of **5** (bottom). Colour code: Ni^{II}, green; N, blue; O, red; C, grey. The hydrogen atoms are omitted for clarity.

Table 5 Selected interatomic distances (Å) and angles (°) for **5**.

Bonds			
Ni1-N6	2.039(3)	Ni1-O3	2.042(2)
Ni1-N3	2.055(3)	Ni1-N4	2.088(3)
Ni1-O6	2.096(2)	Ni1-N1	2.128(3)

Angles			
N6-Ni1-O3	94.88(10)	N6-Ni1-N3	166.70(11)
O3-Ni1-N3	90.63(11)	N6-Ni1-N4	77.48(12)
O3-Ni1-N4	172.28(12)	N3-Ni1-N4	97.07(13)
N6-Ni1-O6	89.56(10)	O3-Ni1-O6	87.17(9)
N3-Ni1-O6	102.81(10)	N4-Ni1-O6	91.57(9)
N6-Ni1-N1	89.49(10)	N3-Ni1-N1	76.46(11)
N3-Ni1-N1	76.46(11)	N4-Ni1-N1	91.84(10)
O6-Ni1-N1	176.57(10)		

Compounds **1**–**3** and **5** are the first metal coordination polymers bearing pyaoxH$_2$ and rare examples of such species with any type of a 2-pyridyl oxime in general.[26] The identity, purity and stability of these compounds has been also studied by pxrd studies (**Figures S3–S6** in the Supplementary Material).

3.3. Photoluminescence studies

The solid state emission spectra of **1** was recorded at room temperature. Upon excitation at 325 nm, **1** shows a maximum emission peak at 440 nm and a visible shoulder at 467 nm (**Figure 5**), which can be assigned to the coordinated

pyaoxH$_2$ and bdc^{2-} ligands, respectively.[14b,25] Note that the free H$_2$bdc and pyaoxH$_2$ ligands are non-luminescent. The origin of the photoluminescence of **1** is likely coming from an intra-ligand π–π*⁄ or n-π⁄ transition.[14b, 25]

The photoluminescence properties of **1** are in good agreement with the literature. In particular, two mononuclear Zn^{2+} complexes have been reported bearing a chelate pyaoxH$_2$ ligand and two terminal carboxylates (acetate and benzoate); these compounds have been found to exhibit photoluminescence at 406 nm upon excitation at 345 nm.[25] The peak at 440 nm in **1** is red-shifted compared to that of the mononuclear complexes, which could be attributed to the more rigid coordination environment of the metal in the polymeric chain. Furthermore, a three dimensional Zn^{2+} coordination polymer, containing the bdc^{2-} ligand, displays emission at 452 nm upon excitation at 330 nm.[14b]
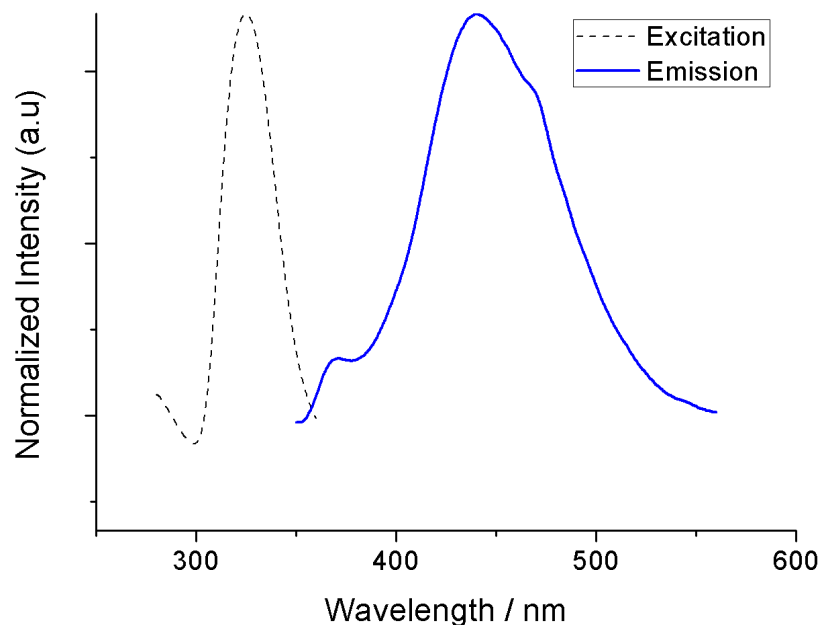
Figure 5. Excitation (---) and PL emission (…) spectrum of **1**.

3.4. Thermal stability studies

The thermal stability properties of **1**, **2**·2DMF, **4**·2H$_2$O, and **5** have been studied by using the thermogravimetric analysis (TGA) technique in temperature range 20–600 °C and heating rate 10 °C min^{-1}. The TGA curves for these compounds are shown in the Supplementary Material (**Figures S7–S10**).

The TGA plot for **1** shows a gradual weight loss of 19.6% from 20 °C to 355 °C, which corresponds to the loss of two H$_2$O molecules and the terminally ligated DMF molecule; the former can be assigned to solvate molecules that have not been crystallographically located, or humidity. The following weight decrease of 53% (between 355 °C and 522 °C) is associated with the loss of one bdc^{2-} and one pyaoxH$_2$ ligands, leading to the full deterioration of the polymeric chain. In the case of **2**, a plateau is observed in the temperature range 20 °C to 157 °C, followed by a weight loss of 16% up to 229 °C, which corresponds to the removal of the two DMF lattice molecules. A second mass loss of 68% (290 °C–582 °C) reveals the thermal decomposition of the polymer; this corresponds to the loss of the two bdc^{2-} and two pyaoxH$_2$ ligands.

The latter occurs in two steps as revealed by the two different slopes in Fig. S8. The first one lies in the range of 290 °C to 340 °C and corresponds to a mass decrease of 30%, indicative of the removal of the chelating pyaoxH$_2$ ligand; the second step is associated with the decomposition of the 1D chain (mass loss: 38%). **5** displays a thermal stability from 20 °C to 341 °C followed by the decomposition of the compound. The absence of the lattice solvent molecules in **5** is in agreement with the elemental analysis and the crystal structure of the compound.

0D compound **4** loses two H$_2$O lattice molecules between 121 and 171 °C (mass loss: 4.4%). Then, there is a plateau from 171 °C to 281 °C followed by the

destruction of the complex upon the removal of the organic ligands. The temperature range from 121 °C to 171 °C, in which the removal of the two H_2O molecules occurs, is an indication of the strong hydrogen bonding interactions between the H_2O molecules and the polymeric chains in **4**. It is noteworthy that the mononuclear complex **4** is the least thermally stable compared to the one dimensional coordination polymers **1**, **2**·2DMF, and **5**; this is a proof of the enhanced stability and rigidity an infinite polymeric chain or network can provide.

4. Conclusions

The study of the ligand blend pyaoxH$_2$/H$_2$bdc or H$_3$btc has afforded the mononuclear compound [Ni(H$_2$btc)$_2$(pyaoxH$_2$)$_2$]·2H$_2$O (**4**·2H$_2$O), as well as four 1D coordination polymers [Zn(bdc)(pyaoxH$_2$)(DMF)]$_n$ (1), {[Ni(bdc)(pyaoxH$_2$)$_2$]·2DMF}$_n$ (**2**·2DMF), [Mn(bdc)(pyaoxH$_2$)$_2$]·2DMF}$_n$ (**3**·2DMF) and {[Ni(Hbtc)(pyaoxH$_2$)$_2$}$_n$ (**5**). The coordination chemistry of 2-pyridyl oximes with polycarboxylic acids is rather unexplored and, as such the reported compounds are unusual examples of metal coordination polymers with any type of this family of oximic ligands and the first examples of such species with pyaoxH$_2$ or its anions.[26] The polymerization of **4**·2H$_2$O has been also achieved through its reaction with an excess of base, which provided access to **5**. The repeating units in **1**–**3** and **5** are held together through bridging carboxylates (bdc^{2-} in **1**, **2**·2DMF and **3**·2DMF; Hbtc^{2-} in **5**), whereas the pyaoxH$_2$ ligand is neutral adopting a *N,N'*-bidentate chelating mode in all cases. Thermogravimetric and pxrd studies confirmed the stability and purity of the compounds. Photoluminescence studies were performed in **1**, which showed a

maximum emission peak at 440 nm and a visible shoulder at 467 nm, assigned to the pyaoxH$_2$ and bdc^{2-} ligands, respectively.[14b,25] The isolation of compounds **1**–**5** demonstrates the potential of the essentially unexplored coordination chemistry of the 2-pyridyl oximes in combination with polycarboxylic acids to become a fruitful source of new coordination polymers. Further studies towards the synthesis of coordination polymers with higher dimensionality (2D, 3D) are currently in progress and will be reported in due course.

Acknowledgement

Appendix A. Supplementary data

CCDC 1832944–1832947 contains the supplementary crystallographic data for **1**, **2**·2DMF, **4**·2H2O, and **5**, respectively. These data can be obtained free of charge via *HTTP://WWW.CCDC.CAM.AC.UK/CONTS/RETRIEVING.HTML*, or from the Cambridge Crystallographic Data Centre, 12 Union Road, Cambridge CB2 1EZ, UK; fax: (+44)1223-336-033; or e-mail: *DEPOSIT@CCDC.CAM.AC.UK*. Supplementary data associated with this article can be found, in the online version, at *HTTPS://DOI.ORG/10.1016/J.POLY.2018.05.027*.

References

1. a) Li, B.; Wen, H.-M.; Zhou, W.; Chen, B. *J. Phys. Chem. Lett.* **2014** 5 (20), 3468. b) Yang, X.; Xu, Q. *Cryst. Growth Des.* **2017** 17 (4), 1450. c) Li, H.;

Wang, K.; Sun, Y.; Lollar, C.T.; Li, J.; Zhou, H.-C. *Mater. Today* **2018** 21 108.

2. a) Qin, J.-S.; Du, D.-Y.; Guan, W.; Bo, X.-J.; Li, Y.-F.; Guo, L.-P.; Su, Z.-M.; Wang, Y.-Y.; Lan, Y.-Q.; Zhou, H.-C. *J. Am. Chem. Soc.* **2015** 137, 7169. b) Ma, L.; Falkowski, J.M.; Abney, C.; Lin, W. *Nat. Chem.* **2010** 2, 838.

3. a) Hu, Z.; Deibert, B.J.; Li, J.; *Chem. Soc. Rev.* **2014** 43, 5815. b) Douvali, A.; Tsipis, A.C.; Eliseeva, S.V.; Petoud, S.; Papaefstathiou, G.S.; Malliakas, C.D.; Papadas, I.; Armatas, G.S.; Margiolaki, I.; Kanatzidis, M.G.; Lazarides, T.; Manos, M.J. *Angew. Chem. Int. Ed.* **2015** 54,1651.

4. a) Wu, M.-X. ; Yang, Y.-W. *Adv. Mater.* **2017** 29,1606134. b) Huxford, R.C.; Rocca, J.D.; Lin, W. *Curr. Opin. Chem. Biol.* **2010** 14 (2),262.

5. a) Ugale, B.; Singh Dhankhar, S.; Nagaraja, C. M. *Cryst. Growth Des.* **2017** 17 (4), 3295. b) Manos, M.J.; Markoulides, M.S.; Malliakas, C.D.; Papaefstathiou, G. S.; Chronakis, N.; Kanatzidis, M.G.; Trikalitis, P.N.; Tasiopoulos, A.J. *Inorg. Chem.* **2011** 50,11297. c) Sezginel, K.B.; Feng, T.; Wilmer, C.E. *Cryst. Eng. Comm.* **2017** 19, 4497.

6. a) Alhamami, M.; Doan, H.; Cheng, C.-H. *Materials* **2014** 7,3198. b) Nouar, F.; Devic, T.; Chevreau, H.; Guillou, N. ; Gibson, E.; Clet, G.; Daturi, M.; Vimont, A.; Grenèche, J.M.; Breeze, M.I.; Walton, R.I.; Llewellyne, P.L.; Serre, C. *Chem. Commun.* **2012** 48,10237.

7. a) Coulon, C.; Miyasaka, H.; Clérac, R. *Struct. Bonding* **2006** 122, 163. b) Jeon, I.-R.; Clérac, R. *Dalton Trans.* **2012** 9569. c) Miyasaka, H.; Julve, M.; Yamashita, M.; Clérac, R. *Inorg. Chem.* **2009** 48, 3420. d) Bernot, K.; Luzon, J.; Sessoli, R.; Vindigni, A.; Thion, J.; Richeter, S.; Leclercq, D.; Larionova,

J.; Van der Lee, A. *J. Am. Chem. Soc.* **2008** 130, 1619. e) Wang, T.-T.; Ren, M.; Bao, S.-S.; Liu, B.; Pi, L.; Cai, Z.-S.; Zheng, Z.-H.; Xu, Z.-L.; Zheng, L.- M. *Inorg. Chem.* **2014** 53, 3117. f) Gatteschi, D.; Sessoli, R. *Angew. Chem. Int. Ed.* **2003** 42, 268. g) Papatriantafyllopoulou, C.; Zartilas, S.; Manos, M.J.; Pichon, C.; Clérac, R.; Tasiopoulos, A.J. *Chem. Commun.* **2014** 50,14873.

8. a) Schoedel, A.; Li, M.; Li, D.; O'Keeffe, M.; Yaghi, O.M. *Chem. Rev.* **2016** 116,12466. b) Kuppler, R.J.; Timmons, D.J.; Fang, Q.-R.; Li, J.-R.; Makal, T.A.; Young, M.D.; Yuan, D.; Zhao, D.; Zhuang, W.; Zhou, H.-C. *Coord. Chem. Rev.* **2009** 253, 3042. c) Furukawa, H.; Cordova, K.E.; O'Keeffe, M.; Yaghi, O.M. *Science* **2013** 341,974.

9. a) Bogani, L.; Wernsdorfer, W. *Nat. Mater.* **2008** 7, 179. b) Leuenberger, M.N.; Loss, D. *Nature* **2001** 410,789.

10. a) Kitagawa, S.; Noro, S. *Comprehensive Coordination Chemistry II Vol. 7, Ch. 7.2, Elsevier256, Amsterdam,* **2004**, 231. b) Batten, S.R.; Champness, N.R.; Chen, X.-M.; Garcia-Martinez, J.; Kitagawa, S.; Ohrstrom, L.; O'Keeffe, M.; Paik Suh, M.; Reedijk, J. *Cryst. Eng. Comm.* **2012** 14, 3001.

11. Papatriantafyllopoulou, C.; Raptopoulou, C.P.; Terzis, A.; Janssens, J.F.; Manessi- Zoupa, E.; Perlepes, S.P.; Plakatouras, J.C. *Polyhedron* **2007** 26, 4053.

12. Pokhodnya, K.I.; Epstein, A.J.; Miller, J.S. *Adv. Mater.* **2000** 12, 410.

13. a) Representative examples: Zhao, X.-L.; Sun W.-Y. *Cryst. Eng. Comm* **2014** 16, 3247. b) Kourtellaris, A.; Moushi, E.E.; Spanopoulos, I.; Tampaxis, C.; Charalambopoulou, G.; Steriotis, T.A.; Papaefstathiou, G.S.; Trikalitis, P.N.; Tasiopoulos, A.J. *Inorg. Chem. Front.* **2016** 3, 1527. c) Chen, Z.; Adil,

K.; Weselinski, L.J.; Belmabkhout, Y.; Eddaoudi, M. *J. Mater. Chem. A* **2015** 3, 6276. d) Moushi, E.E.; Kourtellaris, A.; Spanopoulos, I.; Manos, M.J.; Papaefstathiou, G.S.; Trikalitis, P.N.; Tasiopoulos, A.J. *Cryst. Growth Des.* 2**2015** 15, 185. e) Chandrasekhar, V.; Mohapatra, C.; Metre, R. *Cryst. Growth Des.* **2013** 13, 4607. f) Chen, M.-S.; Chen, M.; Takamizawa, S.; Okamura, T.; Fan, J.; Sun, W.-Y. *Chem. Commun.* **2011** 47, 3787.

14. a) Representative examples and references therein: Li, H.; Eddaoudi, M.; O'Keeffe, M.; Yaghi O.M. *Nature* **1999** 402, 276. b) Sapchenko, S.A.; Dybtsev, D.N.; Damsonenko, D.G.; Fedin, V.P. *New J. Chem.* **2010** 34, 2445. c) Tranchemontagne, D.J.; Hunt, J.R.; Yaghi, O.M. *Tetrahedron* **2008** 64, 8553. d) Clausen, H.F.; Poulsen, R.D.; Bond, A.D.; Chevallier, M.-A.S.; Iversen, B.B. *J. Solid State* **2005** 178, 3342.

15. a) Representative examples and references therein: Davies, K.; Bourne, S.A.; Öhrströmb, L.; Oliver C.L. *Dalton Trans.* **2010** 39, 2869. b) Manos, M.J.; Moushi, E.E.; Papaefstathiou, G.S.; Tasiopoulos, A.J. *Cryst. Growth Des.* **2012** 12 (11), 5471; c) Guesh, K.; Caiuby, C.A.D.; Mayoral, Á.; Díaz-García, M.; Díaz, I.; Sanchez- Sanchez, M. *Cryst. Growth Des.* **2017** 17 (4), 1806. d) Horcajad, P.; Surblé, S.; Serre, C.; Hong, D.-Y.; Seo, Y.-K.; Chang, J.-S.; Grenèche, J.-M.; Margiolaki, I.; Férey, G. *Chem. Commun.* **2007** 2820.

16. a) Chaudhuri, P. *Coord. Chem. Rev.* **2003** 243, 143. b) Pombeiro, A.J.L.; Yu Kukushkin, V. *Comprehensive Coordination Chemistry II, Elsevier, Amsterdam,* **2004** 631–637. c) Milios, C.J.; Piligkos, S.; Brechin, E.K. *Dalton Trans.* **2008** 1809. d) Pathmalingam, T.; Gorelsky, S.I.; Burchell, T.J.; Bédard, A.-C.; Beauchemin, A.M.; Clérac, R.; Murugesu, M. *Chem. Commun.* **2008** 2782. e) Milios, C.J.; Vinslava, A.; Wernsdorfer, W.;

Moggach, S.; Parsons, S.; Perlepes, S.P.; Christou, G.; Brechin, E.K. *J. Am. Chem. Soc.* **2007** 129, 2754. f) Jones, L.F.; Prescimone, A.; Evangelisti, M.; Brechin, E.K. *Chem. Commun.* **2009** 2023.

17. For a comprehensive review, see: Milios, C.J.; Stamatatos, T.C.; Perlepes S.P. *Polyhedron* **2006** 25, 134.

18. a) Stamatatos, T.C.; Foguet-Albiol, D.; Stoumpos, C.C.; Raptopoulou, C.P.; Terzis, A.; Wernsdorfer, W.; Perlepes, S.P.; Christou, G. *Polyhedron* **2007** 26, 2165. b) Stamatatos, T.C.; Foguet-Albiol, D.; Stoumpos, C.C.; Raptopoulou, C.P.; Terzis, A.; Wernsdorfer, W.; Perlepes, S.P.; Christou, G. *J. Am. Chem. Soc.* **2005** 127, 15380. c) Escuer, A.; Vlahopoulou, G.; Mautner, F.A. *Inorg. Chem.* **2011** 50, 2717. d) Mowson, A.M.; Nguyen, T.N.; Abboud, K.A.; Christou, G. *Inorg. Chem.* **2013** 52, 12320. e) Nguyen, T.; Wernsdorfer, W.; Abboud, K.A.; Christou, G. *J. Am. Chem. Soc.* **2011** 133, 20688. f) Nguyen, T.N.; Shiddiq, M.; Ghosh, T.; Abboud, K.A.; Hill, S.; Christou, G. *J. Am. Chem. Soc.* **2015** 137, 7160. g) Nguyen, T.N.; Wernsdorfer, W.; Shiddiq, M.; Abboud, K.A.; Hill, S.; Christou, G. *Chem. Sci.* **2016** 7,1156.

19. a) Papatriantafyllopoulou, C.; Jones, L.F.; Nguyen, T.D.; Matamoros-Salvador, N.; Cunha-Silva, L.; Almeida Paz, F.A.; Rocha, J.; Evangelisti, M.; Brechin, E.K.; Perlepes, S.P. *Dalton Trans.* **2008** 3153. b) Efthymiou, C.G.; Cunha-Silva, L.; Perlepes, S.P.; Brechin, E.K.; Inglis, R.; Evangelisti, M.; Papatriantafyllopoulou, C. *Dalton Trans.* **2016** 17409.

20. Bernasek, E. *J. Org. Chem.* **1957** 22, 1263.

21. Sheldrick, G.M. *Acta Crystallogr., Sect. A: Found. Adv.* **2015** 71, 3.

22. McArdle, P.; Gilligan, K.; Cunningham, D.; Dark, R.; Mahon, M. *Cryst. Eng. Comm.* **2004** 6, 303.

23. Brandenburg, K. *DIAMOND, Version 2003.2001d, Crystal Impact GbR, Bonn, Germany*, **2006**.

24. Addison, A.W.; Rao, T.N.; Reedijk, J.; Rijn, J.v.; Verschoor, G.C. *J. Chem. Soc., Dalton Trans* **1984** 1346.

25. Konidaris, K.F.; Bekiari, V.; Katsoulakou, E.; Raptopoulou, C.P.; Psycharis, V.; Perlepes, S.P.; Stamatatos, T.C.; Manessi-Zoupa, E. *Inorg. Chim. Acta* **2011** 376, 470.

26. Croitor, L.; Coropceanu, E.B.; Siminel, A.V.; Masunov, A.E.; Fonari, M.S. *Polyhedron* **2013** 60, 140.

Supplementary Material

Table S1. Metric parameters of the hydrogen bonding interactions in **4**·$2H_2O$.

D-H···A	D···A (Å)	H···A (Å)	D-H···A (°)
N12-H2(NA)···O25	3.036	2.261	158.80
O1-H1(O1)···O10	2.604	1.790	171.49
O2-H1(O2)···O4	2.595	1.782	170.90
O15-H15···O24	2.601	1.785	172.86
O16-H16(A)···O18	2.593	1.780	171.79
O11-H11(O)···O28	2.621	1.825	163.19

| O19-H19···O8 | 2.624 | 1.841 | 159.64 |

Table S2. Metric parameters of the hydrogen bonding interactions in **5**.

D-H···A	D···A (Å)	H···A (Å)	D-H···A (°)
O2-H1(O2)···O4	2.622	1.751	170.93
N2-H2(N2)···O4	2.896	2.040	170.42
O8-H1(O8)···O5	2.634	1.865	155.62
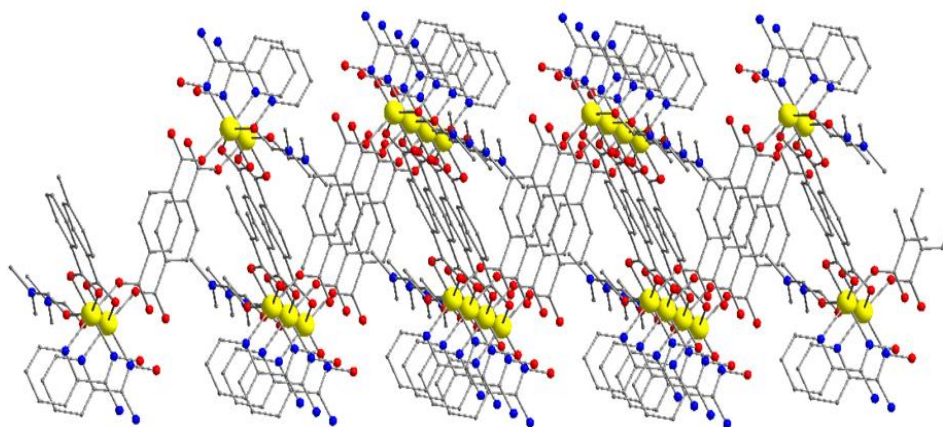
Figure S1. Representation of the two dimensional network in **1**.
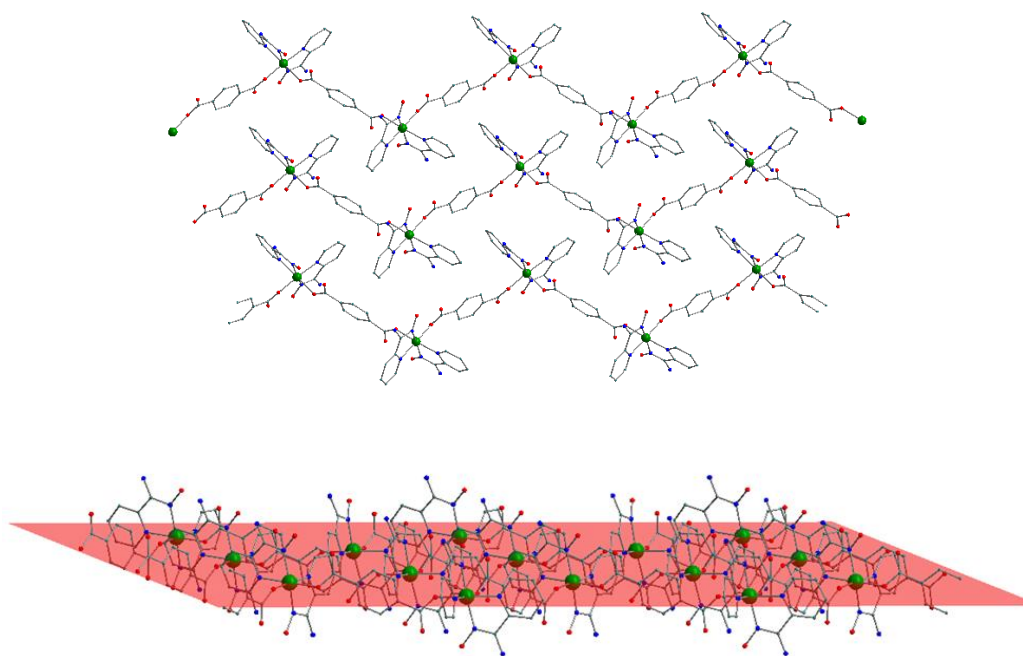
Figure S2. Different views of the 2D network in **2**·2DMF.
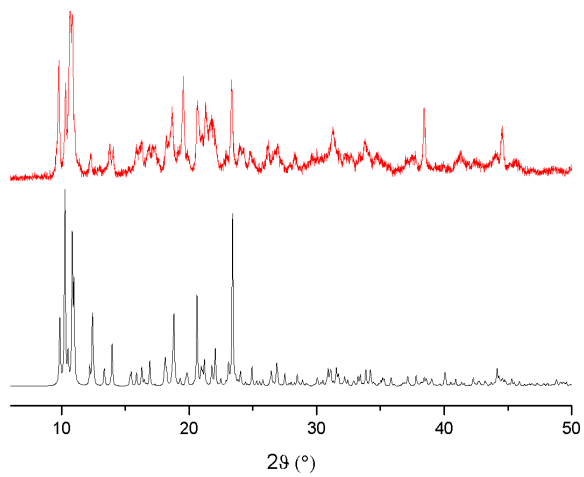
Figure S3. The theoretical (bottom) and experimental (top) pxrd pattern diagrams for **1**.
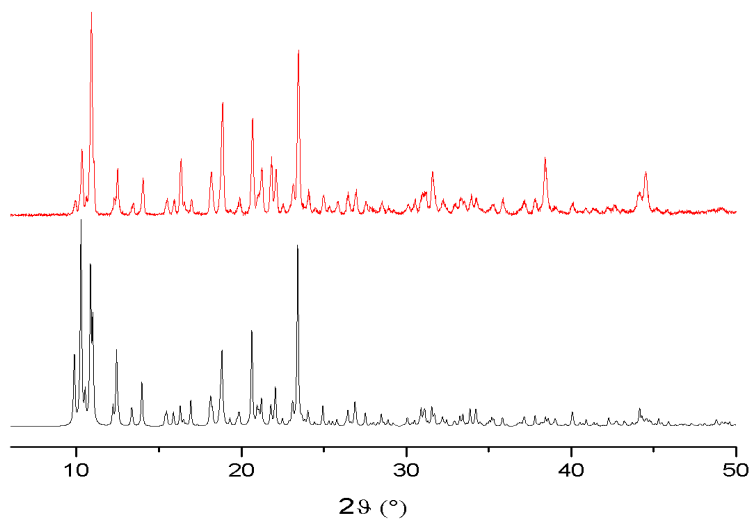
Figure S4. The theoretical (bottom) and experimental (top) pxrd pattern diagrams for **2**.2DMF.
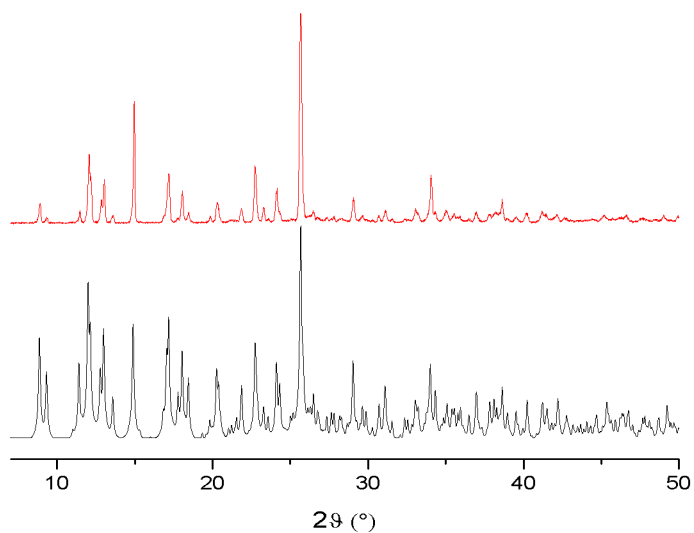
Figure S5. The theoretical (bottom) and experimental (top) pxrd pattern diagrams for **4.**2H$_2$O.
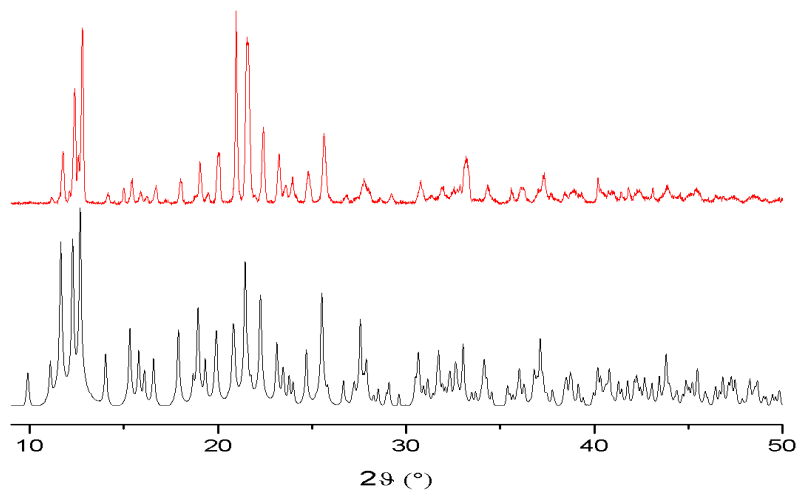
Figure S6. The theoretical (bottom) and experimental (top) pxrd pattern diagrams for **5**.
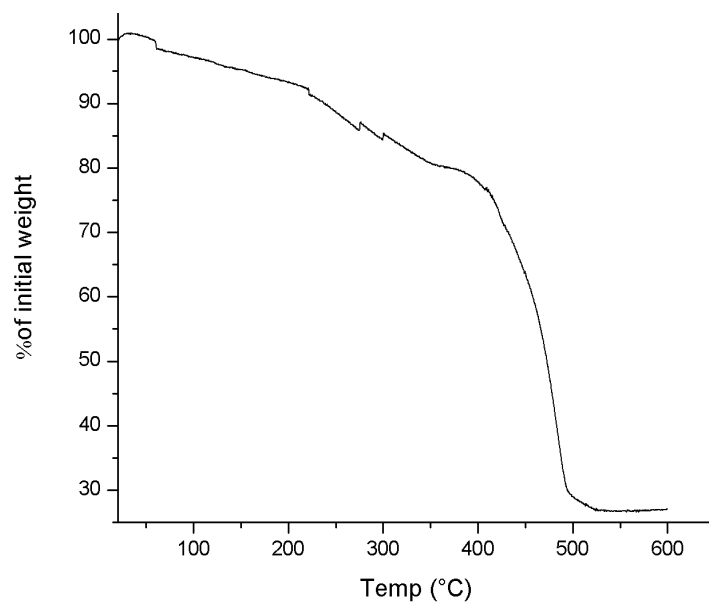
Figure S7. The TGA diagram for **1**.
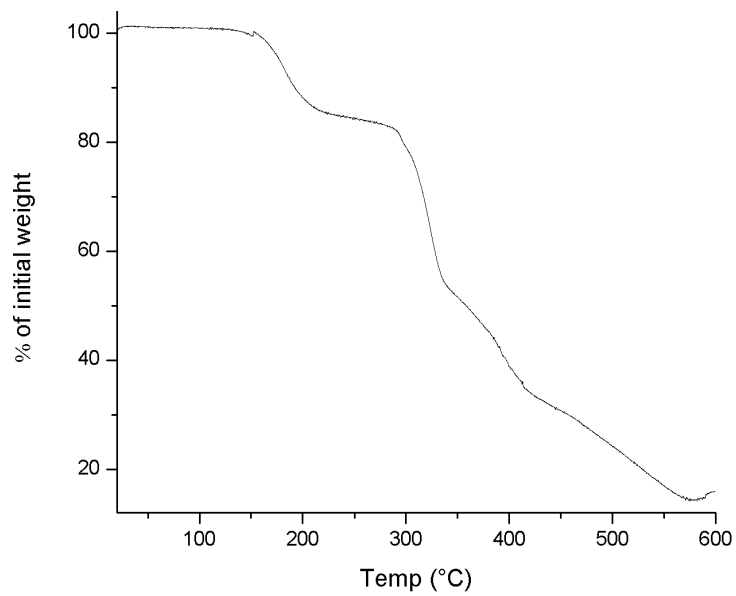
Figure S8. The TGA diagram for **2**.
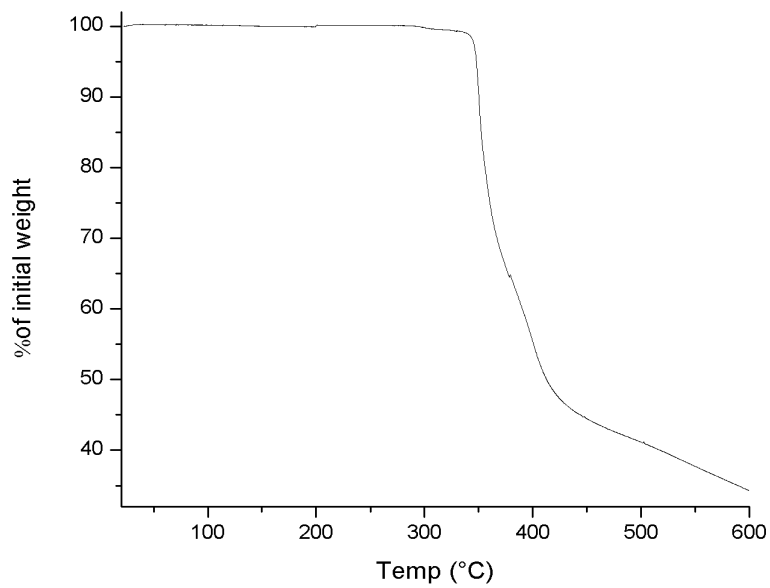
Figure S9. The TGA diagram for compound **5**.
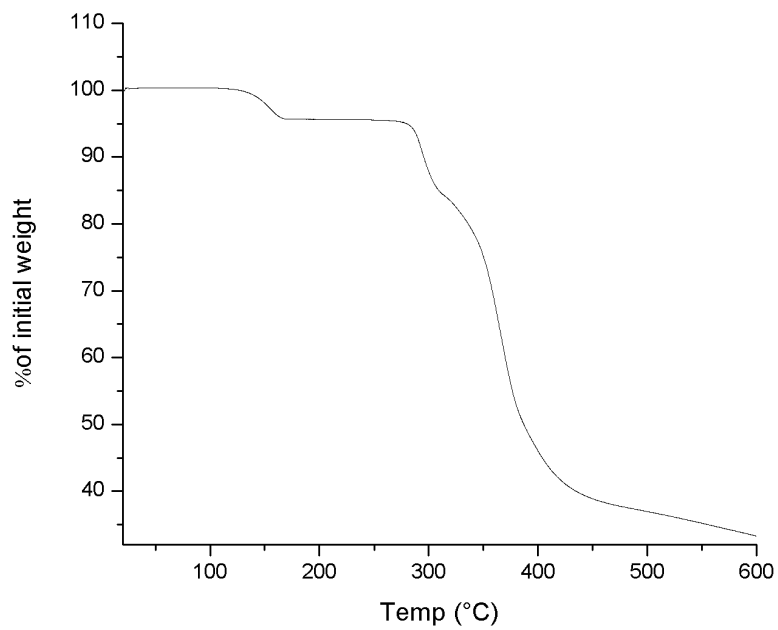
Figure S10. The TGA diagram for **4**.
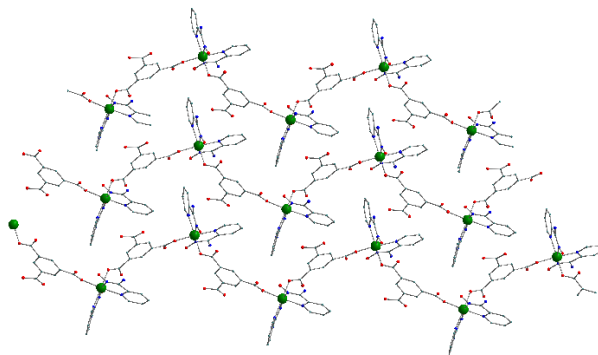
Figure S11. The 2D supramolecular network in **5**.

2.2 Brief description of the paper

In this article are represented the synthetic approach of using 1D coordination polymer for the formation of MOFs, the synthesis of novel MOFs and the use of a Cu4-MOF as a magnetic sensor for the selective encapsulation of Fe(III).

Open Access | Article

From 1D Coordination Polymers to Metal Organic Frameworks by the Use of 2-Pyridyl Oximes

by Ioannis Mylonas-Margaritis [1] ✉ 🆔, Auban Gérard [1] ✉, Katerina Skordi [2] ✉, Julia Mayans [3] ✉ 🆔, Anastasios Tasiopoulos [2] ✉, Patrick McArdle [1] ✉ and Constantina Papatriantafyllopoulou [1,*] ✉

[1] School of Chemistry, College of Science and Engineering, National University of Ireland Galway, SSPC, Synthesis and Solid State Pharmaceutical Centre, University Road, Galway H91 TK33, Ireland
[2] Department of Chemistry, University of Cyprus, 1678 Nicosia, Cyprus
[3] Instituto de Ciencia Molecular (ICMol), Universidad de Valencia, Catedrático José Beltran 2, 46980 Paterna (Valencia), Spain
* Author to whom correspondence should be addressed.

Download PDF | Browse Figures | Citation Export

Abstract

The synthesis and characterization of coordination polymers and metal–organic frameworks (MOFs) has attracted a significant interest over the last decades due to their fascinating physical properties, as well as their use in a wide range of technological, environmental, and biomedical applications. The initial use of 2-pyridyl oximic ligands such as pyridine-2 amidoxime (H_2pyaox) and 2-methyl pyridyl ketoxime (Hmpko) in combination with 1,2,4,5-benzene tetracarboxylic acid (pyromellitic acid), H_4pma, provided access to nine new compounds whose structures and properties are discussed in detail. Among them, [Zn_2(pma)(H_2pyaox)$_2$(H_2O)$_2$]$_n$ (3) and [Cu_4(OH)$_2$(pma)(mpko)$_2$]$_n$ (9) are the first MOFs based on a 2-pyridyl oxime with 9 possessing a novel 3,4,5,8-c net topology. [Zn_2(pma) (H_2pyaox)$_2$]$_n$ (2), [Cu_2(pma)(H_2pyaox)$_2$(DMF)$_2$]$_n$ (6), and [Cu_2(pma)(Hmpko)$_2$(DMF)$_2$]$_n$ (8) join a small family of coordination polymers containing an oximic ligand. 9 exhibits selectivity for Fe^{III} ions adsorption, as was demonstrated by a variety of techniques including UV-vis, EDX, and magnetism. DC magnetic susceptibility studies in 9 revealed the presence of strong antiferromagnetic interactions between the metal centers, which lead to a diamagnetic ground state; it was also found that the magnetic properties of 9 are affected by the amount of the encapsulated Fe^{3+} ions, which is a very desirable property for the development of magnetism-based sensors.

Keywords: coordination polymers; metal–organic frameworks (MOFs); carboxylates; pyridyl oximes; mixed-ligand; detection; encapsulation; iron(III); magnetism

Author's contribution:

I. Mylonas-Margaritis: All the synthetic work, preparation of first draft, tables, figures.

A. Gerard: UV- studies.

K. Skordi, Prof. A. J. Tasiopoulos, Prof. Patrick McArdle: Collection and analysis of the crystallographic data.

Dr. J. Mayans: Magnetic Studies

Dr. Constantina Papatriantafyllopoulou: Managed the project **and** reviewed the manuscript before the submission and during the revision process.

From 1D Coordination Polymers to Metal Organic Frameworks by the Use of 2-Pyridyl Oximes

Ioannis Mylonas-Margaritis [1], Auban Gérard [1], Katerina Skordi [2], Julia Mayans [3], Anastasios Tasiopoulos [2], Patrick McArdle [1] and Constantina Papatriantafyllopoulou [1,*]

1 School of Chemistry, College of Science and Engineering, National University of Ireland Galway, SSPC, Synthesis and Solid State Pharmaceutical Centre, University Road, Galway H91 TK33, Ireland; *I.MYLONAS-MARGARITIS1@NUIGALWAY.IE* (I.M.-M.); *AUBAN.GERARD@UHA.FR* (A.G.); *PATRICK.MCARDLE@NUIGALWAY.IE* (P.M.)

2 Department of Chemistry, University of Cyprus, 1678 Nicosia, Cyprus; *SKORDI.KATERINA@UCY.AC.CY* (K.S.); *ATASIO@UCY.AC.CY* (A.T.)

3 Instituto de Ciencia Molecular (ICMol), Universidad de Valencia, Catedrático José Beltran 2, 46980 Paterna (Valencia), Spain; *JULIA.MAYANS@QI.UB.EDU*

* Correspondence: *CONSTANTINA.PAPATRIANTAFYLLOPO@NUIGALWAY.IE*; Tel.: +353-91-493462

Abstract

The synthesis and characterization of coordination polymers and metal–organic frameworks (MOFs) has attracted a significant interest over the last decades due to their fascinating physical properties, as well as their use in a wide range of technological, environmental, and biomedical applications. The initial use of 2-pyridyl oximic ligands such as pyridine-2 amidoxime (pyaox H_2) and 2-methyl pyridyl ketoxime (mpkoH) in combination with 1,2,4,5-benzene tetracarboxylic acid (pyromellitic acid), H_4pma, provided access to nine new compounds whose structures and properties are discussed in detail. Among them, $[Zn_2(pma)(pyaoxH_2)_2(H_2O)_2]_n$ (**3**) and $[Cu_4(OH)_2(pma)(mpko)_2]_n$ (**9**) are the first MOFs based on a 2-pyridyl oxime with **9** possessing a novel 3,4,5,8-c net topology. $[Zn_2(pma)(pyaoxH_2)_2]_n$ (**2**), $[Cu_2(pma)(pyaoxH_2)_2(DMF)_2]_n$ (**6**), and

$[Cu_2(pma)(mpkoH)_2(DMF)_2]_n$ (**8**) join a small family of coordination polymers containing an oximic ligand. **9** exhibits selectivity for Fe^{III} ions adsorption, as was demonstrated by a variety of techniques including UV-vis, EDX, and magnetism. DC magnetic susceptibility studies in **9** revealed the presence of strong antiferromagnetic interactions between the metal centers, which lead to a diamagnetic ground state; it was also found that the magnetic properties of **9** are affected by the amount of the encapsulated Fe^{3+} ions, which is a very desirable property for the development of magnetism-based sensors.

1. Introduction

The synthesis and characterization of metal coordination polymers has attracted an intense research interest over the recent years due to their applications in a variety of fields, including catalysis, drug delivery sensing, etc.[1–7]. The structure of such species is based on mononuclear or low nuclearity inorganic units that are held together through organic ligands forming multidimensional networks whose properties are strongly affected by the nature of the metal ions and the organic linkers. For example, 1D coordination polymers of paramagnetic metal ions can display single chain magnetism (SCM) behavior, i.e., they can exhibit slow relaxation of magnetization stemming from strong intrachain exchange interactions between high spin structural building units along the chain.[8–14] SCMs are excellent candidates for applications in high-density information storage, molecular spintronics, quantum computation, etc.[15–21]. As the dimensionality of the network increases, the induced porosity can be combined

with magnetism and/or another physical property (e.g., photoluminescence, etc.), leading to the development of hybrid multifunctional materials. The synergistic effect between two different properties often enhances the performance of such species in a variety of significant applications including sensing, catalysis, drug delivery, spintronics, photonics, and others.

One growing family of multifunctional materials is the one of metal–organic frameworks (MOFs) [22–24]; MOFs are crystalline porous materials built from inorganic secondary building units (SBUs) that are connected through polytopic organic linkers. They display a range of appealing structural features such as large surface area, high porosity, flexible structure, an amphiphilic internal microenvironment, and the possibility of introducing functional groups in the pores and frameworks in a spatially controlled way. The unique properties of MOFs and their structural tuneability [25–29] make these materials especially suitable for encapsulating a large variety of guest molecules, and hence they are promising candidates for a plethora of environmental and biomedical applications.[30–35] Restricting further discussion to the ability of MOFs to capture and remove toxic compounds from the environment, MOFs display all the desirable features in terms of water stability, porosity, and surface area, and can be used as alternate adsorbents for the adsorption and removal of toxic species. [36–47] In addition to their capturing capacity, MOFs often have sensing properties, which are based on the change to the physical properties caused by the encapsulated metal ion.[48,49] Although there are a few reports that take advantage of the impact of the guest species on the color, electrochemical, and other properties for the development of sensors, the vast majority of them display luminescence-based sensing, which happens due to the change of the emission and/or lifetime after the toxic chemical capture. One recent such example is the FJI-C8 MOF, which exhibits a high sensitivity for Fe^{3+} with the detection limit

being 0.0233 mM [48]; it contains a π-conjugated aromatic ligand with free/uncoordinated N- and O-atoms, which interact strongly with the encapsulated Fe^{3+} ions affecting the emission spectrum of the anionic FJI-C8 MOF. Other luminescent-active MOFs have also been studied as metal ion sensors, including examples of Ru-, Ln-MOFs, etc. [50–54].

The wide range of applications of MOFs and coordination polymers constitute an increasing need for the development of new such species with suitable porosity, high stability, and fine-tuning properties.[55–63] A large number of organic linkers have now been employed in MOFs synthesis including imidazolates, pyridine, carboxylates, etc. [64–74], with the latter being one of the most commonly used, resulting in MOFs with a wide range of pores sizes and shapes. The decoration of the ligands with free (non-coordinated) groups provide valuable opportunity for the insertion of additional functionalities to the framework, which can be useful for environmental and biomedical applications; for example, the presence of pendent sulfonates enhances the MOF ability for the adsorption and removal of heavy metals from aqueous systems, whereas the presence of π-electron-rich N-donor groups enhances the sensing performance towards electron-deficient nitroaromatic explosives.[75,76]

Although the impact of the ligand combination on the framework topology and porosity has been well investigated, this is not the case for the nuclearity and properties of the SBU itself.[72–78] In fact, the SBUs significantly affect the properties of the overall framework; it has been shown that the presence of an heterometal has a positive impact on the breathing effect, whereas the increase of the metal nuclearity is possible to enhance the MOF's pore size and surface area.[79–81] Thus, it is essential that ligands with high bridging capability that have the potential to lead to species with unprecedented metal topologies and/or high nuclearity SBUs be introduced into this field; to this purpose, we decided to use

2-pyridyl oximes for the isolation and characterization of new MOFs and coordination polymers. 2-pyridyl oximes is a family of ligands that have been extensively used in metal cluster chemistry due to their ability to bridge a large number of metal ions and, often, promote ferromagnetic interactions between the metal centers.[82–95] Although the use of such ligands has led to significant breakthroughs in the areas of single-molecule and single-chain magnetism, they have never been employed for MOF synthesis.[82–95]

Herein, we report on the synthesis, structural characterization, and physical properties of nine new coordination polymers, including the first oxime-based MOFs, by the use of a 2-pyridyl oxime (pyridine-2 amidoxime, pyaoxH$_2$, and 2-methyl pyridyl ketoxime, mpkoH) in combination with 1,2,4,5-benzene tetracarboxylic acid (pyromellitic acid), H$_4$pma (Scheme 1); the latter has been employed in the field of MOFs [96–104], but its combination with an oximic ligand is unexplored. The 3D MOF [Cu$_4$(OH)$_2$(pma)(mpko)$_2$](**9**) displays selectivity for Fe^{3+} adsorption.

R = -NH$_2$; pyaoxH$_2$
R = -Me; mpkoH
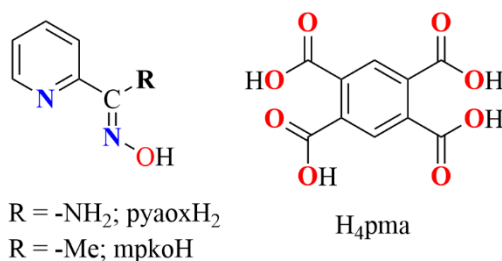
H$_4$pma

Scheme 1. Schematic representation of the 2-pyridyl oximes (**left**) and the ligand H$_4$pma (right) discussed in this work.

98

2. Materials and Methods

2.1. Materials, Physical, and Spectroscopic Measurements

All the manipulations were performed under aerobic conditions using materials (reagent grade) and solvents as received. mpkoH and pyaoxH$_2$ was prepared as described elsewhere.[105,106] WARNING: Perchlorate salts are potentially explosive; such compounds should be used in small quantities and treated with utmost care at all times.

Elemental analysis (C, H, N) were performed by the in-house facilities of National University of Ireland Galway, School of Chemistry. IR spectra (4000–400 cm^{-1}) were recorded on a PerkinElmer Spectrum 400 FT-IR spectrometer. Powder X-ray diffraction data (pxrd) were collected using an Inex Equinoz 6000 diffractometer. Solid-state, variable-temperature, and variable-field magnetic data were collected on powdered samples using an MPMS5 Quantum Design magnetometer operating at 0.03 T in the 300 to 2.0 K range. Diamagnetic corrections were applied to the observed susceptibilities using Pascal's constants. TGA experiments were performed on a STA625 thermal analyzer from Rheometric Scientific (Piscataway, New Jersey). The heating rate was kept constant at 10 °C/min, and all runs were carried out between 20–600 °C. The measurements were made in open aluminum crucibles, nitrogen was purged in ambient mode, and calibration was performed using an indium standard.

2.2. Compound Synthesis

2.2.1. Synthesis of [Zn(H$_2$pma)(pyaoxH$_2$)(H$_2$O)$_2$] (**1**)

Zn(ClO$_4$)$_2$·6H$_2$O (0.149 g, 0.4 mmol) and pyaoxH$_2$ (0.027 g, 0.20 mmol) were dissolved in H$_2$O (20 mL). The resultant solution was put in the oven and heated at 100 °C for 1 h. Then, solid H$_4$pma (0.025 g, 0.1 mmol) was added, the solution was stirred for 15 min, and the vial was left at R.T. for 24 h, after which X-ray quality colorless crystal needles of **1** were formed. The crystals were collected by filtration, washed with cold MeCN (2 mL) and Et$_2$O (2 x 5 mL), and dried in air. Yield 80%. Anal. Calc. for **1**: C, 39.16; H, 3.08; N, 8.56. Found: C, 39.47; H, 3.29; N, 8.17%. IR data: v (cm^{-1}) = 3504m, 3403m, 3123w, 1725s, 1669m, 1609m, 1583s, 1497s, 1414m, 1376s, 1321m, 1295w, 1267w, 1218s, 1168s, 1118s, 1087m, 1062w, 1029s, 1015m, 944m, 916m, 858b, 816w, 794s, 761m, 744m, 725w, 701w, 679w, 667w, 651w.

2.2.2. Synthesis of [Zn$_2$(pma)(pyaoxH$_2$)$_2$]$_n$ (**2**)

Zn(ClO$_4$)$_2$·6H$_2$O (0.149 g, 0.4 mmol) and pyaoxH$_2$ (0.027 g, 0.20 mmol) were dissolved in H$_2$O (10 mL). The resultant solution was put in the oven and heated at 100 °C for 1 h. Solid H$_4$pma (0.025 g, 0.1 mmol) was then added and the vial was placed into the oven for 24 h, after which X-ray quality colorless crystal needles of **2** were formed. The crystals were collected by filtration, washed with cold MeCN (2 mL) and Et$_2$O (2 x 5 mL), and dried in air. Yield 39%. Anal. Calc. for 2: C, 40.33; H, 2.46; N, 12.83. Found: C, 40.56; H, 2.49; N, 13.09%. IR data: v (cm^{-1}) = 3399w, 3215w, 2931w, 1603s, 1402m, 1369s, 1322w, 1253w, 1138w, 1103m, 1061w, 1039m, 915w, 865m, 813m, 783w, 762w, 739w, 683m, 664w.

*2.2.3. Synthesis of [Zn$_2$(pma)(pyaoH$_2$)$_2$(H$_2$O)$_2$]$_n$ (**3**)*

Zn(ClO$_4$)$_2$·6H$_2$O (0.149 g, 0.4 mmol) and pyaoxH$_2$ (0.027 g, 0.20 mmol) were dissolved in H$_2$O (20 mL). The resultant solution was put in the oven and heated at 100 °C for 1 h. Solid H$_4$pma (0.025 g, 0.1 mmol) was then added and the vial was placed into the oven for 2 h, after which X-ray quality colorless polyhedral crystals of **3** were formed. The crystals were collected by filtration, washed with cold MeCN (2 mL) and Et$_2$O (2 x 5 mL), and dried in air. Yield 50%. Anal. Calc. for 3: C, 38.23; H, 2.92; N, 12.16. Found: C, 37.91; H, 2.63; N, 11.93%. IR data: v (cm^{-1}) = 3423w, 3316w, 3202w, 2786w, 1675m, 1648w, 1619w, 1575w, 1548s, 1494s, 1415w, 1372s, 1324m, 1292w, 1267w, 1178w, 1158w, 1138m, 1097w, 1040s, 980w, 942m, 874m, 850w, 813m, 786s, 747s, 690m, 651w.

*2.2.4. Synthesis of [Co$_2$(pma)(pyaoxH$_2$)$_2$(H$_2$O)$_6$] (**4**)*

Co(ClO$_4$)$_2$·6H$_2$O (0.146 g, 0.4 mmol) and pyaoxH$_2$ (0.027 g, 0.2 mol) were dissolved in DMF/H$_2$O (10/10 mL). The resultant solution was put in the oven and heated at 100 °C for 1 h. Solid H$_4$pma (0.025 g, 0.1 mmol) was then added and the vial was placed into the oven for 24 h, after which X-ray quality orange crystals of **4** were formed. The crystals were collected by filtration, washed with cold MeCN (2 mL) and Et$_2$O (2 x 5 mL), and dried in air. Yield 45%. Anal. Calc. for 4: C, 35.22; H, 3.76; N, 11.20. Found: C, 35.17; H, 3.68; N, 11.19%. IR data: v (cm^{-1}) = 3421w, 3308w, 3202w, 2780w, 1667w, 1648w, 1618w, 1573w, 1552s, 1493m, 1412m, 1368s, 1324m, 1293w, 1157w, 1137m, 1096m, 1096w, 1034s, 981m, 942m, 872m, 829w, 812m, 784s, 748m, 689m, 665w.

2.2.5. Synthesis of [Mn$_2$(pma)(pyaoxH$_2$)$_2$(H$_2$O)$_6$] (5)

Mn(ClO$_4$)$_2$·6H$_2$O (0.102 g, 0.4 mmol) and pyaoxH$_2$ (0.0549 g, 0.4 mmol) were dissolved in H$_2$O (10 mL). The resultant yellow solution was put in the oven and heated at 100 °C for 1 h. Then, solid H$_4$pma (0.025 g, 0.1 mmol) was added and the vial was placed into the oven for 24 h, after which X-ray quality colorless needles of **5** were formed. The crystals were collected by filtration, washed with cold MeCN (2 mL) and Et$_2$O (2 x 5 mL), and dried in air. Yield 50%. Anal. Cal. for **5**: C, 35.59; H, 3.80; N, 11.32. Found: C, 35.72; H, 4,06; N, 11.23%. IR data: v (cm^{-1}) = 3358w, 3280w, 2814w, 2229w, 1859m, 1667m, 1649m, 1602m, 1571w, 1545s, 1476s, 1440m, 1418s, 1368s, 1314s, 1259m, 1193w, 1175w, 1165m, 1141s, 1101m, 1071w, 1042s, 968w, 923m, 896w, 853m, 837w, 811w, 792m, 774s, 745s, 689s, 669m, 660w, 651w.

2.2.6. Synthesis of [Cu$_2$(pma)(pyaoxH$_2$)$_2$(DMF)$_2$]$_n$ (6)

Cu(ClO$_4$)$_2$·6H$_2$O (0.149 g, 0.4 mmol) and pyaoxH$_2$ (0.027 g, 0.20 mmol) were dissolved in DMF/H$_2$O (7/7 mL). The resultant solution was put in the oven and heated at 100 °C for 1 h. Then, solid H$_4$pma (0.025 g, 0.1 mmol) was added and the vial was placed into the oven for 24 h, after which X-ray quality green crystal needless of **6** were formed. The crystals were collected by filtration, washed with cold MeCN (2 mL) and Et$_2$O (2 x 5 mL), and dried in air. Yield 39%. Anal. Calc. for **6**: C, 42.16; H, 3.79; N, 14.05. Found: C, 41.87; H, 3.64; N, 13.83%. IR data: v (cm^{-1}) = 3355w, 3226w, 1647s, 1605m, 1483w, 1437w, 1407w, 1363m, 1322w, 1300w, 1245m, 1211m, 1142w, 1098s, 1063w, 1041m, 945w, 928w, 893w, 860w, 844w, 811w, 784m.

2.2.7. Synthesis of [Zn$_2$(pma)(mpkoH)$_2$(H$_2$O)$_4$]·2H$_2$O (7·2H$_2$O)

Zn(ClO$_4$)$_2$·6H$_2$O (0.149 g, 0.4 mmol) and mpkoH (0.027 g, 0.20 mmol) were dissolved in DMF/H$_2$O (7/7 mL). The resultant solution was put in the oven and heated at 100 C for 1 h. Solid H$_4$pma (0.025 g, 0.1 mmol) was then added and the vial was placed into the oven for 24 h, after which X-ray quality colorless crystal needles of **7** were formed. The crystals were collected by filtration, washed with cold MeCN (2 mL) and Et$_2$O (2 x 5 mL), and dried in air. Yield 40%. Anal. Calc. for **7**: C, 37.87; H, 3.97; N, 7.36. Found: C, 38.10; H, 3.93; N, 7.91%. IR data: v (cm^{-1}) = 3102w, 1661m, 1619w, 1548s, 1490m, 1428m, 1375s, 1326s, 1259w, 1187w, 1140m, 1102w, 1046m, 1024w, 969w, 919w, 871m, 827m, 814m, 780w, 762w, 745w, 689m, 664w, 651w.

2.2.8. Synthesis of [Cu(pma)$_{0.5}$(mpkoH)(DMF)]$_n$ (8)

Cu(ClO$_4$)$_2$·6H$_2$O (0.148 g, 0.4 mmol) was added to a solution of mpkoH (0.027 g, 0.2 mmol) in DMF/H$_2$O (10/10 mL). The vial was placed into the oven (100 °C) and, after 1 h, H$_4$pma (0.025 g, 0.1 mmol) was added. The vial was then left in the oven for a further 1 h, after which X-ray quality green crystals of **8** were observed. The crystals were collected by filtration, washed with cold MeCN (2 mL) and Et$_2$O (2 x 5 mL), and dried in air. Yield 45%. Anal. Calc. for **8**: C, 45.28; H, 4.05; N, 10.56. Found: C, 45.41; H, 4.06; N, 10.64%. IR data: v (cm^{-1}) = 3073w, 2342w, 2202w, 2168w, 2068w, 2018w, 1990w, 1623s, 1603w, 1572s, 1480m, 1438w, 1421w, 1399w, 1358bs, 1329w, 1308w, 1297w, 1273w, 1250w, 1170m, 1145m, 1101s, 1064s, 1047m, 1034w, 971w, 925s, 860s, 820w, 811s, 788s, 760s, 715m, 685s, 664s.

*2.2.9. Synthesis of [Cu4(OH)$_2$(pma)(mpko)$_2$]$_n$ (**9**)*

Method A: 9 was prepared in the same manner as **8**, but was left in the oven for 4 h, instead of 1 h in **9**. The crystals were collected by filtration, washed with cold MeCN (2 mL) and Et$_2$O (2 x 5 mL), and dried in air. Yield 80%. Anal. Calc. for **9**: C, 35.65; H, 2.24; N, 6.93. Found: C, 35.73; H, 2.52; N, 6.33%. IR data: *v* (cm^{-1}) = 3339b,1651w, 1616w, 1602w, 1567w, 1547w, 1481s, 1440m, 1416s, 1360s, 1316s, 1270w, 1165s, 1140m, 1102w, 1090m, 1046w, 1023w, 969b, 918m, 899w, 861m, 808s, 773s, 757m, 747m, 707s, 688m, 666w.

Method B: **9** (0.0760 g, ~0.1 mmol) in DMF/H$_2$O (10/10 mL) was placed into the oven (100 °C) for 4 h, after which time green crystals of **9** were formed; the crystals were collected by filtration washed with MeCN (2 x 5 mL) and dried under vacuum. Yield: 80%. The product was characterized by PXRD and IR comparison with the authentic material.

2.3. Single-Crystal X-ray Crystallography

Single-crystal diffraction data for **1**, **5**, **6**, and **8** were collected in an Oxford Diffraction XcaliburCCD diffractometer, whereas crystallographic data for **2**–**4**, **7**, and **9** were collected in an Oxford-Diffraction SuperNova A diffractometer. Mo Ka radiation (λ = 0.71073 Å) was used for **1**, **3**, **5**, **6**, and **8**, and Cu Ka radiation (λ = 1.54184 Å) was used for **2**, **4**, **7**, and **9**. The structures were solved using SHELXT [107], embedded in the OSCAIL software [108]. The non-H atoms were treated anisotropically, whereas the hydrogen atoms were placed in calculated, ideal positions and refined as riding on their respective carbon atoms. Molecular graphics were produced with DIAMOND [109]. Unit cell data and structure refinement details for **1**–**9** are listed in Table 1. CIF files

can be obtained free of charge from the Cambridge Crystallographic Data Centre, Cambridge, UK with the REF codes 2022403-2022411 for **1**–**9**, respectively.

Table 1. Crystallographic data for complexes **1**-**9**.

Complex	**1**	**2**	**3**
Empirical formula	$C_{16}H_{15}N_3O_{11}Zn$	$C_{11}H_8N_3O_5Zn$	$C_{11}H_{10}N_3O_6Zn$
Formula weight	490.68	327.57	346.60
Crystal system	Triclinic	Triclinic	Monoclinic
Space group	$P\bar{1}$	$P\bar{1}$	$P2_1/n$
a (Å)	8.1151(3)	6.9864(7)	11.4913(8)
b (Å)	9.8550(4)	8.9530(8)	6.6261(5)
c (Å)	11.8506(5)	10.4524(9)	16.1381(12)
α (°)	93.283(3)	83.697(7)°	90
β (°)	105.135(3)	94.887(2)	104.335(8)°
γ (°)	92.769(3)	71.582(9)°	90
V (Å^3)	911.40(6)	612.98(10)	1190.54(16)
Z	2	2	4

ρ_{calc} (g cm^{-3})	1.788	1.775	1.934
Radiation, λ (Å)	0.71073	1.54184	0.71073
μ (mm^{-1})	1.420	3.042	2.099
Temperature (K)	297.9(6)	100(2)	100(2)
Measd/independent reflns (R_{int})	4250 /3667 (0.0439)	3860/ 2400 (0.0451)	4714/2088 (0.0371)
Parameters refined	316	197	197
GoF (on F^2)	1.059	1.078	1.055
$R_1{}^a$ ($I > 2\sigma(I)$)	0.0352	0.0517	0.0353
$wR_2{}^b$ ($I > 2\sigma(I)$)	0.0834	0.1377	0.0879
$(\Delta\rho)_{max}/(\Delta\rho)_{min}$ (e Å^{-3})	0.572/-0.504	2.839 / -0.831	0.573 /-0.632

Complex	**4**	**5**	**6**
Empirical formula	$C_{22}H_{28}Co_2N_6O_{16}$	$C_{22}H_{28}Mn_2N_6O_{16}$	$C_{14}H_{15}CuN_4O_6$
Formula weight	750.36	742.38	398.84
Crystal system	Monoclinic	Monoclinic	Triclinic

Space group	$P2_1/n$	$P2_1/n$	$P\bar{1}$
a (Å)	10.9732(9)	11.1773(8)	6.5039(4)
b (Å)	11.7514(8)	12.2116(8)	10.0104(9)
c (Å)	11.6014(13)	11.5293(9)	12.7604(9)
a (°)	90	90	96.743(6)
β (°)	107.619(10)	106.542(7)	91.660(5)
γ (°)	90	90	108.375(7)
V (Å^3)	1425.8(2)	1508.5(2)	781.05(11)
Z	2	2	2
ρ_{calc} (g cm^{-3})	1.748	1.634	1.696
Radiation, λ (Å)	1.54184	0.71073	0.71073
μ (mm^{-1})	9.917	0.921	1.440
Temperature (K)	100(2)	298.0(2)	299.0(1)
Measd/independent reflns (R_{int})	5285/2830 (0.0324)	3603/2795 (0.0680)	3616/2040 (0.1137)
Parameters refined	212	244	240

GoF (on F^2)	1.112	1.047	0.873
$R_1{}^a$ ($I > 2\sigma(I)$)	0.0547	0.0479	0.0526
$wR_2{}^b$ ($I > 2\sigma(I)$)	0.1500	0.1076	0.0868
$(\Delta\rho)_{max}/(\Delta\rho)_{min}$ (e Å^{-3})	0.586 -0.602	0.825/-0.399	0.823/-0.678

Complex	**7·2H$_2$O**	**8**	**9**
Empirical formula	$C_{24}H_{34}N_4O_{18}Zn_2$	$C_{30}H_{32}Cu_2N_6O_{12}$	$C_{12}H_9Cu_2N_2O_6$
Formula weight	797.29	795.69	404.29
Crystal system	Triclinic	Monoclinic	Monoclinic
Space group	$P\bar{1}$	$P2_1/c$	$I2/a$
a (Å)	7.1623(7)	6.4617(3)	16.3272(7)
b (Å)	8.3966(8)	25.5232(9)	10.4575(4)
c (Å)	13.4476(10)	10.1083(5)	15.0472(7)
a (^{o})	106.056(8)	90	90
β (^{o})	104.078(8)	106.321(5)	102.188(5)
γ (^{o})	90.547(8)	90	90

V (Å^3)	751.27(12)	1599.91(13)	2511.27(19)
Z	1	2	8
ρ_{calc} (g cm^{-3})	1.762	1.652	2.139
Radiation, λ (Å)	1.54184	0.71073	1.54184
μ (mm^{-1})	2.785	1.404	4.522
Temperature (K)	100(2)	299.0(2)	100(2)
Measd/independent reflns (R_{int})	4859 / 2943 (0.0323)	3877/2762 (0.0754)	4290/2480 (0.0297)
Parameters refined	225	233	204
GoF (on F^2)	1.087	0.954	1.097
$R_1{}^a$ ($I > 2\sigma(I)$)	0.0638	0.0433	0.0501
$wR_2{}^b$ ($I > 2\sigma(I)$)	0.1890	0.0978	0.1471
$(\Delta\rho)_{max}/(\Delta\rho)_{min}$ (e Å^{-3})	0.957/-1.077	0.450/-0.496	1.587/-1.066

[a] $R1 = \Sigma(|Fo|-|Fc|)/\Sigma(|Fo|)$.

[b] $wR_2 = \{\Sigma[w(Fo^2-Fc^2)2]/\Sigma[w(Fo^2)^2]\}^{1/2}$.

2.4. Metal Ion and 2-methyluracil Adsorption Kinetic and Thermodynamic Studies

The metal adsorption capacity of **9** was investigated as described below: a salt of a metal ion (0.027 g, 0.1 mmol for $FeCl_3$; 0.040 g, 0.1 mmol for $Fe(NO_3)_3$) was added to a glass vial containing distilled H_2O (10 mL) and stirred until all solid is dissolved. Solid **9** (0.242 g) was then added and the mixture was left stirring at room temperature. For the kinetic study, small volumes of aliquots were taken at designated time intervals, centrifuged, and the metal content in the supernatant solution was determined by spectroscopic (UV-vis) techniques. For the thermodynamic study, the same procedure was repeated with varying **9**: metal ratios; the mixture was stirred for 20 min, filtered, and the filtrate was analyzed for its metal content. The metal encapsulation was also confirmed by magnetism studies. The 2-methyluracil adsorption capacity of **9** was investigated following the same method used for the metal adsorption studies.

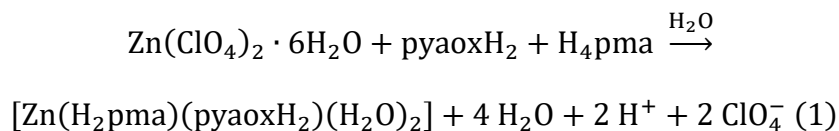## 3. Results and Discussion

3.1. Synthetic Discussion

We have developed an intense interest over the last years in the synthesis of metal clusters and SMMs by the use of 2-pyridyl oximes as bridging ligands. These research efforts have resulted in a large number of new homo- and heterometallic new species with interesting structural features and magnetic properties, e.g., Ni_5, Ni_{12}, Ni_{16}, Ni_2Ln_2, Ni_8Ln_8, Ni_2Mn_2, Mn_8, etc. [83–89]. We recently decided to explore the ability of such ligands to favor the formation of MOFs, when combined with di- and tricarboxylic ligands, such as 1,4-benzenedicarboxylic
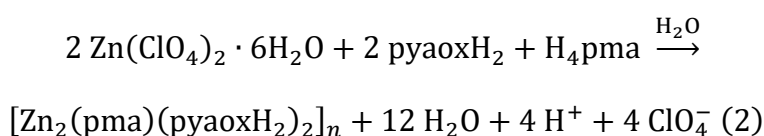
110

and 1,3,5-benzenetricarboxylic acid.[110] This study yielded a new family of 1D chains and prompted us to expand this work using a tetracarboxylic ligand with higher bridging capability, in order to further increase the potential of the reaction system to provide access to new MOFs. The ligand that was chosen, and discussed herein, is the pyromellitic acid, H_4pma. A variety of experiments were performed, studying how the different synthetic parameters (presence/absence or kind of base, molar ratio of the reactants, metal sources, etc.) affect the identity of the isolated product. In particular, the use of other metal sources instead of perchlorates (e.g., chlorides, nitrates, acetates, etc.) led to the precipitation of amorphous materials that could not be further characterized.

In order to ensure the coordination of both the oxime and carboxylic ligand in the metal center, the solution containing the metal salt and the oxime was left under stirring for at least one hour before the addition of the H_4pma. It is noteworthy that the appropriate ratio of oxime/H_4pma, which is able to yield binary species, was found to be 2:1; a 1:1 ratio results in known compounds that contain only the teracarboxylic ligand, whereas a high excess of oxime leads to the formation of oximato metal complexes, preventing the coordination of the ligand H4pma either in its neutral or anionic form.
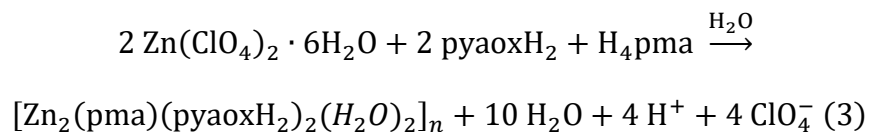
The reaction mixture of $Zn(ClO_4)_2 \cdot 6H_2O$/pyaoxH_2/H_4pma (4:2:1) in H_2O gave a colorless solution from which crystals of $[Zn(H_2pma)(pyaoxH_2)(H_2O)_2]$ (**1**) were subsequently isolated. Following a similar reaction but by increasing the reaction temperature from R.T. to 100 °C, compounds $[Zn_2(pma)(pyaoxH_2)_2]_n$ (**2**) and $[Zn_2(pma)(pyaoxH_2)_2(H_2O)_2]_n$ (**3**) were isolated, depending on the reaction time; **2** is an 1D polymer and is formed after 24 h, whereas **3** is a 2D MOF, which is formed after 2 h of reaction. The stoichiometric equation of the reactions that lead to the formation of **1**–**3** is represented in Equations (**1**)–(**3**).
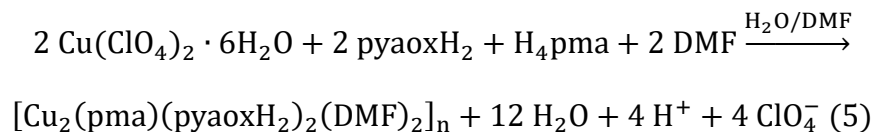
$$Zn(ClO_4)_2 \cdot 6H_2O + pyaoxH_2 + H_4pma \xrightarrow{H_2O}$$

$$[Zn(H_2pma)(pyaoxH_2)(H_2O)_2] + 4\,H_2O + 2\,H^+ + 2\,ClO_4^-\ (1)$$

1

$$2\,Zn(ClO_4)_2 \cdot 6H_2O + 2\,pyaoxH_2 + H_4pma \xrightarrow{H_2O}$$

$$[Zn_2(pma)(pyaoxH_2)_2]_n + 12\,H_2O + 4\,H^+ + 4\,ClO_4^-\ (2)$$

2

$$2\,Zn(ClO_4)_2 \cdot 6H_2O + 2\,pyaoxH_2 + H_4pma \xrightarrow{H_2O}$$

$$[Zn_2(pma)(pyaoxH_2)_2(H_2O)_2]_n + 10\,H_2O + 4\,H^+ + 4\,ClO_4^-\ (3)$$
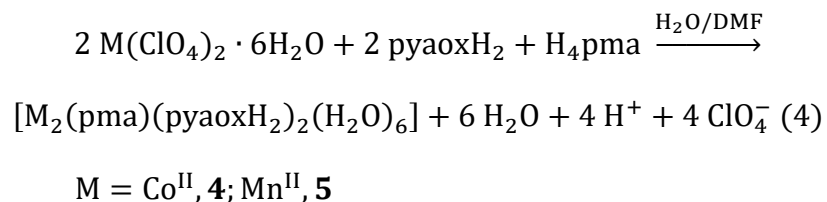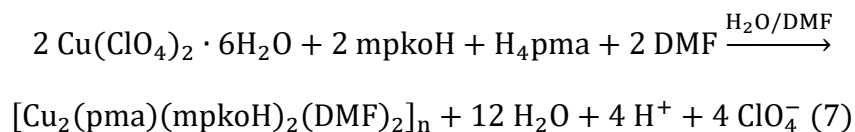
3

After the determination of the crystal structures of **1**–**3**, which revealed that small modification in the reaction conditions affect the dimensionality of the compound (1, 0D; 2, 1D; 3, 2D), we decided to investigate the impact of the kind of the metal ion on the identity of the isolated products. Thus, compounds $[Co_2(pma)(pyaoxH_2)_2(H_2O)_6]$ (**4**), $[Mn_2(pma)(pyaoxH_2)_2(H_2O)_6]$ (**5**), and $[Cu_2(pma)(pyaoxH_2)_2(DMF)_2]_n$ (**6**) were isolated in good yield by a similar reaction to the one that provided access to **1** and **2** (Equations (4) and (5)). **4** and **5** are discrete complexes (0D), whereas **6** is a 1D double chain.

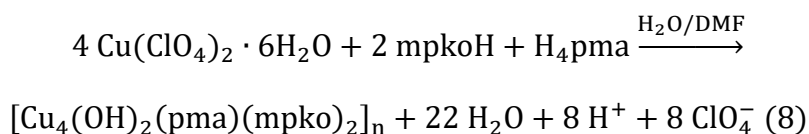$$2 \text{ M(ClO}_4)_2 \cdot 6\text{H}_2\text{O} + 2 \text{ pyaoxH}_2 + \text{H}_4\text{pma} \xrightarrow{\text{H}_2\text{O/DMF}}$$

$$[\text{M}_2(\text{pma})(\text{pyaoxH}_2)_2(\text{H}_2\text{O})_6] + 6 \text{ H}_2\text{O} + 4 \text{ H}^+ + 4 \text{ ClO}_4^- \text{ (4)}$$

$$\text{M} = \text{Co}^{\text{II}}, \textbf{4}; \text{Mn}^{\text{II}}, \textbf{5}$$

$$2 \text{ Cu(ClO}_4)_2 \cdot 6\text{H}_2\text{O} + 2 \text{ pyaoxH}_2 + \text{H}_4\text{pma} + 2 \text{ DMF} \xrightarrow{\text{H}_2\text{O/DMF}}$$

$$[\text{Cu}_2(\text{pma})(\text{pyaoxH}_2)_2(\text{DMF})_2]_n + 12 \text{ H}_2\text{O} + 4 \text{ H}^+ + 4 \text{ ClO}_4^- \text{ (5)}$$

$$\textbf{6}$$

Series of experiments were also performed in order to investigate the influence of the electronic properties of the oximic ligand on the identity and structural properties of the isolated products; to this end, 2-methyl pyridyl ketoxime (mpkoH) was used instead of H$_2$pyaox. The reaction of M(ClO$_4$)$_2\cdot$6H$_2$O (M = Zn, Cu), Hmpko and H$_4$pma in a 4:2:1 molar ratio in DMF/H$_2$O provided access to [Zn$_2$(pma)(mpkoH)$_2$(H$_2$O)$_4$]·2H$_2$O (**7**·2H$_2$O) and [Cu$_2$(pma)(mpkoH)$_2$(DMF)$_2$]$_n$ (**8**), according to the stoichiometric Equations (6) and (7).

$$2 \text{ Zn(ClO}_4)_2 \cdot 6\text{H}_2\text{O} + 2 \text{ mpkoH} + \text{H}_4\text{pma} \xrightarrow{\text{H}_2\text{O/DMF}}$$

$$[\text{Zn}_2(\text{pma})(\text{mpkoH})_2(\text{H}_2\text{O})_4] \cdot 2\text{H}_2\text{O} + 6 \text{ H}_2\text{O} + 4 \text{ H}^+ + 4 \text{ ClO}_4^- \text{ (6)}$$

$$\textbf{7} \cdot 2\text{H}_2\text{O}$$

$$2 \text{ Cu(ClO}_4)_2 \cdot 6\text{H}_2\text{O} + 2 \text{ mpkoH} + \text{H}_4\text{pma} + 2 \text{ DMF} \xrightarrow{\text{H}_2\text{O/DMF}}$$

$$[\text{Cu}_2(\text{pma})(\text{mpkoH})_2(\text{DMF})_2]_n + 12 \text{ H}_2\text{O} + 4 \text{ H}^+ + 4 \text{ ClO}_4^- \text{ (7)}$$
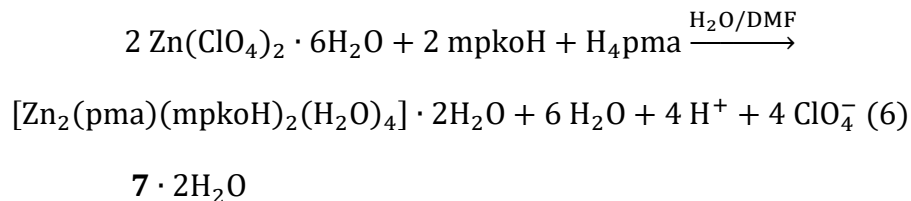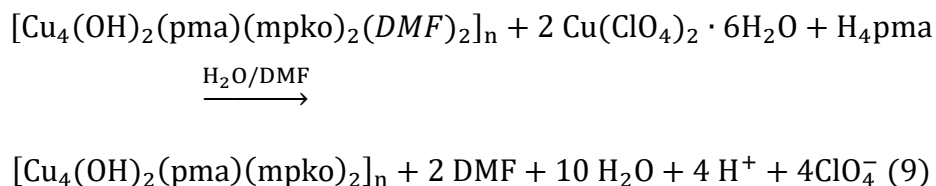
$$\textbf{8}$$

Following that, we investigated all the synthetic parameters that could lead to a different product and the deprotonation of the oximic ligand, i.e., the molar ratio of reactants, presence/kind of base, reaction conditions, metal source, etc. Indeed, by following the same experimental procedure, but by increasing the time from h to 4h, green crystals of $[Cu_4(OH)_2(pma)(mpko)_2]_n$ (**9**) were isolated. The formation of **9** is summarized in the stoichiometric Equation (8). **9** can be also produced in good yield by reacting **8** and $Cu(ClO_4)_2 \cdot 6H_2O$ in a 1:2 ratio, according to the stoichiometric Equation (**9**). Note that the OH⁻ ions in the structure of **9** come from the dissociation of H_2O molecules.

$$4\ Cu(ClO_4)_2 \cdot 6H_2O + 2\ mpkoH + H_4pma \xrightarrow{H_2O/DMF}$$

$$[Cu_4(OH)_2(pma)(mpko)_2]_n + 22\ H_2O + 8\ H^+ + 8\ ClO_4^- \quad (8)$$

$$\textbf{9}$$

$$[Cu_4(OH)_2(pma)(mpko)_2(DMF)_2]_n + 2\ Cu(ClO_4)_2 \cdot 6H_2O + H_4pma$$

$$\xrightarrow{H_2O/DMF}$$

$$[Cu_4(OH)_2(pma)(mpko)_2]_n + 2\ DMF + 10\ H_2O + 4\ H^+ + 4ClO_4^- \quad (9)$$

$$\textbf{9}$$

3.2. Description of Structures

Representations of the molecular structures of **1**–**9** are shown in Figures 1–7 and **Figures S1–S5** (Supplementary Information). Selected interatomic distances and angles are listed in **Tables S1–S9**.

1 crystallizes in the triclinic space group P$\bar{1}$. Its structure (Figure 1) consists of mononuclear [Zn(H$_2$pma)(pyaoxH$_2$)(H$_2$O)$_2$] species. The coordination sphere of the metal centre is completed by one terminal *N,N′*-bidentate chelating pyaox H$_2$ ligand, two terminal water molecules, and one double deprotonated pmaH$_2^-$ ligand. Zn1 is five-coordinate adopting a distorted trigonal bipyramidal geometry (τ = 0.8) with O2 and N3 occupying the axial positions.[111]
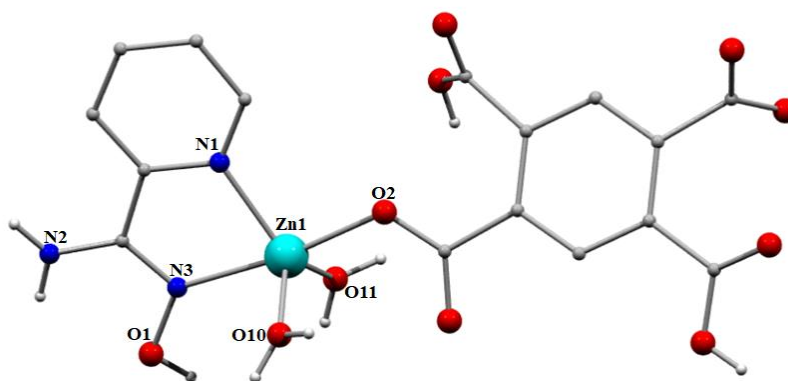

Figure 1. Representation of the mononuclear complex **1**. Color code: Zn, turquoise ; N, navy blue; O, red; C, grey.

A network of intermolecular hydrogen bonding interactions stabilizes the crystal structure of **1**; this involves the protonated carboxylic groups (O4, O9), the amino group (N2), and the terminal H$_2$O molecules (O10, O11) as donors, and carboxylic groups from neighboring compounds (O3, O5, O6, O7, and O8) as acceptors. Details of the metric parameters of the crystallographically established hydrogen bonds in **1** are listed in **Table S10**.

2 crystallizes in the triclinic space group P$\bar{1}$; its structure (Figure 2) is a 1D double chain formed by the connection of [Zn(pma)$_{0.5}$(pyaoxH$_2$)] repeating units through the μ_4-κO; κO'; κO''; κO''' pma4$^-$ ligand. The coordination sphere of the metal ion is completed by two terminally ligated carboxylate groups from two different pma4$^-$ ligands, and one neutral *N,N'*-bidentate chelating pyaoxH$_2$ ligand. Zn^{2+} adopts a tetrahedral coordination geometry. Both hydrogen atoms from the NH$_2$ group participate in hydrogen bonding interactions in which carboxylate groups from neighboring chains act as acceptors (N3$\cdots$O3 = 2.959 Å, H1N$\cdots$O3 = 2.091 Å, N3-H1N$\cdots$O3 = 168.57°; N3$\cdots$O4 = 3.046 Å, H2N$\cdots$O4 = 2.292 Å, N3-H1N$\cdots$O4 = 150.68°). The extensive hydrogen bonding interactions in **2** result in the formation of a 3D network (**Figure S1** in Supplementary Materials).
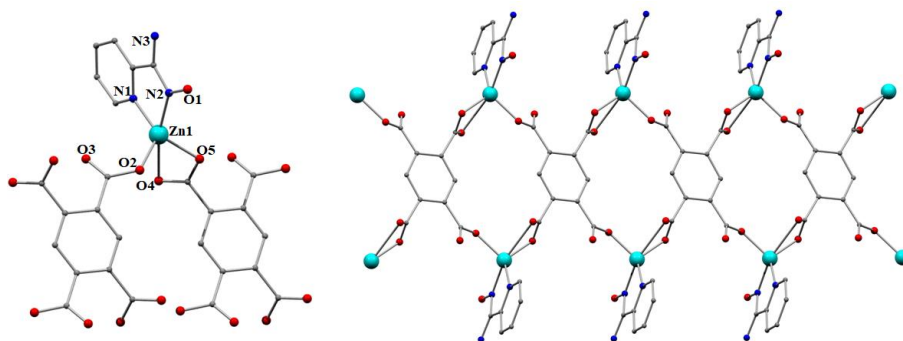

Figure 2. Representation of the repeating unit (left) and a part of the 1D double chain of **2** (right). Color code: Zn, cyan; N, navy blue; O, red; C, grey. The hydrogen atoms are omitted for clarity.

3 crystallizes in the monoclinic space group P2$_1$/n and is a 2D coordination polymer based on the secondary building unit [Zn(pma)$_{0.5}$(pyaoxH$_2$)(H$_2$O)] (**Figure 3**).The latter possesses a similar formula to that of the repeating unit in

2 with the main difference being the ligation of a terminal H_2O molecule. Similar to **2**, the two oximic ligands are neutral adopting an *N,N'*-bidentate chelating coordination mode. The pma^{4-} ligands bridge four neighboring SBUs with two of the carboxylate groups adopting a chelating coordination mode, whereas the other two being terminally ligated. It is noteworthy that the different coordination mode of the pma^{4-} ligand in comparison to that in **2**, in addition to the presence of H_2O molecule in the coordination sphere of the metal centre, result in the Zn being six-coordinated with a distorted octahedral coordination geometry. Note that the coordination geometry of the metal ion in **2** is tetrahedral. This difference in the coordination geometry of the metal ions in **2** and **3** leads to a different orientation of the ligands around the metal ion, favouring the formation of a two-dimensional framework in **3**.
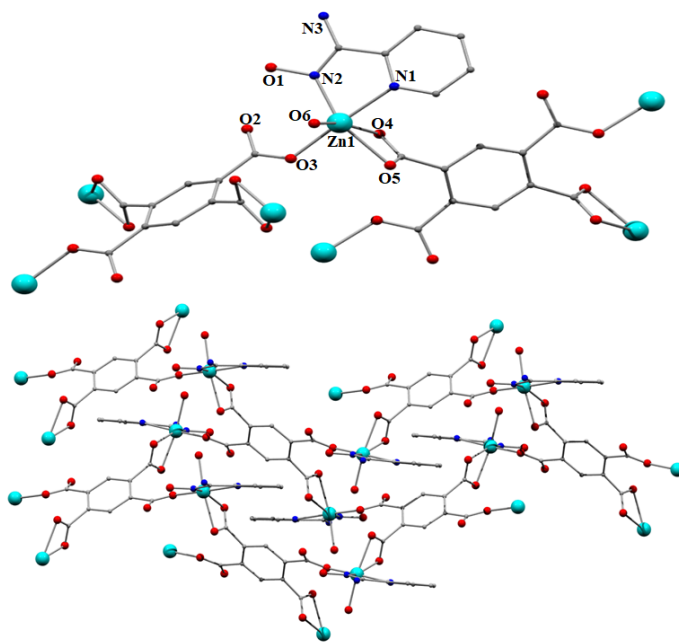

Figure 3. Representation of the repeating unit (top) and a part of the 2D chain of **3** (bottom). Color code: Zn^{2+}, turquoise; N, navy blue; O, red; C, grey. The hydrogen atoms are omitted for clarity.

A network of hydrogen bonding interactions provide stability in the framework in **3**; these are formed between the oximic group (O1, donor) and an oxygen atom (O2, acceptor) from a carboxylate group (O1⋯O2 = 2.610 Å, H1A⋯O2 = 1.816 Å, O1-H1A⋯O2 = 162.55°), as well as between the terminally ligated H$_2$O molecule (O6, donor) and a different carboxylate oxygen atom (O4, acceptor; O4⋯O6 = 2.726 Å, H6B⋯O4 = 2.032 Å, O6-H6B⋯O4 = 137.01°).

Compounds **4** and **5** display related structures with their main difference being the type of the 3d metal ion (**4**, Co^{2+}; **5**, Mn^{2+}). Thus, only the structure of **4** will be discussed in detail. Compound **4** crystallize in the monoclinic space group P2$_1$/n and its structure consists of the dinuclear complex [Co$_2$(pma)(H$_2$pyaox)$_2$(H$_2$O)$_6$] (**Figure 4**). The dinuclear molecules lie on a crystallographic inversion center with Co^{2+} atoms being bridged by the μ-κO;κO′ pma^{4-} ligand. The coordination sphere of each metal ion is neutral *N′*-bidentate chelating H$_2$pyaox, and three terminal water molecules. The metal ion is six-coordinated displaying a slightly distorted octahedral geometry as a result of the relatively small bite angle of the chelating ligand (N1-Co1-N2 = 75.1(2)°).
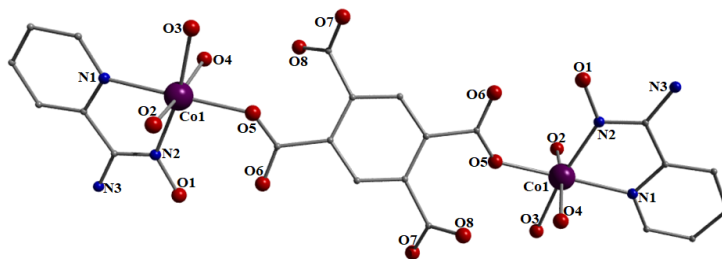

Figure 4. Representation of the molecular structure of the dinuclear complex **4**. Color code: Co^{2+}, purple; N, navy blue; O, red; C, grey. The hydrogen atoms are omitted for clarity.

The crystal structure of **4** is stabilized by a strong intramolecular H bonding interaction between the oximic oxygen atom (O1) as a donor and an oxygen atom (O6) from the pma^{4-} ligand as an acceptor (O1$\cdots$O6 = 2.533 Å, H1$\cdots$O6 1.716 Å, O1-H1$\cdots$O6 172.26°). A network of intermolecular hydrogen bonding interactions is formed between the terminal H_2O molecules (O2, O3, O4) as donors and carboxylic groups from neighboring molecules as acceptors. The metric parameters of the crystallographically established, intermolecular hydrogen bonds for **4** are listed in **Table S11** in the Supplementary Material.

6 crystallizes in the triclinic space group P$\bar{1}$; its structure (**Figure 5**) is based on the connection of [Cu(pma)$_{0.5}$(pyaoxH$_2$)(DMF)] repeating units that result in the formation of a 1D double chain coordination polymer. The pma4- ligand bridges four neighboring repeating units, adopting μ$_4$- κO; κO′; κO″; κO‴ ligation mode. The coordination sphere of the metal ion is completed by two terminally ligated carboxylate groups from two different pma^{4-} ligands, one neutral *N,N′*-bidentate chelating H$_2$pyaox ligand, and one terminal DMF molecule. Cu^{2+} is five-coordinate with a square pyramidal coordination geometry (τ = 0.15) with O6 from the DMF molecule occupying the axial position.[111] Both hydrogen atoms from the NH$_2$ group form hydrogen bonds with oxygen atoms of carboxylate groups from neighboring chains (N2$\cdots$O3 = 2.813 Å, H2N2$\cdots$O3 = 1.937 Å, N2-H2N2$\cdots$O3 = 176.69°; N2$\cdots$O4 = 2.873 Å, H1N2$\cdots$O4 = 2.065 Å, N2-H1N2$\cdots$O4 = 150.10°). Furthermore, an intrachain hydrogen bond between the oximic group (O1) and an oxygen atom of a carboxylate group (O4) provide additional stability to the crystal structure (O1$\cdots$O4 = 2.701 Å, H1O1$\cdots$O4 = 1.921 Å, O1-H1O1$\cdots$O4 = 146.29°).
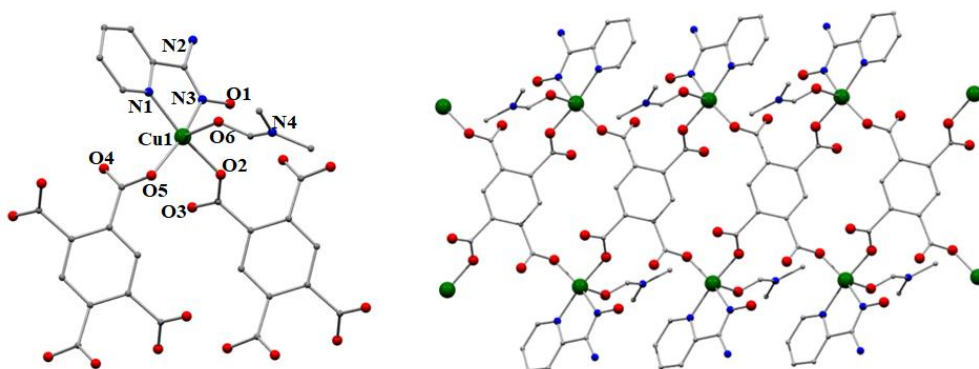
Figure 5. Representation of the repeating unit (left) and a part of the double 1D chain of **6** (right). Color code: Cu, green; N, navy blue; O, red; C, grey. The hydrogens are omitted for clarity.

Compound **7**·$2H_2O$ crystallizes in the triclinic group $P\overline{1}$ and its crystal structure is related to that of **4**, with the main differences being: 1) the type of the 3d metal ion (**4**, Co^{2+}; **7**, Zn^{2+}), 2) the type of the oximic ligand (**4**, pyaoxH$_2$; **7**, mpkoH), and 3) the presence of two solvate H_2O molecules in the crystal structure of **7**. The coordination sphere of the metal ions and the coordination modes of the ligands in both compounds is similar (**Figure S3**). The crystal structure of **7** is stabilized by two strong intramolecular H bonding interactions, which involve: 1) the oximic oxygen atom (O1) as a donor and an oxygen atom (O6) from the pma^{4-} ligand as an acceptor (O1···O6 = 2.656 Å, H1···O6 = 1.846 Å, O1-H1···O6 = 170.36°), and 2) the solvate H_2O molecule (O9, donor) and a carboxylic oxygen atom (O6, acceptor), O9···O6 = 2.815 Å, H9B···O6 = 1.965 Å, O9-H9B···O6 = 176.96°. A network of intermolecular hydrogen bonding interactions is formed between the terminal H_2O molecules (O2, O3, O4; donors) and carboxylic groups (O7, O8; acceptors) or the solvate H_2O molecule (O9) from neighboring molecules. The metric

parameters of the intermolecular hydrogen bonding interactions for **7** are listed in Table S12 in the Supplementary Material.

Compound **8** crystallizes in the monoclinic space group $P2_1/c$. Its structure consists of $[Cu(pma)_{0.5}(mpkoH)(DMF)]n$ repeating units that are held together to form a 1D-double chain. (Figure 6) The coordination sphere of the Cu^{2+} atom is completed by one *N,N'*-bidentate chelating mpkoH ligand, one terminal DMF molecule, and two O atoms (O3 and O6) that come from two different pma^{4-} ions; the symmetry equivalent atom of O6 (O60) links the neighboring building units forming a one-dimensional chain, whereas O30 bridges two Cu atoms from two parallel chains, forming a 1D-double chain.
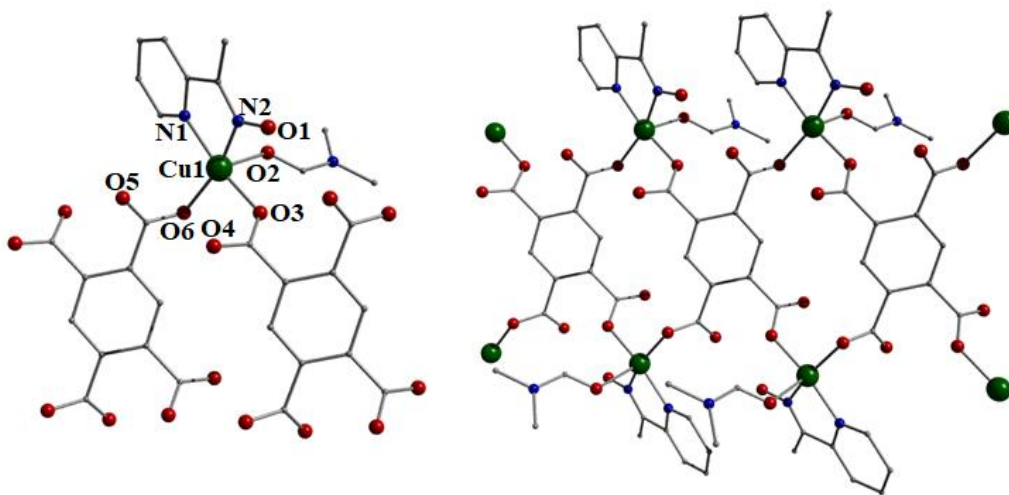

Figure 6. Representation of the repeating unit (left) and a part of the 1D double chain of **8** (right). Color code: Cu^{II}, green; N, navy blue; O, red; C, grey. The hydrogens are omitted for clarity.

Cu1 is five-coordinate adopting a tetragonal pyramidal geometry ($\tau = 0.01$) with O3, O6, N1, and N2 occupying the basal plane vertices and O2 the apical position [111]. There are strong intrachain hydrogen bonding interactions that stabilize the crystal structure of **8**; these are formed between the oximic group (O1, donor), and the carboxylic group of the pma^{4-} ion (O5), which acts as the acceptor (O1$\cdots$O5 = 2.669 Å, H1O1$\cdots$O5 = 1.912Å, O1-H1O1$\cdots$O5 = 155.10°). The shortest Cu$\cdots$Cu distance (6.5 Å) is between atoms of the same chain, whereas the shortest interchain metal$\cdots$metal distance is 7.7 Å; it is noteworthy that the latter is shorter than the intrachain distance between metal atoms that belong to different chains of the 1D-double chain (8.8 Å) in **8**.

9 crystallizes in the monoclinic space group I$_{2/a}$. Its crystal structure contains a three-dimensional network based on a [Cu$_4$(OH)$_2$(pma)(mpko)$_2$] repeating unit (**Figure 7**). The latter possesses a centrosymmetric "planar-butterfly" [Cu$_4$(μ_3-OH)$_2$]$^{6+}$ core with a Cu4 rhombus topology; the μ_3-OH$^-$ ions lie 0.841 Å above and below the plane formed by the four metal ions. Alternatively, the core of the SBU in **9** can be described as two face-sharing defective cubanes, i.e., with a metal atom missing from one vertex of each cubane; this motif is relatively common in metal cluster chemistry.
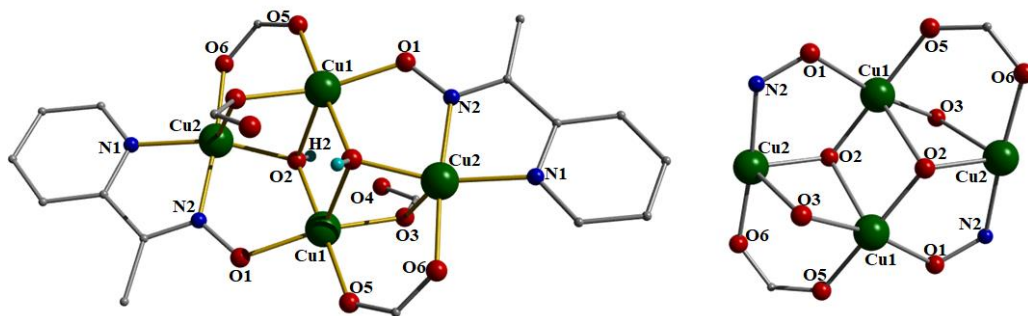
Figure 7. Representation of the repeating unit (left) in **9** and its [Cu$_4$ (μ_3-OH)$_2$]$^{6+}$ "butterfly" shaped core (right). Color code: Cu^{II}, green; N, navy blue; O, red; C, grey. The hydrogen atoms are omitted for clarity, except from the hydrogens from the hydrogens of the hydroxyl groups, which are cyan.

The coordination sphere of the metal atoms in **9** is completed by two doubly bridging anionic mpko$^-$ ligands and four doubly bridging carboxylate groups; the mpko$^-$ adopts the μ-κO; κN; κN' coordination mode. The pma$^-$ ligands link the neighboring SBUs, resulting in the formation of the 3D network, with each one bridging four Cu$_4$ units. All metal atoms in **9** are five-coordinate with a tetragonal pyramidal geometry ($\tau = 0.28$, Cu1, Cu1'; $\tau = 0.20$, Cu2, Cu2'); O2 (for Cu1 and its symmetry equivalent) and O3 (for Cu2 and its symmetry equivalent) occupy the apical positions of the pyramids.[111] The structure of **9** is stabilized by an intramolecular hydrogen bond involving the hydroxo group (O2, donor) and one of the carboxylate groups (O4, acceptor) of the pma^{4-} in (O2$\cdots$O4 = 2.722Å, H2$\cdots$O4 = 2.113 Å, O2-H2$\cdots$O4 = 133.52°), **Figure S4**.

The original framework in **9** can be simplified to its underlying net following two different, approaches, the so-called standard and cluster representations.[112–114] Applying the first one, each Cu atom and the center of the mass of the organic ligands are the nodes, which leads to a 3,4,5,8-c net with point symbol

(3.42)2(3.43.52)2(3.44.53.62)2(412.1016) [112–114]. This topology (**Figure S5**) has not been observed in the past, thus, **9** exhibits a network with an unprecedented architecture. On the other hand, following the cluster representation, in which the Cu atoms with the organic ligands are considered as a single four-coordinated node (ZA, ZB), a unimodal 4-c net is formed with lvt topology (**Figure S6**) and a (42)(84) point symbol.

1–**9** are a new family of oximic metal compounds, coordination polymers and MOFs that display unprecedented structural features. Among them, **3** and **9** are the first MOFs based on a 2-pyridyl oxime with **9** possessing a novel framework topology. **2**, **6**, and **8** join a small family of coordination polymers containing an oximic ligand.[110] The purity and stability of these compounds has been verified by pxrd studies.

3.3. Adsorption Studies

Thermal stability studies (**Figure S17**) in **9** indicated a promising adsorption potential (ca 30% mass loss below 100 °C corresponding to adsorbed solvent), which prompted us to assess its metal adsorption capacity in detail. The metal encapsulation studies for **9** were carried out by soaking MOF crystals into aqueous solutions of $Fe(NO_3)_3 \cdot 9H_2O$. The MOF crystals were activated prior to the Fe^{3+} encapsulation in order to reduce the amount of solvent present; this was carried out by stirring the crystals in acetone for several hours and exchanging this solvent with volatile acetone, which is easily removed at 80 °C. The metal encapsulation was initially investigated by batch studies using UV-vis spectroscopy. The maximum loading capacity obtained for Fe^{3+} in the case of $Fe(NO_3)_3 \cdot 9H_2O$ as a metal source is 104 mg Fe3+/g **9** (1.50 mol Fe^{3+}/mol **9**). The

Fe^{3+} adsorption by **9** exhibits fast kinetics; there is a smooth increase in the adsorption capacity over time, which after 5 min reaches a plateau (**Figure 8**, left). No metal adsorption is observed after 5 min. In order to get a better insight into the adsorption mechanism, the experimental kinetic data were fitted to a theoretical model; pseudo-first order and pseudo-second order kinetic models were used according to Equations (**10**) and (**11**), respectively.[115–117]

$$\ln(q_e - q_t) = \ln q_e - k_1 t \quad (10)$$

$$\frac{t}{q_e} = \frac{1}{k_2 q_e{}^2} + \frac{1}{q_e}t \quad (11)$$

where k_1 and k_2 are the rate constants for the pseudo-first and pseudo-second kinetic models, respectively. A good fit was obtained for the pseudo-second kinetic model (**Figure 8**, right), which is indicative of a chemisorption mechanism, i.e., the formation of a strong interaction between the encapsulated Fe^{3+} and **9**. The corresponding fitting parameters are $R_2 = 0.9968$, $q_e = 107.83$ g Fe^{3+}/g **9**, which is in very good agreement with the experimental data.
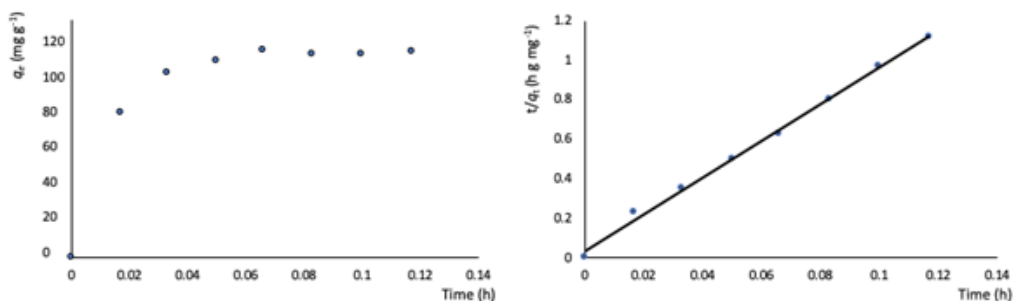
Figure 8. Left: metal adsorption capacity (mg g^{-1}) versus time (h) plot; right: simulation of the experimental data to the pseudo order kinetic model. The solid lines represent the fitting of the data.

The impact of the Fe^{3+} source, and in particular the impact of the kind of counterion, on the kinetic and/or thermodynamic properties of the metal encapsulation by **9** was also studied by using FeCl$_3$ instead of Fe(NO$_3$)$_3$. It was found that the maximum loading capacity is 105 mg Fe^{3+}/g **9** (1.52 mol Fe^{3+}/mol **9**) and is reached after 7 min stirring. The metal adsorption equilibrium data are plotted in **Figure 9**. The best fitting of the data is provided by the Langmuir model,[118,119] considering a monolayer adsorption with a finite number of homogeneous and equivalent active sites Equation (**12**):

$$\frac{C_e}{q_e} = \frac{C_e}{q_s} + \frac{1}{q_s K_L} \quad (12)$$

where q$_e$ (mg/g) is the amount of metal ion per gram of **9** at the equilibrium concentration C$_e$ (ppm of metal ion remaining in solution), q$_s$ is the maximum adsorption capacity of **9**, and K$_L$ is the Langmuir constant; the fitting parameters are = 129.87 mg Fe/g **9**, K$_L$ = 5 x 102 (L mol^{-1}) and R$_2$ = 0.9996. The corresponding kinetic plot is shown in Figure S8. Hence, the nature of the counterion of the Fe^{3+} source does not affect the metal encapsulation capacity of

9. Other metal ions were also tested, including Co^{2+}, Ni^{2+}, Mn^{2+}, and Cr^{3+}; however, no adsorption was observed even after one day stirring, indicating that **9** exhibits high selectivity for Fe^{3+}.
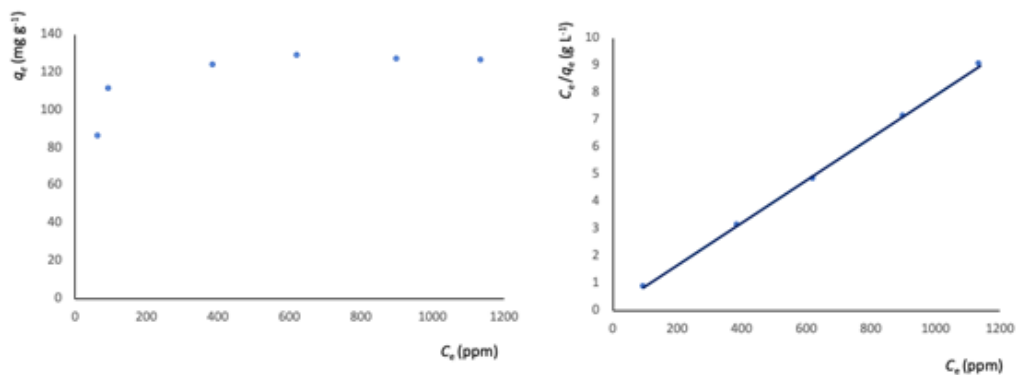

Figure 9. Left: Equilibrium data for the metal adsorption by **9** (contact line: 20 min); right: fitting of the metal adsorption data to the Langmuir model.

The Fe^{3+} adsorption capacity of **9** was further investigated by EDX studies. Figure 10 shows the EDX spectra of **9** and **Fe@9**; Cu, C, and O are detected in both samples, with the second sample displaying one additional peak corresponding to the Fe^{3+} ion that has been adsorbed, hence confirming the metal uptake. It is noteworthy that **9** can be easily regenerated from **Fe@9** by treatment with a 0.2M EDTA solution. The activated MOF displays an identical sorption capacity with that of the original **9**, which is retained for three cycles of regeneration/reuse experiments (**Figure S9**). Thus, **9** is reusable, a [rp[erty which is paramount for practical applications.
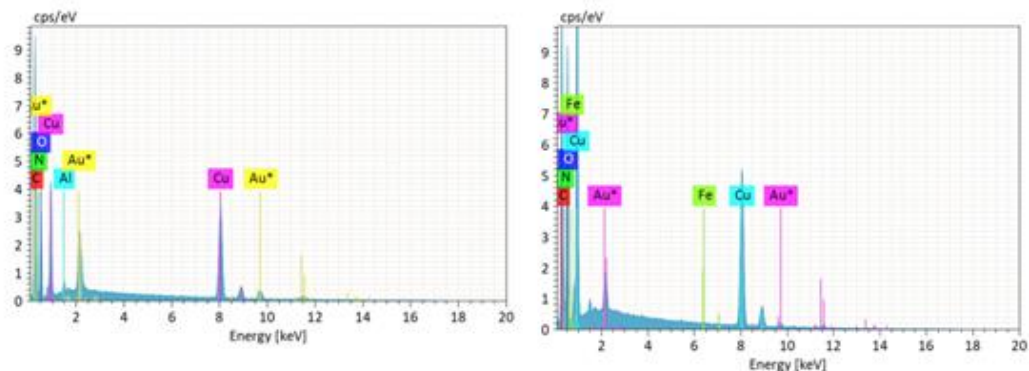
Figure 10. EDX spectra of **9** (left) and Fe@**9** (right).

The good Fe^{3+} adsorption capacity of **9** prompted us to evaluate its encapsulation performance for other species. 6-methyluracil is a compound for which the development of new sorbents or sensors is of great importance; it is a key component of many drugs, including anti-ulcer agents, radiation protective agents, and immunological adjuvants which help enhance immune responses, but on the other hand, it can also be encountered as a toxic byproduct in the synthesis of biologically important DNA adducts. If small impurities of such byproducts are not identified and removed, it could have devastating consequences for the corresponding biological assays and medical treatments. Thus, the development of efficient carriers/sorbents for the delivery or removal of these species would provide new insight into drug manufacturing. Considering also the fact that MOFs have not yet been used for drug purification, this would expand the range of potential applications of MOFs. With the above in mind, and following a similar process to the one used for metal adsorption, the 6-methylyracil capacity of **9** was investigated. This is an ongoing project, but preliminary results (Figure S10) indicate that **9** possess a good performance in 6-methyluracil adsorption; the maximum uptake capacity is 167 mg 6-methyluracil/g **9** for a 1:1 ratio 6-

methyluracil:**9** in an aqueous solution. It exhibits fast kinetics with the maximum encapsulation being reached after 6 min stirring. It is noteworthy, though, that the regeneration of the MOF after the 6-methyluracil adsorption is not feasible. These initial results show the potential of **9**, and MOFs in general, to be used in purification processes during drug manufacturing. Investigations are now in progress to assess the selectivity of 9 for 6-methyluracil and other toxic byproducts, which is a requirement for the use of MOFs in such applications.

3.4. Magnetism Studies

Solid state DC magnetic susceptibility measurements were performed on a polycrystalline sample of **9** in an applied field 0.03 T and temperature range 2–300 K. The obtained data are shown as a MT vs. T plot in **Figure 11**. The MT value at 300 K is 0.075 $cm^3 \cdot mol^{-1}$ K, appreciably lower than the spin-only (g = 2) value of 1.5 $cm^3 \cdot mol^{-1}$ K expected for four non-interacting Cu^{2+} centres (S = 1/2), revealing strong antiferromagnetic coupling within the framework SBU. This is further supported by the overall profile of the plot, which is indicative of strong antiferromagnetic interactions and a diamagnetic ground state for **9**.
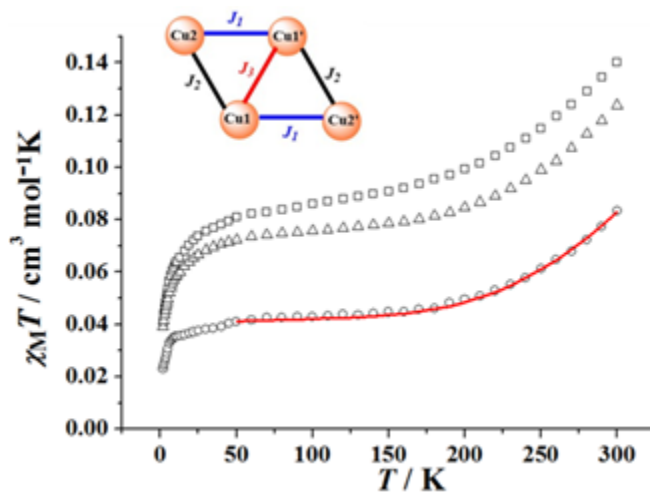
Figure 11. $\chi_M T$ *vs.* T plot for **9** (circles) Fe@**9**-1 (triangles) and Fe@**9**-2 (squares). Solid line represents the best fir for 9. Inset: the exchange interactions in **9**.

The isotropic Heisenberg spin Hamiltonian for 9 is given by Equation (13), where J_1 is associated with the Cu1$\cdots$Cu2' interactions through a diatomic oximato group; J_2 is associated with the Cu1$\cdots$Cu2 interaction through one monoatomic carboxylate bridge; and J3 describes the coupling of Cu1$\cdots$Cu1' through a μ_3-OH$^-$ group (**Figure 11**).

$$\mathcal{H} = -2J_1\left(\hat{S}_{Cu1} \cdot \hat{S}_{Cu2'} + \hat{S}_{Cu1'} \cdot \hat{S}_{Cu2}\right) - 2J_2\left(\hat{S}_{Cu1} \cdot \hat{S}_{Cu2} + \hat{S}_{Cu1'} \cdot \hat{S}_{Cu2'}\right)$$
$$- 2J_3\left(\hat{S}_{Cu1} \cdot \hat{S}_{Cu1'}\right) \quad (13)$$

The fitting of the experimental data to the Hamiltonian was performed using the PHI software [120] and is shown with a solid line in **Figure 10**; the fitting parameters are $J_1 = -508$ cm^{-1}, $J_2 = -1.45$ cm^{-1}, $J_3 = -8.77$ cm^{-1}, and g = 2.07.

130

J_1 is significantly stronger than J_2 and J_3; this high value of antiferromagnetic coupling is common in complexes containing oximes and Cu ions; such complexes often exhibit diamagnetic behavior.[82] J_2 and J_3 are too small to take them as reliable values because at the temperature they start to operate, the complex is diamagnetic due to the extremely high value of J_1.

An initial investigation of the potential of magnetism to be used for the development of novel MOF-based sensors was performed by exploring the impact of the encapsulated metal ion on then magnetic properties of **9**. To this end, DC magnetic susceptibility studies were performed on the polycrystalline samples of Fe@**9**-1 and Fe@**9**-2, where Fe@**9**-1 is the Fe@**9** aggregate after 1 min stirring, during which **9** is expected to have reached ca. its half metal encapsulation capacity, and Fe@**9**-2 is the aggregate at its maximum metal adsorption capacity. A closer inspection in **Figure 11** shows that, although the overall profile of the three plots is similar, the increase of the paramagnetic component in the MOF pores have an effect on the observed $\chi_M T$ value at room temperature; the latter increases from 0.073 $cm^3 \cdot mol^{-1}$ K (for **9**) to 0.115 $cm^3 \cdot mol^{-1}$ K (for Fe@**9**-1) and 0.135 $cm^3 \cdot mol^{-1}$ K (for Fe@**9**-2), indicating that the magnetic properties of the Fe@**9** aggregate are affected by the amount of metal encapsulated in the MOF pores.

4. Conclusions

The initial employment of a 2-pyridyl oxime (pyridine-2 amidoxime, pyaoxH$_2$; 2-methyl pyridyl ketoxime, mpkoH) in combination with 1,2,4,5-benzene tetracarboxylic acid (pyromellitic acid), H$_4$pma, provided access to nine new compounds with interesting structural features, paving the way to the development of an alternative synthetic route towards new MOFs and

coordination polymers. $[Zn_2(pma)(pyaoxH_2)_2(H_2O)_2]_n$ (**3**) and $[Cu_4(OH)_2(pma)(mpko)_2]_n$ (**9**) are the first examples of MOFs based on a 2-pyridyl oxime, whereas $[Zn_2(pma)(pyaoxH_2)_2]_n$ (**2**), $[Cu_2(pma)(pyaox H_2)_2(DMF)_2]_n$ (**6**), and $[Cu_2(pma)(mpkoH)_2(DMF)_2]_n$ (**8**) are new members of a small family of coordination polymers bearing this type of ligands. **9** has a novel 3,4,5,8-c net topology and is based on a butterfly-shaped Cu_4 SBU. DC magnetic susceptibility studies revealed that there are strong antiferromagnetic interactions between the metal centers in **9**, which lead to a diamagnetic ground state.

The metal encapsulation capacity of **9** was tested for a variety of different metal ions and showed that it exhibits selectivity for Fe^{3+} adsorption. It is noteworthy that the magnetic properties of **9** depend on the amount of Fe^{3+} present in to the MOF pores, revealing that magnetism can be an alternative technique for the detection of environmentally hazardous chemicals, and this can be especially useful for species that do not affect the photoluminescence properties or the color of a compound, hence they cannot be detected by the commonly used sensors. Treatment of the Fe@**9** aggreagate with a 0.2 M EDTA solution leads to the removal of the metal ions from the MOF pores and the regeneration of the latter. **9** retains its metal adsorption capacity for three cycles of regeneration/reuse experiments.

Supplementary Materials: The following are available online at *HTTP://WWW.MDPI.COM/1996-1944/13/18/4084/S1*, **Figure S1**: Representation of the 3D network formed through hydrogen bonding interactions in **2**. **Figure S2**: Representation of the molecular structure of the dinuclear complex **5**. **Figure S3**: Representation of the molecular structure of the dinuclear complex **7**. **Figure S4**: Representation of the intramolecular hydrogen bonding interactions in **9**. **Figure**

S5: Representation of the underlying 3,4,5,8-coordinated net in the standard representation in **9**. **Figure S6**: The underlying net in the cluster representation with the lvt topology with Point Symbol (42)(84) in **9**. **Figure S7**: Comparison of the theoretical and experimental pxrd pattern for **9**. **Figure S8**: Left: metal adsorption capacity (mg g^{-1}) versus time (h) plot for the encapsulation of $FeCl_3$ by **9**; right: simulation of the experimental data to the pseudo-second order kinetic model. The solid lines represent the fitting of the data. The corresponding fitting parameters are R_2 = 0.9937, qe = 103.09 mg Fe^{3+}/g **9**, in very good agreement with the experimental data. **Figure S9**: Comparison of the pxrd pattern of the initial **9** with that of the regenerated material. **Figure S10**: UV studies of the 6-methyluracil adsorption by **9**; (a) 0.05 mmol 9/0.1 mmol 6-methyluracil and (b) 0.1 mmol **9**/0.1 mmol 6-methyluracil (in 10 mL of water). **Tables S1–S9**: Selected interatomic distances (Å) and angles for **1–9**. **Table S10**: Hydrogen bonding details for 1. **Table S11**: Intermolecular hydrogen bonding details for **4**. **Table S12**: Intermolecular hydrogen bonding details for **7**.

Conflicts of Interest: The authors declare no conflict of interest.

References

1. Qin, J.-S.; Du, D.-Y.; Guan,W.; Bo, X.-J.; Li, Y.-F.; Guo, L.-P.; Su, Z.-M.;Wang, Y.-Y.; Lan, Y.-Q.; Zhou, H.-C. *J. Am. Chem. Soc.* **2015** 137, 7169–7177.

2. Ma, L.; Falkowski, J.M.; Abney, C.; Lin, W. *Nat. Chem.* **2010** 2, 838–846.

3. Kuznetsova, A.; Matveevskaya, V.; Pavlov, D.; Yakunenkov, A.; Potapov, A. *Materials* **2020** 13, 2699.

4.Wu, M.-X.; Yang, Y.-W. *Adv. Mater.* **2017** 29, 1606134.

5. Huxford, R.C.; Rocca, J.D.; Lin, W. *Curr. Opin. Chem. Biol.* **2010** 14, 262–268.

6. Hu, Z.; Deibert, B.J.; Li, J. *Chem. Soc. Rev.* **2014** 43, 5815–5840.

7. Douvali, A.; Tsipis, A.C.; Eliseeva, S.V.; Petoud, S.; Papaefstathiou, G.S.; Malliakas, C.D.; Papadas, I.; Armatas, G.S.; Margiolaki, I.; Kanatzidis, M.G.; et al. *Angew. Chem. Int.Ed.* **2015** 54, 1651.

8. Coulon, C.; Miyasaka, H.; Clérac, R. *Struct. Bonding* **2006** 122, 163–206.

9. Jeon, I.-R.; Clérac, R. *Dalton Trans.* **2012** 41, 9569–9586.

10. Miyasaka, H.; Julve, M.; Yamashita, M.; Clérac, R. *Inorg. Chem.* **2009** 48, 3420–3437.

11. Bernot, K.; Luzon, J.; Sessoli, R.; Vindigni, A.; Thion, J.; Richeter, S.; Leclercq, D.; Larionova, J.; Van der Lee, A. *J. Am. Chem. Soc.* **2008** 130, 1619–1627.

12. Wang, T.-T.; Ren, M.; Bao, S.-S.; Liu, B.; Pi, L.; Cai, Z.-S.; Zheng, Z.-H.; Xu, Z.-L.; Zheng, L.-M. *Inorg. Chem.* **2014** 53, 3117–3125.

13. Gatteschi, D.; Sessoli, R. *Angew. Chem. Int. Ed.* **2003** 42, 268–297.

14. Papatriantafyllopoulou, C.; Zartilas, S.; Manos, M.J.; Pichon, C.; Clérac, R.; Tasiopoulos, A.J. *Chem. Commun.* **2014** 50, 14873–14876.

15. Bogani, L.; Wernsdorfer, W. *Nat. Mater.* **2008** 7, 179–186.

16. Leuenberger, M.N.; Loss, D. *Nature* **2001** 410, 789–793.

17. Chen, L.; Ji, Q.;Wang, X.; Pan, Q.; Ccao, X.; Xu, G. *CrystEngComm* **2017** 19, 5907–5914.

18. Hui, J.; Kishida, H.; Ishiba, K.; Takemasu, K.; Morikawa, M.; Kimizuka, N. *Chem Eur. J.* **2016** 22, 14213–14218.

19. Wang, H.-N.; Meng, X.; Dong, L.-Z.; Chen, Y.; Li, S.-L.; Lan, Y.-Q. *J. Mater. Chem. A* **2019** 7, 24059–24091.

20. Givaja, G.; Amo-Ochoa, P.; Gomez-Garcia, C.; Zamora, F. *Chem. Soc. Rev.* **2012** 41, 115–147.

21. Yue, Q.; Gao, E.-Q. *Coord. Chem. Rev.* **2019** 382, 1–31.

22. Zhou, H.-C.; Kitagawa, S. *Chem. Soc. Rev.* **2014** 43, 5415–5418.

23. Yan, S.; Feng, L.;Wang, K.; Pang, J.; Bosch, M.; Lollar, C.; Sun, Y.; Qin, J.;Wang, X.; Zhang, P.; et al. *Adv. Mater.* **2018** 37, 1704303.

24. Eddaoudi, M.; Moler, D.B.; Li, H.; Chen, B.; Rheineke, T.M.; O'Keefe, M.; Yaghi, O.M. *Acc. Chem. Res.* **2001** 34, 319–330.

25. Ugale, B.; Singh Dhankhar, S.; Nagaraja, C.M. *Cryst. Growth Des.* **2017** 17, 3295–3305.

26. Manos, M.J.; Markoulides, M.S.; Malliakas, C.D.; Papaefstathiou, G.S.; Chronakis, N.; Kanatzidis, M.G.; Trikalitis, P.N.; Tasiopoulos, A.J. *Inorg. Chem.* **2011** 50, 11297–11299.

27. Sezginel, K.B.; Feng, T.; Wilmer, C.E. *CrystEngComm* **2017** 19, 4497–4504.

28. Alhamami, M.; Doan, H.; Cheng, C.-H. *Materials* **2014** 7, 3198–3250.

29. Nouar, F.; Devic, T.; Chevreau, H.; Guillou, N.; Gibson, E.; Clet, G.; Daturi, M.; Vimont, A.; Grenèche, J.M.; Breeze, M.I.; et al. *Chem. Commun.* **2012** 48,10237–10239.

30. Li, H.;Wang, K.; Sun, Y.; Tollar, C.; Li, J.; Zhou, H.-C. *Mater. Today* **2018** 21, 108–121.

31. Li, H.; Li, L.; Lin, R.-B.; Zhou,W.; Zhang, Z.; Xiang, S.; Chen, B. *EnergyChem* **2019** 1, 100006.

32. Giménez-Marqués, M.; Hidalgo, T.; Serre, C.; Horcajada, P. *Coord. Chem. Rev.* **2016** 307, 342–360.

33. Xue, T.; Xu, C.; Wang, Y.; Wang, Y.; Tian, H.; Zhang, Y. *Biomater. Sci.* **2019** 7, 4615–4623.

34. Mínguez Espallargas, G.; Coronado, E. *Coord. Chem. Rev.* **2018** 47, 533–557.

35. Pascanu, V.; González Miera, G.; Ken Inge, A.; Martín-Matute, B. *J. Am. Chem. Soc.* **2019** 141, 7223–7234.

36. Ricco, R.; Styles, M.J.; Falcaro, P. Metal-Organic Frameworks (MOFs) for Environmental Applications; Ghosh, S.K., Ed.; *Elsevier: Amsterdam, The Netherlands*, **2019** 383–426.

37. Molavi, H.; Hakimian, A.; Shojaei, A.; Raeiszadeh, M. *Appl. Surf. Sci.* **2018** 445, 424–436.

38. Kobielska, P.A.; Howarth, A.J.; Farha, O.K.; Nayak, S. *Coord. Chem. Rev.* **2018** 358, 92–107.

39. Vellingiri, K.; Szulejko, J.E.; Kumar, P.; Kwon, E.E.; Kim, K.-H.; Deep, A.; Boukhvalov, D.W.; Brown, R.J.C. *Sci. Rep.* **2016** 6, 27813.

40. Ahmed, I.; Jhung, S.H. *J. Hazard. Mater.* **2016** 301, 259–276.

41. Seo, P.W.; Bhadra, B.N.; Ahmed, I.; Khan, N.A.; Jhung, S.H. *Sci. Rep.* **2016** 6, 34462.

42. Yang, J.; Hou, B.; Wang, J.; Tian, B.; Bi, J.; Wang, N.; Li, X.; Huang, X. *Nanomaterials* **2019** 9, 424.

43. Zanin, E.; Scapinello, J.; de Oliveira, M.; Rambo, C.L.; Franscescon, F.; Freitas, L.; de Mello, J.M.M.; Fiori, M.A.; Oliveira, J.V.; Magro, J. *Process Saf. Environ. Prot.* **2017** 105, 194–200.

44. Dias, E.M.; Petit, C. *J. Mater. Chem. A* **2015** 3, 22484–22506.

45. Zhao, L.; Azhar, M.R.; Li, X.; Duan, X.; Sun, H.;Wang, S.; Fang, X. *J. Colloid Interface Sci.* **2019** 542, 421–428.

46. Barreto, J.; Xavier, M.D.G.; Ribeiro, R.P.P.L.; Martins, D.; Esteves, I.A.A.C.; Branco, M.; Tirolien, T.; Mota, J.P.B.; Bonfait, G. Neon *J. Chem. Eng. Data* **2019** 64, 5407–5414.

47. Ramanayaka, S.; Vithanage, M.; Sarmah, A.; An, T.; Kim, K.-H.; Sik Ok, Y. *RSC Adv.* **2019** 9, 34359–34376.

48. Chen, C.-H.; Wang, X.-S.; Li, L.; Huang, Y.-B.; Cao, R. *Dalton Trans.* **2018** 47, 3452–3458.

49. Lustig,W.P.; Mukherjee, S.; Rudd, N.D.; Desai, A.V.; Li, J.; Ghosh, S.K. *Chem. Soc. Rev.* **2017** 46, 3242–3285.

50. Shum, J.; Kam-Keung Leung, P.; Kam-Wing Lo, K. *Inorg. Chem.* **2019** 58, 2231–2247.

51. Amudhan Senthana, S.; Alexander, V. *New J. Chem.* **2016** 40, 10064–10070.

52. Ji, G.; Liu, J.; Gao, X.; Sun, W.; Wang, J.; Zhao, S.; Liu, Z. *J. Mater. Chem. A* **2017** 5, 10200–10205.

53. Yan, B. *Acc. Chem. Res.* **2017** 50, 2789–2798.

54. Cui, Y.; Xu, H.; Yue, Y.; Cuo, Z.; Yu, J.; Chen, Z.; Gao, J.; Yang, Y.; Qian, G.; Chen, B. *J. Am. Chem. Soc.* **2012** 134, 3979–3982.

55. Kou,W.-T.; Yang, C.-X.; Yan, X.-P. *J. Mater. Chem. A* **2018** 6, 17861–17866.

56. Ardila-Suárez, C.; Díaz-Lasprilla, A.M.; Díaz-Vaca, L.A.; Balbuena, P.B.; . Baldovino-Medrano, V.G.; Ramírez-Caballero, G.E. *CrystEngComm* **2019** 21, 3014–3330.

57. Garibay, S.J.; Cohen, S.M. *Chem. Commun.* **2010** 46, 7700–7702.

58. Mai, Z.; Liu, D. *Cryst. Growth Des.* **2019** 19, 7439–7462.

59. Yaghi, O.M.; O'Keeffe, M.; Ockwig, N.W.; Chae, H.K.; Eddaoudi, M.; Kim, J. *Nature* **2003** 423, 705–714.

60. Klinowski, J.; Almeida Paz, F.A.; Silva, P.; Rocha, J. *Dalton Trans.* **2011** 40, 321–330.

61. Vinu, M.; Lin,W.-C.; Senthil Raja, D.; Han, J.-L.; Lin, C.-H. *Polymers* **2017** 9, 498.

62. Chen, D.; Zhao, J.; Zhang, P.; Dai, S. *Polyhedron* **2019** 162, 59–64.

63. Wang, Z.; Li, Z.; Ng, M.; Milner, P.J. *Dalton Trans.* **2020**. Advance Article.

64. Zhao, X.-L.; Sun, W.-Y. *Cryst. Eng. Comm.* **2014** 16, 3247–3258.

65. Kourtellaris, A.; Moushi, E.E.; Spanopoulos, I.; Tampaxis, C.; Charalambopoulou, G.; Steriotis, T.A.; Papaefstathiou, G.S.; Trikalitis, P.N.; Tasiopoulos, A.J. *Inorg. Chem. Front.* **2016** 3, 1527–1535.

66. Moushi, E.E.; Kourtellaris, A.; Spanopoulos, I.; Manos, M.J.; Papaefstathiou, G.S.; Trikalitis, P.N.; Tasiopoulos, A.J. *Cryst. Growth Des.* **2015** 15, 185–193.

67. Chen, Z.; Adil, K.; Weselinski, L.J.; Belmabkhout, Y.; Eddaoudi, M.J. *Mater. Chem. A* **2015** 3, 6276–6281.

68. Li, H.; Eddaoudi, M.; O'Keeffe, M.; Yaghi, O.M. *Nature* **1999**, 402, 276–279.

69. Sapchenko, S.A.; Dybtsev, D.N.; Damsonenko, D.G.; Fedin, V.P. *New J. Chem.* **2010** 34, 2445–2450.

70. Tranchemontagne, D.J.; Hunt, J.R.; Yaghi, O.M. *Tetrahedron* **2008** 64, 8553–8557.

71. Clausen, H.F.; Poulsen, R.D.; Bond, A.D.; Chevallier, M.-A.S.; Iversen, B.B. *J. Solid State* **2005**, 178, 3342–3351.

72. Manos, M.J.; Moushi, E.E.; Papaefstathiou, G.S.; Tasiopoulos, A.J. *Cryst. Growth Des.* **2012** 12, 5471–5480.

73. Guesh, K.; Caiuby, C.A.D.; Mayoral,Á.;Díaz-García, M.;Díaz, I.; Sanchez-Sanchez, M. *Cryst. Growth Des.***2017** 17, 1806–1813.

74. Horcajada, P.; Surblé, S.; Serre, C.; Hong, D.-Y.; Seo, Y.-K.; Chang, J.-S.; Grenèche, J.-M.; Margiolaki, I.; Férey, G. *Chem. Commun.* 2**007** 2820–2822.

75. Shimizu, G.K.H.; Vaidhyanathan, R.; Taylor, J.M. *Chem. Soc. Rev.* **2009** 38, 1430–1449.

76. Singh, N.; Singh, U.P.; Butcher, R.J. *CrystEngComm* **2017** 19, 7009–7020.

77. ZareKarizi, F.; Johariana, M.; Morsali, A. *J. Mater. Chem. A* **2018** 6, 19288–19329.

78. Yin, Z.; Zhou, Y.-L.; Zeng, M.-H.; Kurmoo, M. *Dalton Trans.* **2015** 44, 5258–5275.

79. Abednatanzi, S.; Gohari Derakhshandeh, P.; Depauw, H.; Coudert, F.-X.; Vrielinck, H.; Van Der Voort, P.; Leus, K. *Chem. Soc. Rev.* **2019** 48, 2535–2565.

80. Masoomi, M.Y.; Morsali, A.; Dhakshinamoorthy, A.; Garcia, H. *Angew. Chem. Int. Ed.* **2019** 58, 15188–15205.

81. Zhai, Q.-G.; Bu, X.; Mao, C.; Zhao, X.; Feng, P. *J. Am. Chem. Soc.* **2016** 138, 2524–2527.

82. Milios, C.J.; Stamatatos, T.C.; Perlepes, S.P. *Polyhedron* **2006** 25, 134–194.

83. Papatriantafyllopoulou, C.; Jones, L.F.; Nguyen, T.D.; Matamoros-Salvador, N.; Cunha-Silva, L.; Almeida Paz, F.A.; Rocha, J.; Evangelisti, M.; Brechin, E.K.; Perlepes, S.P. *Dalton Trans.* **2008** 3153–3155.

84. Efthymiou, C.G.; Cunha-Silva, L.; Perlepes, S.P.; Brechin, E.K.; Inglis, R.; Evangelisti, M.; Papatriantafyllopoulou, C. *Dalton Trans.* **2016** 17409–17419.

85. Papatriantafyllopoulou, C.; Stamatatos, T.C.; Wernsdorfer, W.; Teat, S.J.; Tasiopoulos, A.J.; Escuer, A.; Perlepes, S.P. *Inorg. Chem.* **2010** 49, 10486–10496.

86. Polyzou, C.D.; Efthymiou, C.G.; Escuer, A.; Cunha-Silva, L.; Papatriantafyllopoulou, C.; Perlepes, S.P. *Pure Appl. Chem.* **2013** 85, 315–327.

87. Papatriantafyllopoulou, C.; . Stamatatos, T.C.; . Efthymiou, C.G.; Cunha-Silva, L.; Almeida Paz, F.A.; Perlepes, S.P.; Christou, G. *Inorg. Chem.* **2010** 49, 9743–9745.

88. Papatriantafyllopoulou, C.; Estrader, M.; Efthymiou, C.G.; Dermitzaki, D.; Gkotsis, K.; Terzis, A.; Diaz, C.; Perlepes, S.P. *Polyhedron* **2009** 28, 1652–1655.

89. Efthymiou, C.G.; Mylonas-Margaritis, I.; Das Gupta, S.; Tasiopoulos, A.; Nastopoulos, V.; Christou, G.; Perlepes, S.P.; Papatriantafyllopoulou, C. *Polyhedron* **2019** 171, 330–337.

90. Nguyen, T.N.; Wernsdorfer, W.; Shiddiq, M.; Abboud, K.A.; Hill, S.; Christou, G. *Chem. Sci.* **2016** 7, 1156–1173.

91. Nguyen, T.N.; Shiddiq, M.; Ghosh, T.; Abboud, K.A.; Hill, S.; Christou, G. *J. Am. Chem. Soc.* **2015** 137, 7160–7168.

92. Ghosh, T.; Abboud, K.A.; Christou, G. *Polyhedron* **2019** 173, 114145.

93. Stamatatos, T.C.; Foguet-Albiol, D.; Stoumpos, C.C.; Raptopoulou, C.P.; Terzis, A.; Wernsdorfer, W.; Perlepes, S.P.; Christou, G. *Polyhedron* **2007** 26, 2165–2168.

94. Escuer, A.; Vlahopoulou, G.; Mautner, F.A. *Inorg. Chem.* **2011** 50, 2717–2719.

95. Mowson, A.M.; Nguyen, T.N.; Abboud, K.A.; Christou, G. *Inorg. Chem.* **2013** 52, 12320–12322.

96. Fabelo, O.; Pasan, J.; Canadillas-Delgado, L.; Delgado, F.S.; Lloret, F.; Julve, M.; Ruiz-Perez, C. *Inorg. Chem.* **2008** 47, 8053–8061.

97. Zhong, D.-C.; Guo, H.-B.; Deng, J.-H.; Chen, Q.; Luo, X.-Z *CrystEngComm* **2015** 17, 3519–3525.

98. Jia, H.-P.; Li,W.; Ju, Z.-F.; Zhang, J. *DaltonTrans*. **2007** 33, 3699–3704.

99. Luo, Y.-H.; Tao, C.-Z.; Zhang, D.-E.; Ma, J.-J.; Liu, L.; Tong, Z.-W.; Yu, X. *Polyhedron* **2017** 123, 69–74.

100. Ji,W.-J.; Hu, M.-C.; Li, S.-N.; Jiang,Y.-C.; Zhai, Q.-C. *CrystEngComm* **2014** 16, 3474–3477.

101. Geng, J.-P.; Wang, Z.-X.; He, Z.; Xiao, H.-P.; Li, M.-X. *Inorg. Chem. Commun.* **2011** 14, 997–1000.

102. Sun, L.-P.; Niu, S.-Y.; Jin, J.; Yang, G.-D.; Ye, L. *Eur. J. Inorg. Chem.* **2006** 5130–5137.

103. Sanselme, M.; Greneche, J.M.; Riou-Cavellec, M.; Ferey, G. *Chem. Commun.* **2002** 2172–2173.

104. Olchowka, J.; Falaise, C.; Volkringer, C.; Henry, N.; Loiseau, T. *Chem.-Eur. J.* **2013** 19, 2012–2022.

105. Bernasek, E. *J. Org. Chem.* **1957** 22, 1263.

106. Orama, M.; Saarinen, H.; Korvenranta, J. *J. Coord. Chem.* **1990** 22, 183–190.

107. Sheldrick, G.M. SHELXT–Integrated space-group and crystal-structure determination. *Acta Crystallogr. Sect. A Found. Adv.* 2015, 71, 3–8.

108. McArdle, P.; Gilligan, K.; Cunningham, D.; Dark, R.; Mahon, M. *CrystEngComm* **2004** 6, 303–309.

109. Brandenburg, K. *DIAMOND, Version 2003.2001d; Crystal Impact GbR: Bonn, Germany,* **2006**.

110. Mylonas-Margaritis, I.;Winterlich, M.; Efthymiou, C.G.; Lazarides, T.; McArdle, P.; Papatriantafyllopoulou, C. *Polyhedron* **2018** 151, 360–368.

111. Addison, A.W.; Rao, T.N.; Reedijk, J.; van Rijn, J.; Verschoor, G.C. *J. Chem. Soc. Dalton Trans* **1984** 1346–1356.

112. Blatov, V.A.; Shevchenko, A.P.; Proserpio, D.M. *Cryst. Growth Des.* **2014** 14, 3576–3586.

113. O'Keeffe, M.; Peskov, M.A.; Ramsden, S.J.; Yaghi, O.M. *Acc. Chem. Res.* **2008** 41, 1782–1789.

114. Alexandrov, E.V.; Blatov,V.A.; Kochetkov, A.V.; Proserpio, D.M. *CrystEngComm* **2011** 13, 3947–3958.

115. Lagergren, S. Zur Theorie der Sogenannten Absorption Gelöster Stoe; *PA Norstedt & Söner: Stockholm, Sweden*, **1898** 1–39.

116. Ho, Y.S.; Mckay, G. *Process Biochem.* **1999** 34, 451–465.

117. Zhang, K.-D.; Tsai, F.-C.; Ma, N.; Xia, Y.; Liu, H.-L.; Zhan, X.-Q.; Yu, X.-Y.; Zeng, X.-Z.; Jiang, T.; Shi, D.; et al. *Materials* **2017**, 10, 205.

118. Langmuir, I. *J. Am. Chem. Soc.* **1915** 38, 2221–2295.

119. Ayawei, N.; Ebelegi, A.N.;Wankasi, D. *J. Chem.* **2017** 2017, 3039817.

120. Chilton, N.F.; Anderson, R.P.; Turner, L.D.; Soncini, A.; Murray, K.S. *J. Comput. Chem.* **2013** 34, 1164–1175.

Supplementary Material

Table S1. Selected interatomic distances (Å) and angles for **1**.

Bonds			
Zn1-N1	2.059(2)	Zn1-O11	1.987(2)
Zn1-N3	2.139(2)	Zn1-O2	2.049(2)
Zn1-O10	1.995(2)		
Angles			
O10-Zn1-O2	91.54(8)	O2-Zn1-N3	172.22(7)
O10-Zn1-O11	121.30(8)	O2-Zn1-N1	95.54(7)
O10-Zn1-N3	91.78(8)	O11-Zn1-N3	90.93(8)
O10-Zn1-N1	111.61(8)	O11-Zn1-N1	125.97(8)
O2-Zn1-O11	93.34(7)	N1-Zn1-N3	76.69(8)

Table S2. Selected interatomic distances (Å) and angles for **2**.

Bonds			
Zn1-O2	1.954(3)	Zn1-N2	2.031(4)

Zn1-N1	2.019(3)	Zn1-O5	1.966(4)
Angles			
O2-Zn1-O5	98.2(1)	N1-Zn1-O5	113.4(1)
O2-Zn1-N1	127.9(1)	N1-Zn1-N2	80.1(1)
O2-Zn1-N2	108.6(1)	N2-Zn1-O5	126.1(1)

Table S3. Selected interatomic distances (Å) and angles for **3**.

Bonds			
Zn1-O6	2.056(3)	Zn1-N2	2.058(3)
Zn1-O5	2.228(2)	Zn1-N1	2.198(2)
Zn1-O4	2.292(2)	Zn1-O3	2.027(2)
Angles			
O5-Zn1-O3	88.44(9)	O6-Zn1-O3	82.62(1)
O3-Zn1-N2	108.1(1)	O6-Zn1-N2	96.88(1)
N2-Zn1-N1	75.4(1)	O4-Zn1-N2	97.76(9)
N1-Zn1-O5	88.99(9)	O4-Zn1-N1	84.47(9)
O6-Zn1-N1	95.33(1)	O4-Zn1-O5	58.28(8)
O6-Zn1-O5	106.54(9)	O4-Zn1-O3	96.64(9)

Table S4. Selected interatomic distances (Å) and angles for **4**.

Bonds

Co1-N2	2.100	Co1-O3	2.132
Co1-O2	2.110	Co1-O4	2.070
Co1-O5	2.089	Co1-N1	2.162

Angles

N1-Co1-O2	89.92(1)	N2-Co1-O4	93.9(1)
O2-Co1-O5	83.74(9)	N2-Co1-N1	75.1(1)
O5-Co1-O4	94.8(1)	O3-Co1-O4	83.7(1)
O4-Co1-N1	92.2(1)	O3-Co1-N1	95.8(1)
N2-Co1-O2	97.6(1)	O3-Co1-O2	84.78(9)
N2-Co1-O5	101.9(1)	O3-Co1-O5	87.5(9)

Table S5. Selected interatomic distances (Å) and angles for **5**.

Bonds

Mn1-O6	2.149(3)	Mn1-O2	2.136(2)
Mn1-N1	2.304(3)	Mn1-N3	2.244(2)
Mn1-O8	2.170(2)	Mn1-O7	2.191(2)

Angles

N3-Mn1-O2	97.69(8)	O7-Mn1-O6	82.3(1)
N3Mn1-O8	99.04(8)	O7-Mn1-N1	94.45(9)
N3-Mn1-N1	70.46(8)	O6-Mn1-O2	95.4(1)
N3-Mn1-O6	94.7(1)	O6-Mn1-N1	92.0(1)
O7-Mn1-O8	83.63(9)	O2-Mn1-O8	85.79(8)
O7-Mn1-O2	97.66(8)	O8-Mn1-N1	89.74(8)

Table S6. Selected interatomic distances (Å) and angles for **6**.

Bonds

Cu1-O6	2.307(3)	Cu1-N1	1.992(4)
Cu1-O2	1.926(3)	Cu1-N3	1.970(4)
Cu1-O5	1.961(3)		

Angles

O5-Cu1-O2	90.9(1)	O6-Cu1-O2	88.0(1)
O2-Cu1-N3	93.5(1)	O6-Cu1-N3	101.8(1)
N3-Cu1-N1	79.2(2)	O6-Cu1-N1	90.2(1)
N1-Cu1-O5	97.0(1)	O6-Cu1-O5	95.1(1)

Table S7. Selected interatomic distances (Å) and angles for **7**.

Bonds			
Zn1-O4	2.062(3)	Zn1-N1	2.056(4)
Zn1-O2	2.100(3)	Zn1-O5	2.019(4)
Zn1-N2	2.041(4)	Zn1-O3	2.100(3)

Angles			
O4-Zn1-N2	91.1(1)	O2-Zn1-O5	85.0(1)
O4-Zn1-N1	91.1(1)	O2-Zn1-O3	89.7(1)
O4-Zn1-O5	91.9(1)	N2-Zn1-O5	103.8(1)
O4-Zn1-O3	92.2(1)	O5-Zn1-O3	83.0(1)
O2-Zn1-N2	87.4(1)	O3-Zn1-N1	94.5(1)
O2-Zn1-N1	92.0(1)	N1-Zn1-N2	78.5(1)

Table S8. Selected interatomic distances (Å) and angles for **8**.

Bonds			
Cu1-N1	1.972(3)	Cu1-O3	1.903(3)
Cu1-N2	2.032(3)	Cu1-O6	1.965(2)
Cu1-O2	2.269(2)		

Angles			
O2-Cu1-N1	88.6(1)	N2-Cu1-O3	93.2(1)

O2-Cu1-N2	100.7(1)	O3-Cu1-O6	91.75(9)
O2-Cu1-O3	88.63(9)	O6-Cu1-N1	97.2(1)
O2-Cu1-O6	99.58(8)	N2-Cu1-N1	78.8(1)

Table S9. Selected interatomic distances (Å) and angles for **9**.

Bonds			
Cu1-O1	1.943(3)	Cu2-O2	1.906(3)
Cu1-O2	1.920(3)	Cu2-O3	2.410(3)
Cu1-O2	2.334(3)	Cu2-O6	1.960(3)
Cu1-O3	1.958(3)	Cu2-N2	1.984(4)
Cu1-O5	1.961(3)	Cu2-N1	1.988(4)
Angles			
N2-Cu2-O2	87.2(1)	O2-Cu2-O3	82.4(1)
N2-Cu2-O3	90.4(1)	Cu2-O2-Cu1	94.2(1)
N2-Cu2-O6	174.3(2)	Cu2-O3-Cu1	90.5(1)
N2-Cu2-N1	80.4(2)	O3-Cu1-O5	89.6(1)
O1-Cu1-O2	92.0(1)	O3-Cu1-O2	83.3(1)

Table S10. Hydrogen bonding details for **1**[a].

D – H … A	D … A (Å)	H … A (Å)	DHA (°)	Symmetry operator of A
O(1) – H(1O4) … O(8)	2.693	1.839	165.12	*x*, -1+*y*, *z*
N(2) – H(2N2) … O(5)	3.069	2.399	135.16	*x*,-1+*y*, 1+*z*
O(10) – H(10A) …O(7)	2.729	1.870	170.65	*x*, *y*, -1+*z*
O(9) – H(1O9) … O(6)	2.577	1.713	166.14	1-*x*, 1-*y*, 1-*z*
O(11) – H(11B) … O(3)	2.673	1.831	161.60	1-*x*, 1-*y*, 2-*z*

[a] A=acceptor, D=donor

Table S11. Hydrogen bonding details for **4**[a].

D – H … A	D … A (Å)	H … A (Å)	DHA (°)	Symmetry operator of A
O(2) – H(2B) … O(7)	2.643	1.804	162.64	-1+*x*, *y*, *z*
O(3) – H(3B) … O(6)	2.711	1.667	166.11	-1+*x*, *y*, *z*
O(2) – H(2A) … O(4)	2.936	2.326	126.06	-1/2+*x*, ½-*y*, ½+*z*
O(4) – H(4B) … O(6)	2.656	1.646	155.62	-1/2+*x*, ½-*y*, ½+*z*

[a] A=acceptor, D=donor

Table S12. Hydrogen bonding details for **7**[a].

D – H … A	D … A (Å)	H … A (Å)	DHA (°)	Symmetry operator of A
O(3) – H(3B) … O(7)	2.759	1.909	166.16	-1+x, -1+y, z
O(2) – H(2A) … O(8)	2.602	1.739	178.63	-1+x, -1+y, z
O(2) – H(2B) … O(9)	2.876	2.066	151.29	x, -1+y, z
O(4) – H(4B) … O(8)	2.674	1.860	157.81	-1/2+x, ½-y, ½+z
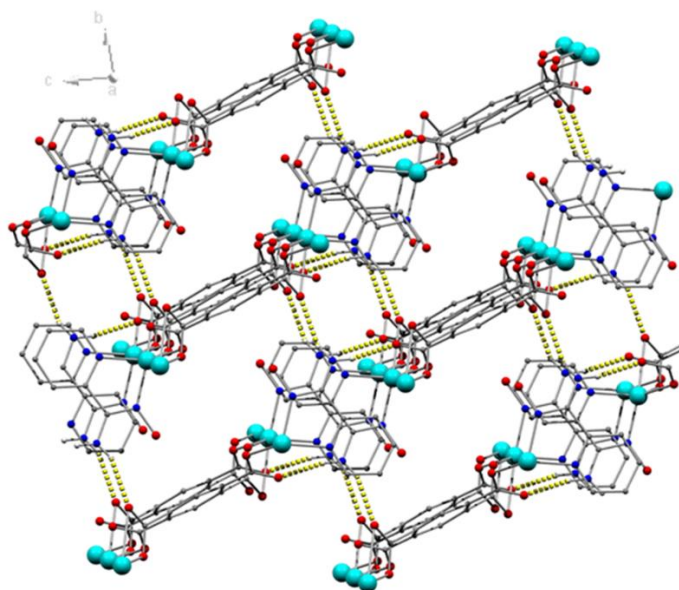
[a] A=acceptor, D=donor

Figure S1. Representation of the 3D network formed through hydrogen bonding interactions in **2**. Colour code: Zn, turquoise; N, navy blue; O, red; C, grey.
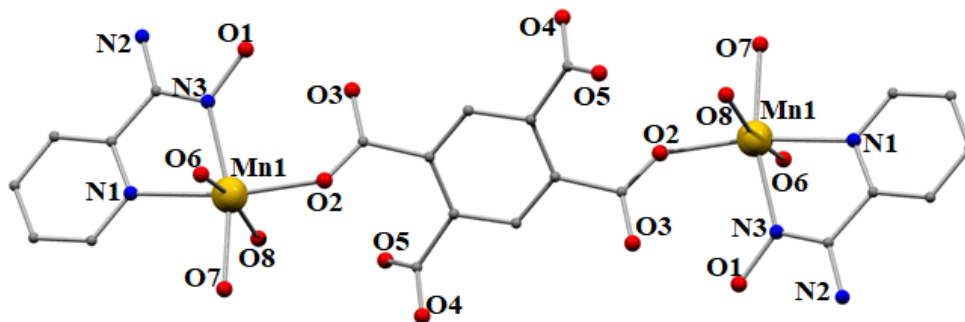
Figure S2. Representation of the molecular structure of the dinuclear complex **5**. Colour code: Mn^{II}, yellow; N, navy blue; O, red; C, grey. The hydrogen atoms are omitted for clarity.
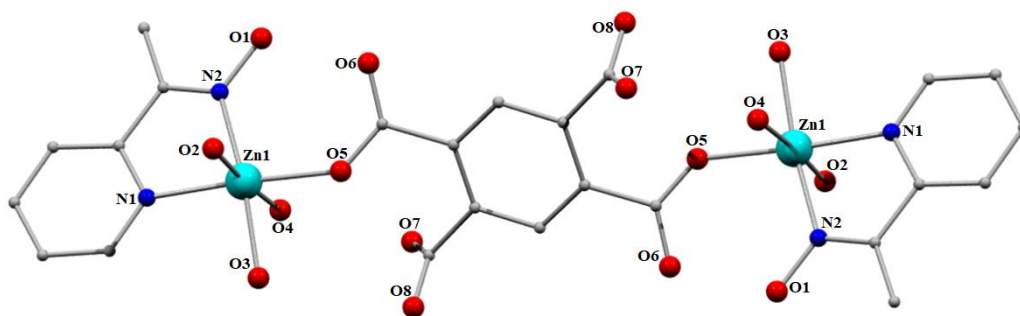
Figure S3. Representation of the molecular structure of the dinuclear complex **7**. Colour code: Zn^{II}, cyan; N, navy blue; O, red; C, grey. The hydrogen atoms are omitted for clarity.

Figure S4. Representation of the intramolecular hydrogen bonding interactions in **9**.

Figure S5. Representation of the underlying 3,4,5,8-coordinated net in the standard representation in **9**.

Figure S6. The underlying net in the cluster representation with the lvt topology with Point Symbol $(4^2)(8^4)$ in **9**.

Figure S7. Comparison of the theoretical and experimental pxrd pattern for **9**.

Figure S8. Left: metal adsorption capacity (mg g^{-1}) versus time (h) plot for the encapsulation of FeCl$_3$ by **9**; right: simulation of the experimental data to the pseudo-second order kinetic model. The solid lines represent the fitting of the data. The corresponding fitting parameters are R^2=0.9937, q$_e$=103.09 mg Fe^{3+} / g **9**, in very good agreement with the experimental data.

Figure S9. Comparison of the pxrd pattern of the initial **9** with that of the regenerated material.

Figure S10. UV studies of the 6-methyluracil adsorption by **9**; (a) 0.05mmol **9** / 0.1 mmol 6-methyluracil and (b) 0.1mmol **9** / 0.1mmol 6-methyluracil (in 10ml of water).

Figure S11. The TGA diagram for **1**.
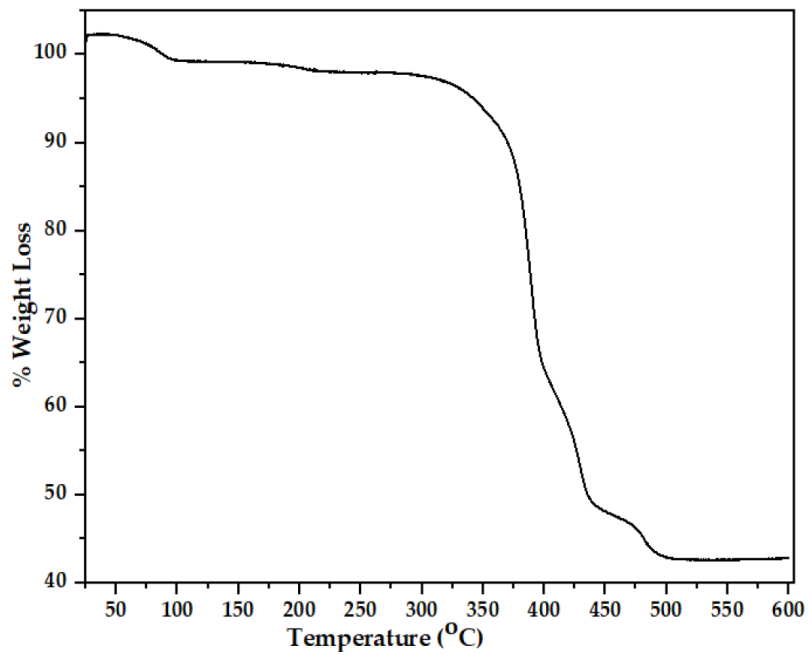
Figure S12. The TGA diagram for **2**.
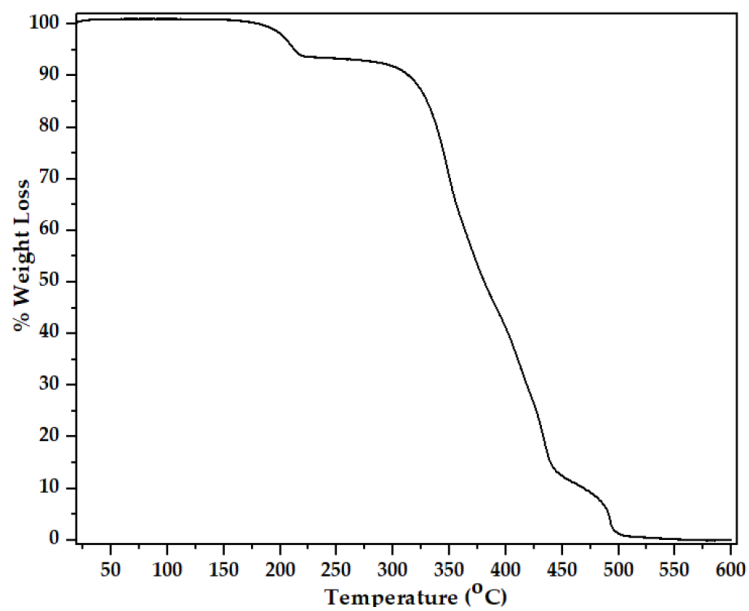
Figure S13. The TGA diagram for **3**.
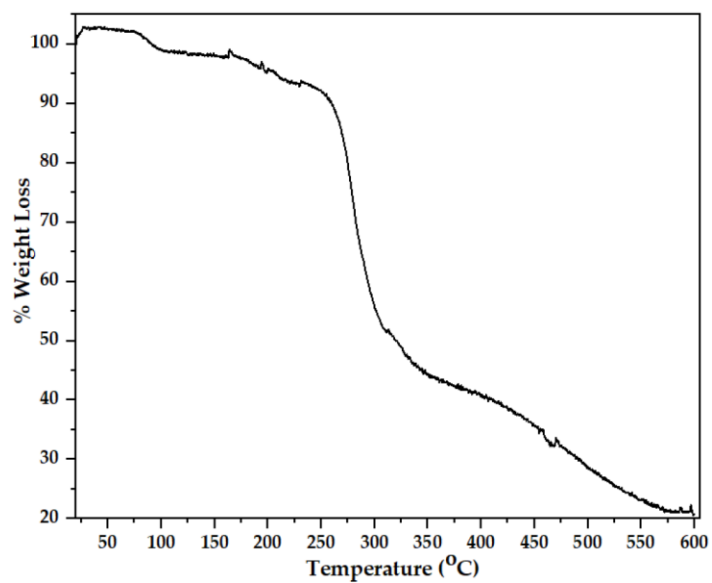
Figure S14. The TGA diagram for **6**.
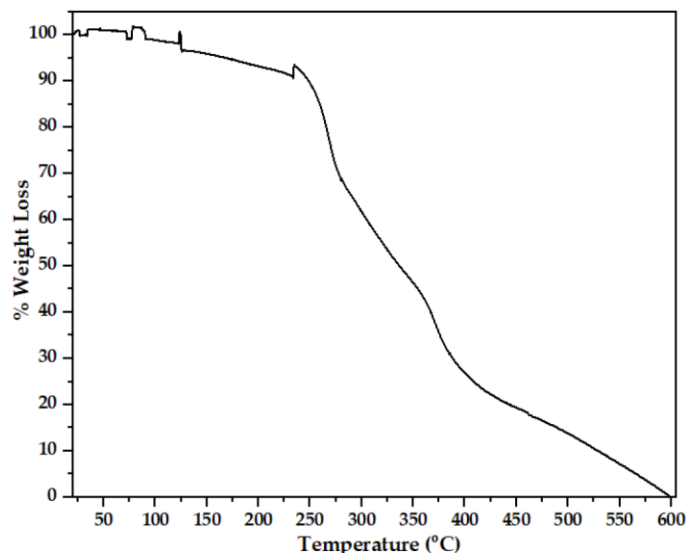
Figure S15. The TGA diagram for **7**.
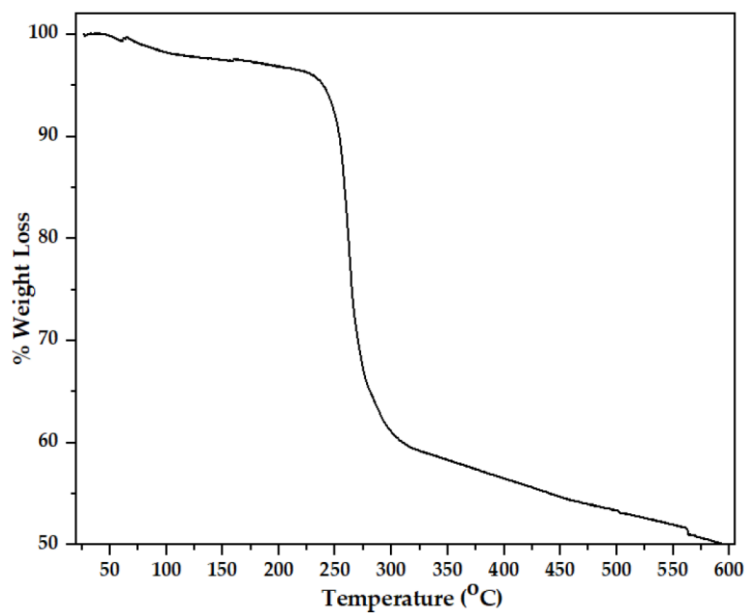
Figure S16. The TGA diagram for **8**.
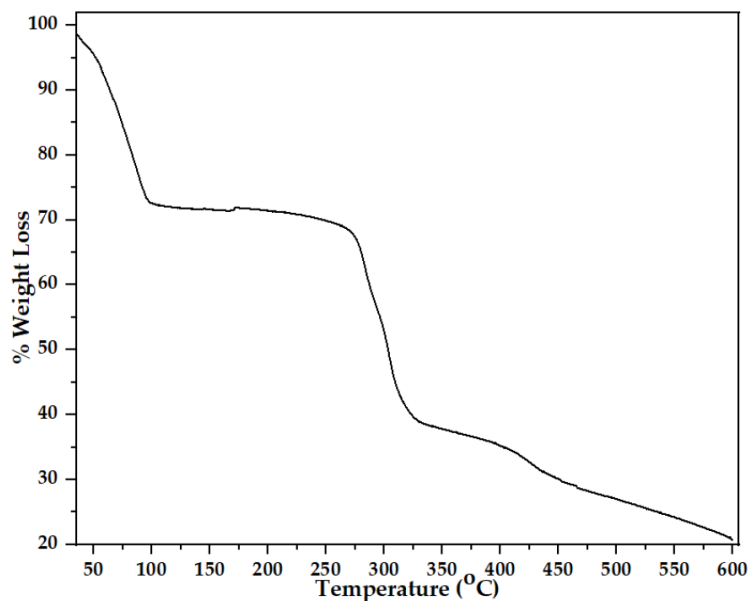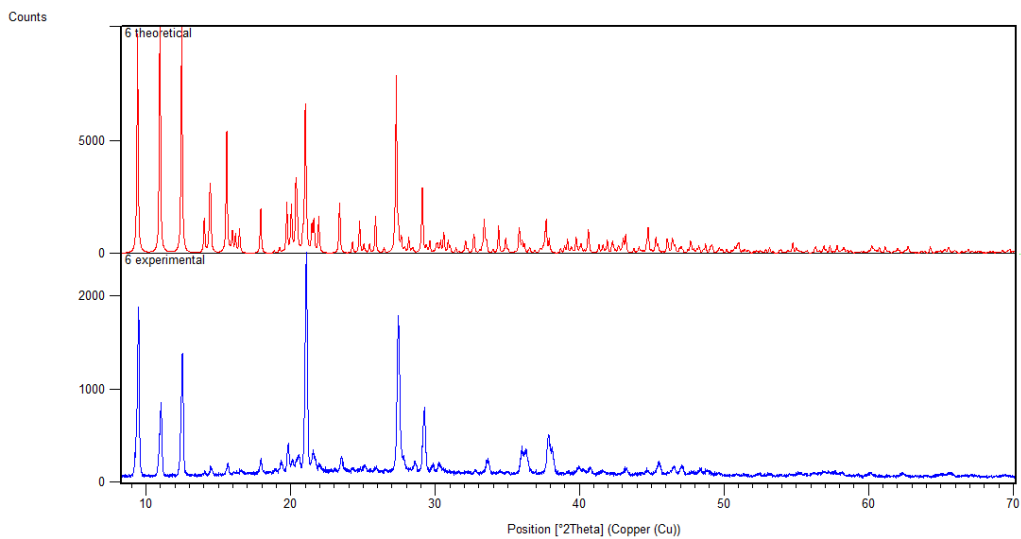
Figure S17. The TGA diagram for **9**.
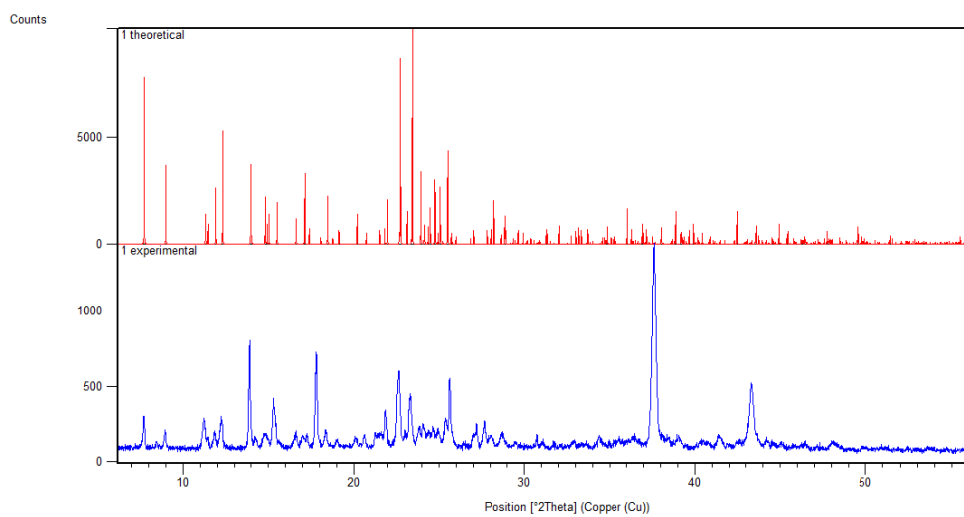
Figure S18. The experimental (bottom) and theoretical (top) pxrd pattern diagrams for **1**.
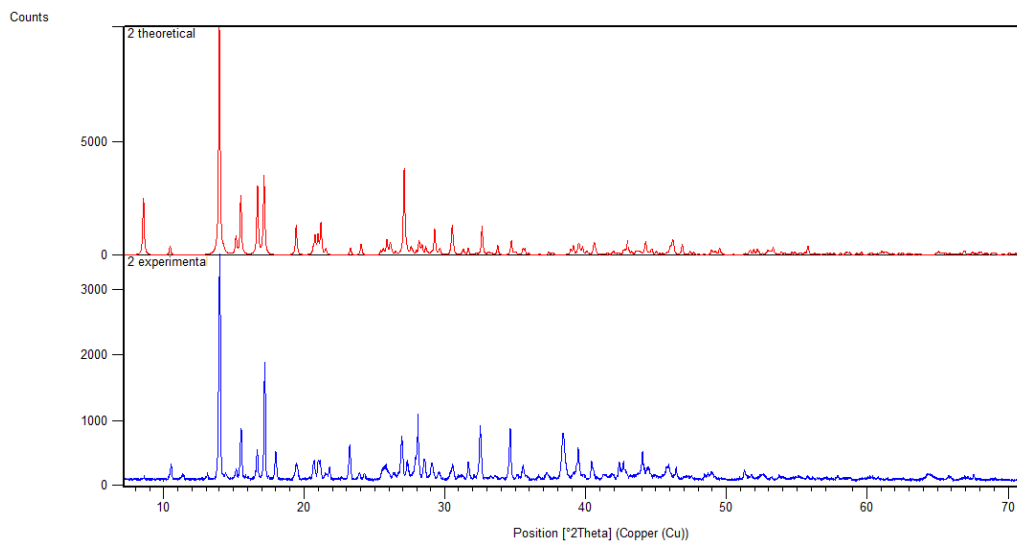
Figure S19. The experimental (bottom) and theoretical (top) pxrd pattern diagrams for **2**.
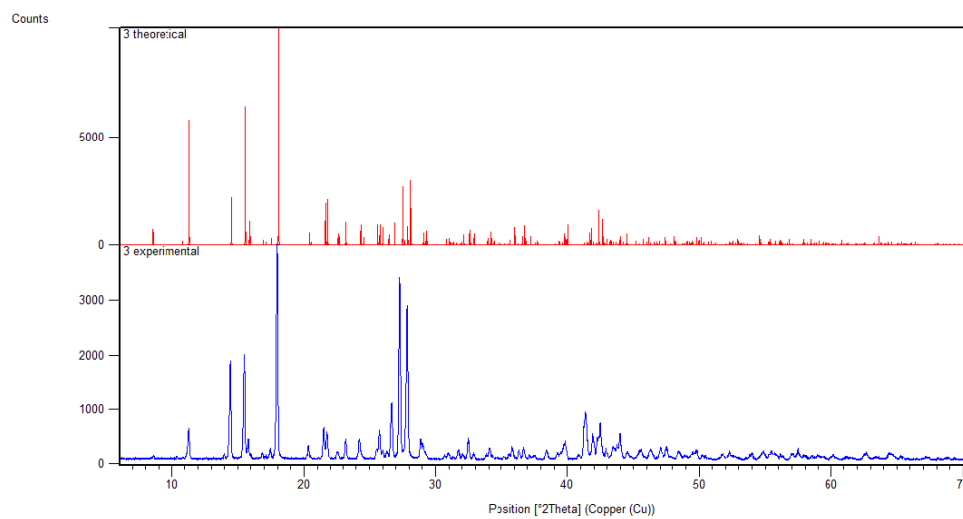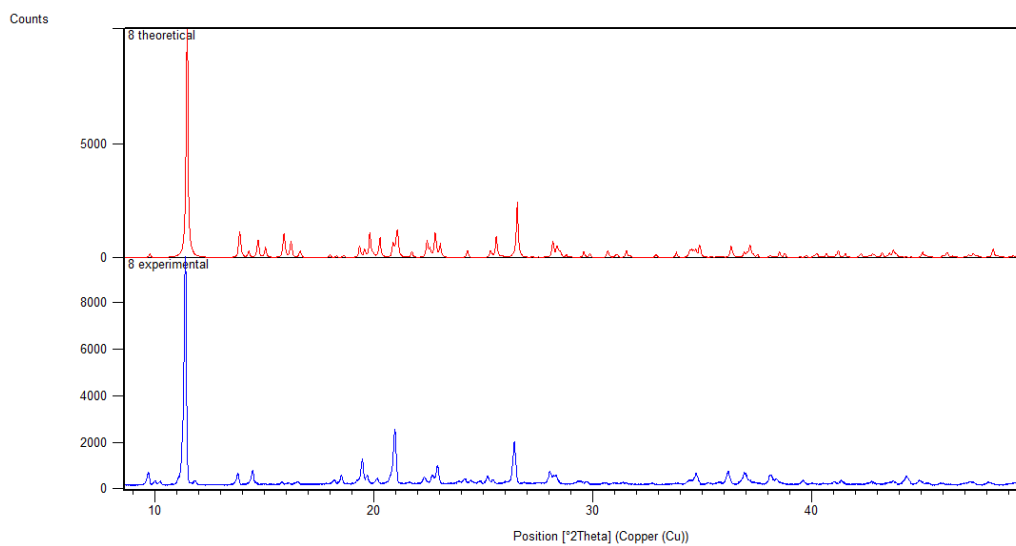

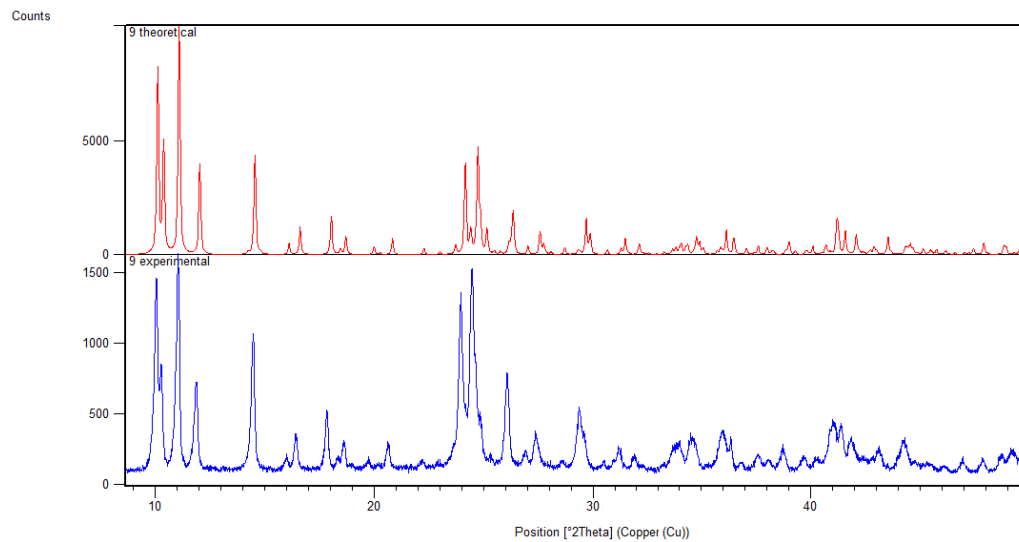**Figure S20.** The experimental (bottom) and theoretical (top) pxrd pattern diagrams for **3**.

Figure S21. The experimental (bottom) and theoretical (top) pxrd pattern diagrams for **6**.

Figure S22. The experimental (bottom) and theoretical (top) pxrd pattern diagrams for **8**.
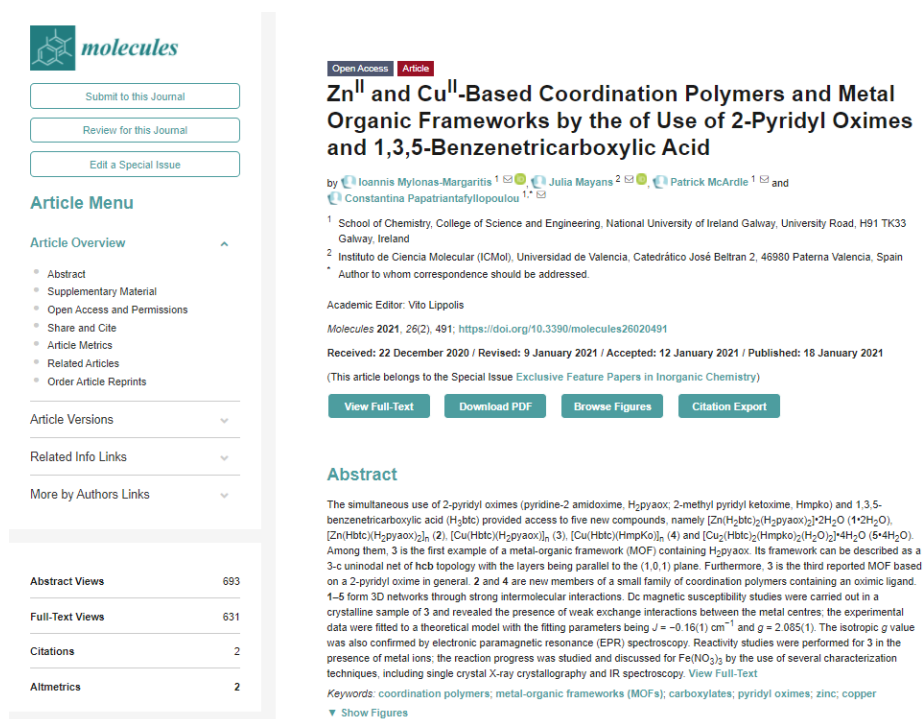
Figure S23. The experimental (bottom) and theoretical (top) pxrd pattern diagrams for **9**.

2.3 Brief description of the paper

In this article are represented Zn(II) and Cu(II) coordination polymers and MOFs by the simultaneous use of 2-pyridyl oximes and trimesic acid. The Cu(II) MOF was magnetically studied and its reactivity studies with Fe(III) metal salts were explored through IR spectroscopy and X-ray crystallography.

by Ioannis Mylonas-Margaritis [1], Julia Mayans [2], Patrick McArdle [1] and Constantina Papatriantafyllopoulou [1,*]

[1] School of Chemistry, College of Science and Engineering, National University of Ireland Galway, University Road, H91 TK33 Galway, Ireland
[2] Instituto de Ciencia Molecular (ICMol), Universidad de Valencia, Catedrático José Beltran 2, 46980 Paterna Valencia, Spain
* Author to whom correspondence should be addressed.

View Full-Text | Download PDF | Browse Figures | Citation Export

Abstract

The simultaneous use of 2-pyridyl oximes (pyridine-2 amidoxime, H_2pyaox; 2-methyl pyridyl ketoxime, Hmpko) and 1,3,5-benzenetricarboxylic acid (H_3btc) provided access to five new compounds, namely $[Zn(H_2btc)_2(H_2pyaox)_2]\cdot 2H_2O$ (1·2H_2O), $[Zn(Hbtc)(H_2pyaox)_2]_n$ (2), $[Cu(Hbtc)(H_2pyaox)]_n$ (3), $[Cu(Hbtc)(HmpKo)]_n$ (4) and $[Cu_2(Hbtc)_2(Hmpko)_2(H_2O)_2]\cdot 4H_2O$ (5·4H_2O). Among them, 3 is the first example of a metal-organic framework (MOF) containing H_2pyaox. Its framework can be described as a 3-c uninodal net of hcb topology with the layers being parallel to the (1,0,1) plane. Furthermore, 3 is the third reported MOF based on a 2-pyridyl oxime in general. 2 and 4 are new members of a small family of coordination polymers containing an oximic ligand. 1–5 form 3D networks through strong intermolecular interactions. Dc magnetic susceptibility studies were carried out in a crystalline sample of 3 and revealed the presence of weak exchange interactions between the metal centres; the experimental data were fitted to a theoretical model with the fitting parameters being $J = -0.16(1)$ cm^{-1} and $g = 2.085(1)$. The isotropic g value was also confirmed by electronic paramagnetic resonance (EPR) spectroscopy. Reactivity studies were performed for 3 in the presence of metal ions; the reaction progress was studied and discussed for Fe(NO_3)$_3$ by the use of several characterization techniques, including single crystal X-ray crystallography and IR spectroscopy. View Full-Text

Keywords: coordination polymers; metal-organic frameworks (MOFs); carboxylates; pyridyl oximes; zinc; copper

▼ Show Figures

Author's contribution:

I. Mylonas-Margaritis: All the synthetic work, preparation of first draft, tables, figures.

Dr. J. Mayans: Magnetic Studies

Prof. Patrick McArdle: Collection and analysis of the crystallographic data.

Dr. Constantina Papatriantafyllopoulou: Managed the project **and** reviewed the manuscript before the submission and during the revision process.

Zn^{II} and Cu^{II}-Based Coordination Polymers and Metal Organic Frameworks by the of Use of 2-Pyridyl Oximes and 1,3,5-Benzenetricarboxylic Acid

Ioannis Mylonas-Margaritis[1], Julia Mayans[2], Patrick McArdle[1] and Constantina Papatriantafyllopoulou[1,*]

[1] School of Chemistry, College of Science and Engineering, National University of Ireland Galway, University Road, H91 TK33 Galway, Ireland; *I.MYLONAS-MARGARITIS1@NUIGALWAY.IE* (I.M.-M.); *PATRICK.MCARDLE@NUIGALWAY.IE* (P.M.)

[2] Instituto de Ciencia Molecular (ICMol), Universidad de Valencia, Catedrático José Beltran 2, 46980 Paterna Valencia, Spain; *JULIA.MAYANS@QI.UB.EDU*

[*] Correspondence: constantina.papatriantafyllopo@nuigalway.ie; Tel.: +353-91-493-462

Abstract:

The simultaneous use of 2-pyridyl oximes (pyridine-2 amidoxime, H$_2$pyaox; 2-methyl pyridyl ketoxime, mpkoH) and 1,3,5-benzenetricarboxylic acid (H$_3$btc) provided access to five new compounds, namely [Zn(H$_2$btc)$_2$(pyaoxH$_2$)$_2$]·2H$_2$O (**1**·2H$_2$O), [Zn(Hbtc)(pyaoxH$_2$)$_2$]$_n$ (**2**), [Cu(Hbtc)(pyaoxH$_2$)]$_n$ (**3**), [Cu(Hbtc)(mpKoH)]$_n$ (**4**) and [Cu$_2$(Hbtc)$_2$(mpkoH)$_2$(H$_2$O)$_2$]·4H$_2$O (**5**·4H$_2$O). Among them, **3** is the first example of a metal-organic framework (MOF) containing H$_2$pyaox. Its framework can be described as a 3-c uninodal net of hcb topology with the layers being parallel to the (1,0,1) plane. Furthermore, **3** is the

third reported MOF based on a 2-pyridyl oxime in general. **2** and **4** are new members of a small family of coordination polymers containing an oximic ligand. **1**–**5** form 3D networks through strong intermolecular interactions. Dc magnetic susceptibility studies were carried out in a crystalline sample of **3** and revealed the presence of weak exchange interactions between the metal centres; the experimental data were fitted to a theoretical model with the fitting parameters being J = -0.16(1) cm^{-1} and g = 2.085(1). The isotropic g value was also confirmed by electronic paramagnetic resonance (EPR) spectroscopy. Reactivity studies were performed for **3** in the presence of metal ions; the reaction progress was studied and discussed for $Fe(NO_3)_3$ by the use of several characterization techniques, including single crystal X-ray crystallography and IR spectroscopy.

Keywords: coordination polymers; metal-organic frameworks (MOFs); carboxylates; pyridyl oximes; zinc; copper.

1. Introduction

The synthesis and characterization of metal coordination polymers and metal-organic frameworks (MOFs) have attracted a considerable research interest worldwide over the last decades, which stems from their technological, environmental and biomedical applications in sensing, catalysis, imaging, drug delivery, etc. [1–10]. Such species consist of mononuclear or low nuclearity inorganic units, which are linked through organic linkers with the nature of the metal ions and the organic linkers affecting their structure, having also the potential to introduce additional functionalities and physical properties in to the

framework, e.g., photoluminescence, magnetism. For example, some 1D coordination polymers exhibit single chain magnetism (SCM) behaviour, and are promising candidates for applications in quantum computing, high-density information storage, etc. [11–24]. As the dimensionality of the framework increases, the induced porosity is combined in a synergistic way with its other physical properties, leading to the formation of hybrid multifunctional materials, with enhanced performance in a variety of applications (spintronics, photonics, catalysis and others).

Restricting further discussion to MOFs [8–10], they display a wide range of desirable structural features, such as large surface area, high porosity, flexible structure, stability and the possibility of controlled and targeted introduction of functional groups into the framework. Furthermore, some MOFs possess phenomena that affect their porosity and stability, namely the interpenetration and the breathing effect.[25–29] The former refers to the cases where more than one networks are catenated with each other [25–27], which potentially results in the increase of the surface area and stability of the MOF, and in the decrease of its pore diameter. The breathing effect is related to the change of the MOF pore dimensions upon encapsulation of a guest molecule as a result of the change of the intermolecular interactions.[28,29] The unique properties of MOFs and their structural tunability make these materials especially suitable for encapsulating a plethora of different guest molecules.

The wide range of applications of MOFs and coordination polymers constitute an increasing need for the development of efficient synthetic approaches towards new species with enhanced porosity and stability. The vast majority of MOFs has been synthesized using solvothermal techniques, while other approaches have been developed in recent years, based on post-synthetic, isoreticular, microwave-assisted, mechanochemical and sonochemical synthesis.[30–38] Each of these

synthetic approaches often leads to different species, whose properties are merely dictated by the organic ligands that link the neighbouring SBUs, and by the nuclearity and type of the metal ion that is present in the structure. The organic linkers possess suitable coordination sites for the formation of the framework, providing the desirable flexibility and stability. The hydrogen bonding, π–π stacking, and other intermolecular interactions also affect the architecture of the overall framework and the MOF selectivity towards specific guest molecules. A large number of organic linkers has now been employed in MOFs synthesis including imidazolates, pyridine, carboxylates, etc., with the latter being one of the most commonly used, resulting in MOFs with a wide range of pores sizes and shapes.[39–49] The combination of two different linkers has been also employed for the synthesis of new MOFs; in this case, one of the ligands often plays the role of the pillar that link parallel layers leading to the formation of pillar-layered MOFs with increased dimensionality and novel topologies.[50,51]

Although the impact of the ligand properties on the MOF topology and porosity has been well investigated, this is not the case for the nuclearity and properties of the SBU itself. To this end, we recently decided to introduce for the first time into the field of MOFs the 2-pyridyl oximes (**Scheme 1**), a family of ligands with high bridging capability, that have the potential to lead to high nuclearity species with unprecedented metal topologies. 2-pyridyl oximes have been extensively investigated in metal cluster chemistry and led to a plethora of metal clusters with interesting magnetic properties, including single-molecule and single-chain magnetism behaviour.[52–65]
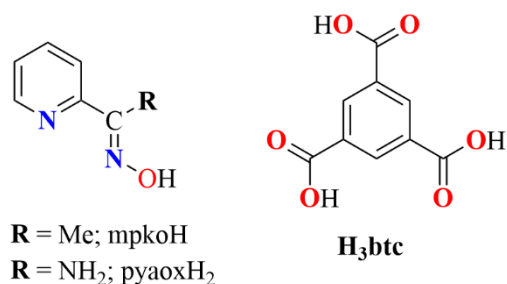
Scheme 1. Schematic representation of the 2-pyridyl oximes (**left**) and the ligand H$_3$btc (**right**) discussed in this work.

The initial combination of 2-pyridyl oximes with a variety of di-, tri- and tetra-carboxylic acids led to the first 2-pyridyl oxime- based MOFs, and other coordination polymers as well.[66,67] It is worth to mention that among the MOFs that we isolated with these ligands, [Cu$_4$(OH)$_2$(pma)(mpko)$_2$]$_n$, where pma^{4-} is the tetra-anion of 1,2,4,5-benzenetetracarboxylic acid (pyromellitic acid) and mpko- is the anionic form of 2-methyl pyridyl ketoxime, is based on a tetranuclear, butterfly-shaped SBU and possesses a novel 3,4,5,8-c net topology. [66] It also exhibits selectivity for Fe^{3+} adsorption with its magnetic properties being strongly related to the amount of metal ion present into the MOF pores.[66]

The promising preliminary results of the employment of 2-pyridyl oximes in the field of MOFs prompted us to explore further this synthetic approach and we, herein, report the synthesis and characterization of five new compounds, by the use of a 2-pyridyl oxime (pyridine-2 amidoxime, pyaoxH$_2$ and 2-methyl pyridyl ketoxime, mpkoH) in combination with 1,3,5-benzenetricarboxylic acid, H$_3$btc (**Scheme 1**). Amongst the reported compounds, [Cu(Hbtc)(pyaoxH$_2$)]$_n$ (**3**) is the first MOF bearing H$_2$pyaox. [Zn(Hbtc)(pyaoxH$_2$)$_2$]$_n$ (**2**) and [Cu(Hbtc)(mpKoH)]$_n$ (**4**) are rare examples of coordination polymers containing

a 2-pyridyl oxime either in its neutral or anionic form. Note that H$_3$btc has been employed in the field of MOFs and has led to the synthesis and characterization of many such species, including the MOFs HKUST, MIL-100, etc., [39,43,68–77] however its combination with an oximic ligand is essentially unexplored.
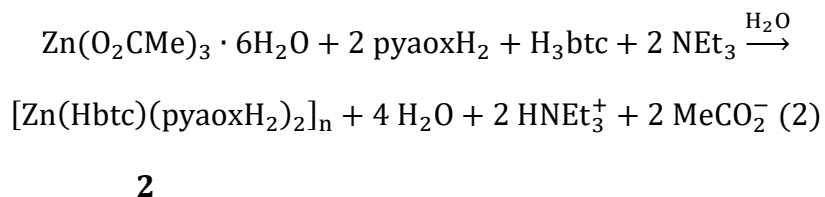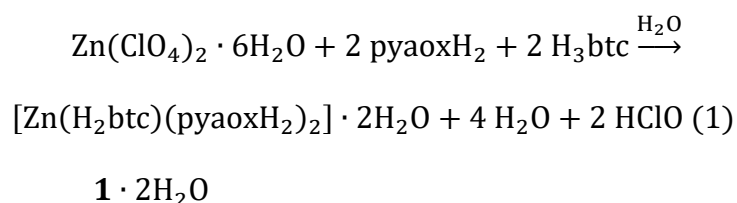
2. Results and Discussion

2.1. Synthetic Discussion

Our group has developed an intense interest over the last years in the synthesis of coordination polymers and MOFs by the use of 2-pyridyl oximes and a polycarboxylic ligand, such as 1,4-benzenedicarboxylic, 1,2,4,5-benzene tetracarboxylic acid, etc. [66,67]. These research efforts have resulted in new species, some of which display new framework topologies and promising sensing properties. It is worth to mention that the initial employment of 1,3,5-benzenetricarboxylic acid (H$_3$btc) in Ni^{II} chemistry in the presence of an oximic ligand has led to the isolation of a 1D coordination polymer.[67] This prompted us to further study this reaction system by the use of different metal ions and investigate its potential to favour the formation of higher dimensionality coordination polymers and/or MOFs. A wide range of experiments was carried out in order to study the impact of the different synthetic parameters (presence/absence or kind of base, metal ratio of the reactants, metal sources, etc.) on the identity and crystallinity of the isolated product.
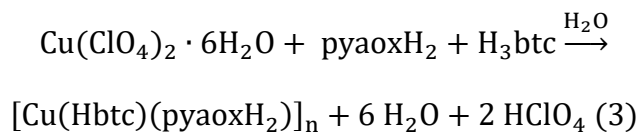
The reaction mixture of Zn(ClO$_4$)$_2$·6H$_2$O/pyaoxH$_2$/H$_3$btc (1:2:1) in H$_2$O at 100 °C gave a colourless solution from which crystals of [Zn(H$_2$btc)$_2$(pyaoxH$_2$)$_2$]·2H$_2$O (**1**·2H$_2$O) were subsequently isolated. Following a similar reaction but using a different Zn^{II} source (Zn(O$_2$CMe)$_2$·6H$_2$O instead

of Zn(ClO$_4$)$_2$·6H$_2$O) and in the presence of NEt$_3$, the 1D coordination polymer [Zn(Hbtc)(pyaoxH$_2$)$_2$]$_n$ (**2**) was isolated in good yield. The stoichiometric equation of the reactions that lead to the formation of **1** and **2** is represented in Equations (**1**) and (**2**). Note that the kind of base does not have any impact on the identity of the isolated compound, but it affects its crystallinity.

$$Zn(ClO_4)_2 \cdot 6H_2O + 2\ pyaoxH_2 + 2\ H_3btc \xrightarrow{H_2O}$$

$$[Zn(H_2btc)(pyaoxH_2)_2] \cdot 2H_2O + 4\ H_2O + 2\ HClO \ (1)$$

$$\mathbf{1} \cdot 2H_2O$$

$$Zn(O_2CMe)_3 \cdot 6H_2O + 2\ pyaoxH_2 + H_3btc + 2\ NEt_3 \xrightarrow{H_2O}$$

$$[Zn(Hbtc)(pyaoxH_2)_2]_n + 4\ H_2O + 2\ HNEt_3^+ + 2\ MeCO_2^- \ (2)$$

$$\mathbf{2}$$
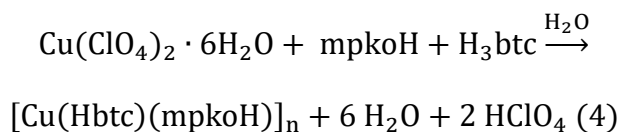
As a next step, we decided to investigate the impact of the metal ion on the identity of the isolated product; thus, by the use of Cu(ClO$_4$)$_2$·6H$_2$O and following a similar synthetic approach to the one that provided access to **1**, green crystals of the 2D coordination polymer [Cu(Hbtc)(pyaoxH$_2$)]$_n$ (**3**) were isolated in good yield. It is noteworthy that the electronic properties of the oximic ligand influence the dimensionality of the reaction product. In particular, by the employment of mpkoH instead of pyaoxH$_2$ and by following the same reaction that yielded **3**, blue crystals of the 1D coordination polymer [Cu(Hbtc)(mpKoH)]$_n$ (**4**) were formed, whereas the use of a different Cu^{II} source (Cu(NO$_3$)$_2$·2.5H$_2$O instead of Cu(ClO$_4$)$_2$·6H$_2$O) provided access to the

compound $[Cu_2(Hbtc)_2(mpkoH)_2(H_2O)_2]\cdot 4H_2O$ (**5**$\cdot$4H$_2$O), according to the stoichiometric Equations (**3**)–(**5**):

$$Cu(ClO_4)_2 \cdot 6H_2O + \text{pyaoxH}_2 + H_3btc \xrightarrow{H_2O}$$

$$[Cu(Hbtc)(\text{pyaoxH}_2)]_n + 6\ H_2O + 2\ HClO_4\ (3)$$

3

$$Cu(ClO_4)_2 \cdot 6H_2O + \text{mpkoH} + H_3btc \xrightarrow{H_2O}$$

$$[Cu(Hbtc)(\text{mpkoH})]_n + 6\ H_2O + 2\ HClO_4\ (4)$$

4

$$2\ Cu(NO_3)_2 \cdot 2.5H_2O + 2\ \text{mpkoH} + 2\ H_3btc + H_2O \xrightarrow{H_2O}$$

$$[Cu_2(Hbtc)_2(\text{mpkoH})_2(H_2O)_2] \cdot 4H_2O + 4\ HNO_3\ (5)$$
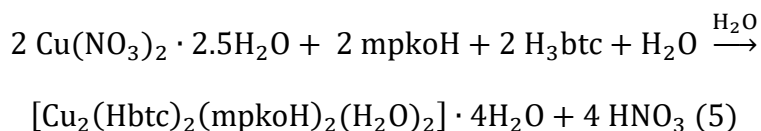
$$\mathbf{5} \cdot 4H_2O$$

2.2. Description of Structures

Representations of the molecular structures of **1**–**5** are shown in **Figures 1–5**, **Figures S1** and **S2** (Supplementary Information). Selected interatomic distances and angles are listed in **Tables S1–S5**.

Compound **1** crystallizes in the triclinic space group $P\bar{1}$. Its structure (**Figure 1**) consists of the mononuclear complex $[Zn(H_2btc)_2(\text{pyaoxH}_2)_2]$ and two lattice

H$_2$O molecules. The coordination sphere of the metal ion is completed by two neutral *N,N'*-bidentate chelating pyaoxH$_2$ ligands and two monodentate single deprotonated H$_2$btc$^-$ ions. Zn^{II} is six coordinated displaying a slightly distorted octahedral geometry due to the relatively small bite angle of the chelating ligand (N1-Zn1-N2 = 75.1(2) and N4-Zn1-N5 = 76.0(2)).

There are strong intermolecular hydrogen bonding interactions in **1** that stabilize its structure and result in the formation of a three-dimensional network (**Figure 1**, right). In particular, there are three different types of hydrogen bonds in **1**, which involve: (1) the oxygen atoms of the oximic groups (O1 and O2), which are the donors, and the carboxylate groups of the H$_2$btc^{-1} ligands (O4, O10), which act as the acceptors (O2···O4 = 2.623 Å, H2A···O4 = 1.857 Å, O2-H2A···O4 = 154.81°; O1···O10 = 2.606 Å, H1···O10 = 1.791 Å, O1-H1···O10 = 172.25°); (2) the oxygen atoms of the neutral carboxylic groups of the H$_2$btc^{-1} ligand (O11, O7; donors) and the deprotonated carboxylate groups (O5, O12; acceptors) of neighbouring species (O11···O5 = 2.645 Å, H11···O5 = 1.86 Å, O11-H11···O5 = 160.15°; O7···O12 = 2.705 Å, H7···O12 = 1.942 Å, O7-H7···O12 = 154.42°) and (3) the amino group of the oximic ligand (N3; donor) and the carboxylate (O8; acceptor) group from a neighbouring complex (N3···O8 = 3.022 Å, H3B···O8 = 2.433 Å, N3-H3B···O8 = 126.27°). Furthermore, the lattice H$_2$O molecules (O15, O16) form hydrogen bonds with the carboxylic (O3, O6, O13 and O4) and the oximic (O1) groups; the non-location of the lattice H$_2$O hydrogen atoms precludes a detailed description of the latter.
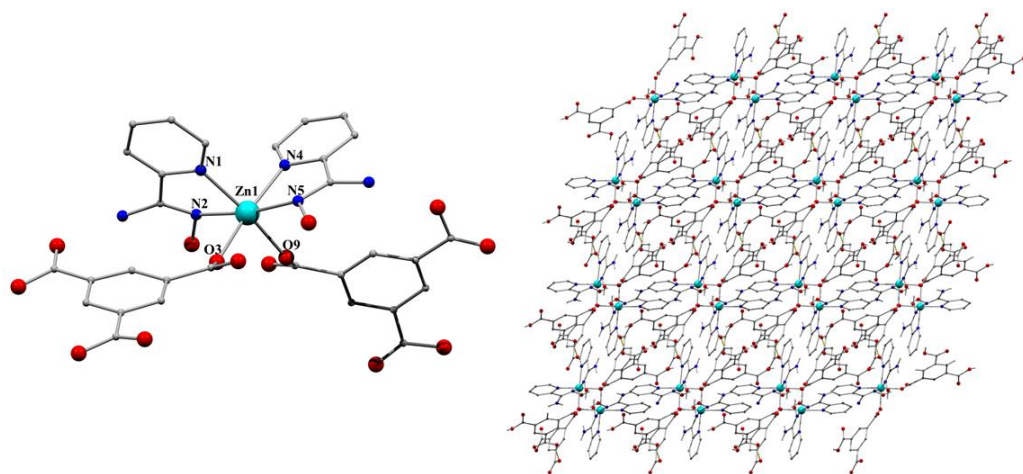
Figure 1. Representation of the molecular structure of compound **1** (left) and the 3D network that is formed through intermolecular interactions along c axis (right). Colour code: Zn^{II}, cyan; N, navy blue; O, red; C, grey.

2 crystallizes in the chiral orthorhombic space group $P2_12_12_1$; its structure contains a one-dimensional chain based on the repeating unit $[Zn(Hbtc)(pyaoxH_2)_2]$. The metal centre is linked to two neutral *N,N'*-bidentate chelating H_2pyaox ligands, and two terminally ligated carboxylate groups coming from two different $Hbtc^{2-}$ ions; the latter bridges two neighbouring repeating units adopting an $\eta^1:\eta^1:\mu$ coordination mode. Zn^{II} is six-coordinate adopting an octahedral geometry. The repeating unit in **2** is similar to compound **1**, with the only difference being the protonation level and, hence, the bridging capability of the carboxylate ligand (**1**, single deprotonated; **2**, double deprotonated carboxylate). The 1D chains in **2** interact strongly through hydrogen bonds, which result in the formation of a 3D network (**Figure 2**, right). The hydrogen bonds involve the oximic, amino and carboxylic groups as donors and the deprotonated carboxylate groups of the $Hbtc^{2-}$ ligands as acceptors. The

metric parameters of the crystallographically established, independent hydrogen bonds are listed in Table S6 in the Supplementary Material.
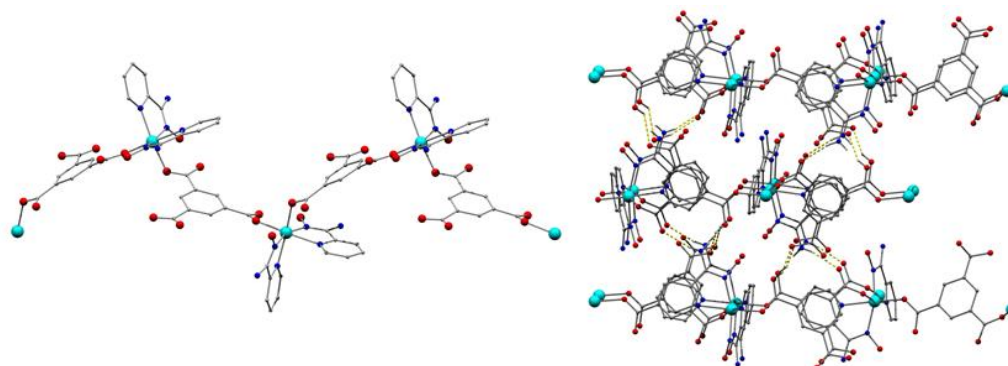

Figure 2. Representation of a part of the 1D chain in **2** (left) and the 3D network that is formed through intermolecular interactions (right). Color code: Zn^{II}, cyan; N, navy blue; O, red; C, grey.

Compound **3** crystallizes in the monoclinic space group $P2_1$/n. Its structure consists of a two-dimensional network based on the dinuclear centrosymmetric repeating unit $[Cu_2(Hbtc)_2(pyaoxH_2)_2]$ (**Figure 3**). The two metal ions within the repeating unit are held together through the two bridging H_2pyaox ligands, and their distance was 4.397 Å. The coordination sphere of Cu^{II} was completed by two $Hbtc^{2-}$ ions, which also linked the neighbouring SBUs resulting in the formation of a 2D framework. The metal ions were penta-coordinated and adopted a square pyramidal geometry ($\tau = 0.05$) with O7 from the oximic group occupying the apical position [78].

Intrachain hydrogen bonds stabilized the crystal structure of **3**; these were formed between: (1) the oximic group (O7), which is the donor, and the carboxylic group

of the Hbtc^{2-} ion (O2), which acts as the acceptor (O7$\cdots$O2 = 2.525 Å, H1(O7)$\cdots$O2 = 1.664 Å, O7-H1(O7)$\cdots$O2 = 173.62°), and (2) the amino group (N2), which is the donor, and the carboxylic group of the Hbtc^{2-} ion (O6), which acts as the acceptor (N2$\cdots$O6 = 2.958 Å, H2(N2)$\cdots$O6 = 2.202 Å, N2-H2(O6)$\cdots$O6 = 147.30°). Furthermore, interchain hydrogen bonds are formed between the oxygen atoms of neighbouring carboxylic groups of the Hbtc^{2-} ions; (O4) acts as a donor and (O6) acts as an acceptor (O4$\cdots$O6 = 2.64 Å, H1(O4)$\cdots$O6= 1.81 Å, O4-H1(O4)$\cdots$O6 = 159.27°), forming a three dimensional network (Figure S1).

The framework in **3** forms a 3-c uninodal net [79–81] of hcb topology (**Figure 4**,left) with the layers being parallel to the (1,0,1) plane.[82–84] Taking also into account the intermolecular interactions between the Hbtc^{2-} ligands, the resulted 3D framework exhibited a utp topological type (**Figure 4**, right).[85–87] Thermal stability studies in **3** revealed that it remains stable until 320 °C (**Figure S2**). In particular, there is a small mass loss (<5%) between room temperature and 320 °C; a sharp mass loss (ca. 60%) is then observed, and the decomposition of the compound continued at a steady rate with a further mass decrease of 12% between 320 and 600 °C.
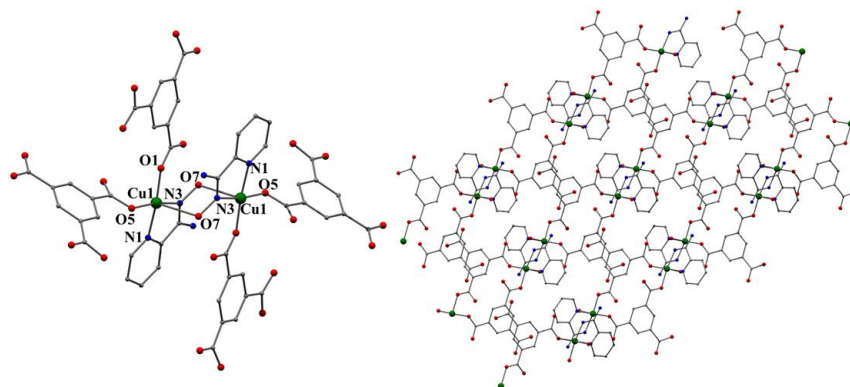
Figure 3. Representation of the repeating unit (left) and a part of the 2D network of **3** (right). Colour code: Cu^{II}, green; N, navy blue; O, red; C, grey. The hydrogens are omitted for clarity.
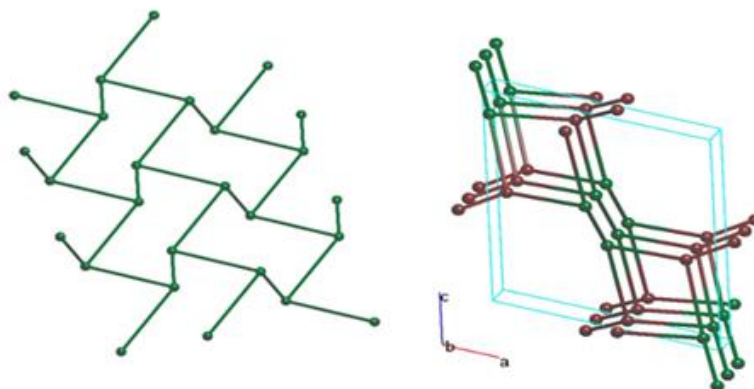

Figure 4. Left: representation of the underlying 3-c net with **hcb** topology in **3**. Right: representation of the 3D network with **utp** topology, which is formed when the intermolecular interactions between the carboxylate ligands are considered. The unit cell is shown with a blue line. Colour code: Cu^{II}, green; $Hbtc^{2-}$, brown.

4 crystallized in the orthorhombic space group *Pna2₁*; it is a zig-zag chain (**Figure 5**, left), formed by the connection of the [Cu(Hbtc)(mpkoH)] repeating units through the $\eta^1:\eta^1:\mu$ Hbtc^{2-} ligands. The coordination sphere of Cu^{II} was completed by one neutral *N,N'*-bidentate chelating mpkoH ligand. Cu^{II} was the tetra-coordinate with a square planar geometry (N1-Cu1-O2 = 173.56°). A strong intramolecular hydrogen bonding interaction was formed between the neutral oximic group (O1, donor) and a carboxylate group (O3, acceptor) from the Hbtc^{2-} ligand (O1···O3 = 2.516 Å, H1O1···O3 = 1.7 Å, O1-H1O1···O3 = 173.11°).
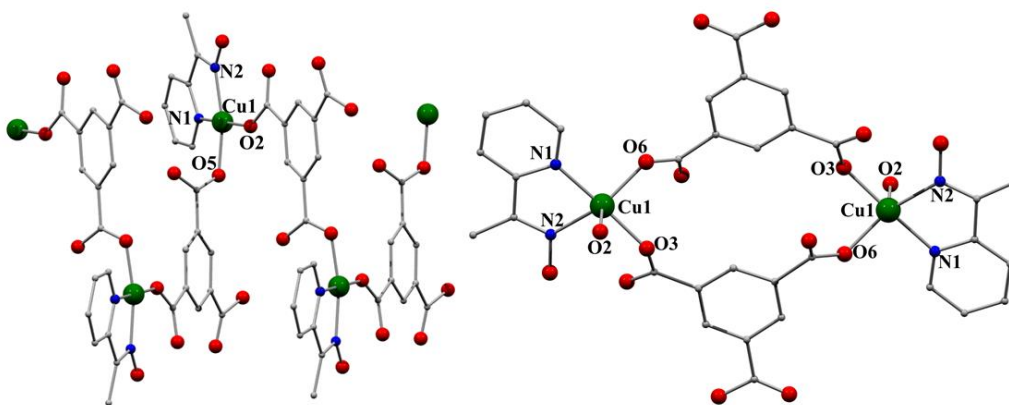

Figure 5. Left representation of a part of the zig-zag chain in **4**. Right: representation of the molecular structure of **5**. Colour code: Cu^{II}, green; N, navy blue; O, red; C, grey. The hydrogens are omitted for clarity.

Compound **5**·4H₂O crystallized in the triclinic space group $P\bar{1}$. Its structure consisted of centrosymmetric dinuclear [Cu₂(Hbtc)₂(mpkoH)₂(H₂O)₂] species (**Figure 5**, right) and H₂O lattice molecules. The two metal centres were held together through the $\eta^1:\eta^1:\mu$ Hbtc^{2-} ions. The coordination sphere of each Cu^{II} was completed by an *N,N'*-bidentate chelating mpkoH ligand and one terminal

H$_2$O molecule. Each cation was penta-coordinated adopting a distorted square pyramidal geometry ($\tau = 0.30$) with the O2 from the terminally ligated H$_2$O to occupy the axial position.[78] There was a strong network of hydrogen bonding interactions that stabilized the structure of **5**·4H$_2$O and result in the formation of a three-dimensional framework (**Figure S3**). These involve the lattice H$_2$O molecules (O9 and O10), which act as both donors and acceptors, the oximic group (O1, donor), the terminally ligated H$_2$O (O2, donor), the neutral carboxylic group (O8, donor) and the carboxylate groups from the Hbtc^{2-} ligands (O4, O5) that act as acceptors. The metric parameters of the crystallographically established, independent hydrogen bonds are listed in **Table S7** in the Supplementary Material. The aromatic rings of the oximic and carboxylic ligands of neighbouring dimers in **5**·4H$_2$O interact further through strong π–π stacking interactions, with the distance between the centroids being 3.8 Å (**Figure S4**).

1–**5** belong to a new family of oximic metal compounds, coordination polymers and MOFs with 3 being the first MOF based on 2-pyridyl amidoxime and 1,3,5-benzenetricarboxylic acid; furthermore, it is only the third example of a MOF based on a 2-pyridyl oxime, in general.[66] **2** and **4** join a small family of coordination polymers containing an oximic ligand.[66,67] The structures of all the reported compounds are stabilized through strong intermolecular interaction, forming three dimensional networks. The purity and stability of **1**–**5** has been verified by pxrd studies (**Figures S5** and **S6**).

2.3. Magnetism Studies

Dc magnetic susceptibility measurements were carried out on a powdered and pressed sample of **3** in the 2–300 K temperature range and under a field of 0.03 T and plotted as χ_MT *vs.* T plot. (**Figure 6**). The $\chi_M T$ for **3** was almost constant

with a room temperature value of 0.8 $cm^3 \cdot Kmol^{-1}$ in good agreement with two non-interacting Cu(II) cations (0.375 $cm^3 \cdot Kmol^{-1}$) with an overall g greater than 2.00.
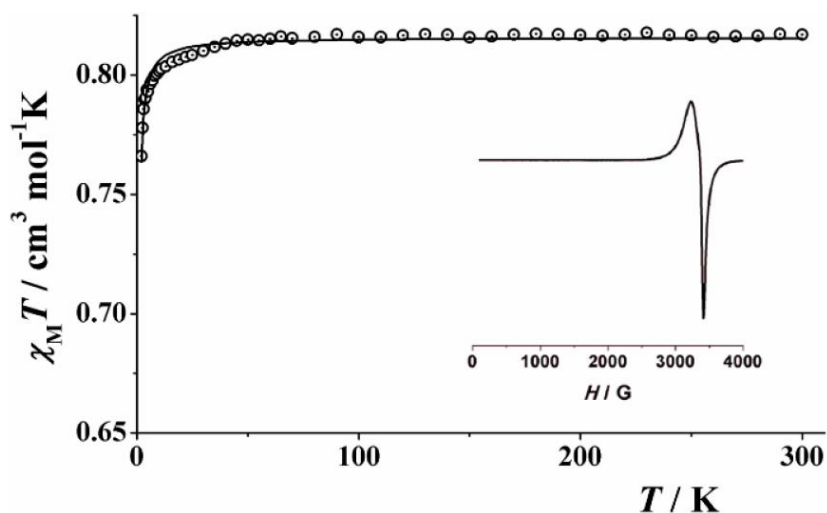

Figure 6. Representation of the $\chi_M T$ as a function of T for **3**. Solid line represents the best fit. Inset, EPR spectrum measured at X-band frequency.

The fitting of the experimental data was performed by using the spin-only Hamiltonian $H = -2J(\hat{S}_1 \cdot \hat{S}_2)$ and PHI software [88] and resulted in almost non-interacting Cu(II) ions with a J = -0.16(1) cm^{-1} and a global g value of 2.085(1). This almost irrelevant value of the super-exchange coupling J is expected due to the relative arrangement of the Cu(II) cations, which determines the overlap along the long bond distance involving the non-magnetic dz^2 orbital and also due the position of the oximes ligands, where the Cu(II)-O-N-Cu(II) torsion angle was 86.8 close to orthogonality. The almost isotropic value of g was confirmed by electronic paramagnetic resonance (EPR) spectroscopy at X-band frequency,

which provides the low temperature $g_{//}$ and $g_\perp$ values of 2.16 and 2.08 (*Figure 6*, inset), being in total agreement with the dc measurements.

2.4. Reactivity Studies

The existence of free (non-coordinated) NH_2- groups in the crystal structure of **3** prompted us to study the ability of this MOF to adsorb or react with metal ions in the aqueous environment. The reactivity studies were carried out by soaking crystals of **3** into solutions of 0.10–0.30 mmol of metal salts ($Fe(NO_3)_3$, $Ni(NO_3)_2$, $Co(NO_3)_2$ and $CrCl_3$) in H_2O (10 mL). The MOF crystals were activated prior to the metal ion encapsulation to remove the amount of solvent present; this was carried out by stirring the crystals in acetone for several hours and then exchanging this solvent with acetone, which is easily removed at 80 °C. The metal encapsulation was initially investigated by batch studies using UV–vis spectroscopy (**Figures S7** and **S8**). The UV-vis studies for $Fe(NO_3)_3$ revealed a substantial decrease of the concentration of the metal ion in the solution over the first 4 min, which was then followed by the appearance of an additional peak at 290 nm (**Figure S5**); the latter can be potentially attributed to Cu^{2+} ions in the solution [89], which indicates that a chemical change takes place in the structure of **3** upon reaction with other metal ions. The progress of the reaction was investigated in the case of $Fe(NO_3)_3$ by means of FTIR and single-crystal X-ray crystallography. During the reaction, the green crystals of **3** had been replaced by a brown precipitate (**Figure S9**) and the initial yellow colour of the solution had turned to pale green. The solution was then filtered and left in a closed vial at room temperature for one day, after which a few green-cyan crystals were formed; the latter were characterized with IR spectroscopy and single crystal X-ray diffraction (unit cell comparison) and were found to be the mononuclear

complex $[Cu(H_2pyca)_2(H_2O)]\cdot(NO_3)_2$, where H_2pyca = pyridine-2-carboxamide. [90] H_2pyca is the product of the hydrolysis of H_2pyaox, which is a reaction often encountered in oximes.[52,91] Concerning the brown precipitate, this was amorphous, which prevented from its further; it is worth to mention, though, that the IR spectrum (**Figure S10**) of the brown precipitate indicates that this could correspond to the previously reported 1D coordination polymer $[Fe_3(H_2O)_{12}(btc)_2]_n$.[76] The absence of bands in the range 1730–1690 cm^{-1} reveals the complete deprotonation of the organic ligand in the product of the reaction.

3. Materials and Methods

3.1. Materials, Physical and Spectroscopic Measurements

All the manipulations were performed under aerobic conditions using materials (reagent grade) and solvents as received. Hmpko and H_2pyaox were prepared as described elsewhere.[92,93] Warning: Perchlorate salts are potentially explosive; such compounds should be used in small quantities and treated with utmost care at all times.

Elemental analysis (C, H and N) was performed by the in-house facilities of National University of Ireland Galway, School of Chemistry. IR spectra (4000–400 cm^{-1}) were recorded on a Perkin-Elmer Spectrum 400 FT-IR spectrometer. Powder X-ray diffraction data (pxrd) were collected using an Inex Equinoz 6000 diffractometer. Solid TGA experiments were performed on a STA625 thermal analyser from Rheometric Scientific (Piscataway, NJ, USA). The heating rate was kept constant at 10°C/min, and all runs were carried out between 20 and 600 °C. The measurements were made in open aluminium crucibles, nitrogen was

purged in ambient mode and calibration was performed using an indium standard. Solid-state, variable-temperature and variable-field magnetic data were collected on powdered samples using an MPMS5 Quantum Design magnetometer operating at 0.03 T in the 300–2.0 K range for the magnetic susceptibility and at 2.0 K in the 0–5 T range for the magnetization measurements. Diamagnetic corrections were applied to the observed susceptibilities using Pascal's constants. EPR spectrum was collected using a

Bruker 300 spectrometer with an X-band frequency measured at room temperature.

3.2. Compound Synthesis

3.2.1. Synthesis of [Zn(H$_2$btc)$_2$(pyaoxH$_2$)$_2$]·2H$_2$O (1·2H$_2$O)

Zn(ClO$_4$)$_2$·6H$_2$O (0.037 g, 0.10 mmol) and pyaoxH$_2$ (0.027g, 0.20 mmol) were dissolved in H$_2$O (10 mL). The resultant solution was put in the oven and heated at 100 °C for 1 h. Then, H$_3$btc (0.021 g, 0.1 mmol) was added and the vial was placed into the oven for 24 h, after which X-ray quality colourless crystal needles of **1**·2H$_2$O were formed. The crystals were collected by filtration, washed with cold MeCN (2 mL) and Et$_2$O (2 x 5 mL) and dried in air. Yield 55 %. Anal. Calc. for **1**·2H$_2$O: C, 45.38; H, 3.55; N, 10.58. Found: C, 45.87; H, 3.71; N, 10.09 %. IR data: v (cm^{-1}) = 3484 m, 3406 m, 3310 m, 2982 m, 2757 m, 2564 m, 2364 w, 1943 w, 1724 m, 1698 m, 1670 m, 1598 s, 1574 m, 1543 s, 1497 m, 1406 m, 1369 m, 1281 m, 1247 m, 1224 s, 1177 s, 1153 m, 1096 m, 1022 s, 907 m, 844 m, 790 s, 745 s, 691 s, 665 m.

3.2.2. Synthesis of [Zn(Hbtc)(pyaoxH$_2$)$_2$]$_n$ (**2**)

Zn(O$_2$CMe)$_2$·6H$_2$O (0.022 g, 0.10 mmol), pyaoxH$_2$ (0.027 g, 0.20 mmol) and Et$_3$N (56 µL, 0.4 mmol) were dissolved in H$_2$O (10 mL). The resultant solution was put in the oven and heated at 100 °C for 1h. H$_3$btc (0.021 g, 0.10 mmol) was added and the vial was placed into the oven for 24 h, after which X-ray quality colourless needless of **2** were formed. The crystals were collected by filtration, washed with cold MeCN (2 mL) and Et$_2$O (2 x 5 mL), and dried in air. Yield 70%. Anal. Calc. for **2**: C, 46.05; H, 3.31; N, 15.34. Found: C, 45.55; H, 3.63; N, 15.18%. IR data: v (cm$^-$1) = 3474 m, 3357 m, 3307 m, 3187 m, 2982 m, 1722 s, 1678 s, 1604 s, 1575 m, 1528 s, 1434 m, 1406 m, 1368 s, 1302 m, 1229 m, 1169 s, 1097 m, 1020 s, 1007 m, 1020 s, 937 m, 896 m, 855 m, 811 m, 790 s, 756 m, 714 s, 687 m, 668 s.

3.2.3. Synthesis of [Cu(Hbtc)(pyaoxH$_2$)]$_n$ (**3**)

Cu(ClO$_4$)$_2$·6H$_2$O (0.037 g, 0.10 mmol) and pyaoxH$_2$ (0.027 g, 0.20 mmol) were dissolved in H$_2$O (10 mL). The resultant solution was put in the oven and heated at 100 °C for 1 h. The colour of the solution turned cyan and H$_3$btc (0.021 g, 0.1 mmol) was then added; the vial was placed into the oven for 24 h, after which X-ray quality green crystals of **3** were formed. The crystals were collected by filtration, washed with cold MeCN (2 mL) and Et$_2$O (2 x 5 mL), and dried in air. Yield 85%. Anal. Calc. for 3: C, 44.07; H, 2.71; N, 10.28. Found: C, 44.32; H, 3.07; N, 10.21 %. IR data: v (cm^{-1}) = 3443 w, 3314 w, 1726 m, 1682 m, 1612 s, 1579 w, 1544 s, 1492 w, 1437 w, 1421 w, 1364 m, 1296 w, 1274 w, 1242m, 1238 m, 1179 m, 1157 w, 1095 m, 1036 s, 951 m, 928 w, 895 w, 836 m, 805 w, 786 s, 743 s, 720 s, 689 w, 669 m.

*3.2.4. Synthesis of [Cu(Hbtc)(mpKoH)]$_n$ (**4**)*

Cu(ClO$_4$)$_2$·6H$_2$O(0.037 g, 0.10 mmol) and mpKoH (0.014 g, 0.10 mmol) were dissolved in H$_2$O (5 mL). The resultant solution was put in the oven and heated at 100 °C for 1 h. H$_3$btc (0.021 g, 0.1 mmol) was then added and the vial was placed into the oven for 24 h, after which X-ray quality blue crystals of **5** were formed. The crystals were collected by filtration, washed with cold MeCN (2 mL) and Et$_2$O (2 x 5 mL), and dried in air. Yield 73%. Anal. Calc. for **4**: C, 47.12; H, 2.97; N, 6.87. Found: C, 46.81; H, 3.14; N, 7.01 %. IR data: v (cm^{-1}) = 2247 w, 2167 w, 1813 m, 1720 m, 1606 m, 1549 s, 1482 w, 1424 m, 1360 s, 1299 w, 1266 w, 1244 s, 1177 s, 1160 s, 1149 w, 1100 w, 1085 m, 1053 w, 1027 w, 978 w, 957 m, 923 m, 803 w, 770 m, 749 s, 718 s, 690 m, 673 s.

*3.2.5. Synthesis of [Cu$_2$(Hbtc)$_2$(mpkoH)$_2$(H$_2$O)$_2$]·4H$_2$O (**5**·4H$_2$O)*

Cu(NO$_3$)$_2$·2.5H$_2$O (0.093 g, 0.40 mmol) and mpkoH (0.014 g, 0.10 mmol) were dissolved in in H$_2$O (10 mL). The resultant solution was put in the oven and heated at 100 °C for 1 h. Then, H$_3$btc (0.021 g, 0.1 mmol) was added and the vial was placed into the oven for 24 h, after which X-ray quality cyan crystals of **5**·4H$_2$O were formed. The crystals were collected by filtration, washed with cold MeCN (2ml) and Et$_2$O (2 x 5 mL), and dried in air. Yield 40%. Anal. Calc. for **5**·4H$_2$O: C, 41.61; H, 3.93; N, 6.07. Found: C, 41.29; H, 4.09; N, 6.34 %. IR data: v (cm^{-1}) = 3393 w, 3032 w, 1714 m, 1606 s, 1548 s, 1435 s, 1363 s, 1335 w, 1249 m, 1235 m, 1189 m, 1144 m, 1103 m, 1074 m, 1028 w, 930 m, 855 w, 803 w, 778 s, 744 s, 714 s, 677 s.

3.3. Single-Crystal X-ray Crystallography

Single crystal diffraction data for **1**–**5** were collected in an Oxford Diffraction Xcalibur CCD diffractometer using graphite-monochromatic Mo Ka radiation (λ = 0.71073 Å) at room temperature. The structures were solved using SHELXT [94], embedded in the OSCAIL software.[95] The non-H atoms were treated anisotropically, whereas the hydrogen atoms were placed in calculated, ideal positions and refined as riding on their respective carbon atoms. The hydrogen atoms on water molecules cannot be calculated accurately and are best located in difference maps and then refined. In the case of compound **1**·$2H_2O$, it was not possible to locate the water H atoms in difference maps. Molecular graphics were produced with DIAMOND.[96]

Unit cell data and structure refinement details are listed in **Table 1**. CIF files can be obtained free of charge at *WWW.CCDC.CAMAC.UK/RETRIEVING.HTML* or from the Cambridge Crystallographic Data Centre, Cambridge, UK with the REF codes 2,054,509–2,054,513 for **1**–**5**.

Table 1. Crystallographic data for complexes **1**-**5**.

Complex	1·$2H_2O$	2	3
Empirical formula	$C_{30}H_{23}N_6O_{16}Zn$	$C_{21}H_{18}N_6O_8Zn$	$C_{15}H_{11}CuN_3O_7$
Formula weight	788.91	547.78	408.81
Crystal system	Triclinic	Orthorhombic	Monoclinic
Space group	$P\bar{1}$	$P2_12_12_1$	$P2_1/n$
a (Å)	10.4432(8)	8.9165(2)	13.6020(5)
b (Å)	11.0391(10)	14.3950(4)	7.8643(3)

c (Å)	16.1331(10)	18.0662(4)	14.5936(6)
α (°)	70.263(7)	90	90
β (°)	71.936(6)	90	106.629(4)
γ (°)	74.980(7)	90	90
V (Å³)	1639.4(2)	2318.85(10)	1495.79(10)
Z	2	4	4
ρ_{calc} (g cm⁻³)	1.598	1.569	1.815
μ (mm⁻¹)	0.837	1.120	1.510
Measd/independent reflns (R_{int})	12784 / 7550 (0.0634)	19382/ 5593 (0.0303)	10552/3386 (0.0279)
Parameters refined	484	350	251
GoF (on F^2)	0.972	1.043	1.069
$R_1{}^a$ ($I > 2\sigma(I)$)	0.0948	0.0340	0.0379
$wR_2{}^b$ ($I > 2\sigma(I)$)	0.2333	0.0763	0.1025
$(\Delta\rho)_{max}/(\Delta\rho)_{min}$ (e Å⁻³)	2.739/-0.619	0.879 / -0.338	0.539/-0.683

Complex	**4**	**5·4H₂O**
Empirical formula	$C_{21}H_{11}CuN_2O_7$	$C_{16}H_{18}CuN_2O_{10}$
Formula weight	466.86	461.86
Crystal system	Orthorhombic	Triclinic
Space group	$Pna2_1$	$P\bar{1}$
a (Å)	14.4904(8)	8.5820(6)
b (Å)	14.2054(6)	10.7135(8)

c (Å)	7.4068(5)	11.0721(8)
a (º)	90	64.108(7)
β (º)	90	86.688(6)
γ (º)	90	83.015(6)
V (Å^3)	2.034	909.01(12)
Z	4	2
ρ_{calc} (g cm^{-3})	2.034	1.687
μ (mm^{-1})	1.494	1.263
Measd/independent reflns (R_{int})	12706/3688 (0.0784)	8056/4204 (0.0377)
Parameters refined	237	286
GoF (on F^2)	0.974	0.963
R_1[a] ($I > 2\sigma(I)$)	0.0544	0.0417
wR_2[b] ($I > 2\sigma(I)$)	0.0869	0.0935
$(\Delta\rho)_{max}/(\Delta\rho)_{min}$ (e Å^{-3})	0.420 /-0.405	0.496 /-0.489

4. Conclusions

The employment of 2-pyridyl oximes (pyridine-2 amidoxime, pyaoxH$_2$; 2-methyl pyridyl ketoxime and mpkoH) in combination with 1,3,5-benzenetricarboxylic acid (H$_3$btc) provided access to five new compounds, including discrete clusters, coordination polymers and MOFs. Among them,

[Cu(Hbtc)(pyaoxH$_2$)]$_n$ (**3**) was based on a 3-c uninodal net of hcb topology being the first reported MOF bearing pyaoxH$_2$; it was also the third MOF example based on a 2-pyridyl oxime in general. [Zn(Hbtc)(pyaoxH$_2$)$_2$]$_n$ (**2**) and [Cu(Hbtc)(mpKoH)]$_n$ (**4**) joined a small family of coordination polymers containing an oximic ligand. **1**–**5** formed a 3D supramolecular network through strong hydrogen bonding interactions.

The exchange interactions between the metal centres in **3** were investigated through dc magnetic susceptibility measurements and were found to be very weak antiferromagnetic (J = -0.16(1) cm^{-1}). Finally, reactivity studies were performed for **3** in the presence of metal ions; in the case of Fe(NO$_3$)$_3$, the reaction products were [Cu(pycaH$_2$)$_2$(H$_2$O)]·(NO$_3$)$_2$, (pyca H$_2$ = pyridine-2-carboxamide, coming from the hydrolysis of the oximic ligand) and [Fe$_3$(H$_2$O)$_{12}$(btc)$_2$]$_n$. The reaction products were characterized by single crystal X-ray crystallography and IR spectroscopic techniques.

Supplementary Materials:

 The **following** are available online, **Figure S1**: Representation of the 3D network formed through hydrogen bonding interactions in **3**, **Figure S2**: Representation of the 3D network formed through hydrogen bonding interactions in **5**·4H$_2$O, **Figure S3**: Comparison of the pxrd patterns for **3** (theoretical, red; experimental: green; CH$_2$Cl$_2$, navy blue; EtOH, grey; H$_2$O, magenta; Me$_2$CO, cyan; MeOH, pink, **Figure S4**: Comparison of the pxrd patterns for **5**·4H$_2$O (theoretical, red; experimental, blue), **Figure S5**: UV-vis plot for the adsorption of iron(III) nitrate nonahydrate by **3** in H$_2$O, **Figure S6**: Photo of crystals of **3** (left) before the reaction and the formed brown compound (right), **Figure S7**: The infrared spectra of the isolated brown precipitated, **Table S1**: Selected

interatomic distances (Å) and angles for **1**·2H$_2$O, **Table S2**: Selected interatomic distances (Å) and angles for **2**, **Table S3**: Selected interatomic distances (Å) and angles for **3**, **Table S4**: Selected interatomic distances (Å) and angles for **4**, **Table S5**: Selected interatomic distances (Å) and angles for **5**·4H$_2$O, **Table S6**: Hydrogen bonding details for **2**, Table S7: Hydrogen bonding details for **5**·4H$_2$O.

Conflicts of Interest: The authors declare no conflict of interest.

Sample Availability: Samples of the compounds **1**–**5** are available from the authors.

References

1. Qin, J.-S.; Du, D.-Y.; Guan, W.; Bo, X.-J.; Li, Y.-F.; Guo, L.-P.; Su, Z.-M.; Wang, Y.-Y.; Lan, Y.-Q.; Zhou, H.-C. *J. Am. Chem. Soc.* **2015** 137, 7169–7177.

2. Kuznetsova, A.; Matveevskaya, V.; Pavlov, D.; Yakunenkov, A.; Potapov, *Materials* **2020** 13, 2699.

3. Hu, Z.; Deibert, B.J.; Li, J. *Chem. Soc. Rev.* **2014** 43, 5815–5840.

4. Douvali, A.; Tsipis, A.C.; Eliseeva, S.V.; Petoud, S.; Papaefstathiou, G.S.; Malliakas, C.D.; Papadas, I.; Armatas, G.S.; Margiolaki, I.; Kanatzidis, M.G.; et al. *Angew. Chem. Int.Ed.* **2015** 54, 1651–1676.

5. Ma, L.; Falkowski, J.M.; Abney, C.; Lin, W. *Nat. Chem.* **2010** 2, 838–846.

6. Wu, M.-X.; Yang, Y.-W. *Adv. Mater.* **2017** 29, 1606134.

7. Huxford, R.C.; Rocca, J.D.; Lin, W. *Curr. Opin. Chem. Biol.* **2010** 14, 262–268.

8. Yan, S.; Feng, L.; Wang, K.; Pang, J.; Bosch, M.; Lollar, C.; Sun, Y.; Qin, J.; Wang, X.; Zhang, P.; et al. *Adv. Mater.* **2018** 37, 1704303.

9. Zhou, H.-C.; Kitagawa, S. *Chem. Soc.Rev.* **2014** 43, 5415–5418.

10. Eddaoudi, M.; Moler, D.B.; Li, H.; Chen, B.; Rheineke, T.M.; O'Keefe, M.; Yaghi, O.M. *Acc. Chem. Res.* **2001** 34, 319–330.

11. Miyasaka, H.; Julve, M.; Yamashita, M.; Clérac, R. *Inorg. Chem.* **2009** 48, 3420–3437.

12. Coulon, C.; Miyasaka, H.; Clérac, R. *Struct. Bonding* **2006** 122, 163–206.

13. Gatteschi, D.; Sessoli, R. *Angew. Chem., Int. Ed.* **2003** 42, 268–297.

14. Givaja, G.; Amo-Ochoa, P.; Gomez-Garcia, C.; Zamora, F. *Chem. Soc. Rev.* **2012** 41, 115–147.

15. Yue, Q.; Gao, E.-Q. *Coord. Chem. Rev.* **2019** 382, 1–31.

16. Leuenberger, M.N.; Loss, D. *Nature* **2001** 410, 789–793.

17. Bogani, L.;Wernsdorfer, W. *Nat. Mater.* **2008** 7, 179–201.

18. Papatriantafyllopoulou, C.; Zartilas, S.; Manos, M.J.; Pichon, C.; Clérac, R.; Tasiopoulos, A.J. *Chem. Commun.* **2014** 50, 14873–14876.

19. Hui, J.; Kishida, H.; Ishiba, K.; Takemasu, K.; Morikawa, M.; Kimizuka, N. *Chem. Eur. J.* **2016** 22, 14213–14218.

20. Chen, L.; Ji, Q.; Wang, X.; Pan, Q.; Ccao, X.; Xu, G. *Cryst. Eng. Comm.* **2017** 19, 5907–5914.

21. Wang, H.-N.; Meng, X.; Dong, L.-Z.; Chen, Y.; Li, S.-L.; Lan, Y.-Q. *J. Mater. Chem. A* **2019** 7, 24059–24091.

22. Jeon, I.-R.; Clérac, R. *Dalton Trans.* **2012** 41, 9569–9586.

23. Bernot, K.; Luzon, J.; Sessoli, R.; Vindigni, A.; Thion, J.; Richeter, S.; Leclercq, D.; Larionova, J.; Van der Lee, A. *J. Am. Chem. Soc.* **2008** 130, 1619–1627.

24. Wang, T.-T.; Ren, M.; Bao, S.-S.; Liu, B.; Pi, L.; Cai, Z.-S.; Zheng, Z.-H.; Xu, Z.-L.; Zheng, L.-M. *Inorg. Chem.* **2014** 53, 3117–3125.

25. Manos, M.J.; Markoulides, M.S.; Malliakas, C.D.; Papaefstathiou, G.S.; Chronakis, N.; Kanatzidis, M.G.; Trikalitis, P.N.; Tasiopoulos, A.J. *Inorg. Chem.* **2011** 50, 11297–11299.

26. Ugale, B.; Singh Dhankhar, S.; Nagaraja, C.M. *Cryst. Growth Des.* **2017** 17, 3295–3305.

27. Sezginel, K.B.; Feng, T.;Wilmer, C.E. *Cryst. Eng. Comm.* **2017** 19, 4497–4504.

28. Nouar, F.; Devic, T.; Chevreau, H.; Guillou, N.; Gibson, E.; Clet, G.; Daturi, M.; Vimont, A.; Grenèche, J.M.; Breeze, M.I.; et al. *Chem. Commun.* **2012** 48, 10237–10239.

29. Alhamami, M.; Doan, H.; Cheng, C.-H. *Materials* **2014** 7, 3198–3250

30. Kou,W.-T.; Yang, C.-X.; Yan, X.-P. *J. Mater. Chem. A* **2018** 6, 17861–17866.

31. Wang, Z.; Li, Z.; Ng, M.; Milner, P.J. *Dalton Trans.* **2020** 49, 16238–16244.

32. Klinowski, J.; Almeida Paz, F.A.; Silva, P.; Rocha, J. *Dalton Trans.* **2011** 40, 321.

33. Vinu, M.; Lin, W.-C.; Senthil Raja, D.; Han, J.-L.; Lin, C.-H. *Polymers* **2017**, 9, 498.

34. Garibay, S.J.; Cohen, S.M. *Chem. Commun.* **2010** 46, 7700–7702.

35. Yaghi, O.M.; O'Keeffe, M.; Ockwig, N.W.; Chae, H.K.; Eddaoudi, M.; Kim, J. *Nature* **2003** 423, 705.

36. Ardila-Suárez, C.; Díaz-Lasprilla, A.M.; Díaz-Vaca, L.A.; Balbuena, P.B.; Baldovino-Medrano, V.G.; Ramírez-Caballero, G.E. *Cryst. Eng. Comm.* **2019** 21, 3014–3030.

37. Chen, D.; Zhao, J.; Zhang, P.; Dai, S. *Polyhedron* **2019** 162, 59–64.

38. Mai, Z.; Liu, D. *Cryst. Growth Des.* **2019** 19, 7439–7462.

39. Horcajada, P.; Surblé, S.; Serre, C.; Hong, D.-Y.; Seo, Y.-K.; Chang, J.-S.; Grenèche, J.-M.; Margiolaki, I.; Férey, G. *Chem. Commun.* **2007** 2820.

40. Kourtellaris, A.; Moushi, E.E.; Spanopoulos, I.; Tampaxis, C.; Charalambopoulou, G.; Steriotis, T.A.; Papaefstathiou, G.S.; Trikalitis,

P.N.; Tasiopoulos, A.J. *Inorg. Chem. Front.* **2016** 3, 1527–1532.

41. Moushi, E.E.; Kourtellaris, A.; Spanopoulos, I.; Manos, M.J.; Papaefstathiou, G.S.; Trikalitis, P.N.; Tasiopoulos, A.J. *Cryst. Growth Des.* **2015** 15, 185–193.

42. Manos, M.J.; Moushi, E.E.; Papaefstathiou, G.S.; Tasiopoulos, A.J. *Cryst. Growth Des.* **2012** 12, 5471–5480.

43. Clausen, H.F.; Poulsen, R.D.; Bond, A.D.; Chevallier, M.-A.S.; Iversen, B.B. *J. Solid State* **2005** 178, 3342–3351.

44. Chen, Z.; Adil, K.; Weselinski, L.J.; Belmabkhout, Y.; Eddaoudi, M. *J. Mater. Chem. A* **2015** 3, 6276–6282.

45. Tranchemontagne, D.J.; Hunt, J.R.; Yaghi, O.M. *Tetrahedron* **2008** 64, 8553–8557.

46. Li, H.; Eddaoudi, M.; O'Keeffe, M.; Yaghi, O.M. *Nature* **1999** 402, 276–299.

47. Sapchenko, S.A.; Dybtsev, D.N.; Damsonenko, D.G.; Fedin, V.P. *New J. Chem.* **2010** 34, 2445–2450.

48. Zhao, X.-L.; Sun,W.-Y. *Cryst. Eng. Comm.* **2014** 16, 3247–3258.

49. Guesh, K.; Caiuby, C.A.D.; Mayoral, Á.; Díaz-García, M.; Díaz, I.; Sanchez-Sanchez, M. *Cryst. Growth Des.* **2017** 17, 1806–1813.

50. Yin, Z.; Zhou, Y.-L.; Zeng, M.-H.; Kurmoo, M. *Dalton Trans.* **2015** 44, 5258–5275.

51. ZareKarizi, F.; Johariana, M.; Morsali, A. *J. Mater. Chem. A* **2018** 6, 19288–19329

52. Milios, C.J.; Stamatatos, T.C.; Perlepes, S.P. *Polyhedron* **2006** 25, 134–194.

53. Escuer, A.; Vlahopoulou, G.; Mautner, F.A. *Inorg. Chem.* **2011** 50, 2717–2719.

54. Mowson, A.M.; Nguyen, T.N.; Abboud, K.A.; Christou, G. *Inorg. Chem.* **2013** 52, 12320–12322.

55. Papatriantafyllopoulou, C.; Jones, L.F.; Nguyen, T.D.; Matamoros-Salvador, N.; Cunha-Silva, L.; Almeida Paz, F.A.; Rocha, J.; Evangelisti, M.; Brechin, E.K.; Perlepes, S.P. *Dalton Trans.* **2008** 3153–3155.

56. Efthymiou, C.G.; Cunha-Silva, L.; Perlepes, S.P.; Brechin, E.K.; Inglis, R.; Evangelisti, M.; Papatriantafyllopoulou, C. *Dalton Trans.* **2016** 17409–17419.

57. Papatriantafyllopoulou, C.; Stamatatos, T.C.;Wernsdorfer,W.; Teat, S.J.; Tasiopoulos, A.J.; Escuer, A.; Perlepes, S.P. *Inorg. Chem.* **2010** 49, 10486–10496.

58. Polyzou, C.D.; Efthymiou, C.G.; Escuer, A.; Cunha-Silva, L.; Papatriantafyllopoulou, C.; Perlepes, S.P. *Pure Appl. Chem.* **2013** 85, 315.

59. Papatriantafyllopoulou, C.; Stamatatos, T.C.; Efthymiou, C.G.; Cunha-Silva, L.; Almeida Paz, F.A.; Perlepes, S.P.; Christou, G. *Inorg. Chem.* **2010** 49, 9743–9745.

60. Papatriantafyllopoulou, C.; Estrader, M.; Efthymiou, C.G.; Dermitzaki, D.; Gkotsis, K.; Terzis, A.; Diaz, C.; Perlepes, S.P. *Polyhedron* **2009** 28, 1652–1655

61. Efthymiou, C.G.; Mylonas-Margaritis, I.; Das Gupta, S.; Tasiopoulos, A.; Nastopoulos, V.; Christou, G.; Perlepes, S.P.; Papatriantafyllopoulou, C. *Polyhedron* **2019** 171, 330–337.

62. Stamatatos, T.C.; Foguet-Albiol, D.; Stoumpos, C.C.; Raptopoulou, C.P.; Terzis, A.;Wernsdorfer,W.; Perlepes, S.P.; Christou, G. *Polyhedron* **2007** 26, 2165–2168.

63. Ghosh, T.; Abboud, K.A.; Christou, G. *Polyhedron* **2019** 173, 114145.

64. Nguyen, T.N.; Shiddiq, M.; Ghosh, T.; Abboud, K.A.; Hill, S.; Christou, G. *J. Am. Chem. Soc.* **2015** 137, 7160–7168.

65. Nguyen, T.N.; Wernsdorfer,W.; Shiddiq, M.; Abboud, K.A.; Hill, S.; Christou, G. *Chem. Sci.* **2016** 7, 1156–1173.

66. Mylonas-Margaritis, I.; Gerard, A.; Skordi, K.; Mayans, J.; Tasiopoulos, A.; McArdle, P.; Papatriantafyllopoulou, C. *Materials* **2020** 13, 4084.

67. Mylonas-Margaritis, I.; Winterlich, M.; Efthymiou, C.G.; Lazarides, T.; McArdle, P.; Papatriantafyllopoulou, C. *Polyhedron* **2018** 151, 360–368.

68. Shen, T.; Liu, T.; Yuan, Z.; Cui, F.; Jin, Y.; Chen, X. *RSC Adv.* **2020** 10, 22881–22890.

69. Álvarez, J.R.; Sánchez-González, E.; Pérez, E.; Schneider-Revueltas, E.; Martínez, A.; Tejeda-Cruz, A.; Islas-Jácome, A.; González- Zamora, E.; Ibarra, I.A. *Dalton Trans.* **2017** 46, 9192–9200.

70. Chui, S.; Lo, S.; Charmant, J.; Opren, G.;Williams, I.D. *Science* **1999** 283, 1148–1150.

71. Davies, K.; Bourne, S.A.; Ohrstrom, L.; Oliver, C.L. *Dalton Trans.* **2010** 39, 2869–2874.

72. Larsen, R.W.; Wojitas, L. *Inorg. Chim. Acta* **2017** 466, 243–248.

73. Rajak, R.; Saraf, M.; Mobin, S.M. *J. Mat. Chem. A* **2019** 7, 1725–1736.

74. He, X.; Wang, W.-N. *Cryst. Growth Des.* **2019** 19, 1095–1102.

75. Venu, B.; Shirisha, V.; Vishali, B.; Naresh, G.; Kishore, R.; Sreedhar, I.; Venugopal, A. *New J. Chem.* **2020** 44, 5972–5979.

76. Riou-Cavellec, M.; Albinet, C.; Greneche, J.-M.; Ferey, G. *J. Mat. Chem.* **2001** 11, 3166–3171.

77. Fang, Y.; Yang, Z.; Liu, X. *Environ. Sci. Pollut. Res.* **2020** 27, 4703–4724.

78. Addison, A.W.; Rao, T.N.; Reedijk, J.; van Rijn, J.; Verschoor, G.C. *J. Chem. Soc. Dalton Trans.* **1984** 1346–1356.

79. Alexandrov, E.V.; Blatov, V.A.; Kochetkov, A.V.; Proserpio, D.M. *Cryst. Eng. Comm.* **2011** 13, 3947–3958.

80. Blatov, V.A.; Shevchenko, A.P.; Proserpio, D.M. *Cryst. Growth Des.* **2014** 14, 3576–3586.

81. O'Keeffe, M.; Peskov, M.A.; Ramsden, S.J.; Yaghi, O.M. *Acc. Chem. Res.* **2008** 41, 1782–1789.

82. Ahamad, M.N.; Khan, M.S.; Shahid, M.; Ashmad, M. *Dalton Trans.* **2020** 49, 14690–14705.

83. Ahamad, M.N.; Shahid, M.; Ashmad, M.; Sama, F. *ACS Omega* **2019** 4, 7738–7749.

84. Li, J.-X.; Qin, Z.-B.; Li, Y.-H.; Cui, G.-H. *Polyhedron* **2018** 151, 530–536.

85. Yang, Q.; Zhao, J.-P.; Liu, Z.-Y. *J. Solid State Chem.* **2012** 196, 52–57.

86. Gabriel, C.; Vangelis, A.A.; Raptopoulou, C.P.; Terzis, A.; Psycharis, V.; Zervou, M.; Bertmer, M.; Salifoglou, *Cryst. Growth Des.* **2015** 15, 5310–5326.

87. Wang, L.; Xue, R.; Li, Y.; Zhao, Y.; Liu, F.; Huang, K. *Cryst. Eng. Comm.* **2014** 16, 7074–7089.

88. Chilton, N.F.; Anderson, R.P.; Turner, L.D.; Soncini, A.; Murray, K.S. *J. Comput. Chem.* **2013** 34, 1164–1175.

89. Hafez, R.S.; El-Khiyami, S. *J. Polym. Res.* **2020** 27.

90. Castro, I.; Faus, J.; Julve, M.; Amigo, J.; Sletten, J.; Debaerdemaeker, T. *Dalton Trans.* **1990** 891–897.

91. Milios, C.J.; Raptopoulou, C.P.; Terzis, A.; Vicente, R.; Escuer, A.; Perlepes, S.P. *Inorg. Chem. Commun.* **2003**, 6, 1056–1060.

92. Bernasek, E. *J. Org. Chem.* **1957** 22, 1263.

93. Orama, M.; Saarinen, H.; Korvenranta, J. *J. Coord. Chem.* **1990** 22, 183–190.

94. Sheldrick, G.M. *Acta Cryst.* **2015** 71, 3–8.

95. McArdle, P.; Gilligan, K.; Cunningham, D.; Dark, R.; Mahon, M. *Cryst. Eng. Comm.* **2004** 6, 303–309.

96. Brandenburg, K. *DIAMOND; Version 2003.2001d; Crystal Impact GbR: Bonn, Germany*, **2006**.

Supplementary Material

Table S1. Selected interatomic distances (Å) and angles (°) for **1**.

Bonds			
Zn1-N5	2.110(8)	Zn1-N2	2.134(7)
Zn1-N4	2.151(5)	Zn1-O3	2.118(4)
Zn1-O0	2.102(4)	Zn1-N1	2.144(6)
Angles			
N5-Zn1-N4	76.0(2)	N1-Zn1-O3	87.4(2)
N4-Zn1-N2	97.2(2)	N1-Zn1-N5	99.6(2)
N2-Zn1-O3	88.7(2)	O4-Zn1-N4	86.2(2)
O3-Zn1-N5	98.4(2)	O4-Zn1-N2	96.7(2)
N1-Zn1-N4	96.3(2)	O4-Zn1-N5	88.7(2)
N1-Zn1-N2	75.1(2)	O4-Zn1-O3	90.9(2)

Table S2. Selected interatomic distances (Å) and angles (°) for **2**.

Bonds			
Zn1-N6	2.091(3)	Zn1-O3	2.055(3)
Zn1-N4	2.282(3)	Zn1-N3	2.111(3)

Zn1-N1	2.172(3)	Zn1-O6	2.084(2)

Angles

N4-Zn1-N1	89.7(1)	N6-Zn1-O6	104.0(1)
N1-Zn1-O6	92.2(1)	N6-Zn1-O3	94.1(1)
O6-Zn1-O3	88.6(1)	N3-Zn1-N4	87.3(1)
O3-Zn1-N4	90.1(1)	N3-Zn1-O3	92.8(1)
N6-Zn1-N1	97.1(1)	N3-Zn1-O6	95.6(1)
N6-Zn1-N4	73.3(1)	N3-Zn1-N1	75.0(1)

Table S3. Selected interatomic distances (Å) and angles (°) for **3**.

Bonds

Cu1-N1	2.006(2)	Cu1-N3	1.977(3)
Cu1-O5	1.942(2)	Cu1-O1	1.918(2)
Cu1-O7	2.629(2)		

Angles

N3-Cu1-O5	170.69	N1-Cu1-N3	79.61
O5-Cu1-O7	97.62	O1-Cu1-O5	87.79
O7-Cu1-N3	83.43	O1-Cu1-O7	88.51
N1-Cu1-O5	91.09	O1-Cu1-N3	101.5
N1-Cu1-O7	97.68		

Table S4. Selected interatomic distances (Å) and angles (°) for **4**.

Bonds			
Cu1-O2	1.924(5)	Cu1-O5	1.934(4)
Cu1-N2	1.982(4)	Cu1-N1	2.001(6)

Angles			
O2-Cu1-N2	101.8(2)	N1-Cu1-O5	90.8(2)
N2-Cu1-N1	79.8(2)	O5-Cu1-O2	88.6(2)

Table S5. Selected interatomic distances (Å) and angles (°) for **5**·4H$_2$O.

Bonds			
Cu1-N2	2.025(2)	Cu1-O2	2.260(2)
Cu1-N1	2.004(3)	Cu1-O6	1.951(2)
Cu1-O3	1.948(2)		

Angles			
O3-Cu1-N1	174.64(8	N2-Cu1-O3	101.57(9)
N1-Cu1-O2	89.09(8)	O6-Cu1-N1	91.78(8)
O2-Cu1-O3	85.60(8)	O6-Cu1-O2	99.72(8)
N2-Cu1-N1	78.72(9)	O6-Cu1-O3	89.88(8)
N2-Cu1-O2	101.49(9)	N2-Cu1-O6	156.55(9)
N1-Cu1-O3	174.64(8)		

Table S6. Hydrogen bonding details for **2**[a].

D-H···A	D···A (Å)	H···A (Å)	DHA (°)	Symmetry operator of A
O1-H1O1···O4	2.648	1.789	165.91	x, y, z
N5-H1N5···O4	2.894	2.147	163.53	1-x, -1/2+y, 1.5-z
O5-H1O5···O8	2.655	1.876	145.31	-x, -1/2+y, 1/2-z

[a] A = acceptor, D = donor

Table S7. Hydrogen bonding details for 5·4H$_2$O[a].

D-H···A	D···A (Å)	H···A (Å)	DHA (°)	Symmetry operator of A
O2-H2O2···O9	2.743	1.907	170.95	x, y, z
O8-H1O8···O10	2.560	1.69	174.02	x, y, z
O1-H1O1···O4	2.510	1.616	174.08	x, y, z
O2-H2O2···O7	2.776	2.061	169.55	x, y, -1+z

[a] A = acceptor, D = donor
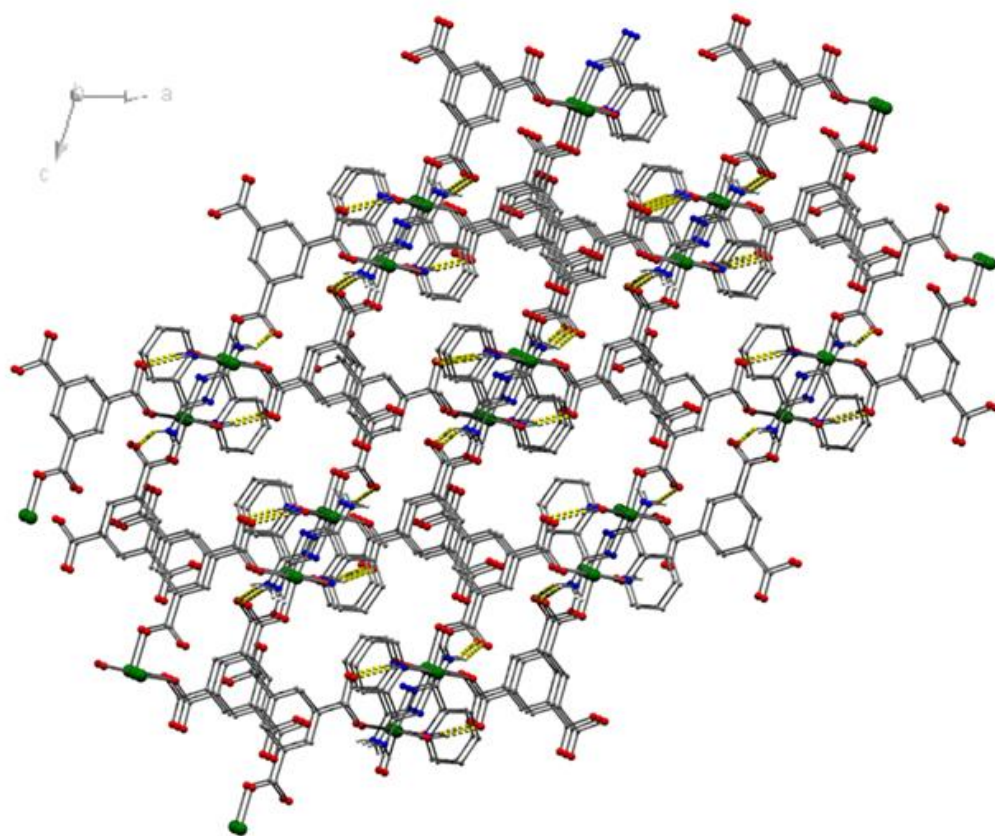
Figure S1. Representation of the 3D network formed through hydrogen bonding interactions in **3**.
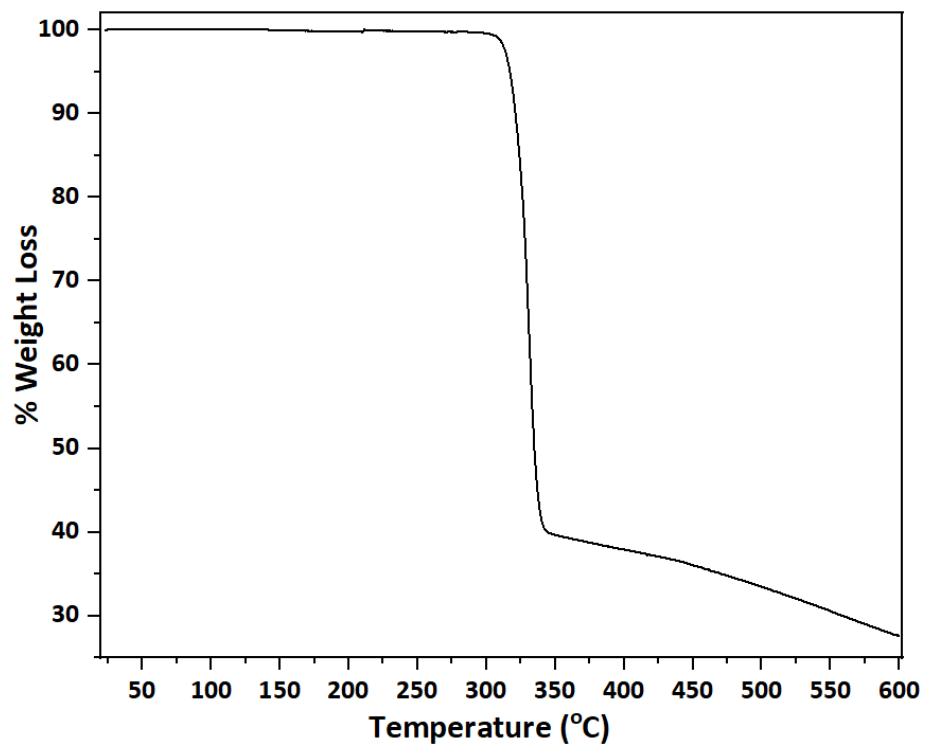
Figure S2. The TGA plot for **3**.
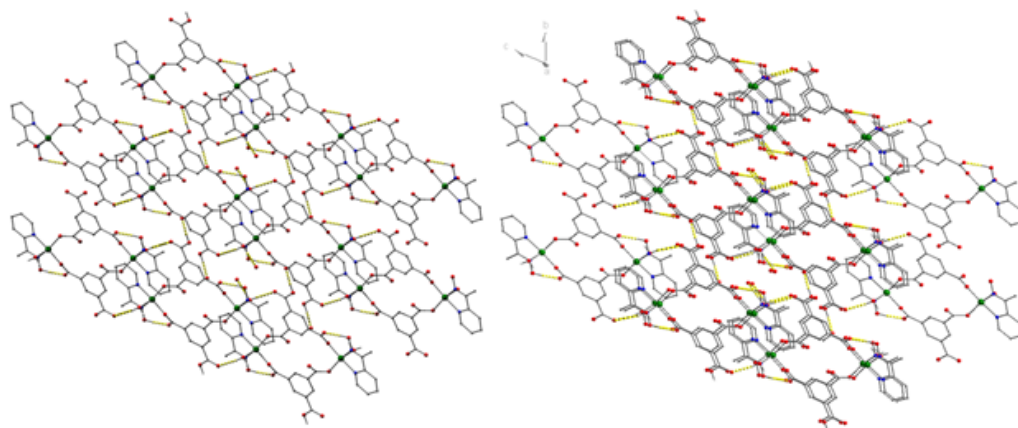
Figure S3. Representation of the 3D network formed through hydrogen bonding interactions in **5**·4H$_2$O.
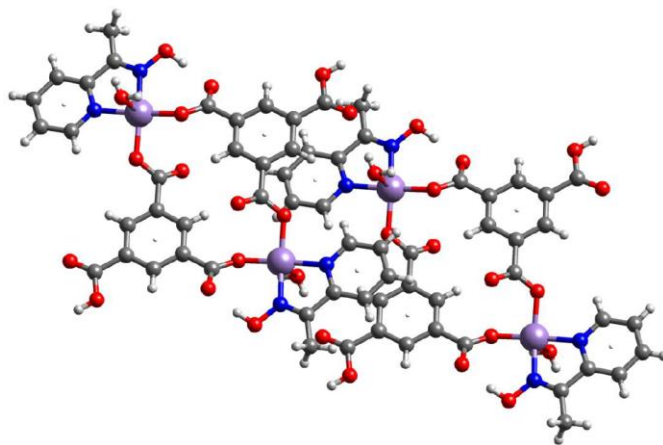
Figure S4. Representation of the intermolecular π-π stacking interactions in **5**·4H$_2$O. The centroids of the interacting aromatic rings are represented with spheres.
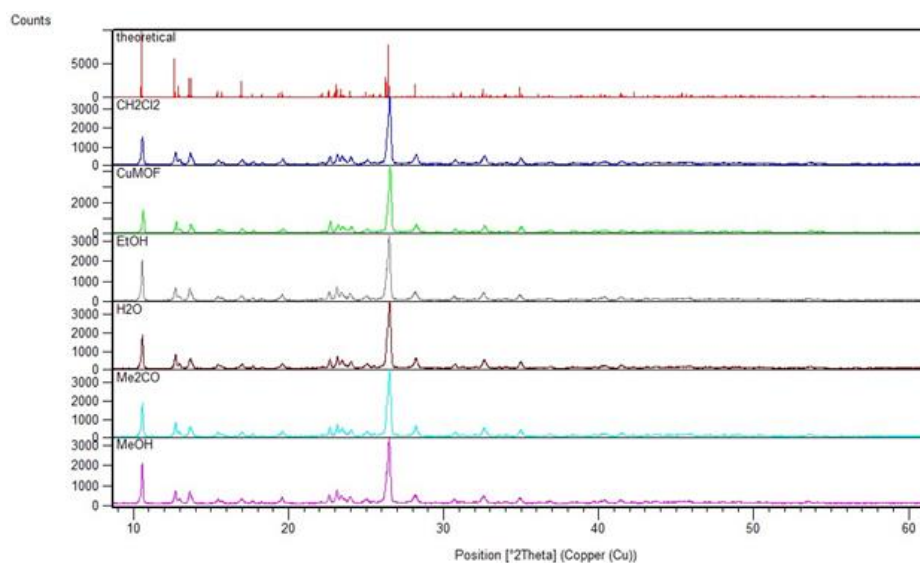
Figure S5. Comparison of the pxrd patterns for **3** (theoretical, red; experimental, green; in CH$_2$Cl$_2$, navy blue; in EtOH, grey; in H$_2$O, magenta; in Me$_2$CO, cyan; in MeOH, pink).
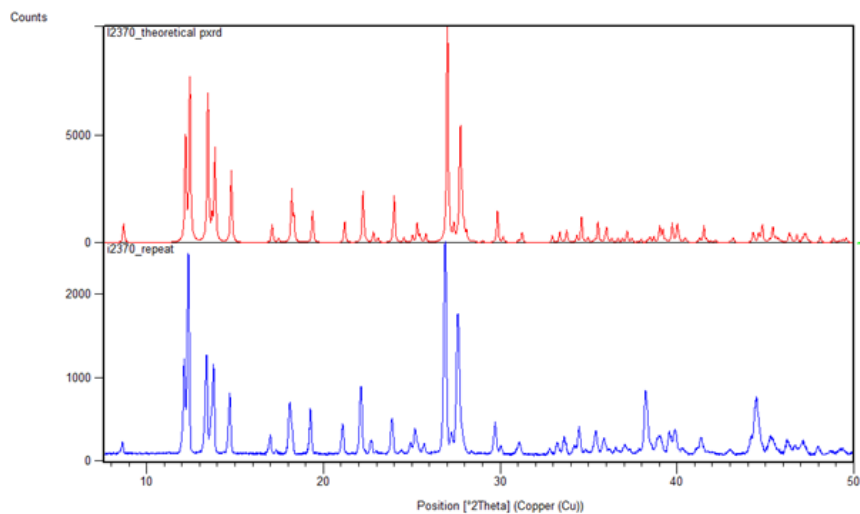
Figure S6. Comparison of the pxrd patterns for **5**·4H$_2$O (theoretical, red; experimental, blue).
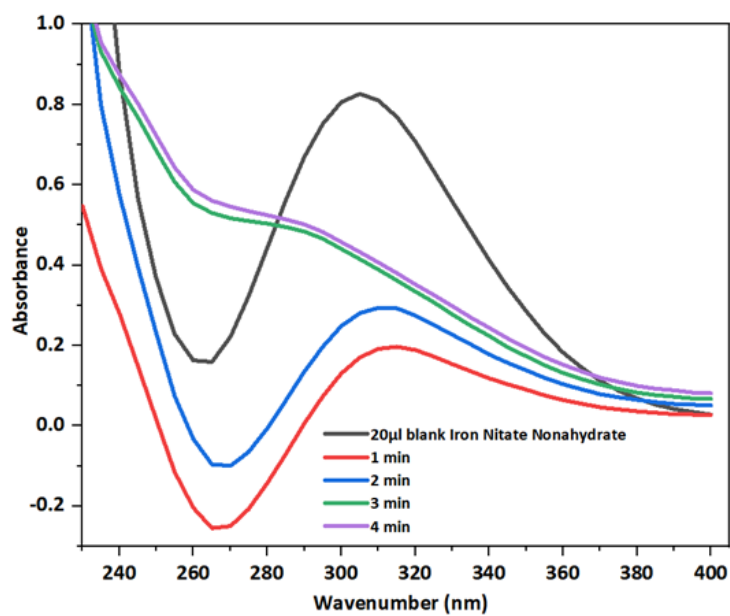
Figure S7. UV-vis plot for the adsorption of iron(III) nitrate nonahydrate by **3** in H$_2$O. Initial concentration: 0.10 mmol Fe(NO$_3$)$_3$ in 10ml of H$_2$O.
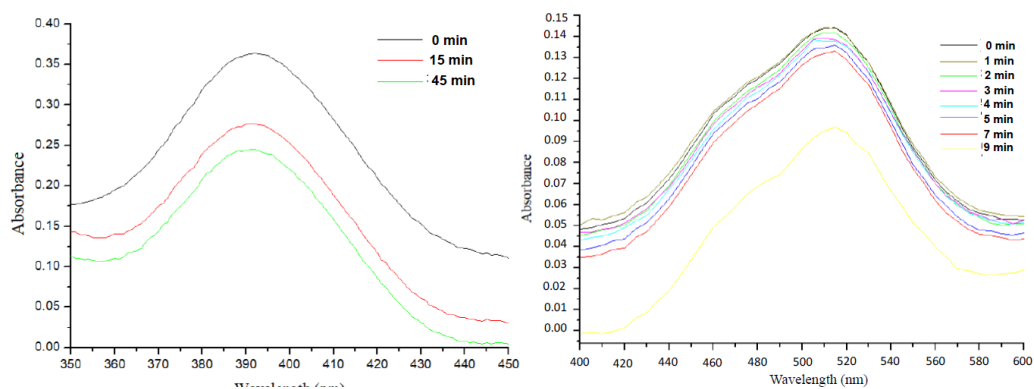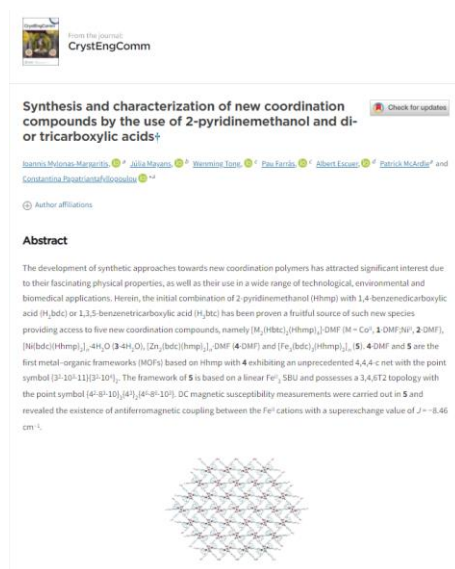
Figure S8. Preliminary results on the adsorption of $Ni(NO_3)_2$ (left) and $Co(NO_3)_2$ (right) by **3** in H_2O.

Figure S9. Photo of crystals of **3** (left) before the reaction and the formed brown compound (right).

207

2.4 Brief description of the paper

In this article is described the synthesis and characterization of new coordination polymers and MOFs by the simulrtaneous use of the 2-pyridinemethanol and terephthalic or trimesic acid. Also, the Fe-MOF was magnetically studied and the Zn-MOF was photoluminescence characterized.

Ioannis Mylonas-Margaritis, Júlia Mayans, Wenming Tong, Pau Farràs, Albert Escuer, Patrick McArdle and Constantina Papatriantafyllopoulou

Author affiliations

Abstract

The development of synthetic approaches towards new coordination polymers has attracted significant interest due to their fascinating physical properties, as well as their use in a wide range of technological, environmental and biomedical applications. Herein, the initial combination of 2-pyridinemethanol (Hhmp) with 1,4-benzenedicarboxylic acid (H_2bdc) or 1,3,5-benzenetricarboxylic acid (H_3btc) has been proven a fruitful source of such new species providing access to five new coordination compounds, namely $[M_2(Hbtc)_2(Hhmp)_4]\cdot DMF$ ($M = Co^{II}$, **1**·DMF; Ni^{II}, **2**·DMF), $[Ni(bdc)(Hhmp)_2]_n\cdot 4H_2O$ (**3**·4H_2O), $[Zn_2(bdc)(hmp)_2]_n\cdot DMF$ (**4**·DMF) and $[Fe_2(bdc)_3(Hhmp)_2]_n$ (**5**). **4**·DMF and **5** are the first metal–organic frameworks (MOFs) based on Hhmp with **4** exhibiting an unprecedented 4,4,4-c net with the point symbol $\{3^2\cdot 10^3\cdot 11\}\{3^2\cdot 10^4\}_2$. The framework of **5** is based on a linear Fe^{II}_3 SBU and possesses a 3,4,6T2 topology with the point symbol $\{4^2\cdot 8^3\cdot 10\}_2\{4^2\}\{4^2\cdot 8^6\cdot 10^3\}$. DC magnetic susceptibility measurements were carried out in **5** and revealed the existence of antiferromagnetic coupling between the Fe^{II} cations with a superexchange value of $J = -8.46$ cm^{-1}.

Author's contribution:

I. Mylonas-Margaritis: All the synthetic work, preparation of first draft, tables, figures.

K. Skordi, Prof. A. J. Tasiopoulos, Prof. Patrick McArdle: Collection and analysis of the crystallographic data.

Dr. J. Mayans; A. Escuer: Magnetic Studies

Dr. W. Tong; Dr. P. Farràs: Photoluminescence studies.

Dr. Constantina Papatriantafyllopoulou: Managed the project **and** reviewed the manuscript before the submission and during the revision process.

Synthesis and Characterization of New Coordination Compounds by the Use of 2-Pyridinemethanol and Di- or Tricarboxylic Acids

Ioannis Mylonas-Margaritis,[a] Júlia Mayans,[b] Wenming Tong,[c] Pau Farràs,[c] Albert Escuer,[d] Patrick McArdle,[a] and Constantina Papatriantafyllopoulou [*][a]

[a]School of Chemistry, College of Sciecne and Engineering, National University of Ireland Galway, Galway, Ireland
E-mail: constantina.papatriantafyllopo@nuigalway.ie; **Tel:** +353 91 493462

[b]Instituto de Ciencia Molecular (ICMol), Universidad de Valencia, Catedrático José Beltran 2, Valencia, 46980 Paterna, Spain

[c]School of Chemistry, Energy Research Centre, Ryan Institute, National University of Ireland, Galway (NUI Galway), University Road, H91 CF50 Galway, Ireland

[d]Departament de Química Inorgànica i Orgànica, Secció Inorgànica and Institute of Nanoscience (IN2UB) and Nanotecnology, Universitat de Barcelona, Marti i Franques 1-11, Barcelona-08028, Spain

Abstract

The development of synthetic approaches towards new coordination polymers has attracted a significant interest due to their fascinating physical properties, as well as their use in a wide range of technological, environmental and biomedical applications. Herein, the initial combination of 2-pyridinemethanol (Hmp) with 1,4-benzenedicarboxylic acid (H_2bdc) or 1,3,5-benzenetricarboxylic acid (H_3btc) has been proven a fruitful source of new such species providing access to five

new coordination compounds, namely $[M_2(Hbtc)_2(Hhmp)_4] \cdot DMF$ ($M=Co^{II}$, **1**·DMF; Ni^{II}, **2**·DMF), $[Ni(bdc)(Hhmp)_2]_n \cdot 4H_2O$ (**3**·$4H_2O$), $[Zn_2(bdc)(hmp)_2]_n$ ·DMF (**4**·DMF) and $[Fe_3(bdc)_3(Hhmp)_2]_n$ (**5**). **4**·DMF and **5** are the first metal-organic frameworks (MOFs) based on Hhmp with **4** exhibiting an unprecedented 4,4,4-c net with point symbol $\{3^2.10^3.11\}\{3^2.10^4\}_2$. The framework in **5** is based on a linear Fe^{II}_3 SBU and possesses a **3,4,6T2** topology with point symbol $\{4^2.8^3.10\}_3\{4^3\}_2\{4^6.8^6.10^3\}$. Dc magnetic susceptibility measurements were carried out in **5** and revealed the existence of antiferromagnetic coupling between the Fe^{II} cations with a superexchange value of $J= -8.46$ cm^{-1}.

1. Introduction

Metal-organic frameworks (MOFs)[1,2] are porous materials that have attracted an intense research interest over the last decades due to their aesthetically pleasing structures and their potential to address contemporary challenges in industrial, biomedical and environmental applications.[3-5] MOFs possess a plethora of attractive properties such as enhanced stability, large surface area, biocompatibility, inexpensive large-scale synthesis, depending on the metal ion and ligand present in their structure, and selective adsorption due to the easibility of targeted introduction of additional functional groups into the framework. Furthermore, they display tuneable and often high porosity, which is also affected by the breathing effect,[6,7] i.e., the property of MOFs to change their pore dimensions upon encapsulation of a guest molecule. The unique properties of MOFs and their structural tuneability make these materials suitable for applications in sensing, catalysis, imaging, drug delivery, etc.[8-15]

The vast range of MOFs' applications along with the increasing need for the isolation of new materials with enhanced porosity, selectivity, and stability, constitute a demand for the development of efficient synthetic approaches towards new such species. Many approaches have now been reported, with some of them (isoreticular synthesis, post synthetic modification) favouring the targeted synthesis of MOFs with desirable properties.[16-24] The latter are affected by the type of the metal ion that is present in the secondary building unit (SBU), and the type of the organic ligand that links the neighbouring SBUs. A large variety of organic linkers or a combination of them has been used for the synthesis of new MOFs, including imidazolates, pyridine, carboxylates, and others.[25-35]

With the above in mind, we recently initiated the exploration of the ligand blend 2-pyridyl oxime/polycarboxylic acids for the synthesis of new MOFs.[36-38] 2-pyridyl oximes were chosen because of their high bridging capability and their potential to introduce interesting magnetic properties to the system.[39] Many oximic ligands, such as pyridine-2-amidoxime and 2-methyl pyridyl ketoxime, were investigated with the simultaneous use of a polycarboxylate (benzene-1,4-dicarboxylic acid, benzene-1,3,5-tricarboxylic acid, benzene-1,2,4,5-tetracarboxylic acid) and yielded the first 2-pyridyl oxime based MOFs, and several coordination polymers. Some of the MOFs display unprecedented metal topologies and good metal ion adsorption capacity. For example, $[Cu_4(OH)_2(pma)(mpko)_2]_n$,[37] where pma^{4-} is the tetra-anion of 1,2,4,5-benzene tetracarboxylic acid (pyromellitic acid) and mpko- is the anionic form of 2-methyl pyridyl ketoxime, exhibits a good Fe^{III} adsorption capacity with its magnetic properties being affected by the amount of the encapsulated metal ions.[37]
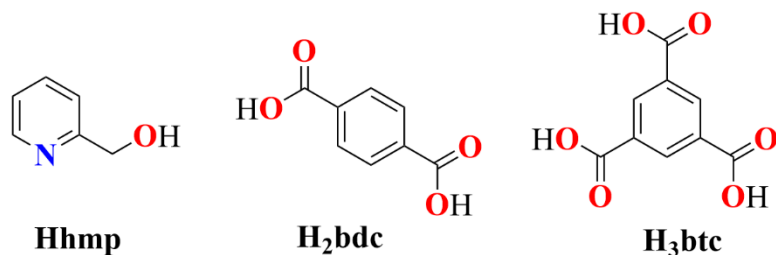
Scheme 1. Schematic representation of the 2-pyridinemethanol (Hhmp, left), terephthalic acid (H$_2$bdc, middle) and trimesic acid (H$_3$btc, right).

Expanding the above described approach for the synthesis of new MOFs, we were prompted to replace the oximes by alkoxy-containing ligands and explore their impact on the structures and physical properties of the isolated compounds.

To this end, we decided to employ 2-pyridinemethanol (Hhmp, **Scheme 1**), which, similarly to oximes, often favours ferromagnetic coupling between the metal centers, and have yielded several polynuclear 3d metal clusters with large *S* values.[40-45] Although Hhmp has been extensively investigated in metal cluster chemistry, it remains essentially unexplored as a source of new MOFs. It is worth to mention that aminoalcohols have been proven to act as templates for the synthesis of new MOFs and coordination polymers.[28,46,47]

Herein, we report on the synthesis, structural characterization and physical properties of five new species by the use of Hhmp in combination with terephthalic acid (H$_2$bdc) or trimesic acid (H$_3$btc). Among them, [Zn$_2$(bdc)(hmp)$_2$]$_n$·DMF (**4**·DMF) and [Fe$_3$(bdc)$_3$(Hhmp)$_2$]$_n$ (**5**) are the first MOFs bearing Hhmp with the former displaying an unprecedented structural topology. Note that both trimesic and terephthalic acid have been extensively

employed for the synthesis of new MOFs, however their combination with 2-pyridinemethanol remains unexplored.

2. Experimental

All manipulations were performed under aerobic conditions using materials (reagent grade) and solvents as received. WARNING: Perchlorate salts are potentially explosive; such compounds should be used in small quantities and treated with the utmost care at all times.

Elemental analysis (C, H, N) were performed by the inhouse facilities of the National University of Ireland Galway, School of Chemistry. IR spectra (4000-400 cm-1) were recorded on a Perkin-Elmer Spectrum 400 FT-IR spectrometer. TGA experiments were performed on an STA625 thermal analyzer from Rheometric Scientific (Piscataway, New Jersey). The heating rate was kept constant at 10°C/min, and all runs were carried out between 20-600°C. The measurements were made in open aluminum crucibles, nitrogen was purged in ambient mode, and calibration was performed using an indium standard.

Solid-state, variable-temperature, and variable-field magnetic data were collected on powdered samples using an MPMS5 Quantum Design magnetometer operating at 0.03 T in the 300–2.0 K range for the magnetic susceptibility and at 2.0 K in the 0–5 T range for the magnetization measurements. Diamagnetic corrections were applied to the observed susceptibilities using Pascal's constants. The fluorescence spectra were measured using an Agilent Eclipes Fluorospectrophotometer with a powder sample holder at room temperature.

2.1. Synthesis of [Co$_2$(Hbtc)$_2$(Hhmp)$_4$]·DMF (**1**·DMF)

Co(ClO$_4$)$_2$·6H$_2$O (0.073g, 0.2mmol) and Hhmp (0.05 ml, 0.53 mmol) were dissolved in DMF (5 ml) into a glass vial with plastic lid. The resultant solution was put in the oven and heated at 100°C for 1h. The solution turned purple; H$_3$btc (0.021 g, 0.1 mmol) was then added and the vial was placed into the oven for 24hours, after which X-ray quality purple crystals of **1** were formed. The crystals were collected by filtration, washed with cold MeCN (2ml) and Et$_2$O (2 x 5 ml), and dried in air. Yield 73%. Anal. Calcd (Found) for **1**·DMF: C, 51.79 (51.87); H, 4.15 (3.99); N, 6.71 (6.89)%. IR data: ν (cm^{-1}) = 1710m, 1663s, 1606s, 1575m, 1555m, 1482w, 1431w, 1411w, 1374s, 1272m, 1239m, 1191w, 1173w, 1159w, 1096m, 1058m, 1042s, 1024w, 967w, 943w, 898w, 819w, 772s, 758s, 709s, 690m, 671m, 659m.

2.2. Synthesis of [Ni$_2$(Hbtc)$_2$(Hhmp)$_4$]·DMF (**2**·DMF)

Ni(ClO$_4$)$_2$·6H$_2$O (0.073g, 0.2mmol) and Hhmp (0.05 ml, 0.53 mmol) were dissolved in 5 ml of DMF into a glass vial with plastic lid. The resultant solution was put in the oven and heated at 100°C for 1h. The solution turned into green. H3btc (0.021 g, 0.1 mmol) was added and the vial was placed into the oven for further 24hours, after which the solution was turned cloudy green and X-ray quality blue crystals of **2** were formed. The crystals were collected by filtration, washed with cold MeCN (2ml) and Et$_2$O (2 x 5 ml), and dried in air. Yield 80%.

Anal. Calc. (Found) for 2.DMF: C, 51.81 (51.90); H, 4.15 (4.32); N, 6.71 (6.80) %. IR data: ν (cm^{-1}) = 2930w, 1716w, 1656s, 1603m, 1576w, 1549m, 1483w, 1437m, 1411w, 1376s, 1289w, 1228m, 1193w, 1173w, 1159w, 1092s, 1058m, 1042s, 1028w, 971m, 909m, 851m, 813m, 797w, 773s, 757m, 717s, 631w, 671w, 659m.

2.3. Synthesis of [Ni(bdc)(Hhmp)$_2$]$_n$·4H$_2$O (**3**·4H$_2$O)

Ni(ClO$_4$)$_2$·6H$_2$O (0.073g, 0.2mmol) and Hhmp (0.05 ml, 0.53 mmol) were dissolved in H$_2$O/DMF (5/5 ml) into a glass vial with plastic lid. The resultant solution was put in the oven and heated at 130°C for 1h. Then H$_2$bdc (0.017 g, 0.1 mmol) was added and the vial was placed into the oven for a further 24hours, after which X-ray green crystals of **3** were formed. The crystals were collected by filtration, washed with cold MeCN (2ml) and Et$_2$O (2 x 5 ml), and dried in air. Yield 60%. Anal. Calc. (Found) for **3**·4H$_2$O: C, 46.82 (47.06); H, 5.11 (5.36); N, 5.46 (5.27) %. IR data: v (cm^{-1}) = 1658w, 1609w, 1576w, 1548m, 1488w, 1438w, 1381s, 1361s, 1296m, 1236w, 1156w, 1108w, 1062w, 1038s, 1014w, 991w, 891w, 811s, 750s, 730w, 650w, 630w, 601w. IR data: v (cm-1) = I2931w, 1649m, 1591m, 1377s, 1253m, 1154w, 1096m, 1062w. 1018m, 888m, 824w, 747s. 662m.

Table 1 Crystallographic data for complexes **1**-**5.**

Complex	1·DMF	2·DMF	3·4H$_2$O	4·DMF	5
Empirical formula	C$_{48}$H$_{48}$Co$_2$N$_6$O$_{18}$	C$_{48}$H$_{48}$Ni$_2$N$_6$O$_{18}$	C$_{20}$H$_{26}$NiN$_2$O$_{10}$	C$_{23}$H$_{22}$N$_3$O$_7$Zn$_2$	C$_{36}$H$_{36}$Fe$_3$N$_2$O$_{14}$
Formula weight	1114.78	1080.2	513.13	583.22	932.28
Crystal system	Orthorhombic	Orthorhombic	Monoclinic	Orthorhombic	Monoclinic
Space group	C_{mca}	C_{mca}	$I_{2/m}$	Pna2$_1$	$P_2$1/n
a (Å)	20.5149(8)	20.5127(6)	11.3588(7)	17.0340(5)	10.4617(10)
b (Å)	16.0901(12)	16.0761(5)	30.0046(12)	11.4043(3)	14.6431(10)
c (Å)	15.5524(5)	15.2569(5)	11.3550(87)	12.6992(3)	12.7995(9)

β (°)	90	90	117.507(9)	90	97.576(7)
V (Å³)	5133.6(5)	5031.2(3)	3713.9(5)	2466.96(11)	1943.7(3)
Z	4	4	8	4	2
ρ_{calc} (g cm⁻³)	1.442	1.426	1.172	1.570	1.593
μ (mm⁻¹)	0.725	0.826	0.815	1.992	1.175
Measd/independent reflns (R_{int})	17757/3286 [R_{int} = 0.0682]	19871/3257 [R_{int} = 0.0316]	15917/3567 [R_{int} = 0.0362]	19183/5937 [R_{int} = 0.0290]	16449/4673 [R_{int} = 0.1128]
Parameters refined	188	176	208	347	270
GoF (on F²)	1.000	0.990	0.996	0.852	0.875
R_1[a] ($I > 2\sigma(I)$)	0.0598	0.0746	0.0671	0.0309	0.0745
wR_2[b] ($I > 2\sigma(I)$)	0.1331	0.1995	0.2170	0.0790	0.1098
(Δρ)max/(Δρ)min (e Å⁻³)	0.654/-0.388	0.803/-0.521	1.910/ -0.679	0.391/-0.263	0.745/-0.669

[a] $R_1 = \Sigma(|F_o| - |F_c|)/\Sigma/ F_o /$; [b] $wR_2 = [\Sigma[w(F_o^2 - F_c^2)^2]/\Sigma[wF_o^2)^2]]^{1/2}$

2.4. Synthesis of [Zn₂(bdc)(hmp)₂]ₙ·DMF (4·DMF)

$Zn(ClO_4)_2 \cdot 6H_2O$ (0.074g, 0.2mmol) and Hhmp (0.05 ml, 0.53 mmol) were dissolved in DMF (5 ml) into a glass vial with plastic lid. The resultant solution was put in the oven and heated at 100°C for 1h. Then H₂bdc (0.016 g, 0.1 mmol) was added and the vial was placed into the oven for a further 24hours, after which X-ray quality colorless crystals of **4** were formed. The crystals were collected by filtration, washed with cold MeCN (2ml) and Et₂O (2 x 5 ml), and dried in air. Yield 40%. Anal. Calc. (Found) for **4**·DMF: C, 47.29 (47.51); H, 3.97 (4.19); N, 7.19 (7.14) %. IR data: ν (cm⁻¹) = 1672s, 16080w, 1571s, 367s, 1287m, 1106w, 1087s, 1045s, 1018m, 820s, 746s.

2.5. Synthesis of [Fe₃(bdc)₃(Hhmp)₂]ₙ (5)

$FeCl_3 \cdot 6H_2O$ (0.054g, 0.2mmol) and Hhmp (0.05 ml, 0.53 mmol) were dissolved DMF (10 ml) into a glass vial with plastic lid. The resultant solution was put in the oven and heated at 100°C for 1h. The solution turned into cloudy brown and H_2bdc (0.017 g, 0.1 mmol) was added; the vial was placed into the oven for a further 72hours, after which the solution was turned into dark red and X-ray quality orange cubes of **5** were formed. The crystals were collected by filtration, washed with cold MeCN (2ml) and Et_2O (2 x 5 ml), and dried in air. Yield 15%. Anal. Calc. (Found) for **5**: C, 49.24 (49.14); H, 2.98 (2.93); N, 3.19 (3.11) %.

3. Results and Discussion

3.1. Synthesis

Several experiments were performed and the effect of the synthetic parameters (presence/absence or kind of base, metal ratio of the reactants, metal sources, etc) were thoroughly studied.

The reaction between a metal salt ($Co(ClO_4)_2 \cdot 6H_2O$, **1**; $Ni(ClO_4)_2 \cdot 6H_2O$, **2**) Hhmp and H_3btc (2:5:1) in DMF at 100°C yielded crystals of $[M_2(Hbtc)_2(Hhmp)_4].DMF$ (M=Co^{II}, **1**·DMF; Ni^{II}, **2**·DMF) in good yield. The stoichiometric equation of the reaction that led to the formation of 1.DMF and **2**·DMF is represented in Eq. (**1**). The presence of further excess of Hhmp leads to the formation of previously reported compounds that do not bear polycarboxylic ligands.
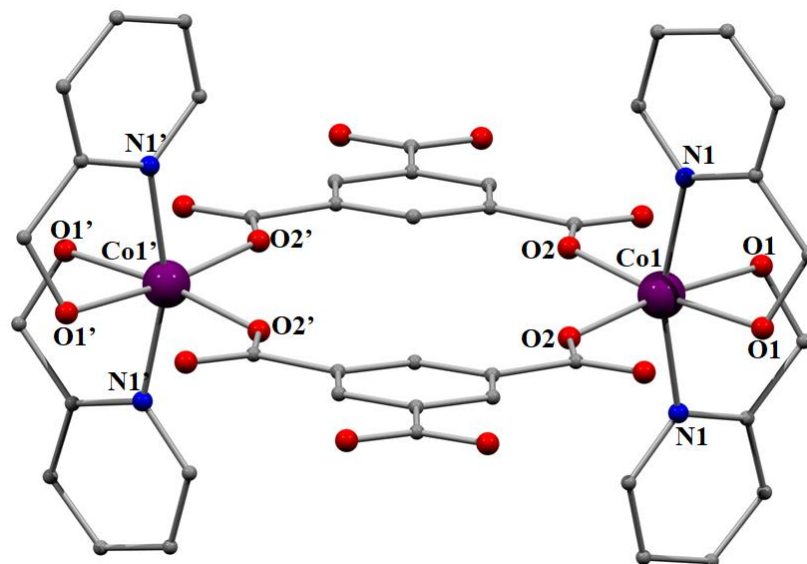
Figure 1: Representation of the molecular structure of **1**·DMF. Color code: Co^{II}, purple; N, navy blue; O, red; C, grey. The hydrogen atoms and the solvate molecules are omitted for clarity.

Following a similar synthetic approach to the one that yielded compounds **1**·DMF and **2**·DMF, but by using H_2bdc instead of H_3btc, $[Ni(bdc)(Hhmp)_2]_n$ ·$4H_2O$ (**3**·$4H_2O$), $[Zn_2(bdc)(hmp)_2]_n$·DMF (**4**·DMF), $[Fe_3(bdc)_3(Hhmp)_2]_n$ (**5**) were isolated as shown in Eqs. (**2**)-(**4**):
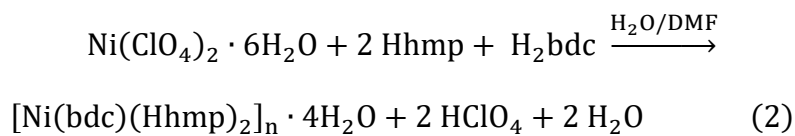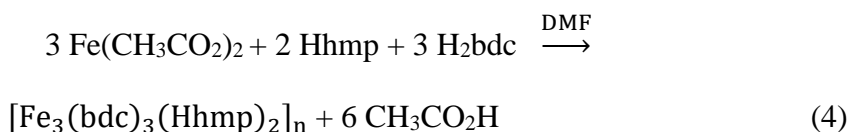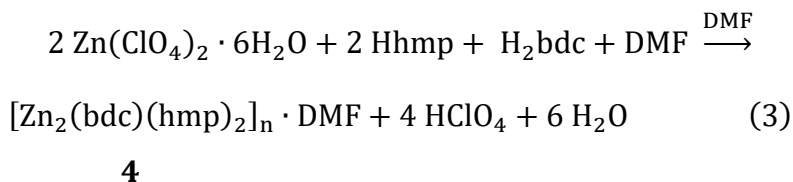
$$Ni(ClO_4)_2 \cdot 6H_2O + 2\ Hhmp + H_2bdc \xrightarrow{H_2O/DMF}$$

$$[Ni(bdc)(Hhmp)_2]_n \cdot 4H_2O + 2\ HClO_4 + 2\ H_2O \qquad (2)$$
$$\mathbf{3}$$

$$2 \, Zn(ClO_4)_2 \cdot 6H_2O + 2 \, Hhmp + H_2bdc + DMF \xrightarrow{DMF}$$

$$[Zn_2(bdc)(hmp)_2]_n \cdot DMF + 4 \, HClO_4 + 6 \, H_2O \qquad (3)$$

$$\textbf{4}$$

$$3 \, Fe(CH_3CO_2)_2 + 2 \, Hhmp + 3 \, H_2bdc \xrightarrow{DMF}$$

$$[Fe_3(bdc)_3(Hhmp)_2]_n + 6 \, CH_3CO_2H \qquad (4)$$

$$\textbf{5}$$

3.2. Description of structures

Representations of the molecular structures of **1**-**5** are shown in **Figures. 1-6, S1** (supplementary information). Selected interatomic distances and angles are listed in **Tables S1-S5**.

Compounds **1**·DMF and **2**·DMF have similar structures with their only difference being the type of the 3d metal ion (**1**·DMF, Co^{II}; **2**·DMF, Ni^{II}). Thus, only the structure of **1**·DMF will be discussed in detail. **1**·DMF crystallizes in the orthorhombic space group C$_{mca}$ and its structure (**Figure 1**) consists of the centrosymmetric complex [Co$_2$(Hbtc)$_2$(Hhmp)$_4$] and lattice DMF molecules. The two Co^{II} ions are held together through two bridging Hbtc^{2-} ions, and the coordination sphere of each metal centre is completed by two terminal, chelate Hhmp ligands. Each metal ion is six coordinated with a slightly distorted octahedral geometry due to the relatively small bite angle of the chelating ligand (N1-Co1-O1 = 77.1(2)°).

Strong intramolecular hydrogen bonding interactions stabilize the crystal structure of **1**·DMF; these are formed between: 1) the neutral alkoxy group of the Hhmp ligand (O1, donor) and an oxygen atom (O3, acceptor) from the Hbtc^{2-} ligand (O1···O3 = 2.609 Å, H1···O3 = 1.778 Å, O1-H1···O3 = 167.13 °), and 2) the protonated carboxylic group of the Hbtc^{2-} ligand (O4, donor) and the lattice DMF molecule (O5, acceptor); O4···O5 = 2.548 Å, H4···O5 = 1.707 Å, O4-H4···O5 = 163.76 °.

Compound **3**·4H$_2$O crystallizes in the monoclinic space group C$_{2/m}$. Its structure consists of two crystallographically independent 1D chains with the formula [Ni(bdc)(Hhmp)$_2$]$_n$, and four lattice H$_2$O molecules. The neighbouring Ni^{II} ions are held together through the bridging bdc^{2-} ligands and form the one-dimensional coordination polymer. Each metal ion is six coordinated, which is completed by two chelate Hhmp ligands, and adopt an octahedral coordination geometry. The structure is stabilized through intermolecular hydrogen bonding interactions, formed between the protonated hydroxyl group (O1, donor) of the Hhmp ligand and the noncoordinated oxygen (O3, acceptor) of the bdc^{2-} ligand (O1···O5 = 2.541 Å). The aromatic rings of the Hhmp ligands of neighbouring chain in **3**·4H$_2$O interact further through strong π-π stacking interactions, with the distance between the centroids being 3.8 Å (**Figure 2**, bottom).
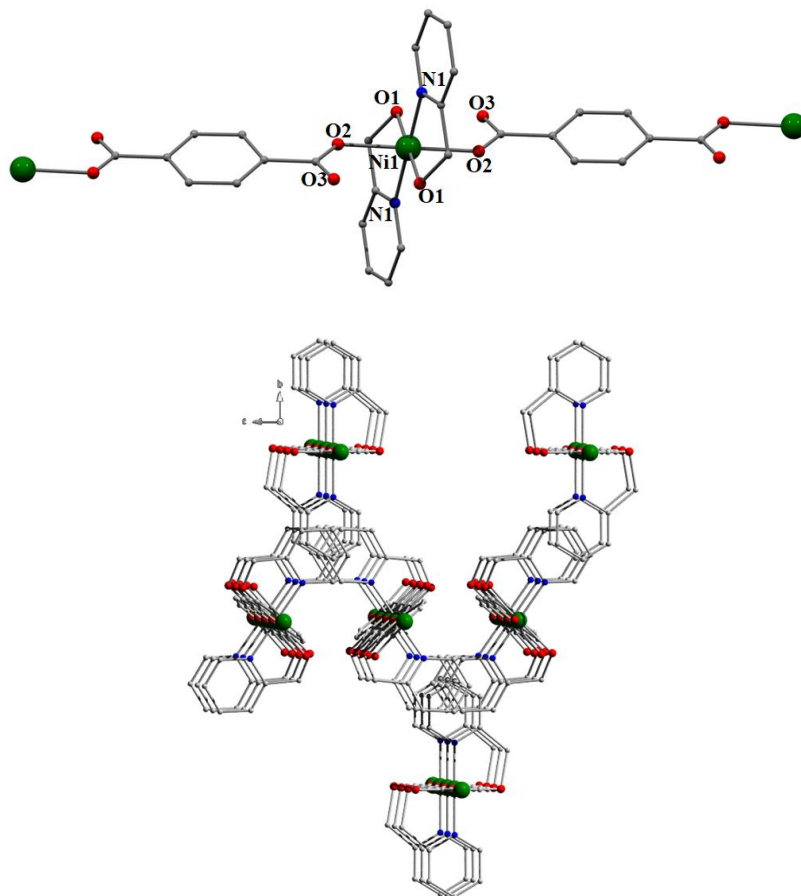
Figure 2: Representation of a part of the one dimensional chain present in **3**·4H$_2$O (top), and representation of the intermolecular π-π stacking interactions in the structure (bottom). Color code: Ni^{II}, dark green; N, navy blue; O, red; C, grey. The hydrogen atoms and the lattice H$_2$O molecules are omitted for clarity.

Compound **4**·DMF is a 3D MOF based on the dinuclear repeating unit [Zn$_2$(bdc)$_2$(hmp)$_2$]$_n$ (**Figure 3**). Solvate DMF molecules are located in the MOF pores. Zn1 is hexa-coordinated adopting octahedral geometry with its

coordination sphere being completed through two terminally chelating hmp⁻ anions and two oxygens coming from two different bdc^{2-} ligands. Zn2 is tetra-coordinated with a tetrahedral geometry; its coordination sphere is completed by two bridging oxygens coming from two hmp⁻ ligands, and O5 and O2, which belong to two different bdc^{2-} anions. Employing a standard representation of the crystal structure of **4**·DMF,[50-52] this gives rise to the formation of a novel three dimensional 4,4,4-c net of the topological type with point symbol $\{3^2.10^3.11\}\{3^2.10^4\}_2$ (**Figure 4**); the latter has never been reported in the past, thus **4**·DMF exhibits a network with a unique architecture. The solvent accessible

volume of **4**·DMF, calculated by PLATON (excluding all solvents from the pores), is 581.5 Å3 and corresponds to the 23.6% of the unit-cell volume (2467.0 Å³).
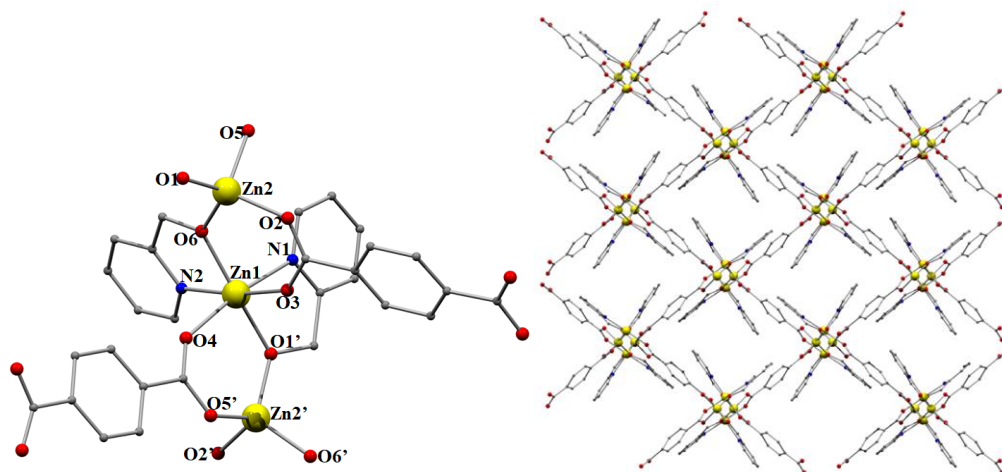
Figure 3: Representations of the repeating unit (left) and a part of the 3D net (right) in **4**·DMF. Color code: Zn^{II}, yellow; N, navy blue; O, red; C, grey. The hydrogen atoms and the lattice DMF molecules are for omitted clarity.
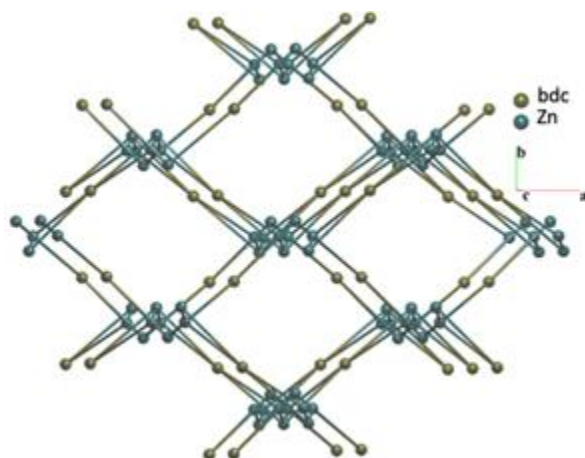
Figure 4: Representation of the 3D 4,4,4-c net with point symbol $\{3^2.10^3.11\}\{3^2.10^4\}_2$ in **4**·DMF.
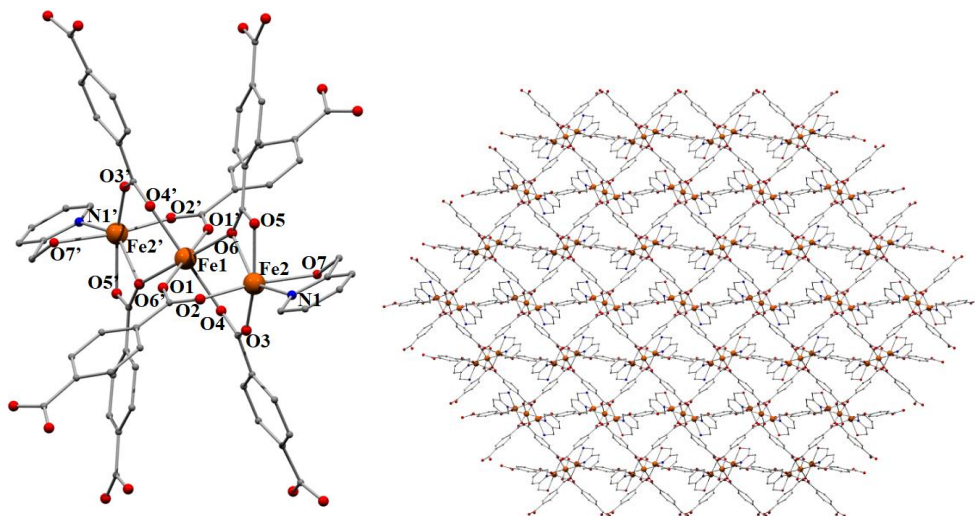
Figure 5: Representations of the repeating unit (left) and a part of the 3D net (right) in **5**. Color code: Fe^{II}, orange; N, navy blue; O, red; C, grey. The hydrogen atoms are for omitted clarity.

5 crystallizes in the monoclinic space group P 2_1/n. Its crystal structure is based on a three-dimensional network with a linear, centrosymmetric $[Fe_3(bdc)_3(Hhmp)_2]_n$ repeating unit (**Figure 5**, left). Fe1 and Fe2 (and its crystallographically equivalent Fe2') are held together through two bridging, and one bridging and chelating bdc^{2-} ligands. The coordination sphere of Fe2 is completed by one chelate Hhmp ligand. The bdc^{2-} ligands link the Fe3 SBU with six neighbouring units resulting in the formation of the 3D network (**Figure 5**, bottom). All metal ions are six-coordinate with an octahedral geometry, which in the case of Fe2 is distorted as a result of the small bite angle of the Hhmp (O7-Fe2-N1 = 76.9(2)°). The metal oxidation state was confirmed through charge considerations and bond-valence sum calculations, BVS (Fe1, 2.03; Fe2, 2.01).[53,54] The framework in **5** can be described as a 3,4,6-c net of the **3,4,6T2** topological type with point symbol $\{4^2.8^3.10\}_3\{4^3\}_2\{4^6.8^6.10^3\}$ (Figure 6).[55-57]
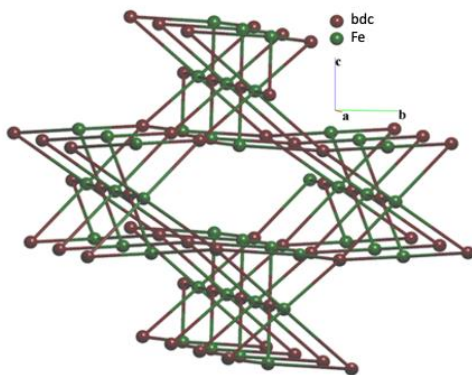
Figure 6: Representation of the 3D 3,4,6-c net of **3,4,6T2** topology in **5**.

1-5 are new coordination compounds resulting from the combination of 2-pyridinemethanol with a di- or tri- carboxylic ligand. In particular, **4** and **5** are

the first examples of MOFs that contain 2-pyridinemethanol; furthermore, **4** possesses a novel three dimensional 4,4,4-c net, whose topology has not appeared in the past in a MOF. **5** joins the relatively small but growing family of Fe MOFs; it is based on linear Fe3 SBU and is described as a 3,4,6-c net of 3,4,6T2 topology. The stability of **1-5** was confirmed by thermal TGA studies (**Figures S2-S5**). All the compounds are decomposed in multiple steps, as expected due to the presence of different ligands in their structures. In addition, the stability of the 3D MOFs **4**·DMF and **5** was investigated via pxrd studies (**Figures S6** and **S7**), which revealed that **4**·DMF retains its crystallinity and structure after its removal from the solution. This is not the case for **5**, which loses crystallinity, yielding a pxrd pattern of poor quality (**Figure S7**). The dimensionality and framework topology of **1-5** are affected by the type of the carboxylate ligand present in the structure and the protonation level of the alkoxy ligand; the latter impacts the coordination ability of the ligand with the anionic form being able to link more metal ions, hence yielding species with a different chemical formula and framework topology.

3.3. Magnetism studies

The magnetic properties of powdered and pressed samples of complex **5** were investigated in the 2-300 K temperature range under a field of 0.03 T and showed as $\chi_M T$ vs. T plots (**Figure 7**).

A large number of iron(II) systems with double carboxylate bridges can be found in the literature, in their majority related to the study of the reduced form of non-heme iron proteins where a variety of exchange couplings can be found depending on the specific geometry of each compound.[58-61] In contrast, linear

trinuclear Fe^{II}/carboxylate are scarce and the only systems with the same core as **5** (double syn-syn and one single O-carboxylate bridge between adjacent iron cations) were reported and magnetically studied by Lippard,[62,63] who established the magnetostructural correlations[62] and the strong zero field splitting that modulates its magnetic behaviour.[63]
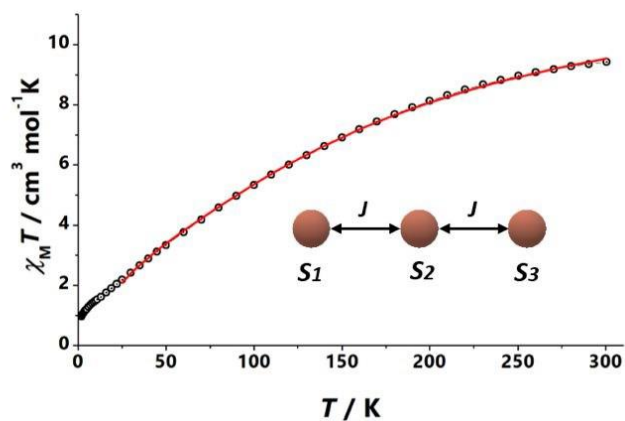
Figure 7: χ_MT vs. T plot for complex **5**. Solid line represents the obtained best fit up to 30 K. Inset, coupling scheme.

Following the magnetic studies of iron complexes mentioned above, we attempted to elucidate the superexhange interactions between the spin carriers in complex **5**; the magnetic coupling strongly depends on the Fe-O distance, where O is the dangling oxygen from the monobridging carboxylate, O5 in **Figure 5**. In particular, the interactions are ferromagnetic for weak Fe-O contacts, and antiferromagnetic when the Fe-O distance lies in the normal bond distance range.[62] Complex **5** belongs to a family of triiron(II) complexes which were

described by Lippard[63] as Class 3 complexes. In this class, the central Fe^{II} atom is located in the crystallographic inversion center, resulting in a linear disposition of the atoms and thus an antiferromagnetic response is expected.

Plot of the $\chi_M T$ vs. T is depicted in **Figure 7**. At room temperature, the $\chi_M T$ is in good agreement with the value for three isolated Fe^{II} cations S=2) and on lowering temperature there is a fully antiparallel spin alignment, yielding in antiferromagnetic coupling between them. The curve has been fitted using PHI software[64] with the spin Hamiltonian H= -2J ($S_1 \cdot S_2 + S_2 \cdot S_3$). By applying the isotropic Hamiltonian, the fit is far from satisfactory and thus a D term was included[65]; this yielded a very good fit in the 25-300 K range of temperature for the parameters J= -8.46(9) cm^{-1}, D = -25.2(4) cm^{-1} and g=2.419(5) which are consistent with similar Fe^{II} in these environment.[62,63,66] The low temperature data (<25 K) was not included in the fit because the weak interaction between trimeric units mediated by the terephthalate bridges requires to include another parameter (zJ') that is strongly correlated with D, resulting in a less reliable fit.[67-69]

3.4. Photoluminescence studies

The photoluminescence (PL) solid state emission spectra of **4**·DMF was recorded at room temperature. Upon excitation at 335 nm, **4**·DMF shows a maximum emission peak at 440 nm (**Figure 8**). The origin of the photoluminescence of **4**·DMF is likely coming from the simultaneous effect of a ligand to metal charge transfer (LMCT) and transitions from the intraligand emission excited state.[36, 70-72] The red shifted emission at 440 nm in **4**·DMF compared to that of the free H_2bdc ligand (410 nm), could be attributed to the rigid coordination environment of the metal in the polymeric network which suppresses the radiationless decay pathways from the intraligand emission excited state.[36,71]

The PL properties of **4**·DMF are in good agreement with the literature with previously reported bdc^{2-} -containing Zn^{2+} coordination polymers, displaying emission in the region of 440 nm upon excitation at 330 nm. [36, 70-72]
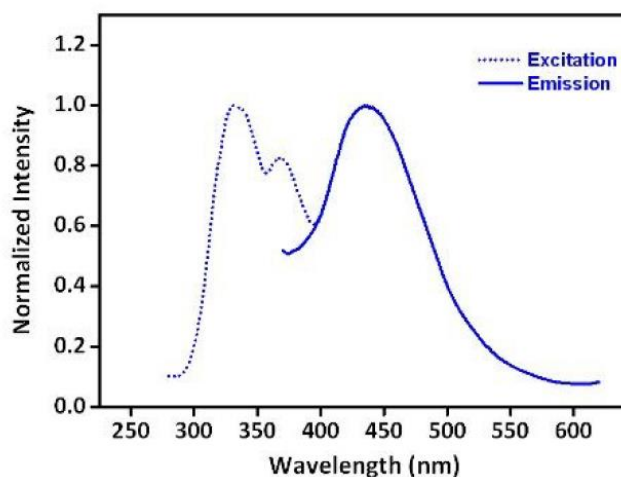
Figure 8: Excitation and PL emission spectrum of **4**·DMF.

4. Conclusions

The simultaneous use of 2-pyridinemethanol and trimesic or terephthalic acid has provided access to five new coordination compounds, which were isolated by the one-pot reaction of a metal source and the ligand blend at high temperature. It is worth to mention that two of the reported compounds, namely $[Zn_2(bdc)(hmp)_2]_n$ ·DMF (**4**·DMF) and $[Fe_3(bdc)_3(Hhmp)_2]_n$ (**5**), are the first MOFs bearing Hhmp in its neutral or ionic form. **4**·DMF is based on a dinucluear SBU and the topology of its 4,4,4-c net has never been reported in the field of MOFs. **5** is a new member of the family of Fe MOFs with its 3,4,6-c net being of a 3,4,6T2 topological type. Dc magnetic susceptibility studies in **5** revealed

antiferromagnetic coupling between the spin carriers in accordance with reported triiron(II) systems.

References

1. a) Schneemann, A.; Bon, V.; Schwedler, I.; Senkovska, I.; Kaskel S.; Fischer, A. R. *Chem. Soc. Rev*. **2014** 43, 6062. b) Furukawa, H.; Cordova, K. E.; O'Keeffe M.; Yaghi, O.M. *Science*, 2013, **341**, 1230444. c) Wang, Q.; Astruc, D. *Chem. Rev.* **2020** 120, 1438.

2. a). Zhou, H.-C. J.; Kitagawa, S. *Chem. Soc. Rev*. **2014** 43, 5415. b) Eddaoudi, M.; Moler, D. B.; Li, H.; Chen, B.; Reineke, T. M.; O'Keeffe, M.; Yaghi, O. M. *Acc. Chem. Res*. **2001** 34, 319. c) Yuan, S.; Feng, L.; Wang, K.; Pang, J.; Bosch, M.; Lollar, C.; Sun, Y.; Qin, J.; Yang, X.; Zhang, P.; Wang, Q.; Zou, L.; Zhang, Y.; Zhang, L.; Fang, Y.; Li , J.; Zhou, H.-C. *Adv. Mater*. **2018** 37, 1704303.

3. a) Horcajada, P.; Chalati, T.; Serre, C.; Gillet, B.; Sebrie, C.; Baati, T.; Eubank, J. F.; Heurtaux, D.; Clayette, P.; Kreuz, C.; Chang, J.-S.; Hwang, Y. K.; Marsaud, V.; Bories, P.-N.; Cynober, L.; Gil, S.; Ferey, G.; Couvreur, P.; Gref, R.   *Nat Mater* **2010** 9, 172. b)   Kumar, P.; Deep, A.; Kim, K.-H. *TrAC Trends Anal. Chem.* **2015** 73, 39.

4. a) Lee, J.; Farha, O. K.; Roberts, J.; Scheidt, K. A.; Nguyen, S. T.; Hupp, J. T. *Chem. Soc. Rev.* **2009** 38, 1450. b) Kurmoo, M. *Chem. Soc. Rev.* **2009** 38, 1353.

5. a) Rosi, N. L.; Eckert, J.; Eddaoudi, M.; Vodak, D. T.; Kim, J.; O'Keeffe, M.; Yaghi, O. *Science* **2003** 300, 1127. b) Horcajada, P.; Serre, C.; Vallet-

Regí, M.; Sebban, M.; Taulelle, F.; Férey, G. *Angew. Chemie Int. Ed*. **2006** 45, 5974.

6. Nouar, F.; Devic, T. ; Chevreau, H.; Guillou, N. ; Gibson, E.; Clet, G. ; Daturi, M. ; Vimont, A.; Grenèche, J. M. ; Breeze, M. I. ; Walton, R. I.; Llewellyne, P. L. ; Serre, C. *Chem. Commun*. **2012** 48, 10237.

7. Alhamami, M.; Doan, H.; Cheng, C.-H. *Materials* **2014** 7, 3198.

8. Kuznetsova, A.; Matveevskaya, V.; Pavlov, D.; Yakunenkov, A.; Potapov, A. *Materials* **2020** 13, 2699.

9. Wu, M.-X.; Yang, Y.-W. *Adv. Mater*., 2017, **29**, 1606134.

10. Huxford, R. C.; Rocca, J. D.; Lin, W. *Curr. Opin. Chem. Biol.* **2010** 14(2), 262.

11. Ma, L.; Falkowski, J. M.; Abney, C.; Lin, W. *Nat. Chem*. **2010** 2, 838.

12. Douvali, A.; Tsipis, A. C.; Eliseeva, S. V. ; Petoud, S. ; Papaefstathiou, G. S.; Malliakas, C. D. ; Papadas, I. ; Armatas, G. S. ; Margiolaki, I.; Kanatzidis, M. G. ; Lazarides, T.; Manos, M. J. *Angew. Chem., Int. Ed*. **2015** 54, 1651.

13. Qin, J.-S.; Du, D.-Y.; Guan, W.; Bo, X.-J.; Li, Y.-F.; Guo, L.-P.; Su, Z.-M.; Wang, Y.-Y.; Lan, Y.-Q.; Zhou, H.-C. *J. Am. Chem. Soc*. **2015** 137, 7169.

14. Chen, L.; Zhang, X.; Cheng, X.; Xie, Z.; Kuang, Q.; Zheng, L. *Nanoscale Adv*. **2020** 2, 2628.

15. Cao, J.; Li, X.; Tian, H. *Curr. Med. Chem.* **2020** 27(35), 5949.

16. Kou, W.-T.; Yang, C.-X.; Yan, X.-P. *J. Mater. Chem. A*. **2018** 6, 17861.

17. Wang, Z.; Li, Z.; Ng, M.; Milner, P. J. *Dalton Trans.* **2020** 49, 16238.

18. Klinowski, J.; Almeida Paz, F. A.; Silva, P.; Rocha, J. *Dalton Trans*. **2011** 40, 321.

19. Vinu, M.; Lin, W.-C. ; Senthil Raja, D. ; Han, J.-L.; Lin, C.-H. *Polymers* **2017** 9, 498.

20. Garibay, S. J.; Cohen, S. M. *Chem. Commun*. **2010** 46, 7700.

21. Yaghi, O. M.; O'Keeffe, M.; Ockwig, N. W.; Chae, H. K.; Eddaoudi, M.; Kim, J. *Nature* **2003** 423, 705.

22. Ardila-Suárez, C.; Díaz-Lasprilla, A. M.; Díaz-Vaca, L. A.; Balbuena, P. B.; Baldovino-Medrano, V. G.; Ramírez-Caballero, G. E. *Cryst. Eng. Comm.* **2019** 21, 3014.

23. Chen, D.; Zhao, J.; Zhang, P.; Dai, S. *Polyhedron* **2019** 162, 59.

24. Mai, Z.; Liu, D. *Cryst. Growth Des*. **2019** 19, 7439.

25. Horcajada, P.; Surblé, S. ; Serre, C.; Hong, D.-Y. ; Seo, Y.-K.; Chang, J.-S.; Grenèche, J.-M.; Margiolaki, I.; Férey, G. *Chem. Commun*. **2007** 2820.

26. Kourtellaris, A.; Moushi, E. E.; Spanopoulos, I.; Tampaxis, C.; Charalambopoulou, G.; Steriotis, T. A.; Papaefstathiou, G. S.; Trikalitis, P. N.; Tasiopoulos, A. J. *Inorg. Chem. Front*. **2016** 3, 1527.

27. Moushi, E. E. ; Kourtellaris, A.; Spanopoulos, I.; Manos, M. J. ; Papaefstathiou, G. S.; Trikalitis, P. N. ; Tasiopoulos, A. J. *Cryst. Growth Des*. **2015** 15, 185.

28. Manos, M. J.; Moushi, E. E.; Papaefstathiou, G. S.; Tasiopoulos, A. J. *Cryst. Growth Des*. **2012** 12(11), 5471.

29. Clausen, H. F.; Poulsen, R. D.; Bond, A. D.; Chevallier, M.-A. S.; Iversen, B. B. *Journal of Solid State* **2005** 178, 3342.

30. Chen, Z.; Adil, K.; Weselinski, L. J.; Belmabkhout, Y.; Eddaoudi, M. *J. Mater. Chem. A* **2015** 3, 6276.

31. Tranchemontagne, D. J.; Hunt, J. R. ; Yaghi, O. M. *Tetrahedron* **2008** 64, 8553.

32. Li, H.; Eddaoudi, M.; O'Keeffe, M.; Yaghi, O. M. *Nature* **1999** 402, 276.

33. Sapchenko, S. A.; Dybtsev, D. N.; Damsonenko, D. G.; Fedin, V. *New J. Chem.*, **2010** 34, 2445.

34. Zhao, X.-L.; Sun, W.-Y. *Cryst. Eng. Comm.* **2014** 16, 3247.

35. Guesh, K.; Caiuby, C. A. D.; Mayoral, Á.; Díaz-García, M.; Díaz, I.; Sanchez-Sanchez, M. *Growth Des*. **2017** 17(4), 1806.

36. Mylonas-Margaritis, I.; Winterlich, M.; Efthymiou, C. G.; Lazarides, T.; McArdle, P.; Papatriantafyllopoulou, C. *Polyhedron* **2018** 151, 360.

37. Mylonas-Margaritis, I.; Gerard, A.; Skordi, K.; Mayans, J.; Tasiopoulos, A.; McArdle, P.; Papatriantafyllopoulou, C. *Materials* **2020** 4084.

38. Mylonas-Margaritis, I.; Mayans, J.; McArdle, P.; Papatriantafyllopoulou, C. *Molecules* **2021** 26, 491.

39. For a comprehensive review, see: Milios, C. J.; Stamatatos, T.; Perlepes, S. P. *Polyhedron* **2006** 25, 134.

40. Abbasi, P.; Quinn, K.; Alexandropoulos, D. I.; Damjanović, M.; Wernsdorfer, W.; Escuer, A.; Mayans, J.; Pilkington M.; Stamatatos, T. C. *J. Am. Chem. Soc*. **2017** 139, 15644.

41. Wang, H.-S.; Chen, Y.; Hu, Z.-B.; Zhang, K.; Zhang, Z.; Song, Y.; Pan, Z.-Q. *New J. Chem*. **2020** 44, 16302.

42. Papatriantafyllopoulou, C.; Abboud, K. A.; Christou, G. *Inorg. Chem*. **2011** 50, 8959.

43. Hooper, T. N.; Schnack, J.; Piligkos, S.; Evangelisti, M.; Brechin, E. K. *Angew. Chem. Int. Ed*. **2012** 51, 4633.

44. Murugesu, M.; Takahashi, S.; Wilson, A.; Abboud, K. A.; Wernsdorfer, W.; Hill, S.; Christou, G. *Inorg. Chem*. **2008** 47, 4095.

45. Roubeau, O.; Clerac, R. *Eur. J. Inorg. Chem.* **2008** 4325.

46. Moushi, E. E.; Kourtellaris, A.; Andreou, E.; Fidelli, A.; Papaefstathiou, G. S.; Plakatouras, J.; Tasiopoulos, A. J. *Cryst. Eng. Comm*. **2020** 22, 2083.

47. Kyprianidou, E. J.; Lazarides, T.; Kaziannis, S.; Kosmidis, C.; Itskos, G.; Manos, M. J.; Tasiopoulos, A. J. *J. Mater. Chem. A* **2014** 2, 5258.

48. Sheldrick, G. M. *Acta Crystallogr., Sect. A: Found. Adv*. **2015** 71, 3.

49. McArdle, P.; Gilligan, K.; Cunningham, D.; Dark, R.; Mahon, M. A. *Cryst. Eng.Comm*. **2004** 6, 303.

50. Blatov, V. A.; Shevchenko, A. P.; Proserpio, D. M. *Cryst. Growth Des*. **2014** 14, 3576.

51. O'Keeffe, M.; Peskov, M. A.; Ramsden, S. J.; Yaghi, O. M. *Acc. Chem. Res*. **2008** 41, 1782.

52. Alexandrov, E. V.; Blatov, V. A.; Kochetkov, A. V.; Proserpio, D. M. *Cryst. Eng. Comm.* **2011** 13, 3947.

53. Liu, W.; Thorp, H.-H. *Inorg. Chem*. **1993** 32, 4102.

54. Brown, I. D.; Altermatt, D. *Acta Crystallogr., Sect. B: Struct. Sci.* **1985** 244, 2.

55. Davies, R. P.; Less, R. J.; Lickiss, P.; White, A. J. P. *Dalton Trans.* **2007** 4, 2528.

56. Wang, X.-F.; Zhang, Y.-B.; Zhang, W.-X.; Xue, W.; Zhou, H.-L.; Chen, X.-M. *Cryst. Eng. Comm.*, 2011, **13**, 4196.

57. a) Kongshaug, K. O.; Fjellvag, H. *Solid State Sci.*, 2003, **5**, 303. b) Rood, J. A.; Noll, B. C.; Henderson, K. W. *Main Group Chem.* **2006** 5, 21.

58. Hartman, J. R.; Rardin, R. L.; Chaudhuri, P.; Pohl, K.; Wieghart, K.; Nuber, B.; Weiss. J.; Papaefthymiou, G. C.; Frankel, R. B.; Lippard, S. J. *J. Am. Chem. Soc.* **1987** 109, 7387.

59. Hagen, K. S.; Lachicotte. R. *J. Am. Chem. Soc.* **1992** 114, 8741.

60. Ménage, S. ; Brennan, B. A. ; Juarez-Garcia, C.; Münck, E.; Que, L. *Jr. Inorg. Chem.,* **1993** 112, 6423.

61. Borovick, A. S.; Hendrich, M. P.; Holman, T. R.; Münck, E.; Papaefthymiou, V.; Que, L. *Jr. J. Am. Chem. Soc.* **1990** 112, 6031.

62. Goldberg, D. P. ; Tesler, J. ; Bastos, C. M.; Lippard, S. J. *Inorg. Chem.* **1995** 34, 3011.

63. Reisne, E.; Tesler, J.; Lippard, S. J. *Inorg. Chem.* **2007** 46, 10754.

64. Chilton, N. F.; Anderson, R. P.; Turner, L. D.; Soncini, A.; Murray, K. S. *J. Comput. Chem.* **2013** 34, 1164.

65. Rardin, R. L.; Poganiuch, P.; Bino, A.; Goldberg, D. P.; Tolman, W. B.; Liu, S.; Lippard. S. J. *J. Am. Chem. Soc.* **1992** 114, 5240.

66. Boča, R. *Coord. Chem. Rev.* **2004** 248, 757.

67. Cano, J.; De Munno, G.; Sanz, J. L.; Ruiz, R.; Faus, J.; Lloret, F.; Julve, M.; Canneschi, A. *J. Chem. Soc., Dalton Trans*. **1997** 1915.

68. Choubey, S.; Roy, S.; Bhar, K.; Ghosh, R.; Mitra, P.; Lin, C.-H.; Ribas, J.; Ghosh, B. K. *Polyhedron* **2013** 55, 1.

69. Choubey, S.; Chattopadhayay, S.; Bhar, K.; Roy, S.; Khan, S.; Ribas, J.; Ghosh, B. K. *J. Chem. Sci*. **2014** 126, 1685.

70. Sapchenko, S. A.; Dybtsev, D. N.; Damsonenko, D. G.; Fedin, V. P. *New J. Chem*., **2010** 34, 2445.

71. Konidaris, K. F.; Bekiari, V.; Katsoulakou, E.; Raptopoulou, C. P. ; Psycharis, V.; Perlepes, S. P.; Stamatatos, T. C.; Manessi- Zoupa, E. *Inorg. Chim. Acta* **2011** 376, 470.

72. Yang, X.; Yan, D. *Chem. Sci.* **2016** 7, 4519.

Table S1. Selected interatomic distances (Å) and angles (°) for **1**.

Bonds			
Co1-N1	2.115	Co1-O1	2.168
Co1-O2	2.043		
Angles			
N1-Co1-O2	96.5(1)	N1-Co1-O1	90.2(4)
N1-Co1-O1	77.1(2)	N1-Co1-O2	95.7(5)

Table S2. Selected interatomic distances (Å) and angles (°) for **2**.

Bonds			
Ni1-O1	2.104	Ni1-O2	2.040
Ni1-N1	2.058		
Angles			
O1-Ni1-O2	92.91	O2-Ni1-O2	86.78
O1-Ni1-N1	79.82	O2-Ni1-N1	94.50
O1-Ni1-O1	87.97	O2-Ni1-N1	95.15
O1-Ni1-N1	90.58		

Table S3. Selected interatomic distances (Å) and angles (°) for **3**.

Bonds			
Ni1-O2	2.058	Ni1-N1	2.052
Ni1-O1	2.085		

Angles			
O1-Ni1-O2	92.48	N1-Ni1-O2	92.88
O2-Ni1-O1	87.52	N1-Ni1-O1	99.75
N1-Ni1-O1	80.25	N1-Ni1-O2	87.12

Table S4. Selected interatomic distances (Å) and angles (°) for **4**.

Bonds			
Zn1 - N2	2.130(3)	Zn2 - O5	1.957(5)
Zn1 - O6	2.010(5)	Zn2 - O1	1.906(4)
Zn1 - O3	2.137(3)	Zn2 - O6	1.915(4)
Zn1 - O1	2.012(4)	Zn2 - O2	1.960(5)
Zn1 - O4	2.149(3)		

Angles			
O4-Zn1-O1	92.8(2)	N2-Zn1-O4	89.8(1)
O4-Zn1-O6	92.1(1)	O2-Zn2-O5	103.6(2)
O6-Zn1-O1	173.0(2)	O5-Zn2-O1	112.4(2)
O3-Zn1-O6	93.8(2)	O1-Zn2-O6	116.7(2)
O3-Zn1-O4	91.6(1)	O6-Zn2-O2	111.8(2)
O3-Zn1-O1	91.0(2)	O2-Zn2-O1	107.8(2)
N2-Zn1-O6	78.5(2)	O5-Zn2-O6	103.9(2)
N2-Zn1-O1	96.6(2)		

Table S5. Selected interatomic distances (Å) and angles (°) for **5**.

Bonds

Fe1-O6	2.149(4)	Fe2-O2	2.089(0)
Fe1-O1	2.073(3)	Fe2-O3	1.969(9)
Fe1-O4	2.187(7)	Fe2-O6	2.321(9)
Fe2-O7	2.314(6)	Fe2-O5	2.121(2)
Fe2-N1	2.166(8)		

Angles

O6-Fe1-O4	92.23	O3-Fe2-O5	158.72
O6-Fe1-O4	87.07	O2-Fe2-O6	99.08
O6-Fe1-O1	89.64	O2-Fe2-N1	98.15
O6-Fe1-O1	90.36	O2-Fe2-O5	96.99
O4-Fe1-O1	90.46	N1-Fe2-O5	87.62
O4-Fe1-O1	89.54	N1-Fe2-O7	76.92
O3-Fe2-O6	100.74	O5-Fe2-O7	87.32
O3-Fe2-O2	85.88	O7-Fe2-O6	87.48
O3-Fe2-N1	112.94	O6-Fe2-O2	99.08
O3-Fe2-O7	91.93		
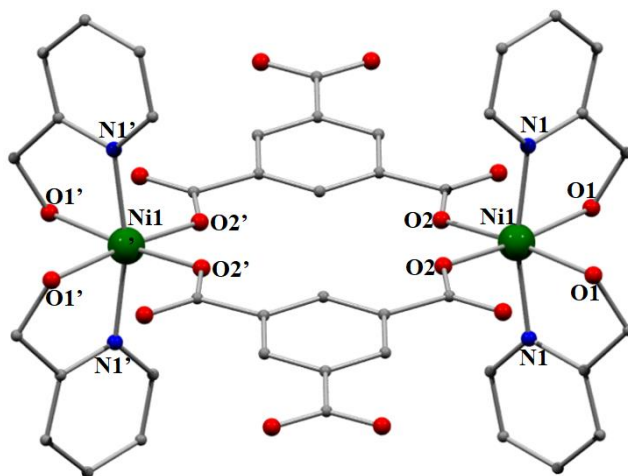
Figure S1. Representation of the molecular structure of **2**·DMF. Color code: Ni^{II}, purple; N, navy blue; O, red; C, grey. The hydrogen atoms and the solvate molecules are omitted for clarity.
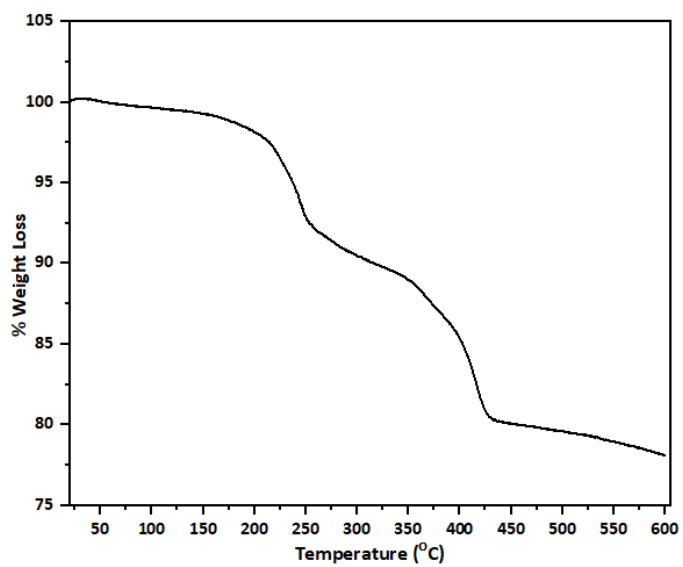
Figure S2. The TGA diagram for **1**.
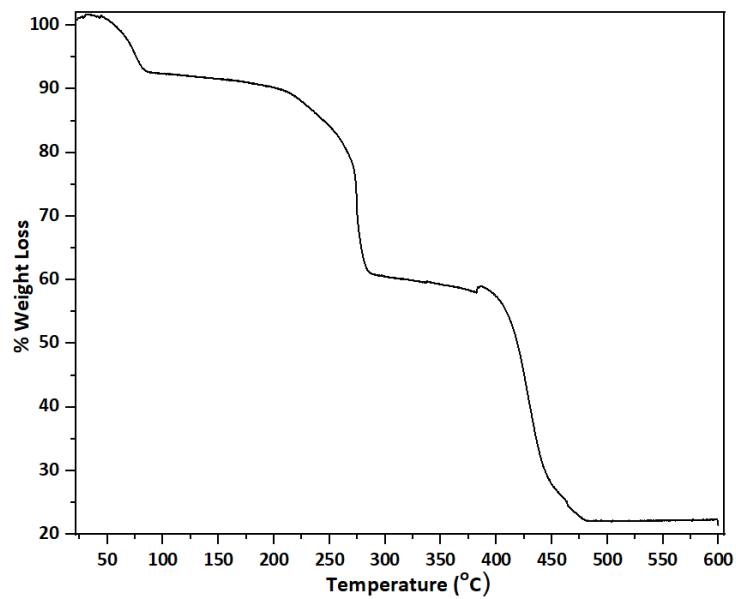
Figure S3. The TGA diagram for **3**.
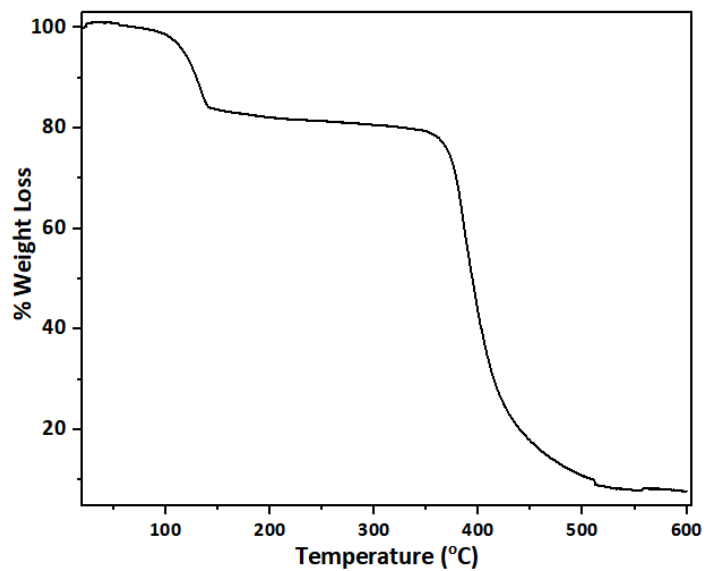
Figure S4. The TGA diagram for **4**·DMF.
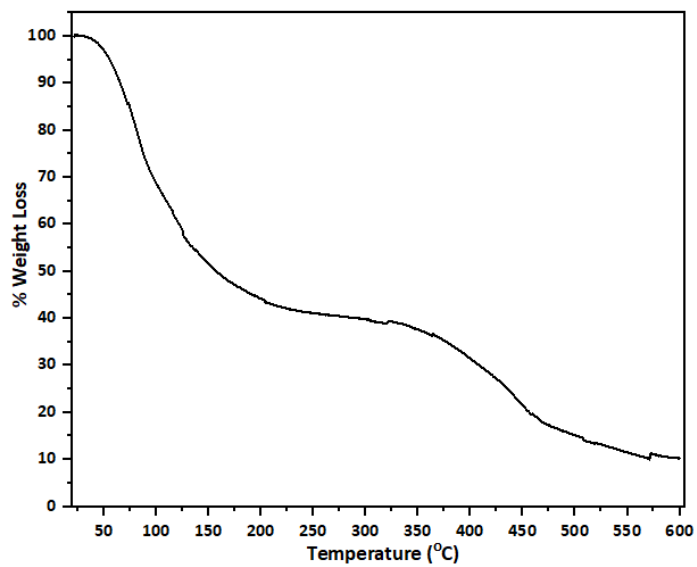
Figure S5. The TGA diagram for **5**.
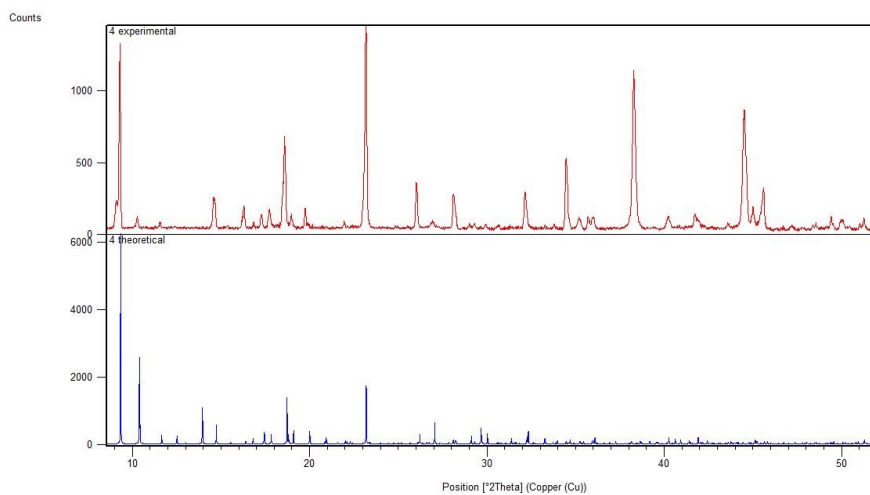
Figure S6. Comparison of the powder patterns for **4**·DMF (theoretical, blue; experimental , red).
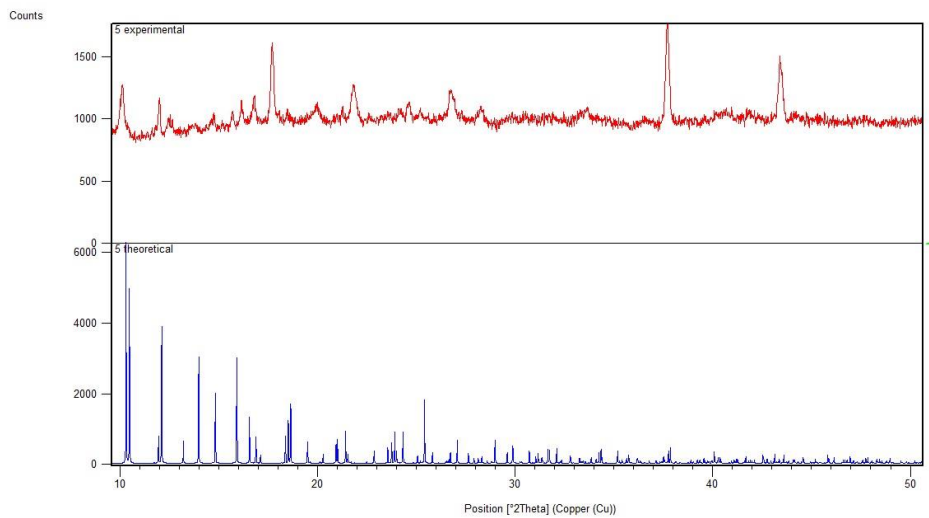
Figure S7. Comparison of the powder patterns for **5** (theoretical, blue; experimental, red).

2.5 Brief description of the paper (manuscript in preparation)

In this article is described the synthesis and characterization of three novel MOFs and a mononuclear complex, by the simultaneous use of the 2,6-pyridinedimethanol and terephthalic acid.

Metal-organic frameworks by the simultaneous use of 2,6-pyridinedimethanol & terephthalate

Abstract

The employment of two different ligands is an alternative approach for the synthesis of new MOFs with enhanced properties. Pyridine-alcohols are broadly studied in the field of single-molecule magnets (SMMs) and they have given compounds that exhibit interesting magnetic properties and topologies. This work is introducing for the first time the combination of 2,6-pyridinedimethanol (H_2pdm) with 1,4-benzene dicarboxylic acid (H_2bdc) in the field of metal-organic frameworks (MOFs). This reaction system provided access to new metal-organic frameworks $[M_3(bdc)_2(Hpdm)_2]_n \cdot DMF$ (where M^{II} = Zn(**1**·DMF), Mn(**2**·DMF)), $[Mn_3(bdc)_3(H_2pdm)_2]_n$ **3**, and $[Mn_3(bdc)_3(DMF)_4]_n$ **4**. The synthesis and crystal structure characterization are discussed in detail.

1. Introduction

MOFs are hybrid porous materials, which are consisted of inorganic and organic secondary building units (sbus). In the last decade, a plethora of scientific groups are working in the isolation of MOFs through the mixed-ligand approach, which demands the control of different parameters. Once the linkers have different

chemical nature, the one-pot-synthetic approach for the solvothermal synthesis is arising issues e.g. solubility, fast precipitation of the synthesized compounds, and also crystallinity. For the aforementioned reasons, new approaches and protocols have to be developed based on the under study system.

Recently, an increasing number of research groups are investigating mixed ligand systems for the formation of new classes of metal-organic frameworks (MOFs).[1] The majority of the published and studied compounds are presenting mixed-ligand pillars for the formation of MOFs with interesting porosity, in an effort to isolate compounds with high surface areas for the adsorption of molecules.[2,3]

Despite the fact that several ligand combinations have been investigated, reports that include the use of mixed ligand systems with the capacity to provide access to MOFs with high nuclearity SBUs are limited. Oximes and pyridine-alcohols belong to this category of ligands; they have high bridging capability and as such have been extensively studied for the formation of low and high nuclearity metal complexes, which exhibit interesting structural features and physical properties. Nevertheless, their use for the synthesis of MOFs has not been systematically investigated.

Our group has been investigating the simultaneous use of oximes and di-, tri- ,and tetra- topic carboxylates (benzene-1,4-dicarboxylic acid, benzene-1,3,5-tricarboxylic acid and 1,2,4,5-benzene tetracarboxylic acid); this reaction system has led to the formation of metal complexes, one-dimensional polymers, and 2D & 3D MOFs.[4] A representative such example is $[Cu_4(OH)_2(pma)(mpkoH)_2(DMF)_2]_n$, which exhibits promising magnetic sensing properties for the selective adsorption of Fe^{III}. Furthermore, the use of pyridine-methanol and combining it with di- and tri- topic carboxylates (benzene-1,4-

dicarboxylic acid was benzene-1,3,5-tricarboxylic acid), provided access to the formation of the first metal complexes and 3D-MOFs.[5] An expansion of this project involves the use of ligands with more than one bridging alkoxy groups and the investigation of how this affects the identity of the isolated products and for this reason 2,6-pyridine-dimethanol (H_2pdm) was employed instead of 2-pyridine-methanol; H_2pdm has been broadly used in the field of single molecule magnets (SMMs), giving high nuclearity metal complexes with interesting magnetic properties e.g. $[Ln^{III}_4(NO_3)_2(pdmH)_6(pdmH_2)_2](NO_3)_4$ ($Ln^{III} = Eu^{III}$, Gd^{III}, Tb^{III}, Dy^{III}, Ho^{III}, Er^{III}, Yb^{III}); $[Fe_{18}O_6(OH)_8(pdm)_{10}(pdmH)_4(H_2O)_4](ClO_4)_{10}$; $\{[Cu_3(O_2CMe)_2(pdm)_2(MeOH)_2][Cu_4(O_2CMe)_2(Hpdm)_4]\}(ClO_4)_2 \cdot 4MeOH$.[6]

Herein, we report on the synthesis, structural characterization and physical properties of four new species including the first MOFs bearing 2,6-pyridinedimethanol (H_2pdm), by the use of H_2pdm in combination with terephthalic acid (H_2bdc). This combination led to the formation of two iso-structural two-dimensional metal-organic frameworks $[M_3(bdc)_2(Hpdm)_2]_n \cdot DMF$ (where M^{II} = Zn(**1**·DMF), Mn(**2**·DMF)), one three-dimensional metal-organic framework $[Mn_3(bdc)_3(H_2pdm)_2]_n$ **3**, and a mononuclear complex $[Ni(H_2pdm)_2](bdc)$ **5**.

H₂pdm   **H₂bdc**
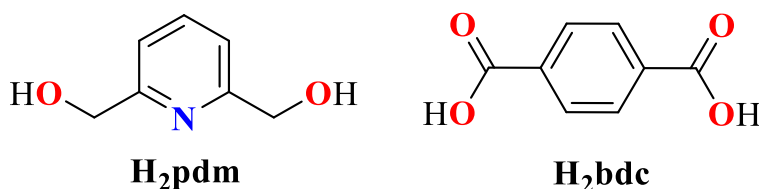
Scheme 1. Schematic representation of the 2,6-pyridinedimethanol (H_2pdm) (left) and the terephthalic acid (H_2bdc) (right) discussed in this work.

2. Materials and Methods

2.1. Materials, Physical and Spectroscopic Measurements

All the manipulations were performed under aerobic conditions using materials (reagent grade) and solvents as received. Warning: Perchlorate salts are potentially explosive; such compounds should be used in small quantities and treated with utmost care at all times.

Elemental analysis (C, H and N) was performed by the in-house facilities of National University of Ireland Galway, School of Chemistry. IR spectra (4000-400 cm^{-1}) were recorded on a Perking-Elmer Spectrum 400 FT-IR spectrometer. Powder X-ray diffraction data (pxrd) were collected using an Inex Equinoz 6000 diffractometer. Solid TGA experiments were performed on a STA625 thermal analyser from Rheometric Scientific (Piscataway, New Jersey). The heating rate was kept constant at 10°C/min, and all runs were carried out between 20 and 600 ^{o}C. Thea measurements were made in open aluminium crucibles, nitrogen was purged in ambient mode and calibration was performed using an indium standard.

2.2. Compounds Synthesis

*2.2.1. Synthesis of [Zn$_3$(bdc)$_2$(Hpdm)$_2$]$_n$·DMF (**1**·DMF)*

Zn(ClO$_4$)$_2$·6H$_2$O (0.075g, 0.2mmol) and H$_2$pdm (0.014g, 0.1 mmol) were dissolved in DMF (5ml). The resultant solution was put in the oven and heated at 100°C for 1h. H$_2$bdc (0.0166g, 0.1mmol) was then added and the vial was placed into the oven for 24h, after which X-ray quality pale yellow crystals of

1·DMF were formed. The crystals were collected by filtration, washed with cold MeCN (2ml) and Et_2O (2 x 5mL) and dried in air. Yield 23%. Anal. Calc. for 1: C, 44.38; H, 2.74; N, 2.72. Found: C, 44.28; H, 2.69; N, 2.64%. IR data (cm^{-1}) = 1655s, 1501w, 1439w, 1386s, 1255m, 1160w, 1093s, 1061w, 822w, 798w, 748m, 659s.

2.2.2. Synthesis of [Mn₃(bdc)₂(Hpdm)₂]ₙ·DMF (2·DMF)

This was prepared in the same manner as **1** but using $Mn(ClO_4)_2 \cdot 6H_2O$ (0.0508g, 0.14mmol) instead of $Zn(ClO_4)_2 \cdot H_2O$. Yield 23%. Anal. Calc. for **2**: C, 45.78; H, 2.83; N, 2.81. Found: C, 45.68; H, 2.78; N, 2.73%. IR data (cm^{-1}) = 1653s, 1497w, 1439w, 1386s, 1255m, 1092s, 1063w, 750w, 659s.

2.2.3. Synthesis of [Mn₃(bdc)₃(H₂pdm)₂]ₙ (3)

$Mn(ClO_4)_2 \cdot H_2O$ (0.051g, 0.14mmol), H_2pdm (0.223g, 1.6 mmol) and Et_3N (416 μl, 3.2mmol) were dissolved in a mixture of DMF/H_2O (25ml/ 25ml). The resultant solution was put in the oven and heated at 130°C for 1h. Then, H_2bdc (0.0166g, 0.1mmol) was added and the vial was placed into the oven for 24h, after which X-ray quality colorless crystals of **3** were formed. The crystals were collected by filtration, washed with cold MeCN (2ml) and Et_2O (2 x 5mL) and dried in air. Yield 23%. Anal. Calc. for **3**: C, 45.69; H, 3.03; N, 2.80. Found: C, 45.59; H, 2.98; N, 2.72%. IR data (cm^{-1}) = 2825m, 1567s, 1470m, 1458m, 1440m, 1343s, 1254w, 1095w, 1024m, 789s, 662w.

2.2.4. Synthesis of {[Mn₃(bdc)₃(DMF)₄]}ₙ (4)

$Mn(ClO_4)_2 \cdot 6H_2O$ (0.0508g, 0.14mmol) and H_2bdc (0.0166g, 0.1mmol) were dissolved in a mixture of DMF (5ml) was put in the oven and heated at 100ºC for 24h, after which X-ray quality colorless crystals of **5** were formed. The crystals were collected by filtration, washed with cold MeCN (2ml) and Et_2O (2 x 5mL) and dried in air. Yield 23%. Anal. Calc. for **5**: C, 42.68; H, 3.98; N, 5.53. Found: C, 42.58; H, 3.93; N, 5.45%. IR data (cm^{-1}) = 1640m, 1612w, 1582w, 1551m, 1499m, 1435w, 1369s, 1293w, 1252w, 843m, 815m, 749s, 663m.

2.3. Single Crystal Xray Crystallography

Single Crystal diffraction for **1**-**5** were collected in an Oxford Diffraction Xcalibur CCD diffractometer using graphite-monochromatic Mo Ka radiation (λ = 0.71073 Å) at room temperature. The structures were solved using SHELXT, embedded in the OSCAIL software. The non-H atoms were treated anisotropically, whereas the hydrogen atoms were placed in calculated, ideal positions and refined as riding on their respective carbon atoms. Molecular graphics were produced with DIAMOND.

Unit cell data and structure refinement details are listed in **Table 1**.

Table 1. Crystallographic data for complexes **1-3**.

Complex	1	2	3

Empirical formula	$C_{30}H_{16}N_2O_{12}Zn_3$, $C_6H_{11}N_2O_2$	$C_{30}H_{16}Mn_3N_2O_{12}$, $2(C_3H_7NO)$	$C_{38}H_{30}Mn_3N_2O_{16}$
Formula weight	935.79	907.46	935.46
Crystal system	Monoclinic	Monoclinic	Monoclinic
Space group	P 21/n	P 21/n	P 21/n
a (Å)	14.8513(9)	14.8480(5)	10.4343(3)
b (Å)	8.4497(4)	8.4497(3)	16.7883(5)
c (Å)	16.5769(11)	16.5953(7)	10.6385(4)
α (°)	90	90	90
β (°)	105.100(6)	105.152(4)	95.378(3)
γ (°)	90	90	90
V (Å^3)	2008.4(2)	2009.68(14)	1855.39(10)
Z	2	2	2
ρcalc (g cm^{-3})	1.547	1.5	1.674
Radiation, λ (Å)	0.71073	0.71073	0.71073
μ (mm^{-1})	1.847	0.998	1.086
Temperature (K)	300 K	299 K	293 K
R_1[a] ($I > 2\sigma(I)$)	0.0477(3441)	0.0615(3408)	0.0341(3201)
wR_2[b] ($I > 2\sigma(I)$)	0.1345(4688)	0.2014(4841)	0.0809(4458)

3. Results and Discussion

3.1 Synthetic Discussion

Several experiments were performed and the effect of the synthetic parameters (temperature, presence/absence of base, metal ratio of reactants, metal sources etc.) was thoroughly studied. By the reaction of $Zn(ClO_4)_2 \cdot 6H_2O$ (**1**) or $Mn(ClO_4)_2 \cdot 6H_2O$ (**2**) with H_2pdm and H_2bdc in a molar ratio 2: 1: 1 at 100°C, crystals of the 2D MOFs $[M_3(bdc)_2(Hpdm)_2]_n$ (M^{II} = Zn (**1**), Mn(**2**)) were isolated in good yield. The stoichiometric equation of the reaction that led to the formation of **1** and **2** is represented in Eq. (1).

$$3\ M(ClO_4)_2 \cdot 6H_2O + 2\ H_2pdm + 2\ H_2bdc + DMF \xrightarrow{DMF}$$
$$[M_3(bdc)_2(Hpdm)_2]_n \cdot DMF\ + 6\ HClO_4 + 18\ H_2O\ (1)$$
$$\mathbf{1} \cdot DMF$$
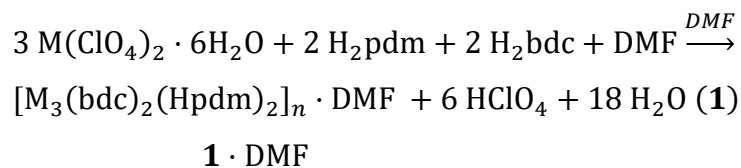
$$\text{where } M^{II} = Zn(\mathbf{1}), Mn(\mathbf{2})$$

The temperature and the presence of a base in the reaction mixture, as well as the nature of the solvents plays a crucial role in the identity of the isolated product. Hence, the reaction of $Mn(ClO_4)_2 \cdot 6H_2O$, Et_3N, H_2pdm and H_2bdc in a molar ratio 0.14: 1.6: 3.2: 0.1 in DMF/H_2O (25ml/25ml) has provided access to **3** in good yield. The stoichiometric equation of the reaction that led to the formation of **3** is represented in Eq. (2).

$$3\ Mn(ClO_4)_2 \cdot 6H_2O + 2\ H_2pdm + 3\ H_2bdc \xrightarrow{DMF/H_2O}$$

$$\{[Mn_3(bdc)_3(H_2pdm)_2]\}_n + 6\ HClO_4 + 18\ H_2O\ (\mathbf{2})$$
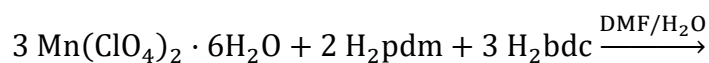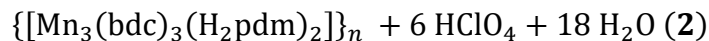
<div align="center">**3**</div>

It is worth mentioning that the reaction that led to the formation of **1**-**3** involve two steps with the first step being a reaction between the metal salt and pdmH$_2$; this results in the formation of a reaction intermediate which then reacts with H$_2$bdc favouring the formation of the products. One step reactions have been also attempted, which led to either precipitates that could not been further characterized or to know compounds. In particular, in the case of Mn the one step reaction yielded the 3D MOF [Mn$_3$(bdc)$_3$(DMF)$_4$]$_n$ (**4**), which has been previously reported in the literature.

Following a similar synthetic approach to the one yielded **1,2** and **3**, but by using Ni^{II},a discrete metal compound was isolated instead of a coordination polymer. Thus, the reaction of 0.2 Ni(ClO$_4$)$_2$6H$_2$O: 1.6 H$_2$pdm: 3.2 Et$_3$N: 0.1 H$_2$bdc yielded xray quality crystals of **5**. The stoichiometric equation for the formation of **5** is shown in Eq. (3).

$$3\ Mn(ClO_4)_2 \cdot 6H_2O + 3\ H_2pdm + 4\ DMF \xrightarrow{DMF}$$
$$\{[Mn_3(bdc)_3(DMF)_4]\}_n + 6\ HClO_4 + 18\ H_2O\ (\mathbf{3})$$
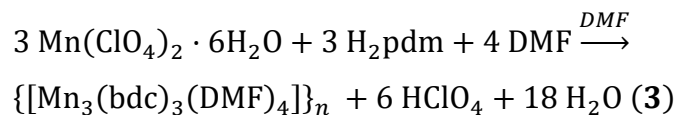
<div align="center">**4**</div>

Following, a similar synthetic approach to the one yielded **1,2** and **3**, but by using Ni^{II}, at 130°C was isolated **5**. At 100°C was not visible the isolation of a crystalline compound either in DMF or in a mixture of DMF/water; for this

reason the temperature was increased to 130°C. Either in the presence or absence of DMF were isolated solids or jells, but once the mixture of water/DMF was used the reaction system changed behavior mixtures of crystals and solid or multicrystalline or sfairoid samples were isolated. Only in a ratio of 0.2 $Ni(ClO_4)_2 6H_2O$: 1.6 H_2pdm: 3.2 Et_3N: 0.1 H_2bdc was possible the isolation of **5** in crystalline form. The stoichiometric quation for the formation of **5** is Eq. (4).
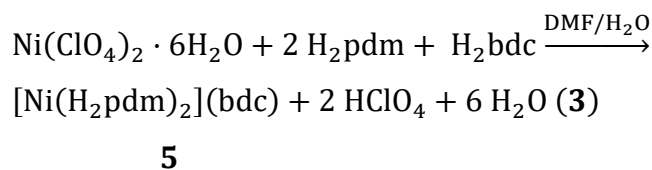
$$Ni(ClO_4)_2 \cdot 6H_2O + 2\,H_2pdm + \,H_2bdc \xrightarrow{DMF/H_2O}$$
$$[Ni(H_2pdm)_2](bdc) + 2\,HClO_4 + 6\,H_2O\;(\mathbf{3})$$
$$\mathbf{5}$$

3.2. Description of Structures

Representations of the molecular structures of **1**-**5** are shown in Figures 1-5. Selected interatomic distances and angles are listed in Tables S1-S5.

1.DMF and **2**.DMF are similar, differing only in the type of the metal ion present in their structure (**1**, Zn; **2**, Mn). Hence, only the structure of **1**.DMF will be described in detail. **1**.DMF crystallizes in the P2$_1$/n monoclinic space group and Its crystal structure forms a 2D network based on the centrosymmetric repeating unit [Zn$_3$(pdmH)$_2$(bdc)$_2$] and lattice DMF molecules. The three metal ions are held together through the two η^2:η^1:η^1:η^1:μ pdmH$^-$ ligands, each one bridging Zn1 and Zn2 (or each symmetry equivalent Zn2'), and four carboxylate groups coming from six different bdc^{2-} ligands. The latter bridges each Zn$_3$ unit with four neighbouring SBUs favouring the formation of the network.
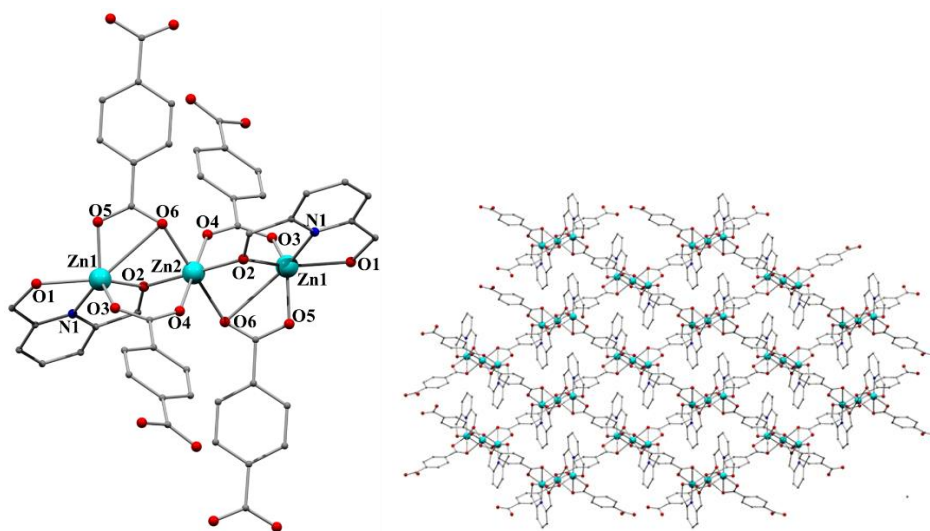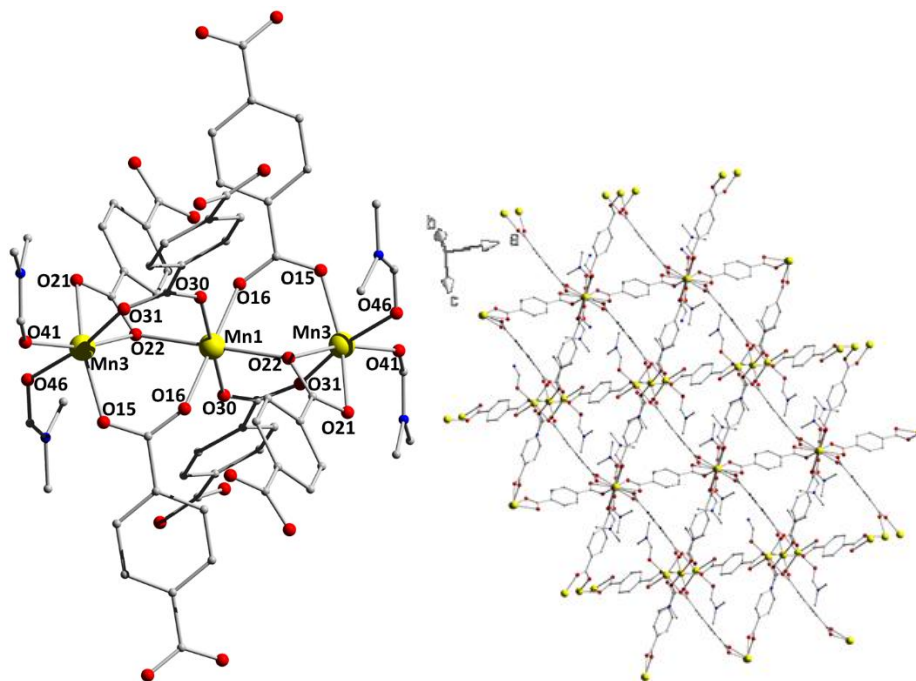
Figure 1. Representation of the repeating unit (left) and a part of the 2D net (right) in **1**. Colour code: Zn, cyan; N, blue; O, red, C, grey. The hydrogen atoms are omitted for clarity.

Zn1 is penta-coordinate adopting a distorted trigonal pyramidal geometry (τ = 0.45); its coordination sphere is completed by two carboxylate groups (O3, O5), which belong to two different bdc^{2-} ions, and one pdmH- ligand which forms two five-member rings through O1, O2 and N1. Zn2 is hexa-coordinated and its coordination sphere is completed through six oxygen atoms, four of them coming from four bdc^{2-} ligands (O4, O6, and their symmetry equivalents) and two from the deprotonated alkoxy groups of the two pdmH$^-$ ligands (O2 and O2'). A strong intramolecular hydrogen binding interaction stabilize the crystal structure; this is formed between hydroxyl group of the pdmH$^-$ ligand (O1, donor), which is the donor, and the lattice DMF molecule (O7, acceptor): **1**, O1$\cdots$O7 = 2.563 Å, H1$\cdots$O7 = 1.776 Å, O1-H1$\cdots$O7 = 160.36°; **2**, O1$\cdots$O7 = 2.667 Å, H1$\cdots$O7 = 1.957 Å, O1-H1$\cdots$O7 = 144.35°.

Compound **3** crystallizes in the monoclinic space group P2$_1$/n. Its structure (**Figure 2**) consists of a three-dimensional network based on the trinuclear centrosymmetric repeating unit [Mn$_3$(bdc)$_3$(H$_2$pdm)$_2$]. The three metal ions within the repeating unit are held together through six bridging carboxylate groups coming from six different bdc^{2-} ligands. The latter link the neighbouring SBUs resulting to the formation of a three dimensional network. The distance of the metal ion within the SBU is 3.500 Å, while the minimum distance between metal ions of different SBUs is 10.434 Å.
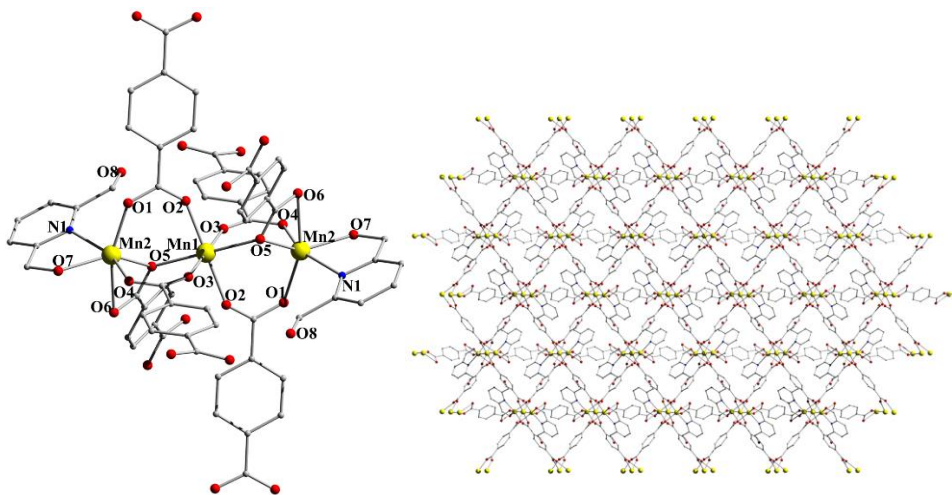
Figure 2. Representation of the repeating unit (left) and a part of the of the 3D net based on the c axis (right) in **3**. Colour code: Mn, yellow; N, blue; O, red, C, grey. The hydrogen atoms are omitted for clarity.

Mn1 is a hexa-coordinated adopting an octahedral geometry and its coordination sphere is completed through six oxygens from six different bdc^{2-} ions; in planar position are located the O2, O5, O2, O5, and in axial position the O3, O3. Mn2

is also hexa-coordinated adopting a deformed octahedral geometry. Its coordination sphere is completed by one chelate $pdmH_2$ ligand (O7, N1) and three carboxylate groups from three different bdc^{2-} ligands (O6, O1, O4, O5). The crystal structure of **3** is stabilized through hydrogen bonding interactions that involve the hydroxyl group of the $pdmH_2$ ligand (O7, O8, donors), and the deprotonated carboxylate groups of the bdc^{2-} ions (O1, O6, acceptors): O7···O1 = 2.696 Å, H1O7···O1 = 1.866 Å, O7-H1O7···O1 = 159.42°; O8···O6 = 3.019 Å, H8···O6 = 2.228Å, O8-H8···O6 = 162.41°.Thermal stability studies in 1 revealed that a sharp mass loss at 202°C (c.a. 32.5%) has occurred, then the compound retained steady till 300°C and between 300-360°C a further 25% and then a third step was observed which led to a further 10% loss prior the complete decomposition of the compound.

4 crystallizes in triclinic space group P-*1*. Its structure (**Figure 3**) consists of a two-dimensional network based on the trinuclear centrosymmetric repeating unit $[Mn_3(bdc)_3(DMF)_4]$. The molecule is centrosymmetric and the axis is passing through the central metal center. The metal distance between Mn1-Mn3 is 3.655 Å. The bdc^{2-} ligands link the Mn3 with six neighbouring repeating units resulting in the formation of the 3D network (**Figure 3**).

Figure 3. Representation of the repeating unit (left) and a part of the 2D net (right) in **4**. Colour code: Mn, yellow; N, blue; O, red, C, grey. The hydrogen atoms are omitted for clarity.

Compound **5** crystallizes in triclinic space group P-*1*. **5** is a mononuclear complex, where Ni1 is hexa-coordinated adopting an octahedral geometry and it is stabilized through two chelating H$_2$pdm molecules. There are strong intermolecular hydrogen bonding interactions in **5** that stabilize its structure and result in the formation of a three-dimensional network (**Figure 6 & Figure S19**). In particular, there is one type of hydrogen bonds that involve the hydrogen of the hydroxyl group (O9, O11, O19, O21), which are the donors, and the doubly deprotonated carboxylate groups of the lattice terephthalate ligands (O29, O32, O33, O30), which act as acceptors (O9···O29 = 2.559 Å, H9···O29 = 2.184 Å, O9-H9···O29 = 106.23°; O21···O30 = 2.510 Å, H21···O30 = 1.753Å, O21-

H21⋯O30 = 145.67°; O11⋯O32 = 2.525 Å, H11⋯O32 = 1.792 Å, O11-H11⋯O32 = 141.91°; O19⋯O33 = 2.510 Å, H19⋯O33 = 1.720 Å, O19-H19⋯O33 = 151.79°).
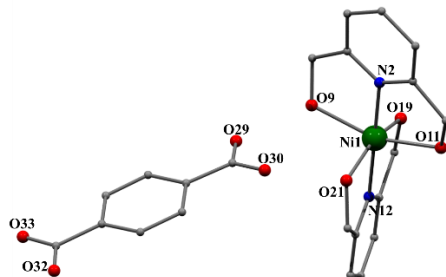
Figure 5. Representation of the mononuclear complex **5**. Colour code: Ni, green; N, blue; O, red, C, grey. The hydrogen atoms are omitted for clarity.
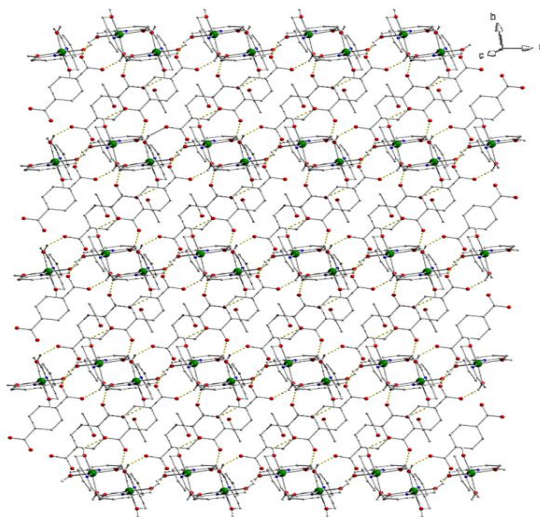
Figure 6. Representation of the 3D hydrogen bonding network for **5**. Colour code: Ni, green; N, blue; O, red, C, grey. The hydrogen atoms are omitted for clarity.

4. Conclusions

The simultaneous use of 2,6-pyridine-dimethanol and terephthalic acid has provided access to three new MOFs and one mononuclear complex, which were isolated by the two-pot reaction approach. It is worth mentioning that the two 2D-MOFs and one 3D-MOF reported here, namely $[M_3(bdc)_3(Hpdm)_2]_n \cdot DMF$ (where M^{II} = Zn (**1**), Mn (**2**)) and $[Mn_3(bdc)_3(H_2pdm)_2]_n$ (**3**), are the first MOFs bearing H_2pdm in its ionic or neutral form respectively with all of them based on a trinuclear sbu. The temperature and the presence of a base in the reaction mixture, as well as the nature of the solvents was found to play a crucial role in the identity of the isolated products. Lower temperature synthesis without the presence of base was found to crystallize only 2D polymers. With the simultaneous increase of temperature in the presence of base (Et_3N), a 3D framework was found to crystallize in case of Mn. In the case of Ni(II), we were not able to isolate a higher dimensional compound, as the 1D polymer is stabilized through strong hydrogen interactions, forming a 3D network. In conclusion, the temperature and the presence of base in the reaction mixture, as well as the nature of the solvents used, plays a crucial role in the dimensionality of the isolated product.

References

1. a) Konavarapu, S. K.; Goswami, A.; Ganesh Kumar, A.; Banerjeeb, S.; Biradha, K. *Inorg. Chem. Front.* **2019** 6,184-191. b) Wang, J.; Pan, Y.; Lu, L.; Xiong, Y. F.; Fang, L.; Luo, W.; Wu, X.; Kumar, A. Journal of Molecular Structure **2019** 1196, 194-200. c) Vizuet, J. P.; Howlett, Th. S.; Lewis, A. L.; Chroust, Z. D.; McCandless, G. T.; Balkus, K. J. *Inorg. Chem.* **2019** 58, 8, 5031–5041. d) Zhaoa, F.-H.; He, Y. -C.; Shen, C.-Y.;

Wang, D. -L.; Lia, Z.-L.; Lia, S.-Y.; Guoa, W.-Y.; Youa, J.-M. *Inorg. Chim. Acta* **2019** 492, 60-65. e) Zhu, K.; Chen, L.; Jin, X.; Qu, C. *Stuctural Chemistry* **2019** 30, 1485-1484. f) Zuo, W.; Fan, Y.; Yang, L.; Cui, L. *Journal of Inorganic and Organometallic Polymers and Materials* **2020** 30, 2105-2113. g) Fridelli, A. M.; Kessler, V. G.; Escuer, A.; Papaefstathiou, G. S. CrystEngComm 2017, 19, 4355-4367. h) Fidelli, A. M.; Armakola, E.; Demadis, K. D.; Kessler, V. G.; Escuer, A.; Papaefstathiou, G. S. *Eur. J. Inorg. Chem.* 2018 1, 91-98.

2. a) Kleist, W.; Jutz, F.; Maciejewski, M.; Baiker, A. *Eur. J. Inorg. Chem.* **2009**, 24, 3552-3561. b) Burrows, A. D. *Cryst Eng Comm.* **2011** 13, 3623-3642.

3. a) Freund, R.; Canossa, S.; Cohen, S. M.; Yan, W.; Deng, H.; Guillerm, V.; Eddaoudi, M.; Madden, D. G.; Fairen-Jimenez, D.; Lyu, H.; Macreadie, L. K.; Ji, Z.; Zhang, Y.; Wang, B.; Haase, F.; Wöll, C.; Zaremba, O.; Andreo, J.; Wuttke, S.; Diercks, C. S. *Angew. Chem. Int. Ed.* **2021** DOI: *HTTPS://DOI.ORG/10.1002/ANIE.202101644*. b) Fan, L.; Liu, X.; Zhang, L.; Kong, X.; Xiao, Z.; Fan, W.; Wang, R.; Sun, D. *Journal of Molecular Structure* **2019** 1197, 87-95. c) Khullara, S.; Thakurb, S.; Mandalb, S. K. Inorg. Chim. Acta **2020** 502, 119281.

4. a) Mylonas-Margaritis, I.; Winterlich, M.; Efthymiou, C. G.; Lazarides, T.; McArdle P.; Papatriantafyllopoulou, C. *Polyhedron* **2018**, 151, 360. b) Mylonas-Margaritis, I.; Gerard, A.; Skordi, K.; Mayans, J.; Tasiopoulos, A.; McArdle, P.; Papatriantafyllopoulou, C. *Materials* **2020**, 4084.; Mylonas-Margaritis, I.; Mayans, J.; McArdle P.; Papatriantafyllopoulou, C. *Molecules* **2021**, 26, 491.

5. Mylonas-Margaritis, I.; Mayans, J.; Escuer, A.; McArdle, P.; Papatriantafyllopoulou, C. *CrystEngCommun.* **2021** DOI: *HTTPS://DOI.ORG/10.1039/D1CE00659B* .

6. a) Alexandropoulos, D. I.; Cuhna-Silva, L.; Bekiari, V.; Christou, G.; Stamatatos, Th. C. *Inorg. Chem.* **2017** 70, 3220-3229. b) Taguchi, T.; Thompson, M. S.; Abboud, K. A.; Christou, G. *Dalton Trans.* **2010** 39, 9131-9139. c) Stamatatos, Th. C.; Vlahopoulou, G. C.; Raptopoulou, C. P.; Terzis, A.; Escuer, A.; Perlepes, S. P. *Inorg. Chem.* **2009** 48 4610-4612.

Supplementary Material

Synthesis of [Ni(H$_2$pdm)$_2$](bdc) (**5**)

Ni(ClO$_4$)$_2$·H$_2$O (0.0731g, 0.2mmol), H$_2$pdm (0.2226g, 1.6 mmol) and Et$_3$N (416 μl, 3.2mmol) were dissolved in a mixture of DMF/H$_2$O (25ml/ 25ml). The resultant cyan solution was put in the oven and heated at 130°C for 1h. Then, H$_2$bdc (0.0166g, 0.1mmol) was added and the vial was placed into the oven for 24h, after which X-ray quality green crystals of **4** were formed. The crystals were collected by filtration, washed with cold MeCN (2ml) and Et$_2$O (2 x 5mL) and dried in air. Yield 23%. Anal. Calc. for **4**: C, 46.80; H, 3.93; N, 4.96. Found: C, 46.70; H, 3.88; N, 4.88%. IR data (cm^{-1}) = 3425w, 2925w, 2864w, 2320w, 1842w, 1664s, 1604w, 1583m, 1498m, 1439m, 1383m, 1352s, 1297w, 1257w, 1240w, 1160m, 1144w, 1090m, 1034w, 1015s, 1001w, 894w, 866w, 794s, 754s, 660s.

Tables S1. Selected interatomic distances (Å) and angles (°) for **1**.

Bonds

Zn1-N1	2.044(3)		Zn1-O2	1.999(3)
Zn1-O1	2.273(3)		Zn2-O2	1.970
Zn1-O3	1.960(2)		Zn2-O4	2.173
Zn1-O5	1.967(3)		Zn2-O6	2.179

Angles

O1-Zn1-O3	89.0(1)		O5-Zn1-O2	100.5(1)
O3-Zn1-O2	106.7(1)		O5-Zn1-N1	125.9(1)
O2-Zn1-N1	80.0(1)		O4-Zn2-O6	88.1
N1-Zn1-O1	73.5(1)		O6-Zn2-O4	91.9
O3-Zn1-N1	113.3(1)		O2-Zn2-O6	93.2
O1-Zn1-O2	152.9(1)		O2-Zn2-O4	89.2
O5-Zn1-O1	90.8(1)		O2-Zn2-O6	86.8
O5-Zn1-O3	117.8(1)		O2-Zn2-O4	90.8

Tables S2. Selected interatomic distances (Å) and angles (°) for **2**.

Bonds

Mn1-N1	2.036(4)		Mn1-O5	1.964(3)
Mn1-O1	2.258(5)		Mn2-O6	2.184
Mn1-O3	1.954(3)		Mn2-O2	1.965
Mn1-O2	1.999(3)		Mn2-O4	2.162

Angles

N1-Mn1-O2	79.9(1)		O3-Mn1-O5	117.7(1)
O2-Mn1-O5	100.9(1)		O3-Mn1-O1	89.5(1)
O5-Mn1-O1	90.5(1)		O6-Mn2-O4	88.5
O1-Mn1-N1	73.6(2)		O4-Mn2-O6	91.5
N1-Mn1-O5	126.0(1)		O2-Mn2-O6	87.0
O1-Mn1-O2	153.0(1)		O2-Mn2-O4	89.3
O3-Mn1-N1	113.5(1)		O2-Mn2-O6	93.0
O3-Mn1-O2	106.2(1)		O2-Mn2-O4	90.7

Tables S3. Selected interatomic distances (Å) and angles (°) for **3.**

Bonds

Mn1-O2	2.113	Mn2-O7	2.143(2)
Mn-O5	2.270	Mn2-O4	2.076(2)
Mn1-O3	2.130	Mn2-O5	2.191(2)
Mn2-N1	2.292(2)	Mn2-O1	2.118(1)

Angles

O2-Mn1-O5	89.53	N1-Mn2-O7	73.37(7)
O5-Mn1-02	90.47	O7-Mn2-O4	83.46(7)
O3-Mn1-O2	87.91	O4-Mn2-N1	156.44(6)
O3-Mn1-05	91.50	O7-Mn2-O5	142.25(6)
O3-Mn1-O2	92.09	O1-Mn2-O4	92.10(6)
O3-Mn1-O5	88.5	O1-Mn2-O5	102.77(6)
O4-Mn2-O5	107.19(6)	O1-Mn2-N1	93.12(6)
O5-Mn2-N1	94.01(6)	O1-Mn2-O7	113.13(6)

Tables S4. Selected interatomic distances (Å) and angles (°) for **4**.

Bonds

Mn3-O41	2.1548	Mn3-O22	2.2711
Mn3-O46	2.243	Mn1-O22	2.2256
Mn3-O21	2.2893	Mn1-O30	2.1255
Mn3-O31	2.1073	Mn1-O16	2.1453
Mn3-O15	2.1191		

Angles

O21-Mn3-O22	57.80	O31-Mn3-O22	95.44
O22-Mn3-O15	92.77	O31-Mn3-O15	105.45
O15-Mn3-O41	101.26	O31-Mn3-O41	82.98
O41-Mn3-O21	108.09	O16-Mn1-O30	93.25
O46-Mn3-O21	83.55	O30-Mn1-O16	86.75
O46-Mn3-O22	90.45	O22-Mn1-O16	92.60
O46-Mn3-O15	82.34	O22-Mn1-O30	88.79
O46-Mn3-O41	89.3	O22-Mn1-O16	87.4
O31-Mn3-O21	92.68	O22-Mn1-O30	91.21

Tables S5. Selected interatomic distances (Å) and angles (°) for **5**.

Bonds

Ni1-N2	1.9856		Ni1-O21	2.0914
Ni1-O9	2.1128		Ni1-O19	2.0991
Ni1-O11	2.1244		Ni1-N12	1.9846

Angles

O21-Ni1-O9	94.20		N2-Ni1-O19	105.56
O9-Ni1-O19	90.25		N12-Ni1-O11	79.15
O19-Ni1-O11	93.54		N12-Ni1-O21	79.67
O11-Ni1-O21	89.97		N12-Ni1-O9	102.11
N2-Ni1-O11	79.15		N12-Ni1-O19	79.02
N2-Ni1-O21	95.74		N12-Ni1-O11	99.53
N2-Ni1-O9	79.31			

Tables S6. Hydrogen bonding for **1**[a].

O1-H1···O7	2.563	1.776	160.36	x, y, z

[a] A = acceptor, D = donor

Tables S7. Hydrogen bonding for **2**[a].

D-H···A	D-A (Å)	H-A (Å)	DHA (°)	Symmetry operator
O1-H1···O7	2.667	1.957	144.35	x, y, z

[a] A = acceptor, D = donor

Tables S8. Hydrogen bonding for **3**[a].

D-H···A	D-A (Å)	H-A (Å)	DHA (°)	Symmetry operator
O7-H1O7···O1	2.696	1.866	159.42	x, y, z
O8-H8···O6	3.019	2.228	162.41	x, y, z

[a] A = acceptor, D = donor

Tables S9. Hydrogen bonding for **5ᵃ**.

D-H···A	D-A (Å)	H-A (Å)	DHA (°)	Symmetry operator
O9-H9···O29	2.559	2.184	106.23	x, y, z
O21-H21···O30	2.510	1.753	145.67	x, y, z
O11-H11···O32	2.525	1.792	141.91	x, y, z
O19-H19···O33	2.510	1.720	151.79	x, y, z

ᵃ A = acceptor, D = donor
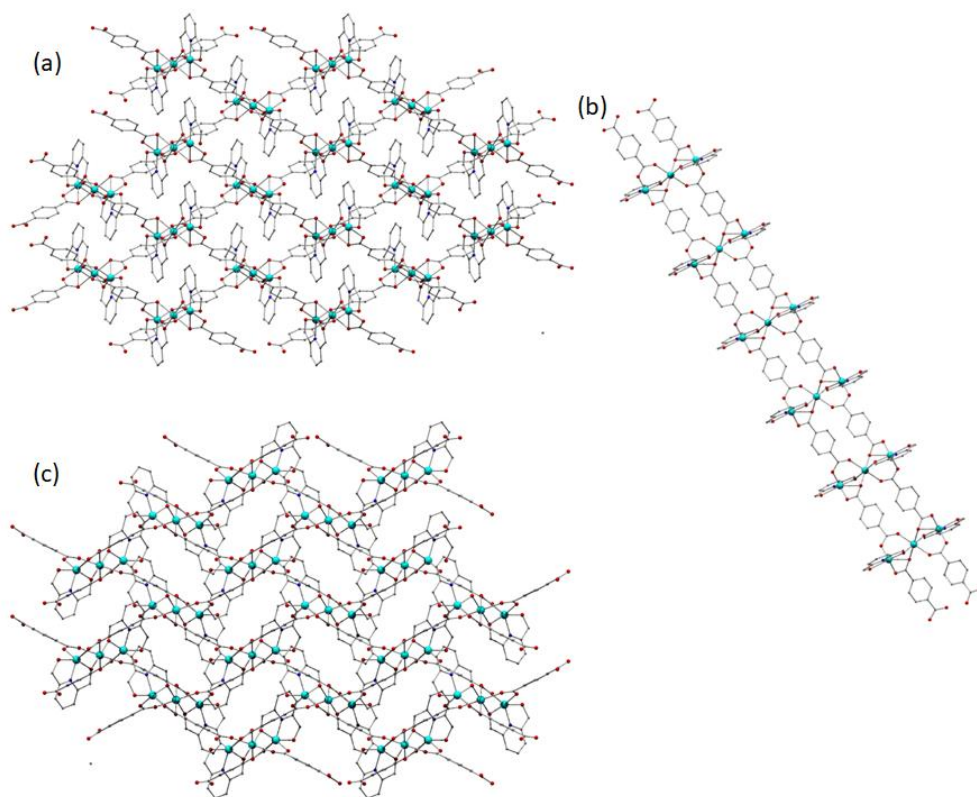
Figure S1. Representation of the 2D network of **1** (a) a-axis, (b) b-axis, (c) c-axis.
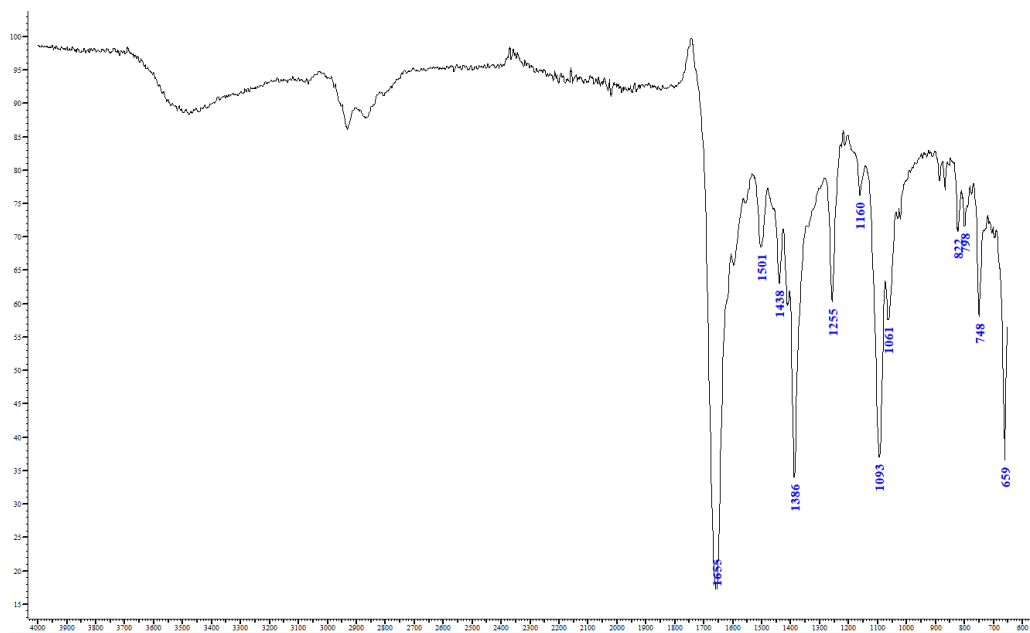
Figure S2. The infrared spectra of **1**.
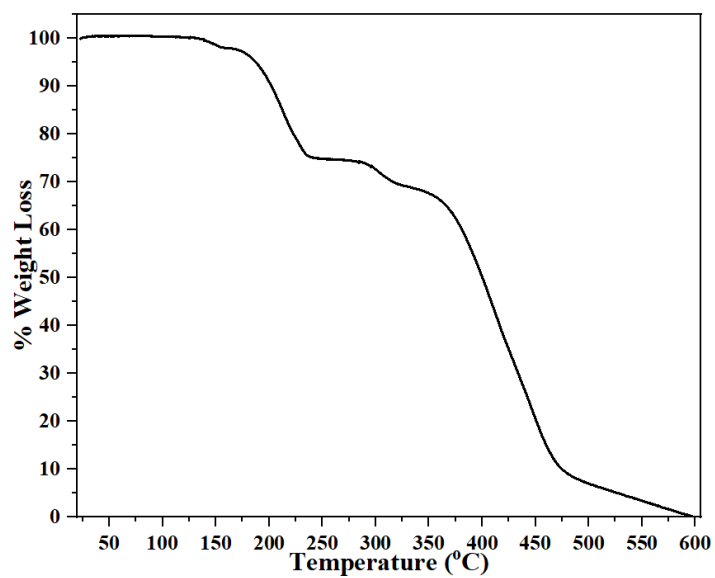
Figure S3. The TGA spectra of **1**.
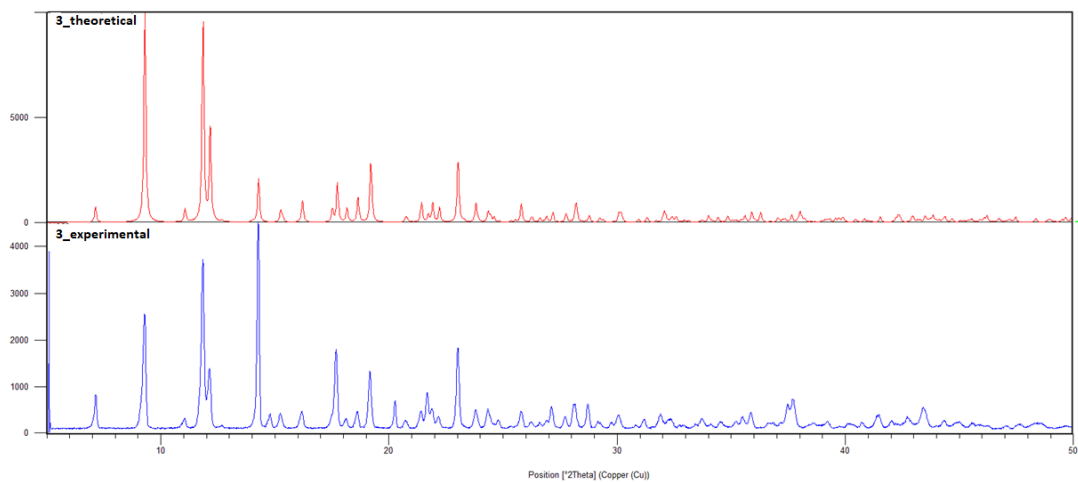
Figure S4. Comparison of the theoretical (top) and the experimental (bottom) pxrd pattern for **1**.
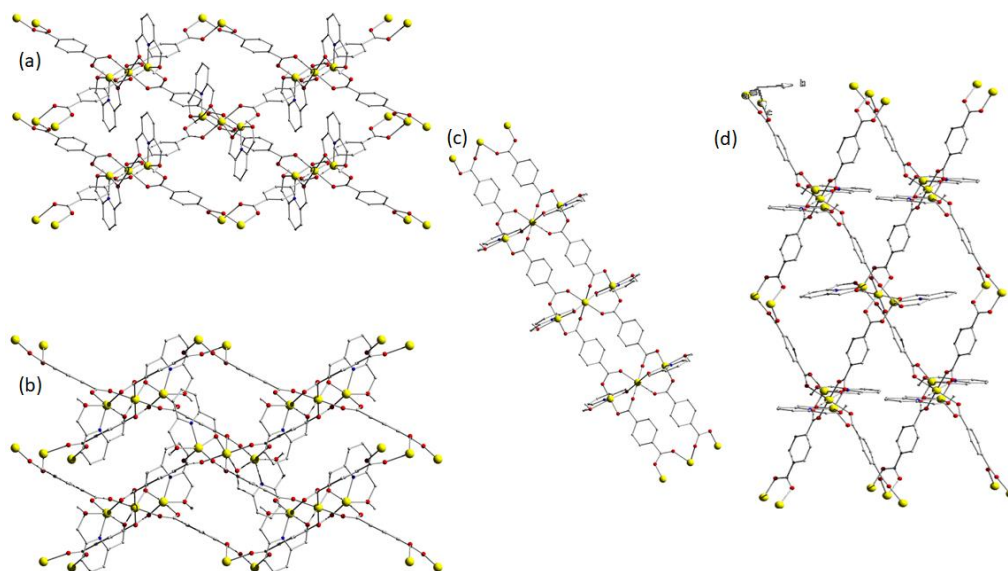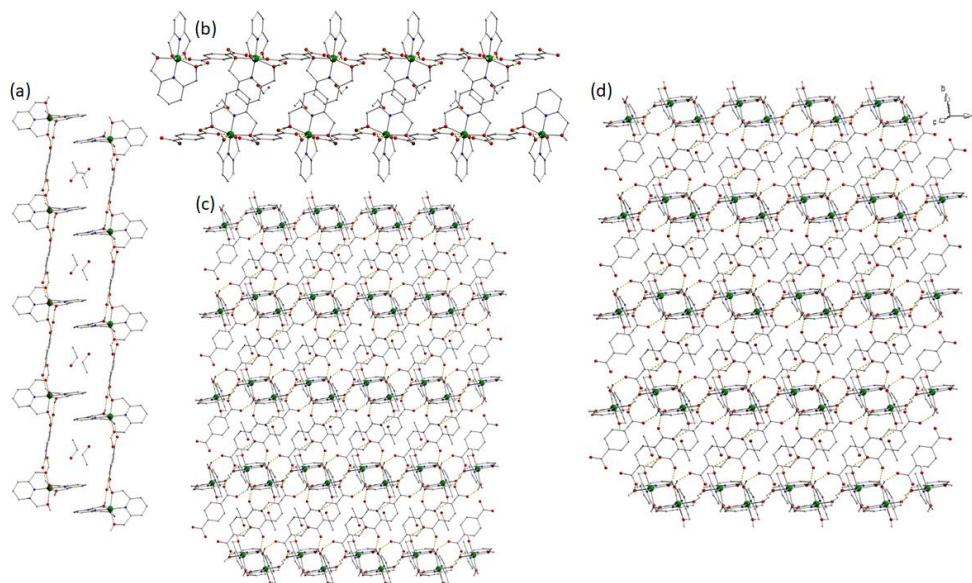

Figure S5. Representation of the 2D network of **2** (a) a-axis, (b) b-axis, (c) c-axis.
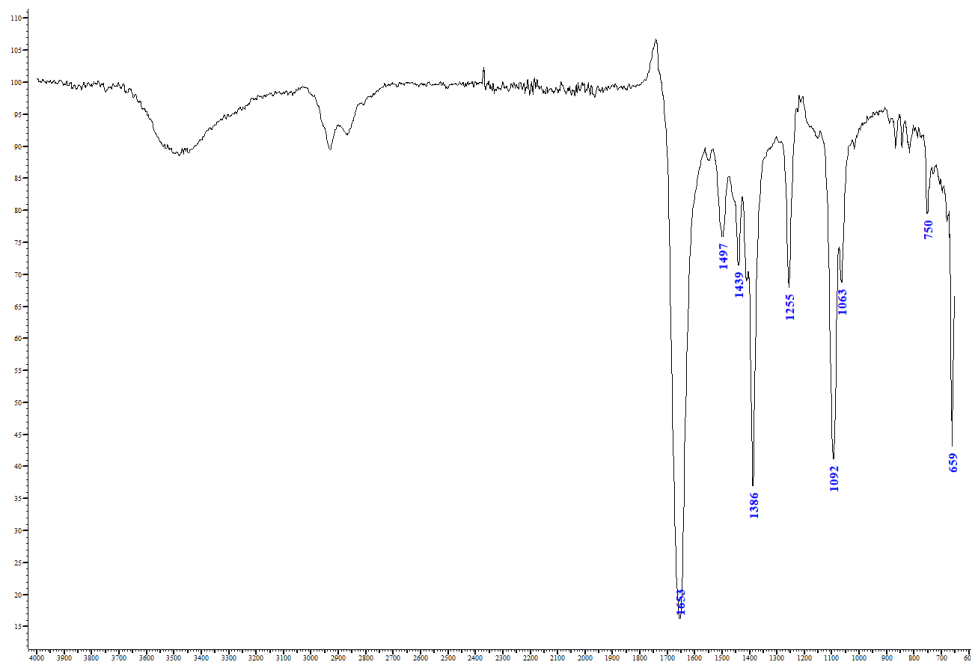
Figure S6. The infrared spectra of **2**.
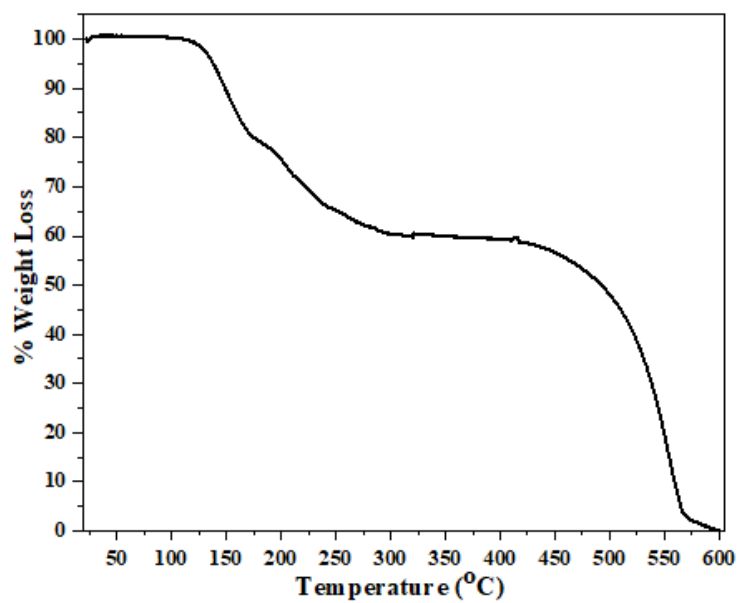
Figure S7. The TGA diagram of **2**.
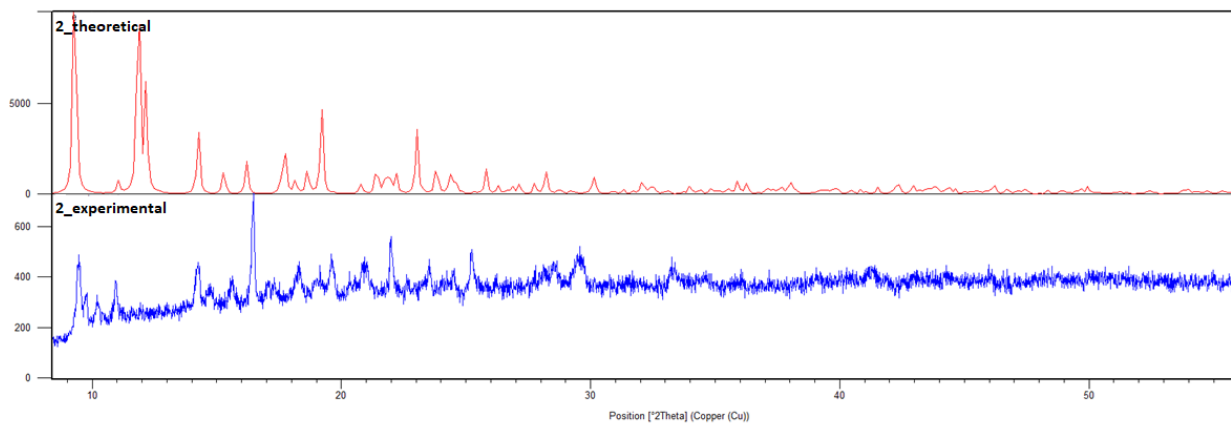
Figure S8. Comparison of the theoretical (top) and the experimental (bottom) pxrd pattern for **2**.
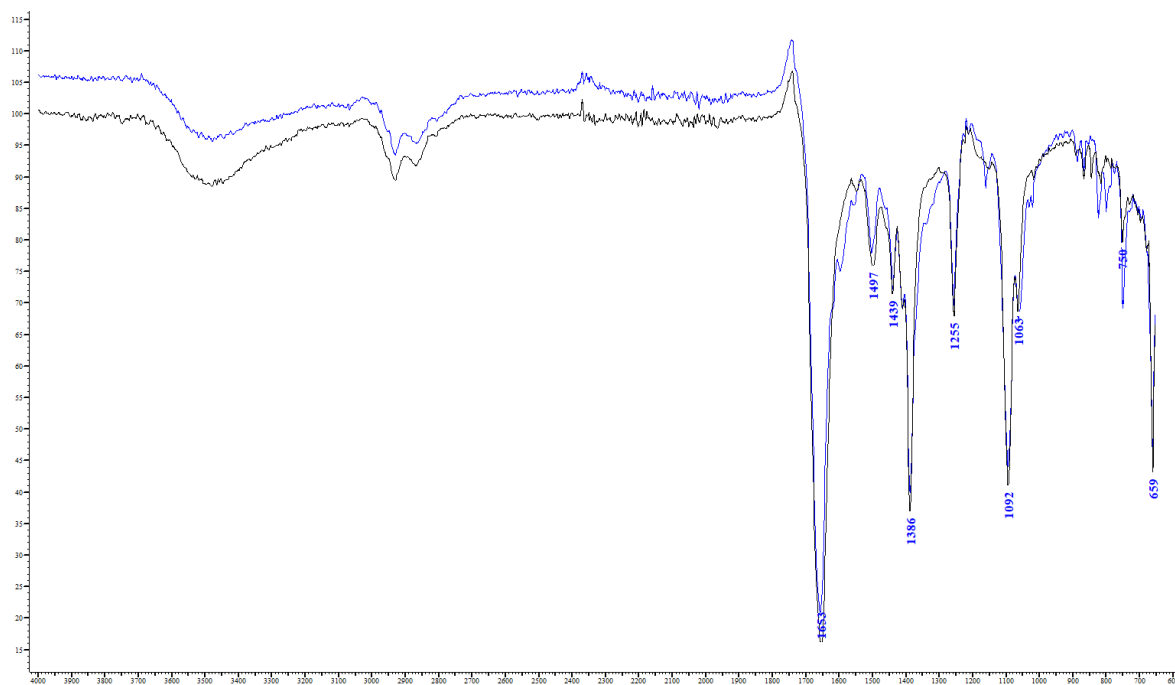
Figure S9. Comparison of the infrared spectra of **1** (black) vs **2** (blue).

Figure S10. Photo of crystals of **3**.
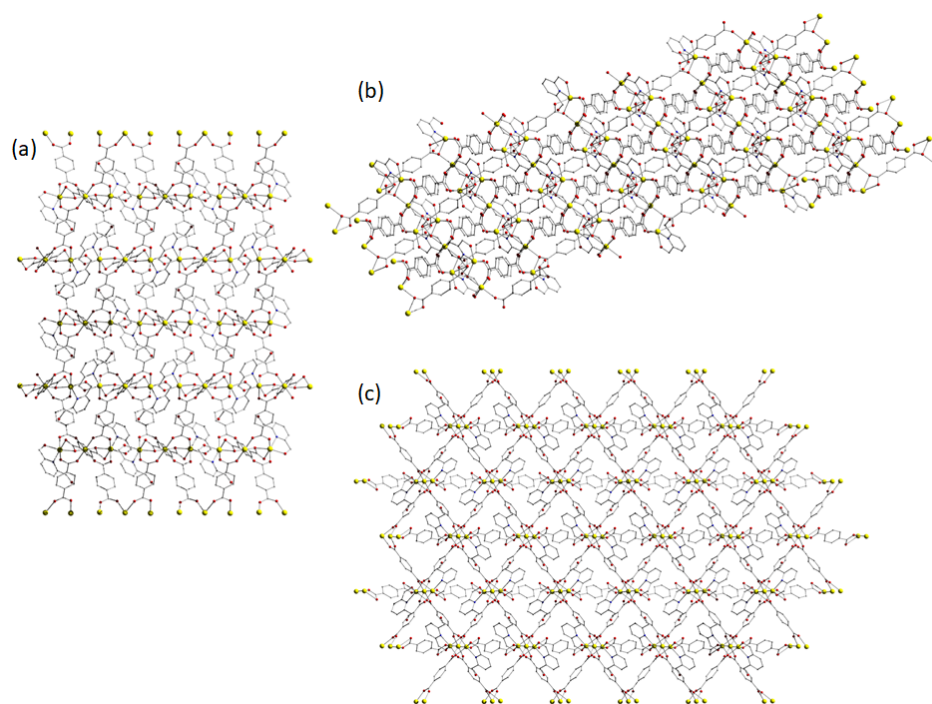
Figure S11. Representation of the 3D network of **3** (a) a-axis, (b) b-axis, (c) c-axis.
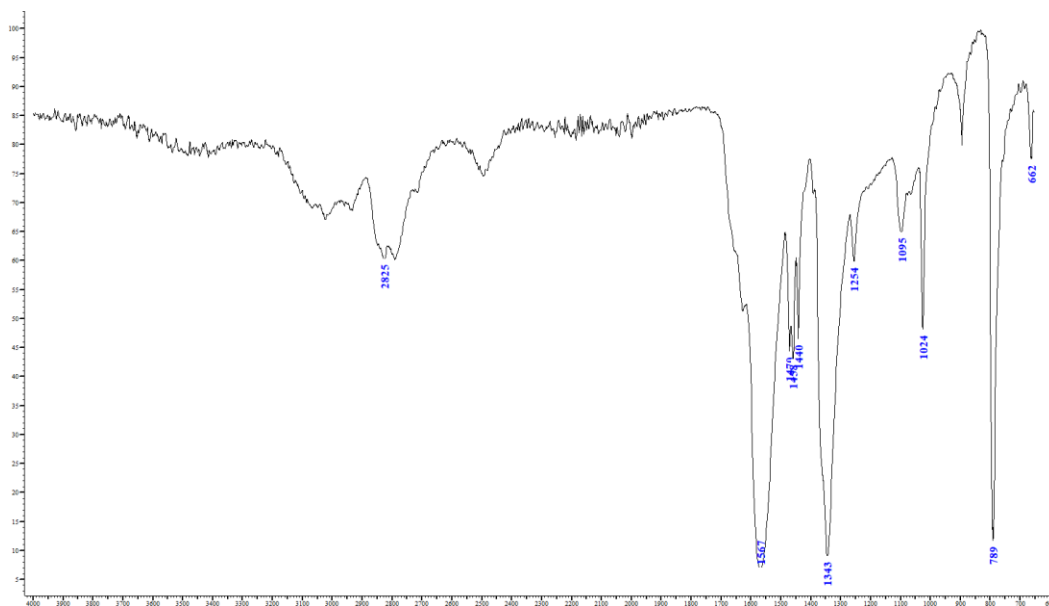
Figure S12. The infrared spectra of **3**.
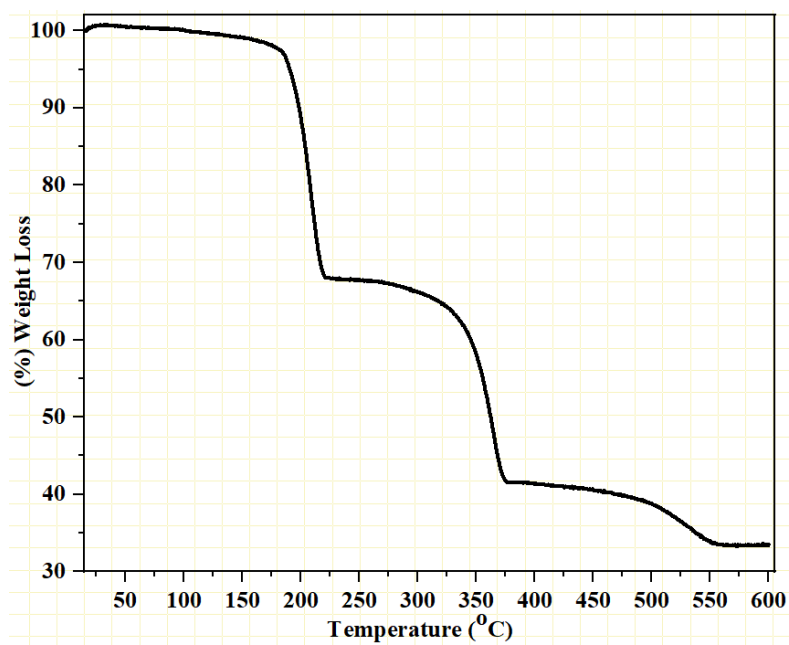
Figure S13. The TGA diagram of **3**.
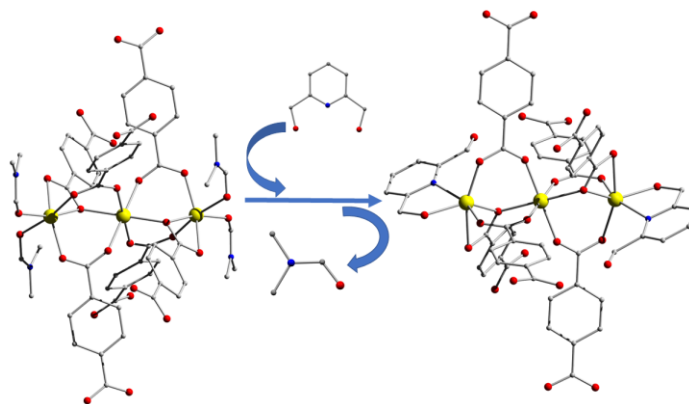
Figure S14. Mechanistic representation of the replacement of DMF molecules of **4** for the formation of **3** by replacing them with H$_2$pdm.
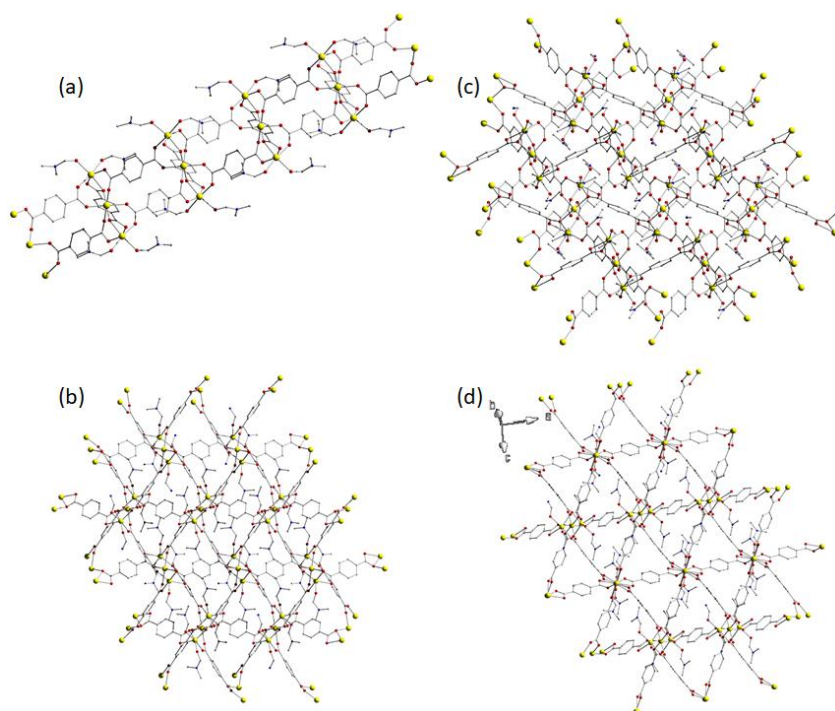
Figure S15. Representation of the 2D network of **4** (a) a-axis, (b) b-axis, (c) c-axis and (d) rotated axis.
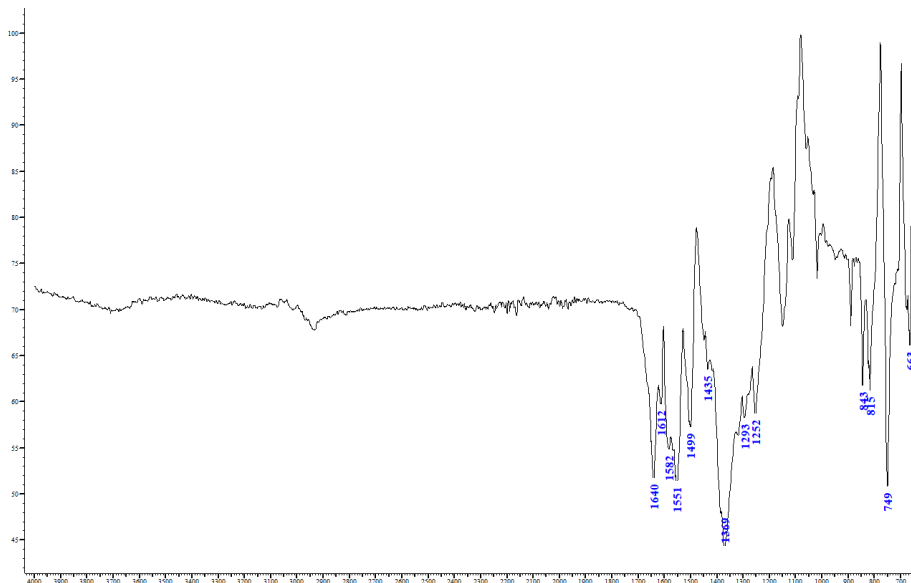
Figure S16. The infrared spectra of **4**.
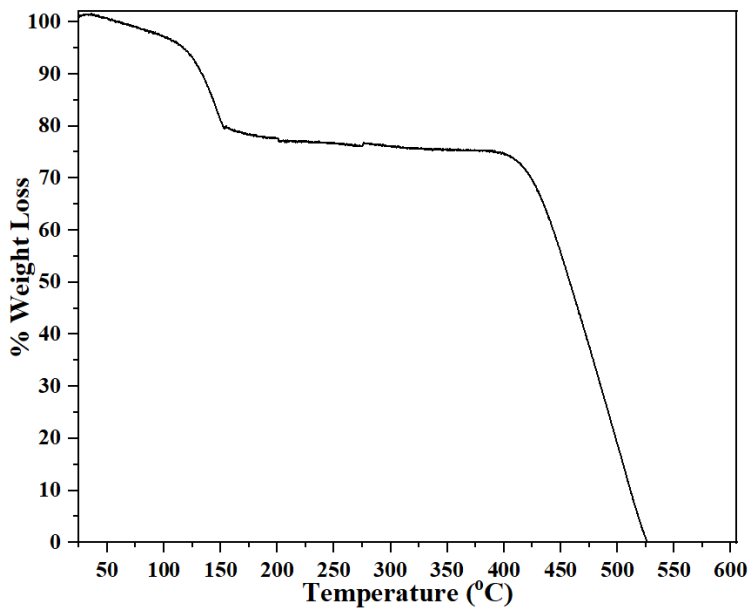
Figure S17. The TGA diagram of **4.**
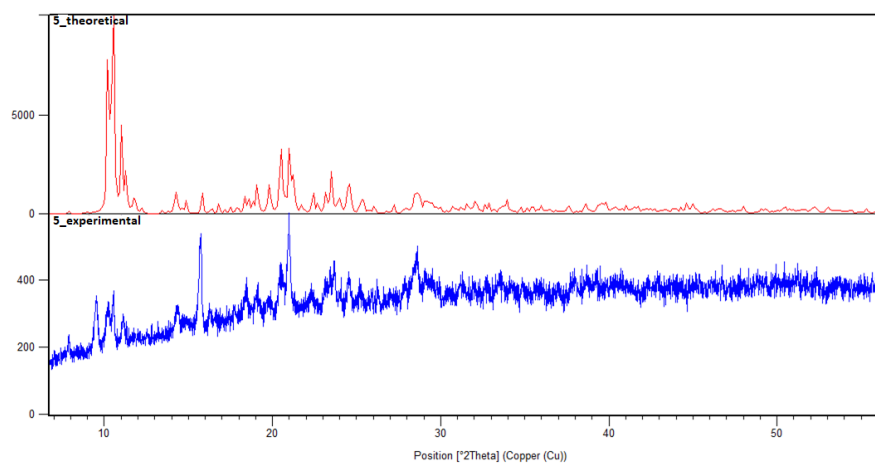
Figure S18. Comparison of the theoretical (top) and the experimental (bottom) pxrd pattern for **4**.

Figure S19. Representation of the 3D hydrogen bonding network of **5** (a) a-axis, (b) b-axis, (c) c-axis and (d)rotated axis.
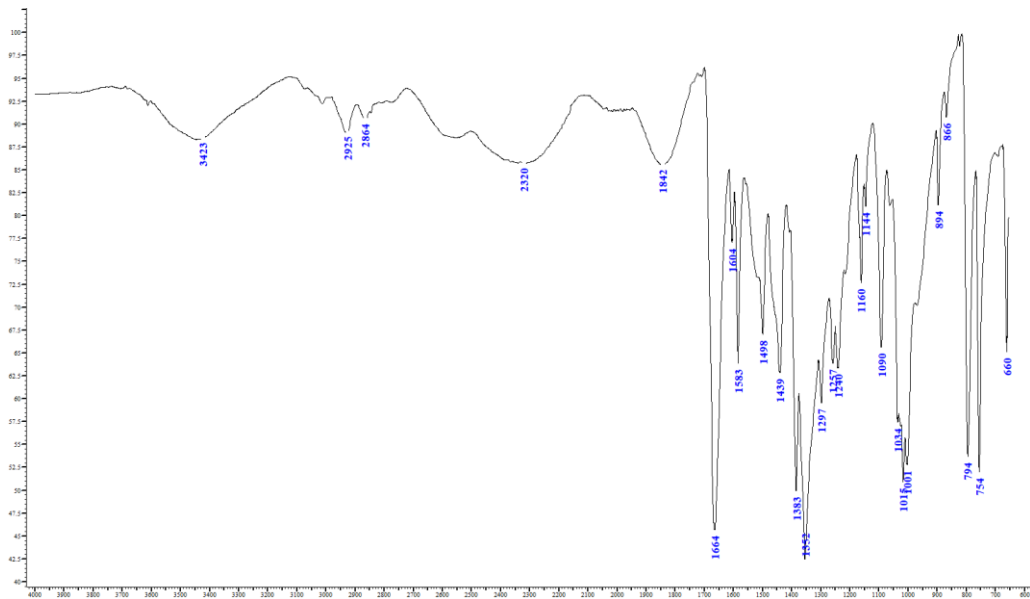
Figure S20. The infrared spectra of **5**.

Chapter 3

Conclusions and Future Work

Outlook and Future Work

This work introduces for the first time small rigid ligands (pyridyl-oximes and alcohols) from the field of single-molecule magnets (SMMs) in the field of metal-organic frameworks, combining them with polycarboxylates (e.g. terephthalic acid, trimesic acid or 1,2,4,5-benzenetetracarboxylic acid) for the formation of the network. This unique combination has led to the isolation of nine metal complexes, eight coordination polymers, and twelve MOFs adopting novel topologies. Pyridyl oximes and alcohols were chosen, as they are able to stabilize homo- and hetero-metallic metal complexes with small and high nuclearities presenting interesting magnetic properties, which is essential for the development of magnetism-based sensors. The development of magnetism-based sensors is crucial as not all the environmental pollutants are photoluminescence active, hence their detection can be challenging. Through this research, it was proven that the chosen ligands are suitable for the development of compounds adopting the required properties and an example of this is the $[Cu_4(OH)_2(pma)(mpko)_2]_n$, which can act as magnetic sensor and it is suitable for the sensing of Fe^{3+} with adsorption capacity 129.89 mg Fe/g MOF.

The combination of pyridyl oximes and terephthalic acid led to the isolation of metal complexes and 1D coordination polymers. Polymerization of the mononuclear complexes to 1D polymers was achieved, but it was not possible to isolate a higher dimensionality polymer. The use of trimesic acid achieved not only the isolation of metal complexes and 1D-polymers, but also the isolation of the first 2D MOF $[Cu(Hbtc)(pyaoxH_2)]_n$ of this combination. Using 1,2,4,5-benzene-tetracarboxylic acid, which has an additional carboxylic group, it was possible to isolate a higher dimensional 3D polymer, which adopts a tetranuclear sbu with the formula $[Cu_4(OH)_2(pma)(mpko)_2]_n$. This was the first example of a

magnetism-based sensor and it was also shown to selectively adsorb Fe^{3+}. The first known 2D polymer of this sbu combination was also isolated, $[Zn_2(pma)(pyaoxH_2)_2(H_2O)_2]_n$.

As the combination of pyridyl-oximes and carboxylates was studied in-depth, we continued to investigate the behavior of an analogue family of small rigid ligands, pyridine alcohols. The oximic group (-N-OH) of pyridyl-oximes was replaced by the hydroxyl group (-OH) of pyridine alcohols. This combination was introduced for the first time in the field of coordination polymers and MOFs. The combination of 2-pyridine methanol with terephthalic acid led to the isolation of two 3D MOFs with formulas $[Zn_2(bdc)(hmp)_2]_n \cdot DMF$,$[Fe_3(bdc)_3(Hhmp)_2]_n$, adopting unique topologies. The use of trimesic acid did not lead to the isolation of any MOF, but of dinuclear complexes, which were not able to be further polymerized.

For further investigation of the addition of an extra hydroxyl group, instead of 2-pyridine methanol, 2,6-pyridine-dimehtanol was used with the simultaneous use of terephthalic acid. This unique combination led to the isolation of two 2D MOFs {$[M_3(bdc)_3(Hpdm)_2]_n \cdot DMF$ (where M^{II} = Zn, Mn)} and a 3D MOF with formula $[Mn_3(bdc)_3(H_2pdm)_2]_n$. The increase of temperature and the simultaneous presence of base (Et_3N) was found to be crucial for the isolation of the 3D MOF. In case of Ni(II), it was not possible to isolate a MOF, but a 1D coordination polymer as the compound is stabilized through strong hydrogen bonding interactions and even with excess base or increased temperature a higher dimension product was unable to be synthesized.

Through this research it was shown that pyridyl-oximes and pyridine-alcohols are good candidates for the formation of unique secondary building units, which present unique magnetic properties and can lead to MOFs with unique topologies

which can possibly be used for future development of magnetic sensors. The vast majority of MOFs in this work present poor porosity. The employment of elongated linkers is expected to provide access to MOFs with enhanced porosity and retention of the analog sbus without affecting the topology. The use of elongated ligands will likely lead to less π -π stacking interactions and strong hydrogen bonding between the two linkers.

Chapter 4: Appendix

2.1. New insights into oximic ligands: Synthesis and characterization of 1D chains by the use of pyridine 2-amidoxime and polycarboxylates
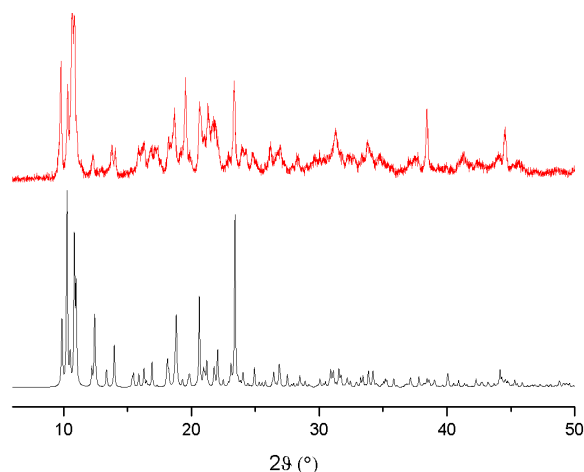
Figure S3. Theoretical (bottom) and experimental (top) pxrd pattern diagrams for **1**

Explanation: The pxrd data of **1** do not match 100%, as a few extra peaks can be observed on the experimental pxrd (red). This is happening due to the fact, that into the vial, a second class of crystals were co-crystallized, whose crystal structure could not be determined. Efforts were done to separate mechanically the two different products, but always a tiny amount of the second class of crystals remained as their size was too small and we could not proceed to further purification of the sample.

2.2. From 1D Coordination Polymers to Metal Organic Frameworks by the Use of 2-Pyridyl Oximes

The encapsulation of Iron(III) was proved through magnetic studies and EDX analysis. The profiles of infrared spectra (**Figure Ap. 1 & 2**), TGA (**Figure Ap. 3 & 4**), and PXRD (**Figure Ap. 5 & 6**) did not change once iron(III) was loaded into **9,** even if UV-vis proves the encapsulation. After the UV-vis encapsulation studies, the samples were filtered and the filtered MOF was further analysed. Through these data, it is proved that the techniques mentioned above were not able to identify the small amounts of adsorbed metal cation.
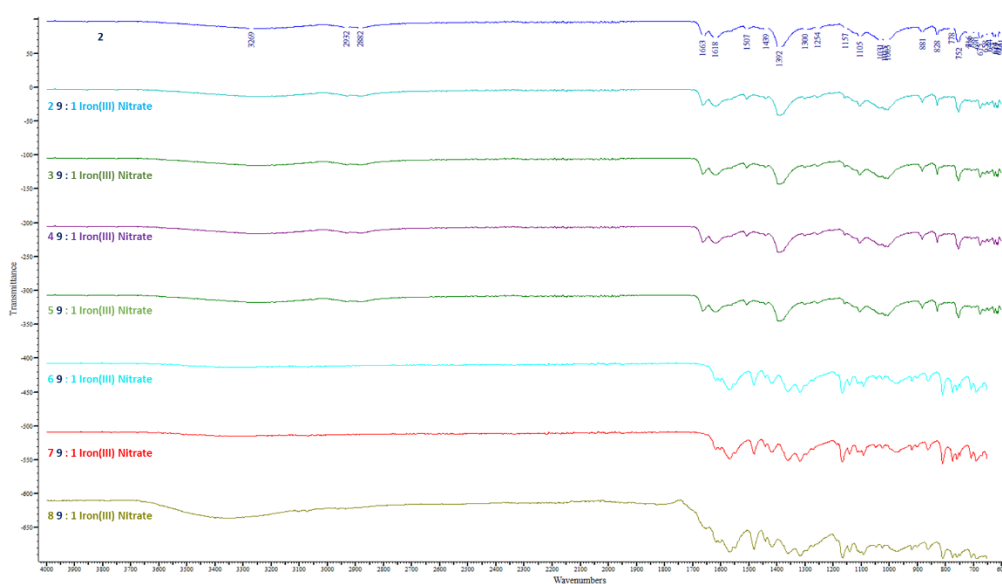
Figure Appendix 1. Comparison of the infrared data of **9** with experimental data after the UV-Vis encapsulation studies for iron(III) nitrate. Blue: Initial MOF (9); Cyan: 2 eq. of **9** vs. 1 eq. of iron(III) nitrate; Green: 3 eq. of **9** vs. 2 eq. of iron(III) nitrate; Purple: 4 eq. of 9 vs. 1 eq. of iron(III) nitrate; Pale Green: 5 eq. of 9 vs. 1 eq. of iron(III) nitrate; Cyan: 6 eq. of 9 vs. 1 eq. of iron(III) nitrate; Red: 7 eq. of 9 vs. 1 eq. of iron(III) nitrate; Ocher: 8 eq. of 9 vs. 1 eq. of iron(III) nitrate.
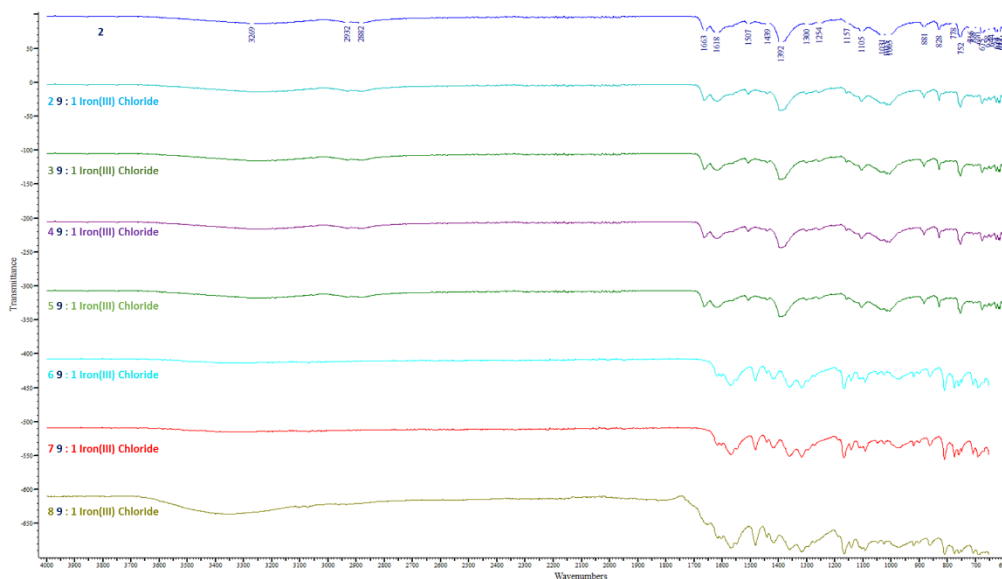
Figure Appendix 2. Comparison of the infrared data of **9** with experimental data after the UV-Vis encapsulation studies with iron (III) chloride. Blue: Initial MOF (**9**); Cyan: 2 eq. of **9** vs. 1 eq. of iron(III) chloride; Green: 3 eq. of **9** vs. 2 eq. of iron(III) chloride; Purple: 4 eq. of 9 vs. 1 eq. of iron(III) chloride; 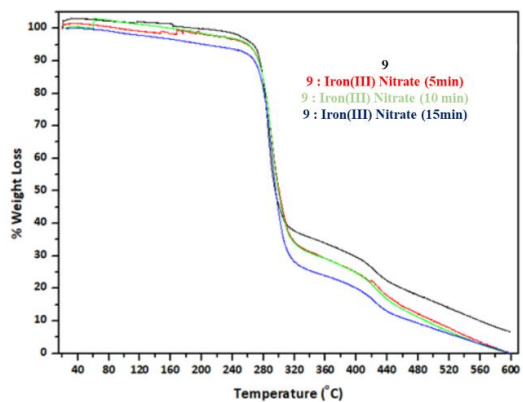Pale Green: 5 eq. of 9 vs. 1 eq. of iron(III) chloride; Cyan: 6 eq. of 9 vs. 1 eq. of iron(III) chloride; Red: 7 eq. of 9 vs. 1 eq. of iron(III) chloride; Ocher: 8 eq. of 9 vs. 1 eq. of iron(III) chloride.

Figure Appendix 3. Comparison of the TGA data of **9** with the experimental data after the UV-Vis encapsulation studies in presence iron (III) nitrate. Black:

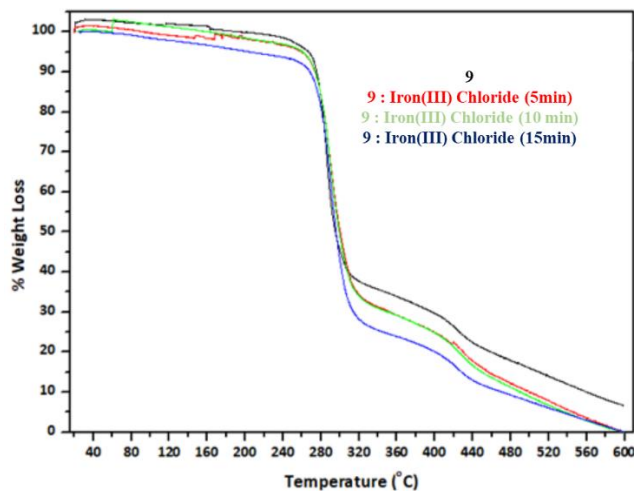Initial **9**. Red: After 5 min of UV-studies. Green: After 10 min of UV-studies. Blue: After 15min of UV-studies.

Figure Appendix 4. Comparison of the TGA data of **9** with the experimental data after the UV-Vis encapsulation studies in presence of iron (III) chloride. Black: Initial **9**. Red: After 5 min of UV-studies. Green: After 10 min of UV-studies. Blue: After 15min of UV-studies.
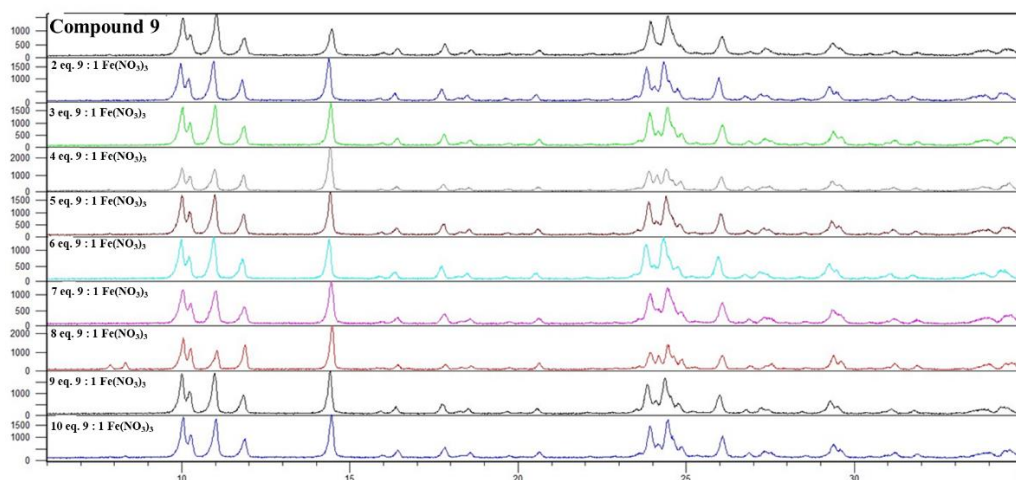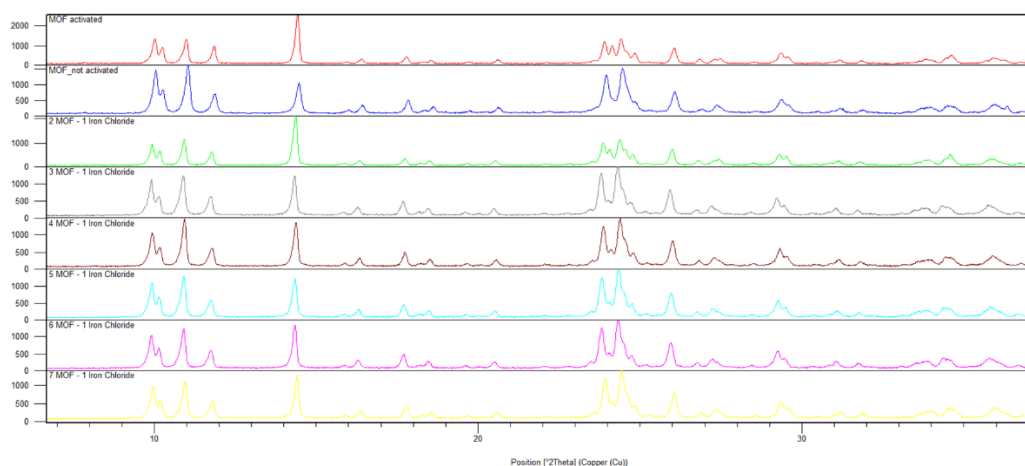

Figure Appendix. 5. Comparison of the PXRD data of **9** with the experimental data after the UV-Vis encapsulation studies for iron(III) nitrate. Black: initial **9**;

Blue: 2 eq. of **9** vs. 1 eq. of iron(III) nitrate; Green: 3 eq. of **9** vs. 1 eq. of iron(III) nitrate; Grey: 4 eq. of 9 vs. 1 eq. of iron(III) nitrate; Brown: 5 eq. of 9 vs. 1 eq. of iron(III) nitrate; Cyan: 6 eq. of 9 vs. 1 eq. of iron(III) nitrate; Purple: 7 eq. of 9 vs. 1 eq. of iron(III) nitrate; Pale brown: 8 eq. of 9 vs. 1 eq. of iron(III) nitrate; Black: 9 eq. of 9 vs. 1 eq. of iron(III) nitrate; Dark blue: 110 eq. of 9 vs. 1 eq. of iron(III) nitrate.

Figure Appendix. 6. Comparison of the PXRD data of **9** with the experimental data after the UV-Vis encapsulation studies of iron(III) chloride. Red: activated **9**; Blue: not activated **9**; Green: 2 eq. of **9** vs. 1 eq. of iron(III) chloride; Grey: 3 eq. of **9** vs. 1 eq. of iron(III) chloride; Brown: 4 eq. of **9** vs. 1 eq. of iron(III) chloride; Cyan: 5 eq. of **9** vs. 1 eq. of iron(III) chloride; Purple: 6 eq. of **9** vs. 1 eq. of iron(III) chloride; Purple: 6 eq. of **9** vs. 1 eq. of iron(III) chloride; Yellow: 7 eq. of **9** vs. 1 eq. of iron(III) chloride.

Apart from the encapsulation of iron(III), a variety of other metal cations were studied, but none of them were adsorbed. The studied species were Co(II), Ni(II), and Cr(III). In **Figure Appendix 7**, the UV-Vis encapsulation studies of the aqueous solutions of cobalt(II) nitrate, nickel(II) nitrate, and chromium(III) nitrate are presented, proving that **9** does not adsorb any of them. Also, in **Figures Appendix 8** and **9** respectively are represented the infrared and PXRD data proving that there is no encapsulation.
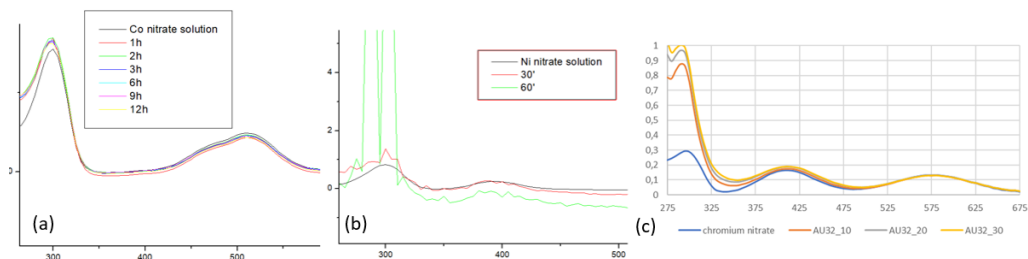
Figure Appendix. 7. (a) UV-vis encapsulation studies for cobalt(II) nitrate. (b) UV-vis encapsulation studies for nickel(II) nitrate. (c) UV-vis encapsulation studies for chromium(III) nitrate.
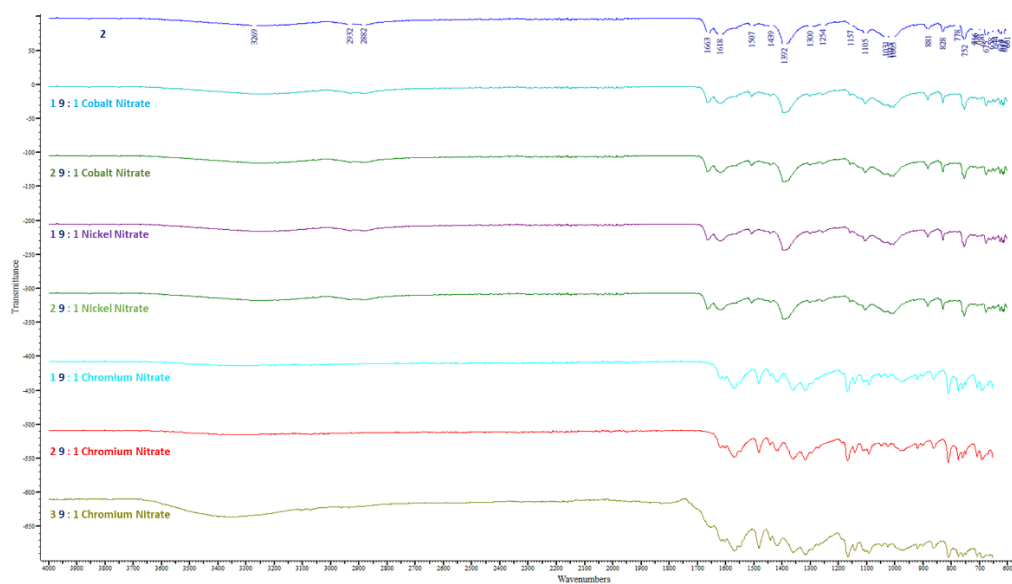

Figure Appendix. 8. Blue: Initial **9**; Pale Blue: initial MOF 9; Pale Blue: 1 eq. 9 vs. 1 eq. of cobalt(II) nitrate; Green: 2 eq. of 9 vs. 1 eq. of cobalt (II) nitrate; Purple: 1 eq. of 9 vs. 1 eq. of nickel(II) nitrate; Green: 2 eq. of 9 vs. 1 eq. nickel(II) nitrate; Cyan: 1 eq. of 9 vs. 1 eq. of chromium(III) nitrate; Red: 2 eq. of 9 vs. 1 eq. of chromium nitrate; Ochre: 2 eq. of 9 vs. 1 eq. of chromium(III) nitrate.
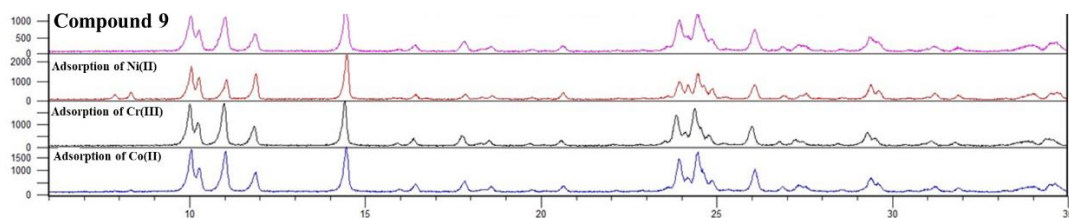
Figure Appendix 9. Comparison of the PXRD data of compound **9** after the encapsulation studies with different metal cations. Purple: Initial 9; Purple: Ni(II) nitrate; Black: Cr(III) nitrate; Blue: Co(II) nitrate.